THÈSE

Pour obtenir le grade de

Docteur

Délivré par **l'Ecole Nationale Supérieure de Chimie de Montpellier (ENSCM)**

Préparée au sein de l'école doctorale **Sciences Chimiques Balard (ED459)**
Et de l'unité de recherche **Institut Européen des Membranes (IEM)**
Spécialité : **Chimie et Physico-Chimie des Matériaux**

Présentée par **Adriana BOTH ENGEL**

Development and optimization of electrospun carbon fiber electrodes designed for enzymatic or hybrid biofuel cells applications

Soutenue le 08 Décembre 2015 devant le jury composé de

M. Nicolas MANO, Directeur de Recherche Université de Bordeaux	Rapporteur
Mme. Isabel Cristina TESSARO, Professeur Univ. Fédérale du Rio Grande do Sul (UFRGS, Brésil)	Rapporteur
M. Kouakou Boniface KOKOH, Professeur Université de Poitiers	Examinateur
M. Philippe MIELE, Professeur ENSCM - IEM	Examinateur
M. David CORNU, Professeur ENSCM - IEM	Directeur de Thèse
Mme. Sophie TINGRY, Chargée de Recherche CNRS - IEM	Co-directrice de Thèse

Remerciements

Ces travaux de thèse ont été réalisés à l'Institut Européen des Membranes (IEM), à Montpellier, France, au Département DM3 (Design des Matériaux Membranaires et Systèmes Multifonctionnels). L'IEM est actuellement dirigé par le Professeur Philippe Miele, à qui je remercie pour l'accueil au sein du laboratoire et par sa gentillesse. Je reconnais aussi le financement de thèse par le programme brésilien Sciences sans Frontières (*Ciência sem Fronteiras*), sans lequel ce travail ne serait pas possible.

Cette thèse a été réalisée sous l'encadrement du Professeur David Cornu et de la Docteur Sophie Tingry, à qui j'adresse mes plus sincères remerciements. David et Sophie m'ont guidé durant cette trajectoire d'une manière exceptionnelle sur le plan professionnel, sans oublier l'amitié, sur laquelle je garde les meilleurs souvenirs.

A mes collaborateurs de Montpellier et Poitiers, un grand merci pour tout l'apprentissage et l'ambiance amicale et amusante.

Au personnel de l'IEM, merci de votre gentillesse, aide et sourires.

Je remercie énormément aux collègues les plus proches, sans lesquels mon expérience en France ne serait pas complète : collègues de l'IEM, de la Galéra et mes stagiaires.

Aux amis brésiliens de Montpellier et ceux restés au Brésil, vous êtes super !

A ma famille et mon cher Leo, votre soutien a été incomparable.

Obrigada !

Index

Abbreviations

ABTS	2,2'-azinobis(3-ethylbenzothiazoline-6-sulfonate) diammonium salt
BAE	Bromide anion exchange
BFC	Biofuel cell
BOD	Bilirubin oxidase
CF	Carbon fiber
CNF	Carbon nanofiber
CNT	Carbon nanotube
CRD	Constant resistance discharge
CRFP	Carbon fiber reinforced polymer
CV	Cyclic voltammetry
CVD	Carbon vapor deposition
DMF	Dimethylformamide
DWNT	Double-walled carbon nanotubes
EDX	Energy dispersive X-ray spectroscopy
EIS	Electrochemical impedance spectroscopy
FC	Fuel cell
FFT	Fast Fourier transform
GBFC	Glucose biofuel cell
GDH	Glucose dehydrogenase
GOx	Glucose oxidase
h-GBFC	Hybrid glucose bifuel cell
MWNT	Multi-walled carbon nanotube
ORR	Oxygen reduction reaction
PAN	Polyacrylonitrile
PBS	Phosphate buffer solution
RHE	Reversible hydrogen electrode
SEM	Scanning electron microscopy
SHE	Standard hydrogen electrode
XRD	X-ray diffraction

This Ph.D. thesis has, to date, been subject to 5 publications in international journals, 1 publication in a French journal, 7 oral presentations in international conferences, 2 presentations in French conferences and 3 poster presentations.

General introduction

Biofuel cells are a specific type of fuel cell that employs biological catalysts (enzymes or microbes) in order to convert the chemical energy of the renewable fuels into electrical energy. It is a growing technology that still needs scientific and technological advances to reach a maturity level required for industrial developments. Research on the topic is therefore intense in order to overcome the existing drawbacks: the stability of the enzymatic catalysts over time and the low delivered power. Advances have so far allowed the application of this interesting technology to feed small electronic devices like music players and, more interestingly, benefiting from the glucose present in living bodies, to create implanted biofuel cells. The field of implanted biofuel cells might, in the future, revolutionize how we power implanted medical devices (artificial organs, pacemakers, hearing devices, etc), since it would be ideal to use our own metabolism to do so, instead of the lithium-ion batteries used nowadays. Not only could the cells be implanted in human bodies, but also in animals, which would guarantee electric power in, for example, military missions, where power is not directly available.

The optimization of biofuel cells is an extensive science that can focus on the design of the cell itself, biofuels (different types of sugars and alcohols), the engineering of new enzymes, the immobilization of such enzymes onto the electrodes and, the electrode material itself. This last feature is the focus of the present work. Electrode materials are evolving from dense metals, which provide lower surface for enzyme immobilization, toward porous structures with high surface allowing better diffusion of species and increased loading of enzymes which reflect in increased current delivered.

In this context, the objective of this thesis was motivated by a previous work realized in our group. This previous work was the first to prove the possibility of use of electrospun carbon nanofibers as electrode material for an enzymatic biocathode undergoing the typical O_2 reduction reaction. Before that, carbon nanofibers had not been explored in the literature as a possible electrode material for biofuel cells applications, even though it presents the crucial features: good electrical conductivity and high specific surface. From that limited background, the objectives of the present dissertation were set: to employ the

electrospun carbon nanofibers as electrode material in a complete biofuel cell assembly and to enhance the performance of this basic electrode material. For that purpose, strategies able to modify the surface property or the electrical conductivity of the material would be developed. Two different strategies were tested: the modification of the carbon fibers with nanostructured materials (carbon nanotubes adsorbed on the surface of fibers and gold particles added *in situ* on and into the fibers), and the approach of aligning the fibers.

This dissertation is divided in three parts. **Part 1** comprises the state of the art of relevant scientific topics: from the emergence of carbon materials until carbon nanofibers; electrospinning technique and details about biofuel cells technology. **Part 2** is dedicated to the elaboration of electrode materials and their physico-chemical characterization. It is divided in three chapters, each one dealing with the synthesis and intrinsic characterization of one different material: randomly organized carbon fibers modified or not with carbon nanotubes, aligned carbon fibers and gold-modified carbon fibers. **Part 3** is dedicated to the modification of the developed electrode materials with enzymes or other abiotic catalysts, and test as anodes or cathodes for biofuel cells applications. This part is also divided in three chapters. The first deals with the optimization of the enzyme immobilization technique onto the fibers and test toward a typical biocathode reaction, which is the O_2 reduction catalyzed by the enzymes. The next two chapters deal with the construction of complete biofuel cells, either fully enzymatic (with enzymatic anode and the enzymatic cathode optimized in the previous chapter) or hybrid (with abiotic catalysts onto carbon nanofibers as anode material, and the optimized biocathodes).

PART 1:

GENERAL STATE OF THE ART

Chapter I. Scientific background

1.1. Carbon and carbon fibers

Carbon is an essential material in the modern society that it is used in a very wide variety of applications. For instance, carbon is used as energy source (charcoal), in water filters and medicines for the digestive system (activated charcoal), in pigments (carbon black), in jewelry (diamond form), in the form of alloys and carbides in the industry of aircrafts, nuclear reactors, high temperature molds, prosthetics or sports equipment, not to mention advanced applications that are emerging with the valorization of carbon nanomaterials (carbon nanotubes, graphene, carbon nanofibers).[1] Furthermore, carbon based materials can be obtained from biosourced polymers, which is a sustainable emerging production route.[2] All this is possible because carbon exists abundantly in nature in very different crystalline forms or allotropes. Since four valence electrons are present, carbon can bond to both electronegative and electropositive elements and, more importantly, it can

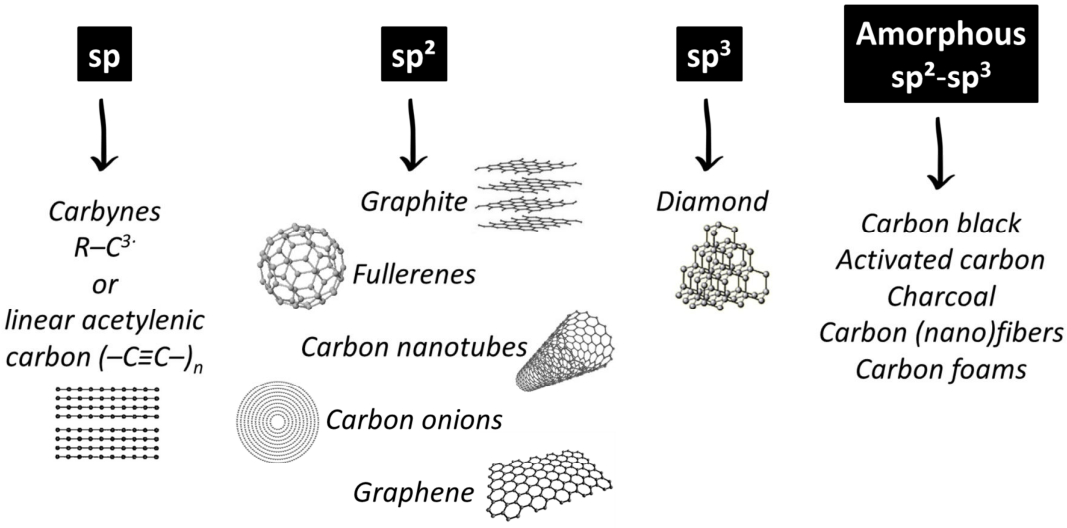

Figure 1.1. *Forms of carbon according to its hybridization, along with schematic representations.*

bond to itself through single, double, or triple bonds, which explains the existence of such a number of carbon allotropes.[3] **Figure 1.1** depicts the majority of carbon allotropes according to its hybridization along with some structural representations. It is important to point out that before the rise of carbon nanotubes and fullerenes, amorphous carbons were considered as an allotropic form of carbon.[4] However, some amorphous carbons contain an important amount of hydrogen, which makes the term "allotrope" unfit for such materials.

Carbon fibers are mostly composed of amorphous carbon with sp^2 hybridization containing a significant amount of sp^3 carbon atoms, and depending on the synthesis conditions they can exhibit different degrees of crystallinity, which will affect the fibers properties and applications.[3] Carbon fibers contain at least 92% of carbon, mean fiber diameters are in the range of 1–10 μm, the most common precursors being polyacrylonitrile (PAN), pitch and rayon.[5] Regardless of the precursor, the fabrication process is similar, as pointed by Huang: "*Precursor fibers are first stabilized at about 200–400 °C in air by an oxidization process. The infusible, stabilized fibers are then subjected to a high temperature treatment at around 1,000 °C in an inert atmosphere to remove hydrogen, oxygen, nitrogen, and other non-carbon elements. This step is often called carbonization. Carbonized fibers can be further graphitized at an even higher temperature up to around 3,000 °C to achieve higher carbon content and higher Young's modulus in the fiber direction*."[5] This fabrication process is nowadays very widespread, an example of an early US Patent (number 3,533,743) explaining such process having been published in 1970 (**Figure 1.2)**.[6]

Before that, the first commercial carbon fiber was made in 1879 by Thomas Edison when creating the incandescent light bulb, where cotton yarns were heated at high temperatures, which lead to their carbonization, thus creating a copy of the starting material composed of carbon (US Patent 223,898).[7] Later, in 1958 at Union Carbide (United States), Roger Bacon reported the first high performance carbon fiber, obtained while working with the melting of graphite under high temperatures and pressures (US Patent 2,957,756).[8] His process was enhanced in the following years at Union Carbide, especially by the use of rayon as precursor material, and by the development of a hot stretching process that gave birth to the first truly high modulus carbon fibers in 1964, which later originated the Thornel line with always increasing modulus for over ten years.[9] At the same time, in the early 60's in Japan, PAN started to be employed as precursor by Akio Shindo, showing modulus three

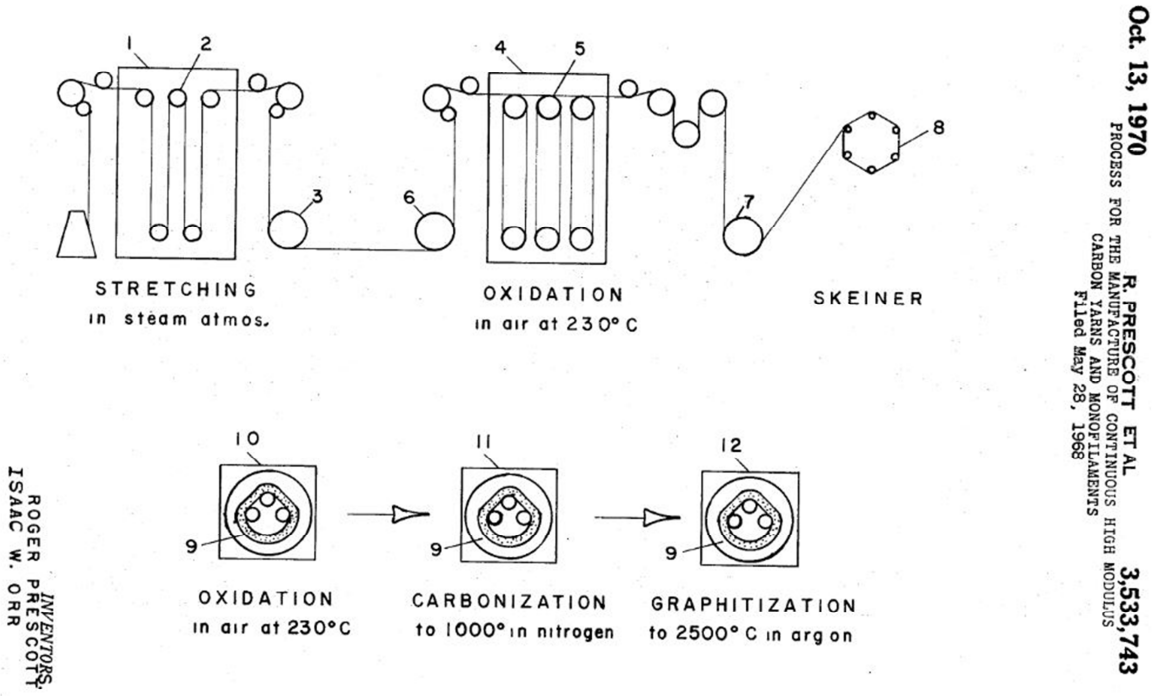

Figure 1.2. *Schematic representation of the thermal treatment of carbon fibers production from a 1970 US Patent[6], showing the three steps of stabilization, carbonization and graphitization (similar process is still used today).*

times better than that of rayon-based carbon fibers (Japan Patent 4,405). In 1964, William Watt developed even stronger PAN-based carbon fibers that were soon commercialized (British Patent 1,110,791), which launched the modern era of carbon fibers as the high performance material we presently know.

PAN is until today the dominant precursor material worldwide, since it provides carbon fibers with good quality at a lower cost. Pitch-based carbon fibers, for example, possess inferior tensile strength, and the processing and purification make it more expensive than PAN ones.[10] Huang explains that "*pitch as a precursor has the advantage of lower material cost, higher char yield, and higher degree of orientation compared with PAN. The graphitic structure also gives pitch based carbon fibers higher elastic modulus and higher thermal and electrical conductivity along the fiber direction. However, the processing cost (mainly from pitch purification, mesophase formation and fiber spinning) to achieve high performance carbon fibers is higher.*"[5] Another advantage of PAN is its higher melting point, thanks to strong intermolecular interactions (presence of polar nitrile groups in PAN molecule), which cause the polymer thermal degradation prior to melting, making it more thermally stable. As

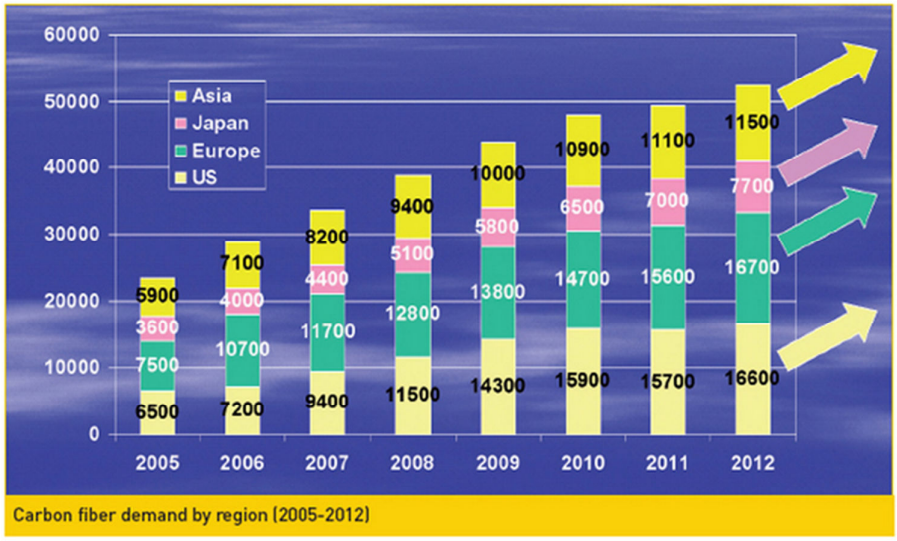

Figure 1.3. *Carbon fiber global demand per region (the regions of the world that most use carbon fibers) in the period of 2005 to 2012, values in million tons. Source: JEC Group.*[12]

pointed by Edie, carbon fibers with high degrees of molecular orientation (like pitch based fibers) exhibit high modulus, while carbon fibers with less ordered structures (like those obtained from polymers) develop higher tensile strengths, which makes PAN based carbon fibers the preferred base material for high strength composites.[11]

The world consumption of carbon fibers is predicted to grow at a more rapid rate during the coming decade. From 2005 to 2012, the average annual growth in Europe was 12 %, and in 2012 the global carbon fiber demand was over 50,000 million tons, the highest demand coming from Asia, Japan, Europe and the United States, as can be observed in **Figure 1.3**, a market analysis by the JEC Group.[12] In 2015, the global market of carbon fiber reinforced polymer (CFRP) composites is forecasted to be worth US$ 29 billion with a consumption of 78 million tons according to a report from Visiongain that predicts "*strong growth of CFRP consumption in automotive, energy and aerospace applications as a result of the higher demand for fuel efficient vehicles and aircrafts. The amount of electric and hybrid vehicles manufactured has also increased considerably in recent years and this has led to higher usage of CFRP composites in the automotive and fuel cells sectors*".[13] The market report from Ceskaa Market Research also predicts an annual growth rate from 2015 to 2020 of 12 %.[14]

1.1.1. Transformations during heat treatment of PAN fibers

In this subsection, a brief review of the stages of transformation of PAN to carbon at the molecular point of view will be made.

PAN is a thermoplastic polymer with glass transition temperature at around 90 °C, and melting temperature at around 320 °C, which molecular structure is represented in **Figure 1.4**. Electrostatic forces between the dipoles of adjacent –C≡N groups generate an intermolecular interaction that restricts the bond rotation, leading to a more rigid chain, which is responsible for its intrinsic properties and superior mechanical properties of the fibers obtained from it.[15]

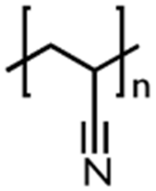

Figure 1.4. *Repeating unit of PAN.*

The three steps for the conversion of PAN fibers to carbon fibers are well known:

1) Stabilization (or oxidation), at mild temperatures (200–300 °C) under air;

2) Carbonization, at temperatures superior to 1000 °C under inert atmosphere;

3) Graphitization, at higher temperatures (around 3000 °C).[10,11,16]

Stabilization is the most important step for the formation of carbon fibers, since the appropriate parameters determine the properties of the resulting material. During stabilization, the chemical structure of the fiber changes, enabling it to support higher temperatures without melting, i.e. it becomes thermally stable. The chemical reactions that occur during this step are cyclization, dehydrogenation, aromatization, oxidation, and crosslinking, leading to the formation of a conjugated ladder structure, in which –C≡N bonds are converted to –C=N bonds (as proposed by Houtz in 1950),[17] and crosslinking occur

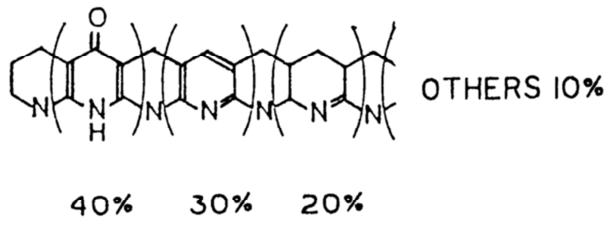

Figure 1.5. *PAN ladder structure obtained after the stabilization step.*[16]

between the PAN molecules.[18] All these reactions will not be more detailed here, but they were carefully studied in a review by Rahaman et al.[10] The final chemical structure of fully stabilized fibers is the one presented in **Figure 1.5**, as published by Morita in 1986.[16]

Regarding the ideal temperature for the stabilization process, there is no consensus amongst researchers. It is usually carried at temperatures between 200 to 300 °C,[5,19] but some state that it must be higher than 300°C for the stabilization to be completed.[20] Quoting Rahaman: "*If the [stabilization] temperature is too high, the fibers can overheat and fuse or even burn. However, if the temperature is too low, the reactions are slow and incomplete stabilization can be resulted, yielding poor carbon fiber properties*",[10] which highlights the importance of this step.

Carbonization is the step that takes place at temperatures from 1000 °C to 1500 °C (the higher the temperature, the higher the degree of carbonization obtained), in a dynamic atmosphere of nitrogen or argon, which prevents oxidation and removes the products of pyrolysis reactions.[21] Two steps take place during carbonization: thermal pyrolysis happens up to 600 °C where dehydrogenation reaction occurs; then at 600 to 1300 °C denitrogenation reaction occurs. These reactions are schematized in **Figure 1.6**, where the final structure obtained after carbonization can be observed.[22] Non carbon elements are removed from the fiber structure in the form of volatile elements like methane, hydrogen, water, carbon monoxide, carbon dioxide, etc., which causes the fiber to loose mass, reducing its diameter. Regarding the heating rate during carbonization, it is important to note: "*Too*

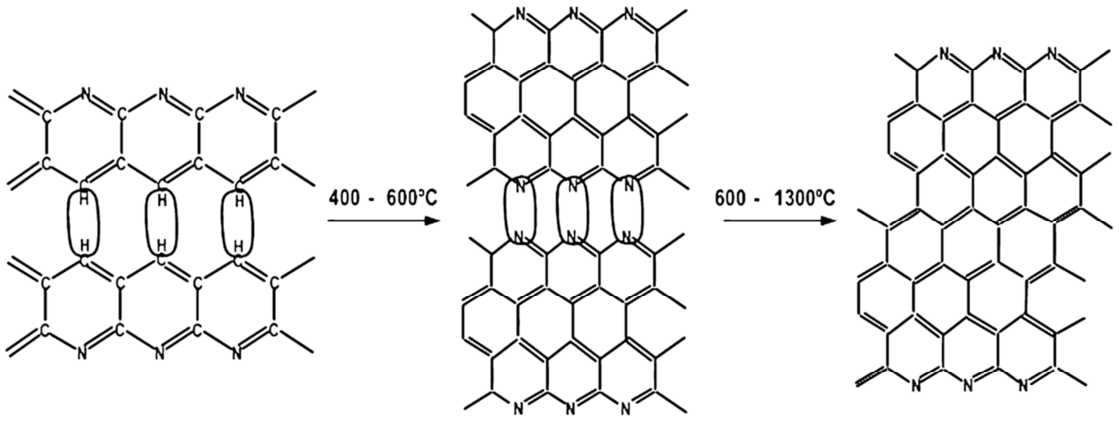

Figure 1.6. *Transformations undergone by the stabilized PAN fibers during the carbonization step. At 400-600 °C: dehydrogenation reaction. At 600-1300 °C: denitrogenation reaction.*[22]

fast a carbonization rate introduces defects in carbon fibers, while low carbonization rate causes the loss of too much nitrogen at the early stages of carbonization, certain amount of which is preferred to achieve high strength carbon fibers".[5] Fitzer showed that while increasing the carbonization temperature until 1600°C the tensile strength of carbon fibers increases.[23] However, at higher temperatures it starts to decrease, which might be explained by the release of nitrogen. Conversely, with increasing the temperature, even higher than 2000 °C, the modulus of fibers increases, thanks to the increase in the degree of preferred orientation of adjacent graphite-like layers within the fiber, which get more aligned in the fiber direction.[5]

Finally, graphitization can be considered as the prolongation of the carbonization step until higher temperatures up to 3000 °C. In this step the carbon structure is transformed into graphite, with up to 99% conversion of PAN polymer into carbon,[10] which is difficult to achieve with other polymers. The result is carbon fibers with improved mechanical properties,[21] and reduced concentration of residual nitrogen on the material to very low levels.[10] Usually argon may be used, because nitrogen can react with carbon at such high temperatures.[5]

1.1.2. The case of carbon nanofibers

Besides industrial carbon fibers which have a mean fiber diameter in the order of 1–10 µm, carbon nanofibers (CNFs) are a special case of carbon fibers that possess a mean fiber diameter in the order of 10–500 nm. It is not clear in the literature whether fibers with diameters ranging from 500 – 1000 nm can be called "nanometric fibers", some authors preferring the term "submicronic fibers". Interest in CNFs gradually increased from the identification of carbon nanotubes by Iijima in 1991.[24] Besides, carbon nanofibers also differ from carbon nanotubes in their intrinsic geometry, since CNTs are hollow structures with mean diameter of some nanometers, while CNFs are massive filaments with higher diameter, as mentioned above.[25] In **Figure 1.7**, a schematic comparison of the mean diameters of these three structures is made to visualize the large difference in size that separates the different forms of carbon fibers, which is one factor strongly affecting their properties.

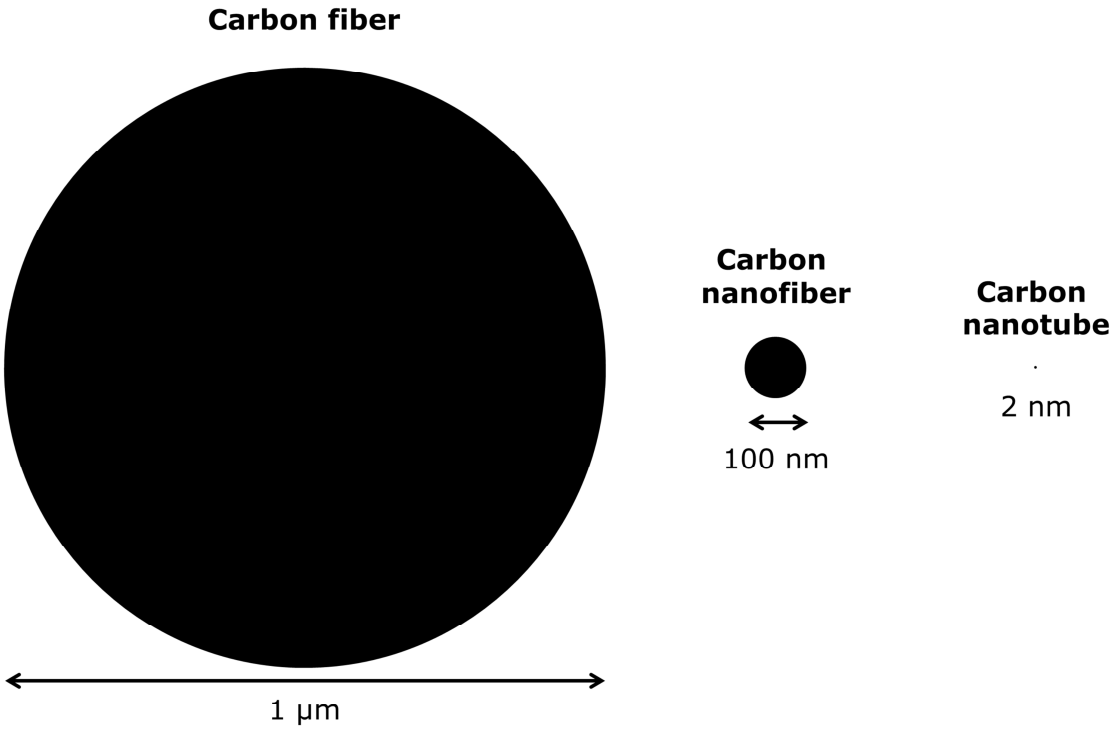

Figure 1.7. *Comparison of mean diameters (arbitrary values for exemplification) of micronic carbon fiber, carbon nanofiber and carbon nanotube.*

Research on high strength carbon nanofibers is an current scientific chalenge.[26–28] The strongest carbon fibers that can be produced today have a tensile strength of merely ~7 GPa (T1000® from Toray, with fiber diameters of 5 µm), while the highest performance electrospun CNFs reported presented tensile strength of 3.5 GPa [27] (fiber diameters between 150 and 500 nm). Concerning the applications, CNFs are a promising material where the advantages of its smaller dimensions and higher specific surface can be beneficial. CNFs applications are normally those that rely on their superior physical properties such as high specific surface area, great electrical conductivity, and good bio-compatibility, which are referred to as functional carbon nanofibers.[29] Hence, most applications are in electrodes for energy conversion and storage (Li-ion batteries, supercapacitors, biofuel cells), catalysis support, sensors, adsorption and biomedical applications.

Carbon nanofibers can be obtained by CVD, for instance, or by electrospinning, an interesting technique that is detailed in the following section.

1.2. Electrospinning technique for the production of CNFs

Electrospinning is a well-known technique for the production of ultrathin polymeric fibers with diameters ranging from tens of nanometers to some micrometers. The fibers can be solid or hollow, with an exceptional length, uniform diameter and several compositions (polymers, composites, ceramics).[30,31] Bognitzki et al. well described the process, as follows:

> *The electrospinning process involves the application of a strong electrostatic field to a capillary connected with a reservoir containing a polymer solution. Under the influence of the electrostatic field, a droplet of the polymer solution at the capillary tip is deformed into a conical shape (Taylor cone). If the voltage surpasses a threshold value, electrostatic forces overcome the surface tension, and a fine charged jet is ejected. The jet moves towards a ground plate acting as counter electrode. Due to the viscosity of the polymer solution and the presence of entanglements, the jet remains stable and does not transform into spherical droplets as expected for a liquid cylindrical thread. The solvent begins to evaporate immediately after the jet is formed. The result is the deposition of a thin polymer fiber on a substrate located above the counter electrode.*[32]

In **Figure 1.8** the scheme[33] of a typical electrospinning set-up is presented.

1.2.1. Brief history

The history of electrospinning might date back to the year 1600 with the first record of the deformation of a liquid drop (later known as Taylor cone) by William Gilbert, followed by some advancement in the 18th and 19th centuries, as detailed by Tucker et al.[34] Electrospinning as a physical phenomenon and as an application to produce tiny fibers was likely first suggested by Morton with a patent submitted in 1900.[35] He created fibrous masses by electrospinning either with a needle and needleless, which at the time was truly state-of-the-art. Formhals in 1930 was the first to patent his works on the electrospinning of plastics,[36] making a significant contribution with a sequence of 22 patents. He is generally recognized as the father of electrospinning technology, even though his first patent[36] did not concern the phenomenon of electrospinning in its essence but its commercial potential, and he even mentioned that the phenomenon itself was already known at the time, probably referring to Morton's work.

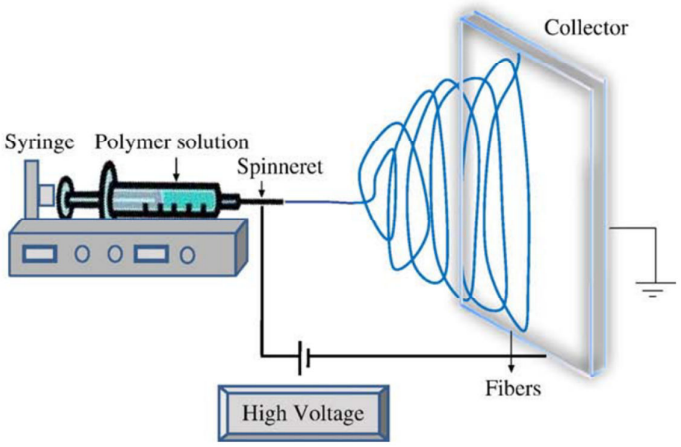

Figure 1.8. *Scheme of electrospinning process. [from Bhardwaj[33]]*

None of those early works in the US "*reached industrial application in spite of the fact that their inventions had high commercial potential. The probable reasons for that might be lack of appropriate equipment that should have enabled the researchers to discover the 'nanodimension' of electrospun fibres, since the first prototype electron microscope came into existence in 1931*.", stated Lukáš et al.[37] However, in 1939 in the former USSR, the first industrial facility for the production of elecrospun filters, named "Petryanov filters" was established in the city of Tver.[34,38] In the US, Donaldson Co., Inc. was the first company to introduce electrospun nanofiber filtering media products commercially, only in the year 1981.[37]

It was with the works of Taylor from 1964 to 1969 that the theoretical foundations of modern electrospinning were set.[39–41] His work was, though, focused on the field of meteorology. He described mathematically the shape of the cone formed by the liquid droplet under the effect of an electric field, named as Taylor cone. Until the year 1993, electrospinning technique was known as "electrostatic spinning", and it was the Reneker group that popularized the name electrospinning,[34] evidencing its nanoscale nature and the high added-value of the resulting nanomaterials.[30,42,43] Ever since, the importance and attention given to this interesting technique have only risen, with works being realized in many fields of science, one example being electrospinning for energy and environmental applications.[31]

Regarding applications, thanks to the smaller pores and higher surface area of electrospun fibers compared to regular fibers, successful applications in several fields have been achieved, such as, nanocatalysis, tissue engineering scaffolds, protective clothing, filtration, biomedical, pharmaceutical, optical electronics, healthcare, biotechnology, defense and security, and environmental engineering.[33]

1.2.2. Electrospinning today

The technology of electrospinning is nowadays very widespread. It can be achieved from a polymer in the melt state, a polymer solution (where the solvent, molecular weight of the polymer and solution viscosity play an important role) or an emulsion (for solutions with insoluble components). The set-up can be horizontal (as shown in **Figure 1.8**) or vertical. It can be realized with a single needle for solution injection, with a system of multiple needles (useful to increase the production rate, thickness of the mats or area of deposition) or with co- or tri-axial needles (where the simultaneous spinning of different liquids is made, allowing the creation of core/shell nanofibers). In **Figure 1.9** the different needle possibilities are presented. Needleless electrospinning also exists, and it normally employs either a thin film of polymer solution, or sharp tips on top of which the charges are concentrated, and from where the polymer jet emerges. Needleless systems are more advantageous than multiple needle systems for industrial upscaling, for example, because the latter can often be impaired by the clogging of the needles. An example of needleless electrospinning

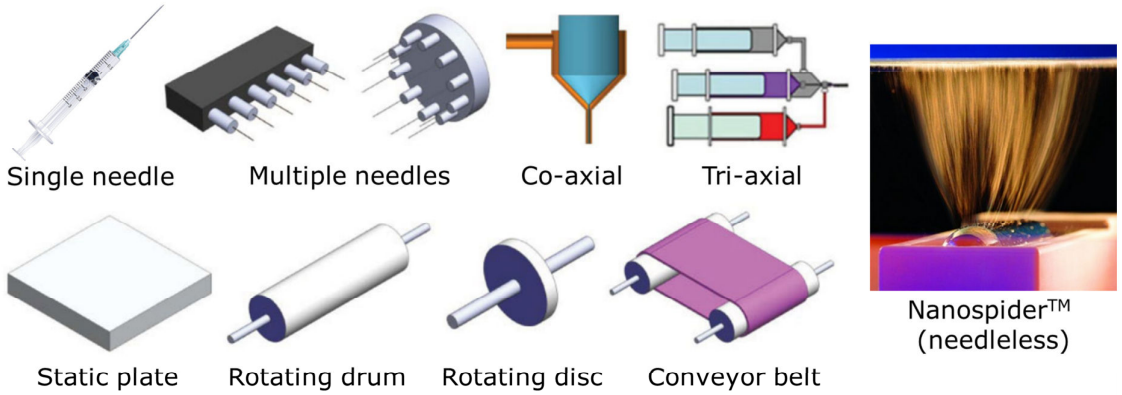

Figure 1.9. *Different needle set-ups possible in electrospinning, as well as the different fiber collector types most normally employed (pictures from Persano et al.[38]). On the right, a picture of the Nanospider™ set-up from Elmarco company, where no needles are employed.*

employed industrially is the Nanospider™, by the Czech company Elmarco, where a rotating cylinder partially immersed in a pool containing the polymer solution serves as nanofiber generator, as shown in **Figure 1.9**. The fiber collector can be a simple static flat plate, a rotating drum, a rotating disc or a conveyor belt (for larger productivities), as also shown in **Figure 1.9**.

It is important to note the vast amount of parameters in electrospinning technology that play a role in the characteristics of the resulting fibers (diameter, surface smoothness, porosity of the fiber, porosity of the mat, etc.). There are three main sources of variations:

SOLUTION CHARACTERISTICS: molecular weight of the polymer and viscosity/concentration, solution conductivity, solvent, surface tension.

PROCESS PARAMETERS: voltage, feed rate, diameter of the needle, tip to collector distance, type of fiber collector.

AMBIENT PARAMETERS: temperature, humidity.

In general, parameters that have an effect on solvent evaporation tend to decrease fiber diameter, like the ambient temperature or the use of a solvent with higher vapor pressure. Increasing the voltage also tends to decrease fiber diameter, because the fiber is stretched more strongly. The molecular weight of the polymer, as well as the viscosity and the solution concentration have a similar effect, which is of increasing fiber diameter, which becomes more uniform, and preventing fibers to fracture when those parameters are higher, since a higher amount of polymer chains will be entangled in the fiber. Another parameter that greatly influences the fiber formation is the solution conductivity, which is a result of the polymer and solvent employed, and the presence of salts or other materials in the solution. Higher solution conductivity significantly decreases fiber diameter, whereas low conductivity results in insufficient elongation of the jet. A more detailed analysis on the effect of electrospinning parameters was made by Ramakrishna et al.[44] and Bhardwaj et al.[33]

1.2.3. Carbon nanofibers from electrospinning and other techniques

PAN in DMF, as mentioned earlier, is the base material of most micrometric carbon fibers around the world. The solution is easily transformed into white-colored nanofiber mats via electrospinning, which has been thoroughly studied[15,45–47]. Further thermal treatment involving stabilization and carbonization, similarly to the treatment for regular carbon fibers, converts PAN nanofibers into carbon nanofibers, thus creating a new material

with totally different properties than those of the original precursor fibers. The subject of CNFs was addressed on the Section 1.1.2, and the objective of this section is to compare the advantages of electrospinning as a technique for the production of CNFs with other possible techniques.

Besides electrospinning, fiber production can be achieved by extrusion techniques, also called spinning techniques. Spinning corresponds to processes that employ a spinneret for the production of continuous polymeric fibers, where the spinneret can have one or many holes with variable diameters for the extrusion to take place. The material to be extruded must be in the liquid form (i.e. melt, solution or emulsion).[48] Spinning process is generally classified as follows:

- **Wet spinning:** a spinneret is immersed in a coagulation bath (i.e. a liquid that is miscible with the solvent, but a non-solvent for the polymer), and a polymeric solution is extruded directly into the bath, so that the solvent is removed from the fiber jet and solidification of the fiber occurs. Wet spinning is the most ancient of the spinning techniques, originated in the mid-1850's by Hilaire de Chardonnet in Besançon (France) to produce cellulosic fibers.[49]
- **Dry spinning:** a polymer solution is forced through a spinneret, and then the solvent is evaporated under a stream of hot air or inert gas, forming a solid fiber. Dry spinning is faster than wet spinning because the mass transfer of the evaporation of solvent is faster than the mas transfer between the solvent and non-solvent liquids. Dry spinning is employed in large-scale production, and results in fibers with irregular cross-sectional morphologies that normally are subsequently stretched to improve fiber properties.
- **Dry-wet spinning (also called gel spinning):** the spinneret is positioned above the coagulation bath, and the filaments are extruded vertically, passing through air and then into the bath. This type of fibers exhibit finer linear density and higher strength, thus becoming more popular.[29]
- **Melt spinning:** a polymer melt is passed through a spinneret, mechanical stretching often occurs at this point in order to reduce the fiber diameter, followed by the cooling of the filaments before solid fibers are recuperated. This is the fastest fiber solidifying process, since no solvent is involved. Thus, several solvent-related issues are absent in melt spinning, like solution concentration,

solvent residues and solvent recovery, not to mention lower cost and higher productivity rates (since the cooling of fibers is fast), making this the favorite spinning method in industry.[48] However, the high viscosity of the polymer melts creates a difficulty for the production of very thin fibers.

From those techniques, polymeric fibers are obtained, which can be further thermally treated to obtain carbon fibers. Moreover, another technique for producing carbon fibers specifically is:

- **Vapor growing:** chemical vapor deposition (CVD) was explored in the 1970's and 1980's[50] and consists in the catalytic decomposition of hydrocarbons (like ethylene or methane) in the presence of metal particles (transition metal catalysts like Fe, Ni) at a temperature of 1000-1300°C.[51]

Electrospinning is similar to conventional processes of fiber spinning, except that instead of mechanical forces, electrostatic repulsions between surface charges are employed for fiber formation. One advantage of electrospinning compared to other spinning techniques is the possibility of generating fibers with much smaller diameters because the elongation of the fiber is achieved with no contact, thanks to the application of an electric field.[52] Even though spinning fibers present in general larger diameters, there are examples of the achievement of small diameters, like the one reported in 2009 of a dry-spinning process using a modified "spinneret based tunable engineering parameter" (STEP) technique for the production of patterned nanofibers with diameters ranging from 50–500 nm, with fiber lengths of several millimeters.[53] Vapor grown carbon fibers also exhibit small diameters (from several nm to hundreds of nm) and small length (from several µm to hundreds of µm),[54] making them short and discontinuous.[55]

Thus, a major advantage of electrospinning compared to all other cited techniques, is the possibility of achieving a free-standing felt of fibers, either if it is polymeric or carbon fibers. This is thanks to the fact that the fibers obtained by electrospinning are very long (can virtually go from several cm up to several meters[44]) and thin, thus allowing their deposition as a non-woven material, which can be of great benefit for certain applications, since no support or bonding material is necessary.

1.3. Energy harvesting through biofuel cells

1.3.1. From traditional to biological fuel cells

Fuel cells are electrochemical devices that convert the chemical energy of fuels directly into electrical energy and produce heat and water as byproduct, with high efficfiency.[56] Their operation is simple and more efficient if compared with internal combustion engines. Fuel cells have power capacity in the order of 200 kW to 2 MW with average efficiency of around 40 to 60 %.[56] For comparison, a typical diesel combustion engine has a power of 500 kW up to 5 MW, but with an efficiency of 35 %.

The first fuel cell was demonstrated in 1839 by British scientist William Grove. Grove built a first device in 1842 which he called a "gas voltaic battery".[57] His device, represented in **Figure 1.10**, was composed of platinum electrodes in a dilute solution of acid as electrolyte. First (**Figure 1.10A**), water is electrolyzed into H_2 and O_2 when an external current flows in the system. Then when the power supply is replaced by an ampere-meter (**Figure 1.10B**), the electrolysis is reversed and a small current is observed.[58] This experiment is, however, very inefficient, especially because the contact area between the gas, the electrode and the electrolyte is very small.

More than a century after Grove's development, the first fuel cell found a commercial use at NASA (National Aeronautics and Space Administration, US), where a compact system was needed to generate electricity for space shuttle applications. An alkaline fuel cell with 12 kW power was developed in the 1970's, supplying reliable power without the need of backup powers like batteries.[56]

Nowadays fuel cell technology is well established, and the electrodes are usually made flat, with a thin layer of electrolyte, as showed in **Figure 1.10C**. The electrode material is porous so that both the electrolyte from one side and the gas from the other can penetrate it aiming to maximize the contact between the electrode, the electrolyte, and the gas. In the simplest and one of the most common types of FC, the acid electrolyte FC, hydrogen gas ionizes in the anode releasing electrons (that pass through an external circuit) and protons, according to the reaction presented in **Figure 1.10C**. At the cathode, oxygen reacts with the electrons and protons arising from the anodic reaction to form water.

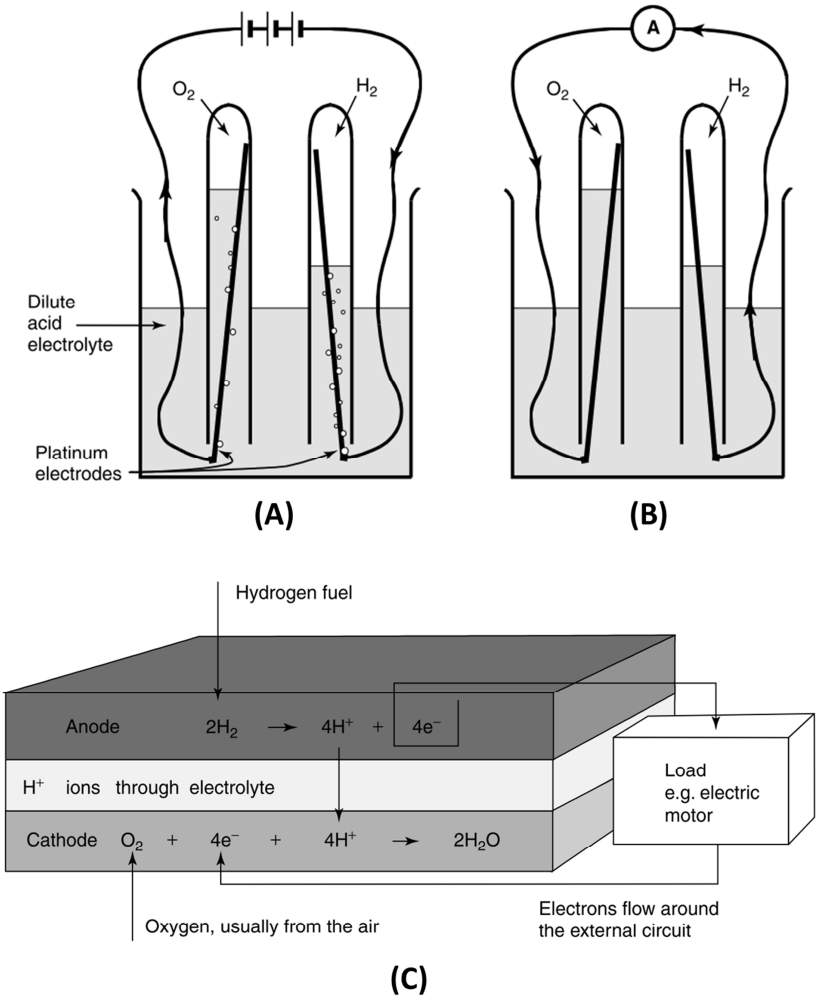

Figure 1.10. *Grove's assay of the first fuel cell: in* ***(A)*** *the electrolysis of water where hydrogen and oxygen are separated through the passage of an external electric current; in* ***(B)*** *a small current is observed when an ampere-meter is added to the system (the arrows represent the flow of electrons from – to +). In* ***(C)****, the basic construction of a present construction of an acid electrolyte FC with electrode reactions. (from Larminie and Dicks.*[58]*)*

Many are the examples of FCs nowadays, with different electrolytes and different reactions at the electrodes, being commercialized or in research scale. Six major types of FCs can be highlighted presently, according to the choice of electrolyte and fuel:

i. Proton exchange membrane fuel cell (PEMFC)

(a) Direct formic acid fuel cell (DFAFC)

(b) Direct Ethanol Fuel Cell (DEFC)

ii. Alkaline fuel cell (AFC)

(a) Proton ceramic fuel cell (PCFC)

(b) Direct borohydride fuel cell (DBFC)

iii. Phosphoric acid fuel cell (PAFC)

iv. Molten carbonate fuel cell (MCFC)

v. Solid oxide fuel cell (SOFC)

vi. Direct methanol fuel cell (DMFC).

These FCs can be divided in two operating temperature ranges: low temperature (50 – 250 °C for PEMFC, AFC and PAFC) and high temperature (650 – 1000 °C, for MCFC and SOFC).[56] Temperatures in FC technology are usually high in order to increase reaction rates, which can also be achieved by the use of catalysts or by increasing the electrode area. This parameter is specifically important for FC technology since the reactions with electrons or protons must take place at the surface of the electrodes, so that electrons can be removed. Therefore, the rate of the reaction is proportional to the area of the electrode, so that FCs performance is often depicted per cm^2. The simple geometric area (i.e. length $\times$ width) of the electrodes is, however, not sufficient, and present electrodes are designed with a highly porous microstructure that can be hundreds or even thousands of times the straightforward geometric area.[58]

Biofuel cells (BFCs) are a specific type of fuel cell that employs biological catalysts and fuels. The first development in this area was realized in the beginning of the 20^{th} century with the works of Potter in England, who placed a platinum electrode into cultures of yeast or *Escherichia coli* and showed that a potential difference could be generated.[59] Later, in 1931, Cohen developed microbial fuel cells that in series were capable of generating 35 V and 2 mA.[60] In the 1960's, Yahiro et al. first described the production of electricity from enzymes, which is the first report on an enzymatic fuel cell.[61] They used the enzyme glucose oxidase at the anode and an O_2 cathode, generating 175–350 mV. A different system with alcohol dehydrogenase in the presence of iron (probable electron transfer mediator) yielded voltages that ranged from 625–750 mV.

Biofuel cells have traditionally been classified according to whether the catalytic enzymes were located inside or outside of living cells (i.e. enzymes separated and purified from living organisms). If living cells are involved (bacteria, yeast), the system is considered to be microbial, and if not, the system is considered enzymatic.[62]

Comparison of both techniques, traditional and biological FCs, is not essential but difficult to avoid, since the basic technology is the same. First, the enormous difference in

power range makes the applications of both types of FCs not competing. Traditional FCs power (from 200 kW to 2 MW) makes them suitable to feed cars, boats and other types of engines and as primary and backup power for commercial and residential buildings, amongst other applications, while enzymatic BFCs deliver powers in the range of few mW allowing them to feed small electronic devices and gadgets, like music players, and possibly implanted medical devices, the fuel being glucose present in the blood. In the case of microbial fuel cells (MFCs) that run with wastewaters, besides the production of electricity, an interesting feature is the possibility to purify or treat the fuel. Second, whereas metallic catalysts employed in FCs are able to catalyze different reactions, enzymes are selective for specific reactions, which diminishes the problem of side reactions and allows the removal of the separation membrane.[63] The price range of both types of catalysts is also a point to consider, enzymes and microbes being lower cost biological and renewable components, while metals come from a limited source, being thus more expensive; not to mention the cost of the fuel, since biofuels like glucose have a negligible price compared to pure hydrogen. In addition, BFCs operate at much milder temperatures than traditional FCs: under 40 °C, whilst the second might operate at temperatures as high as 1000 °C which leads to an energetic concern.

Since the focus of this work is enzymatic BFCs, the subject of MFCs will not be further detailed. The scheme of a typical enzymatic BFC is represented in **Figure 1.11**. The oxidation of the fuel at the anode happens through a specific enzyme that captures the electrons from that reaction, and transfers them to the electrode material with or without the need of an electron transfer mediator. The electrons go through the external circuit and arrive at the cathode, where O_2 is reduced into water with electrons and the protons that resulted from the anodic reaction, via another specific enzyme (also with the aid of an electron transfer mediator or not).

The justification for BFCs technology development is, as pointed out by Katz et al.,[64] the present trend towards the miniaturization and portability of computing and communication devices. These energy-demanding applications require small, light power sources that are able to sustain operation over long periods of time, particularly in remote locations such as space and exploration. Furthermore, advances in the medical sciences are leading to an increasing number of implantable electrically operated devices (pacemakers, artificial organs, and vision and hearing devices). These items need power supplies that will

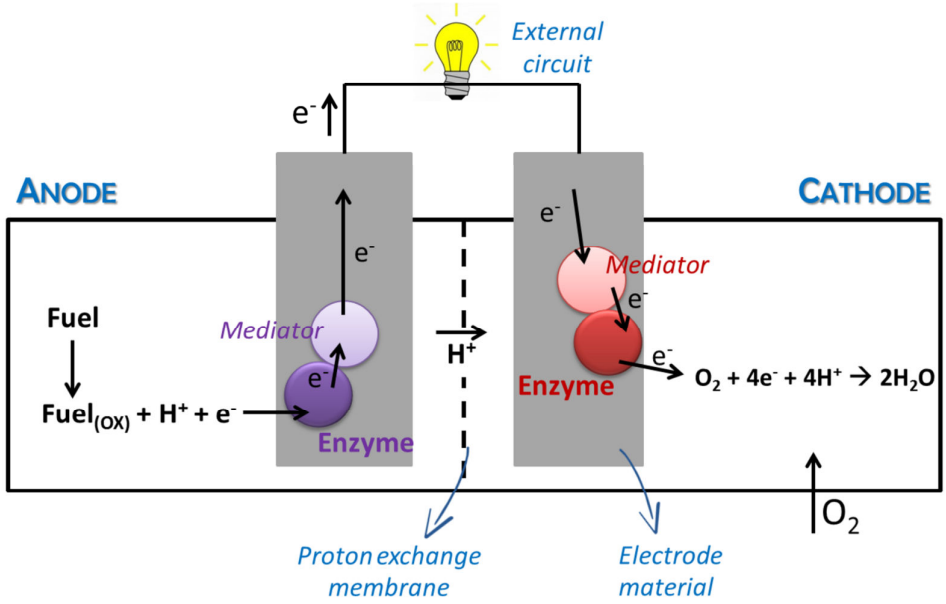

Figure 1.11. *Scheme of a typical enzymatic biofuel cell, with enzymes and electron transfer mediators on both chambers, with typical O_2 cathode and respective reactions.*

operate for extremely long durations as maintenance would implicate in surgery. Ideally, implanted devices would take advantage of the natural fuel substances found in the body, and thus would continue to draw power for as long as the subject lives.[64]

Therefore, general applications of BFCs can be divided in the following three groups depending on the type of fuels employed, according to Barton et al.:[62]

i. implantable power, such as microscale cells implanted in human or animal tissue[65–68] or larger cells implanted in blood vessels[69];

ii. power derived from ambient fuels or oxidants, mainly plants or juices, but extendable to sewage and other waste streams;[70,71]

iii. power derived from conventional fuels, including hydrogen, methanol, and higher alcohols.[72,73]

However, to date, drawbacks exist that prevent this technology to be commercialized massively, unlike the model of traditional fuel cells. Compared to them, research on BFCs is still in early stages, mostly because of the low stability and power delivered, which obliges the use of BFCs in series for reasonable performance to be obtained.[74] Moreover, stability is

a key aspect of any practical fuel cell, and BFCs must have lifetimes ranging from months to years to justify implanted, massively distributed, or consumer portable applications.[62]

Next sections will discuss some specific features of enzymatic BFCs, which is the main subject of this work.

1.3.2. BFCs fuels

Where **fuels for enzymatic BFCs** are concerned, abundant organic raw materials such as methanol, organic acids, or glucose can be used as substrates for the oxidation process, and molecular oxygen or H_2O_2 can act as the substrate being reduced.[64] Glucose is the most obvious fuel for BFCs given its abundance in nature and essential role in human metabolism. Other sugars like fructose[75] and lactose[76] have been employed as well. Methanol has been already identified as one of the best fuels in conventional direct fuel cells, which can be used as power supply for portable applications. Ethanol has attracted more attention being a biofuel that can be produced by fermentation of biomass. Glycerol is also an attractive fuel due to its high energy density, low vapor pressure and low toxicity opposed to other mentioned alcohols (like methanol). Commonly, anodic systems employ only one enzyme that leads to the partial oxidation of the fuel, while enzyme cascades allow better utilization of the chemical energy of the fuel, allowing its complete oxidation to CO_2 and the liberation of more than one electron, however increasing the complexity of the system.[77]

1.3.3. Biological catalysts

Enzymatic anodes. Regarding anodes for BFCs or biosensors powered by glucose, glucose oxidase (GOx) is the most widely used enzyme. GOx catalyzes the oxidation of glucose to gluconolactone according to the **Equation 1.1**, which spontaneously hydrolyzes to gluconic acid. Since GOx reacts naturally with O_2 to form H_2O_2, the presence of O_2 should be avoided when using GOx, preventing the use of membraneless systems. Therefore, O_2 competes with the electrode for the released electrons (the parasite reaction prevents electrons from flowing to the external circuit), which decreases the current density delivered by the anode. GOx normally operates with the redox electron transfer mediator flavin adenine dinucleotide (FAD).[77] Direct electron transfer (DET, a concept that will be introduced later in this chapter) with GOx was shown to be achievable in the presence of CNTs.[78]

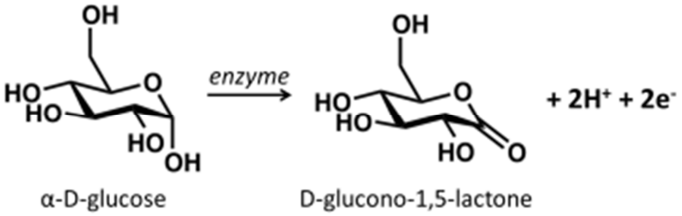

(1.1)

Glucose dehydrogenase (GDH) is another option with the advantage that it does not react with O_2. However, its applications are limited since GDH requires a soluble co-factor: nicotinamide adenine dinucleotide (NADH/NAD^+). Glucose and other monosaccharides can also be oxidized by cellobiose dehydrogenase (CDH), enzyme introduced in 2008 by Gorton et al.[79,80] In addition, PQQ-dependent GDH and fructose dehydrogenase oxidize glucose and fructose, respectively.

Several redox enzymes are able to oxidize different alcohols like methanol, ethanol, glycerol and others. Alcohol dehydrogenases, for instance, normally employ NAD^+/NADH co-factor, as mentioned above with GDH, but DET have been achieved.[81,82] Enzyme cascades can be employed for the complete oxidation of the alcohol to CO_2, for example, a sequence of NAD-dependent alcohol dehydrogenase, aldehyde dehydrogenase and formate dehydrogenase were used for the oxidation of methanol to CO_2.[83] A different multi-enzymatic cascade was employed (aiming the regeneration of the co-factor) by our group for the development of BFCs powered by ethanol.[84] The enzymes alcool desydrogenase (ADH) and diaphorase (DP) were employed, with nicotinamide dinucleotide (NAD) and K3 vitamine (VK3) as mediators. The chain of reactions that take place at the anode is the following: after the oxidation of ethanol into acetaldehyde through ADH (reaction that is depicted in **Equation 1.2**), its mediator NAD captures the electron coming from this reaction.

$$CH_3-CH_2-\mathrm{OH} \xrightarrow{enzyme} CH_3-\mathrm{CH{=}O} + 2H^+ + 2e^- \qquad (1.2)$$

For NAD to be regenerated and continue active, it reacts with the second enzyme DP which possesses its own mediator, VK3. Many species need to be in intimate contact on the surface of the electrode for the course of the anodic reaction to be successful, and good mass transfer is primordial. However, the higher complexity of these cascade systems is a drawback for its application.

Enzymatic cathodes. O_2 is the most widely used oxidant in enzymatic BFCs, being employed in the form of pure gas or air.[77] Laccase and bilirubin oxidase (BOD), widely employed enzymes for BFCs applications, are multicopper oxidoreductase enzymes that catalyze the four-electron reduction of O_2 completely to H_2O (represented in **Equation 1.3**) either through direct electron transfer[85] using carbon nanotubes as promoters for suitable orientation or in the presence of the electron transfer mediator ABTS (the concept of mediated electron transfer will be explained later in this chapter).[86] By oxidizing the mediator $ABTS_{red}$, laccase acquires the necessary electrons to reduce dioxygen into water, and $ABTS_{ox}$ is reduced on the electrode surface.

$$O_2 + 4H^+ + 4e^- \xrightarrow{enzyme} 2H_2O \qquad (1.3)$$

Laccase is a readily affordable enzyme that exhibits activity at slightly acidic conditions, being studied since the 19th century.[87] BOD was isolated in 1981.[88] This enzyme is much more difficult to obtain and more expensive, but retained more atention thanks to its stronger activity at neutral pH and relative resistance to Cl^- ions, which make BOD superior for applications in physiological conditions.[86] Both laccase and BOD are found in various fungus and bacteria, and laccase is also found in plants.[87,88]

Other possible enzymes for O_2 reduction are cytochrome oxidase,[77] ascorbate oxidase,[89] copper efflux oxidase[86] and tyrosinase,[90] used on a lesser extent.

Regarding the enzymatic structure, typical laccases contain in the active center four copper atoms organized in three centers named T_1, T_2 and T_3, as can be observed in **Figure 1.12**.[91] T_1 and T_2 contain one Cu atom each, while T_3 contains 2 Cu atoms. T_2 and T_3 are close to each other (0.04 nm) and form the so-called copper trinuclear cluster. T_1 center is

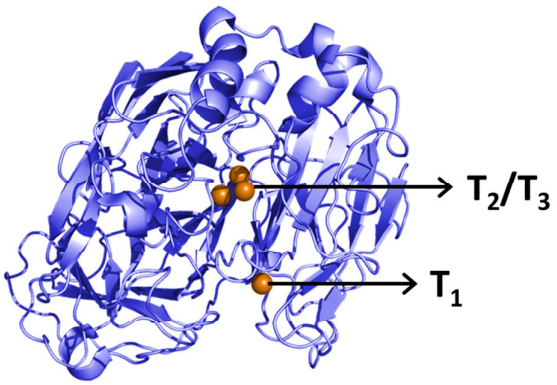

Figure 1.12. *Crystalline structure of laccase, showing the copper centers T_1 and T_2/T_3. (adapted from Armstrong[91])*

approximately 0.13 nm from the T_2/T_3 cluster, and is hidden in a hydrophobic pocket of the protein, being accessible for electrons from the electrode and for organic mediator, which means that T1 is the main electron acceptor.[86,92] It is in T_2/T_3 cluster that binding of dioxygen followed by four-electron reduction to water occurs.[87] One can observe from the laccase structure, as what happens in most multicopper oxidase enzymes, that the redox center is buried inside the protein matrix, hindering the communication with reacting species. This is one reason for the difficulty in achieving DET.

Considering BOD enzyme, which also contains four copper atoms, the exact electronic pathway has not yet been determined, but it is known that T_1 center accepts electrons from organic substrate of the enzyme and relays them to the O_2 reduction site, which is a trinuclear Cu cluster, similarly to laccase.[88] This mechanism is represented in **Figure 1.13**, for BOD from *Magnaporthe oryzae* (PDB code 2L9Y), where arrows show the hypothetical electron transfer, according to Mano et al.[88]

Besides O_2, another oxidant far less employed in BFCs is hydrogen peroxide (H_2O_2). This highly reactive oxygen species has strong oxidizing properties and can be harmful for biological components, which obliges its use in two compartment systems with separating membrane. Enzymes for this purpose are microperoxidase-11 and horseradish peroxidase, for example, which contain iron active sites.[77] The half-cell reaction in this case is shown in **Equation 1.4**:

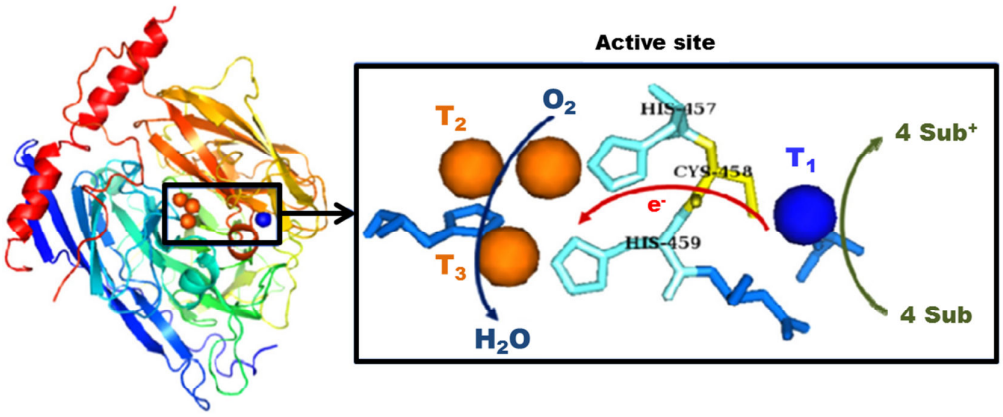

Figure 1.13. *Proposed structure and mechanism for BOD from Magnaporthe oryzae. (from Mano et al.[88])*

$$H_2O_2 + 2H^+ + 2e^- \xrightarrow{enzyme} 2H_2O \quad (1.4)$$

1.3.4. Abiotic catalysts

In the case of hybrid BFCs, abiotic catalysts are employed in one of the compartments, generally the anode. Surely abiotic or biocatalysts have each its own positive and negative points. Some disadvantages of biocatalysts compared to transition metal catalysts were underlined by Ivanov et al.[77] In general, redox proteins tend to exhibit their superior catalytic properties exclusively in their natural environment. This is usually manifested by the difficulty in establishing electrical communication between the protein and the electrode surface and by the limited stability of the biocatalyst-electrode assembly. Another drawback of enzymes from a chemical engineering point of view is the lower volumetric catalyst density. Enzymes are large molecules, so the number of active sites per volume is usually lower compared to conventional metal electrodes.[77] This can directly impact the amount of catalysts per cm^2 of electrode surface, which affects the current density delivered.

Abiotic cathodes. Platinum are the most currently employed metallic catalysts for O_2 reduction reaction, and have been employed in traditional FCs. However, the high cost of this noble metal has led to researches focusing on the development of alternative catalysts composed of non-noble metal catalysts, like metal alloys, carbon materials, quinone and derivatives or transition metals compounds.[93] It is known that all carbon materials have some electrocatalytic activity towards O_2 reduction reaction when in alkaline solutions.[94] Glassy carbon and pyrolytic graphite normally catalyze a 2-electron transfer oxygen reduction, producing H_2O_2. On an oxidized glassy carbon electrode and oxidized graphite electrodes, the H_2O_2 can be further reduced to water at more negative potentials. On carbon nanotubes, the O_2 reduction product is H_2O_2 or a mixture of H_2O_2 and OH^-.[95]

Abiotic anodes. Metallic nanoparticles (NPs) are a range of materials with interesting properties like increased surface area per volume, excellent electrical conductivity, good biocompatibility and high catalytic power. NPs can be either employed as abiotic catalyst in the anode of a BFC, or be incorporated with enzymes as electron "carriers",[96] thus improving the bioelectrocatalytic performance.[97] Examples of metallic NPs that catalyze glucose oxidation reaction are gold,[98] platinum,[99] silver,[100] nickel,[101] palladium,[102] not to mention multimetalic alloys like Au-Pt,[103] Au-Pd,[104] or Au-Pt-Pd [105,106] NPs. The advantage of such

multimetallic NPs is the possibility of developing synergistic properties that might increase the overall performance of the system compared to the use of monometallic NPs.

1.3.5. Electrode materials

After the discussion of BFCs catalysts, it is relevant to address the topic of electrode materials, since it is the part of a BFC onto which catalysts should be immobilized, through which electrons flow from the anode to the external circuit and finally to the cathode. It is basically the site of the reactions. Only electrode materials for enzymatic BFCs will be addressed, even though some similarities with microbial FCs exist. The role of the electrode material in the performance of BFCs is major: its connection with enzymes must be optimal, otherwise the electrons produced in the anode will not reach the cathode. As stated by Yang et al., in comparison with other biodevices or biofunctional materials, electrode materials in biofuel cells are much more specialized and considered as a critical point, being the bioelectrocatalytic efficiency of an immobilized material largely governed by the electrical conductivity between the redox center and the electrode.[107] Some characteristics that the electrode material must present are:

- **High electrical conductivity:** to assure optimal flow of electrons;
- **High specific surface:** to assure enough space for a high amount of enzymes to be effectively connected to the electrode, which is essential for higher current delivered;
- **Biocompatibility:** so that enzymes are not harmed;
- **Chemical stability:** so that corrosion or other reactions do not take place at the working potential range in the electrolyte solutions;
- **Appropriate mechanical strength:** so that electrical contacts can be established properly and the operation can run smoothly without the breaking of the electrode.

Mostly employed materials include gold and several forms of carbon. Not rare examples of indium tin oxide (ITO) as electrode material for BFCs are also found in the literature.[108,109] ITO is a transparent oxide with good electrical conductivity which can be in the form of a film obtained by physical vapor deposition, or nanostructured.[92] Other noble materials like tungsten and titanium carbides or nitrides could also be employed thanks to their high electrical conductivity, despite their higher price.

Gold electrodes are widely employed in research, normally composed of a thin layer of gold that can be synthesized by electrochemical deposition[110] or physical vapor deposition.[84] Gold in the form of nanoparticles can also be employed as "wires" between the enzyme active center and the conductive support, one example is the work of Katz et al.[111] Also, innumerous works report on the modification of gold electrodes with specific molecules for enzyme immobilization, which is the subject of the next section.

Carbon materials are as well widely employed as electrode materials in BFCs, thanks to their excellent properties and multiple presentations, as discussed in section 1.1 of this chapter. Commercial carbon graphite electrodes, presents good electrical conductivity, but its specific surface is governed by its geometric area (none or very small porosity).[112] Glassy carbon, also a dense material, is widely employed in research and has been tentatively used as electrode material in BFCs.[113] An example of carbon-based electrodes is the BFC implanted in a rat realized in Grenoble, France, where the electrodes were composed of compacted graphite particles in the form of a disc containing the enzymes.[67] The evolution of this electrode was realized by substituting the graphite particles by carbon nanotubes, which is presently the highest performance electrode reported.[114]

Considering carbon fibers and carbon nanofibers, which are the subject of this work, they can also be employed as electrode materials, since they present the morphology of graphitic carbon (in variable extents, as discussed in section 1.1 of this chapter), with good electrical conductivities, and increased specific surface, if compared to a dense electrode. First, clear difference must be established between carbon fibers and carbon nanofibers. Carbon fibers present mean diameters in the range of some μm, while nanofibers can have diameters of tens of nm to hundreds of nm. This difference in diameter gives nanofibers more interesting properties as electrode materials, but works with micrometric fibers are also realized. For example, Li et al. employed a single carbon fiber with diameter of 7.0 μm and length of 1.0 mm as a microelectrode for a glucose/O_2 BFC.[115]

Secondly, clear differences have also been observed between carbon nanofibers obtained from chemical vapor deposition or by electrospinning. As previously discussed in section 1.2 of this chapter, CVD-derived CNFs are thinner and small in length, while electrospinning-derived CNFs are thicker and much longer in length, being able to form self-sustained felts. In 2001, CVD-derived graphite nanofibers were started to be used as electrodes for fuel cells, with supported Pt particles.[116] By 2003, a review published on the

subject of carbon nanotubes and nanofibers in catalysis, including fuel cells, did not mention electrospun CNFs, only CVD-derived ones.[117] Electrospun carbon nanofiber felts were employed as electrode materials in electrochemical applications for the first time in 2003, as supercapacitor electrodes.[118] In 2006, electrospun CNFs were employed as anode materials in lithium-ion batteries.[119] Regarding the application of electrospun CNFs as electrodes in BFCs applications, to the best of our knowledge, a previous work of our group in 2011 was the pioneer with the creation of biocathodes for enzymatic BFCs.[120] Also in 2011, this material was employed for the first time as electrode in microbial BFCs.[121]

1.3.6. Enzyme immobilization techniques

Effective immobilization of enzymes (and mediators) onto the electrode surface is an essential task with the role of improving the stability of the bioelectrodes, the enzyme activity, the mass and electron transfer and, consequently, the delivered power of the enzymatic BFC. The need for appropriate immobilization techniques comes mainly from the fact that enzymes are unstable when removed from their natural location, which is a three-dimensional environment with easy flow of substrates and products, to a solid surface where the protein structure might lose its conformation. The enzyme has, thus, the need for certain conditions of pH and temperature, so that durability is a challenge to achieve. Therefore, the immobilization matrix should provide a microenvironment to the enzymes, protecting them from harsh environmental conditions such as shear forces, pH, temperature fluctuations, organic solvents and toxins.[107]

Yang et al. highlighted the three major key points in immobilization technology in BFC, in a scheme that properly sums up the matter with general examples, represented in **Figure 1.14**: **methods** (i.e. the actual procedure of immobilization), **structures** (i.e. the spatial organization of enzymes onto the support) and immobilization **materials**. Only the enzyme immobilization methods will be addressed here.

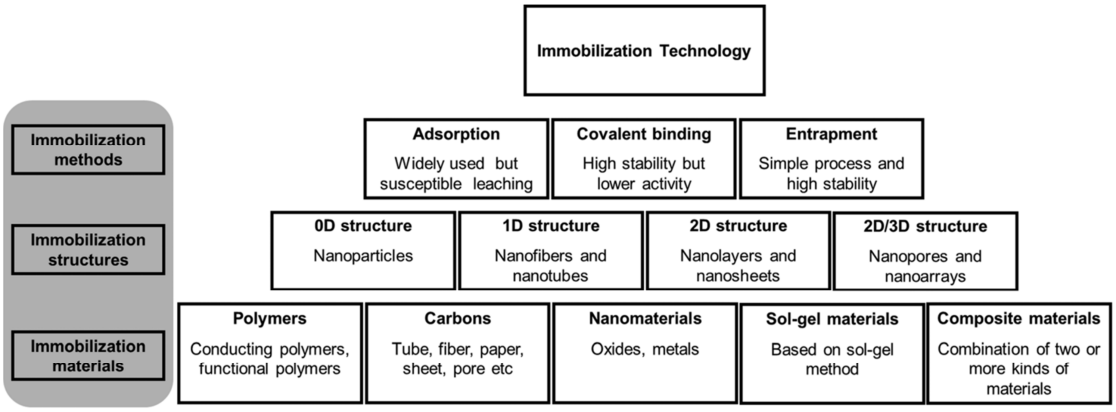

Figure 1.14. *Three key points in immobilization technology in BFCs. (from Yang et al.[107])*

The most common methods of enzyme immobilization in BFCs technology are, presently, adsorption, covalent binding, encapsulation and cross linking (i.e. a type of encapsulation), which are represented in **Figure 1.15**. One point to consider is that regardless of the method, the material in which the enzyme is immobilized must be insoluble in the solvent of the BFC (which is frequently water).[122] Adsorption is the simplest method, which consist on the physical adsorption (by van der Waals forces, hydrophilic/phobic interactions) of the enzymes on the surface of the support, or inside its pores. It is a mild and reversible process which efficiency depends on the physicochemical characteristics of the solutions employed (e.g. pH), as well as those of the support (pore sizes, hydrophilic/phobic character), but the easy leaching of the adsorbed species is a major drawback. Overall, adsorbed enzymes should be employed only in organic solvents or in pure hydrophobic reactants to avoid leaching, which are not the case in BFCs, since in aqueous solutions protein unfolding is favored.[123] One example of this method is the adsorption of enzymes GOx and horseradish peroxidase on the surface of conductive particles (graphite powder).[124]

Covalent binding consists in attaching the enzymes to the support through a chemical bond between a functional group of the enzyme and the support that might have been previously modified for that purpose. In the scheme of **Figure 1.15**, the pink structures represent the support/enzyme covalent bond. The stability of this bioelectrodes is higher (the enzyme is strongly attached to the surface), but at the same time displays lower activity than the native protein, since the enzyme presents limited conformational motion available,

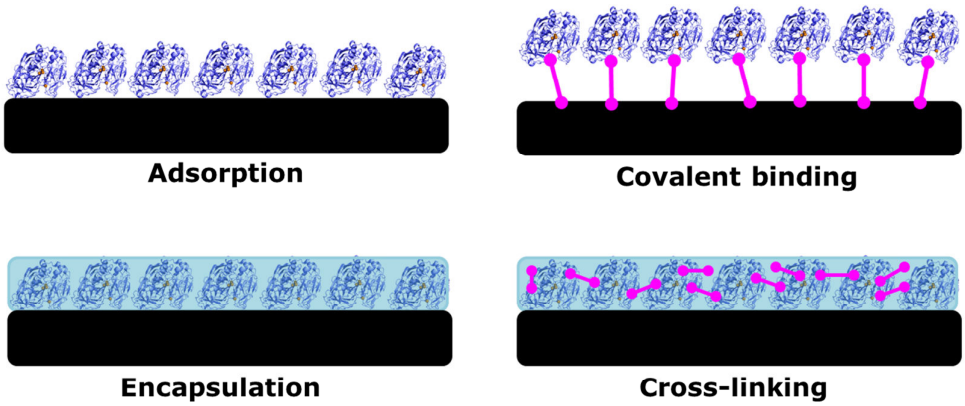

Figure 1.15. *Scheme of enzyme immobilization techniques generally employed in BFCs bioelectrodes.*

blocked by the covalent bond.[107] In a protein (i.e. enzyme), the reactive groups can be amine groups, carboxyl groups, tyrosine or imidazole groups present on histidines.[125] Gutiérrez-Sánchez et al. reported the covalent immobilization of laccase onto a graphite electrode modified by gold nanoparticles (AuNPs), in the absence of electron transfer mediators. The attached AuNPs were functionalized with a mixed monolayer of aromatic diazonium derivative and a thiol for the covalent and oriented immobilization of laccase molecules, which showed fast DET towards O_2 reduction reaction and good operational stability (retention of 40% of the initial current after 4 days of continuous chronoamperometry).[126]

Encapsulation is the technique where enzymes are confined whithin a polymer matrix, a sol-gel or a redox hydrogel, as represented in **Figure 1.15** by the blue film that surrounds the enzymes. Advantages of this method are the easy synthesis process that provides good mechanical strength and stability, while permitting good degree of enzyme movement and simultaneously preventing the leaching of enzymes or mediators and improving stability. One drawback of this method is the limitation in transport of substrate/analyte to the active site of the enzymes.[122] With sol-gel entrapment, the porous structure can provide a beneficial aqueous environment and physiological stability for the enzymes.[107] Redox hydrogels provide the advantage of conducting electrons while still conducting ions and allowing the diffusion of substrate species.[97] Conducting polymers like polypyrrole and polyaniline are also commonly employed for enzyme immobilization, being synthesized by electropolymerization, with the advantage of facilitating electron transfer through the film.[74] Also, polymer chains can be functionalized in order to introduce an electron relay.

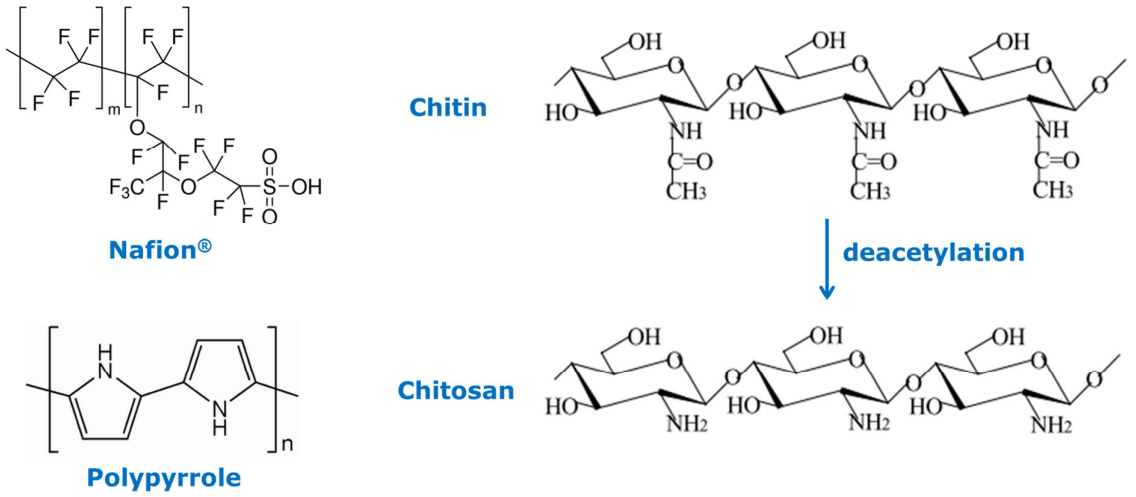

Figure 1.16. *Stucture of the encapsulating polymers employed in this work.*

In this work, polypyrrole, Nafion and chitosan were employed as encapsulating polymers. A brief description of each one will be presented as follows.

Nafion is an ion conducting polymer that was developed by the DuPont Company, generated by the copolymerization of a perfluorinated vinyl ether comonomer with tetrafluoroethilene, resulting in the chemical structure showed in **Figure 1.16**. Nafion films possess excellent chemical stability and have been widely employed as ion exchange membranes in fuel cells and in the formation of polymer modified electrodes in electroanalytical investigations.[127] Although promising results were achieved, some drawbacks of the use of Nafion are the reduced enzymatic activity observed due to the acidic side chains of Nafion that lead to a nonideal environment for the enzymes, besides that Nafion is an expensive polymer that is not biodegradable due to its perfluorinated polymer backbone.[128] It has, however, been vastly employed in the field of enzymatic BFCs, considering the works of Minteer et al. (some of them referenced in a review from 2008 [128]) or others, to cite a few.[129,130]

Polypyrrole, as mentioned, is a conductive polymer obtained from the electropolymerization of the monomer pyrrole, resulting in the structure showed in **Figure 1.16**. In any electrochemical polymerization, the monomer is dissolved in an appropriate solvent containing the desired anionic doping salt, then it is oxidized at the surface of an electrode by application of an anodic potential (oxidation). The choice of the solvent and electrolyte is of particular importance since both should be stable at the oxidation potential

of the monomer and provide an ionically conductive medium. Since pyrrole has a relatively low oxidation potential, electropolymerization can be carried out in aqueous electrolytes which is not possible for thiophene or benzene. Several mechanisms for pyrrole electropolymerization have been proposed, the Diaz's one being the most often found in the literature.[131] Other proposed mechanisms include Kim's, Pletcher's, Reynold's, as described in a review by Sadki et al.[131] Briefly, as a result of the initial oxidation, the radical cation of pyrrole monomer is formed and reacts with other monomers present in solution to form oligomeric products and then the polymer.[131]

Besides the application as enzyme entrapping polymer for BFCs, polypyrrole have been employed in biosensors, gas sensors, microactuators, polymeric batteries and other electronic devices.[132] Polypyrrole was employed in a previous work of our group to efficiently entrap laccase and ABTS onto CNFs electrodes that were tested as biocathodes for O_2 reduction.[120] Functionalization of polypyrrole is a strategy that can allow better affinity for proteins during immobilization. For instance, Lalaoui et al. modified CNTs electrodes via the electrodeposition of polypyrrole either functionalized with pyrene, or with N-hydrohysuccinimide (NHS), for the immobilization of laccase. With NHS, laccase is covalently grafted by amide coupling, whereas in the case of pyrene, the polycyclic aromatic region interacts with the hydrophobic pocket of laccase, leading to both immobilization and orientation of the enzyme.[133] Thanks to the fact that polypyrrole is easily electrodeposited onto an electrode surface from aqueous solutions that it is preferred amongst other conducting polymers for the entrapment of enzymes.

Chitosan is another polymer that has drawn attention as encapsulating polymer for BFCs, thanks to its biological origin (it is the second most abundant biopolymer after cellulose), low price and excellent film properties. It is produced from the deacetylation (i.e. removal of acetyl groups) of chitin, a structural element in crustacean shells (shrimps, crabs), insects and fungal mycelia, as represented in **Figure 1.16**. The degree of deacetylation varies (i.e. not 100% of acetyl groups are removed), which influences the properties of chitosan. Carboxyl and amine side groups of chitosan can serve as protein-binding ligands for enzyme immobilization.[134] For instance, chitosan was employed by El Ichi et al. as encapsulating matrix of CNTs and laccase bioelectrodes, enhancing the long term stability towards O_2 reduction at 37 °C and pH 7, suitable for implantable devices.[135]

Chitosan is inert, hydrophilic and insoluble in water, alkali and organic solvent, being soluble in acidic media (pH < 6.5). This means that a film of chitosan will be completely dissolved in solutions of pH lower than 6.5, which can be harmful depending on the application. For that reason, two strategies become possible: *i)* the neutralization of the chitosan film in an alkaline solution (usually NaOH), which results in the precipitation of solid chitosan, or *ii)* the cross-linking of chitosan with a cross-linking agent, which results in the formation of a gel. This is the fourth immobilization method from **Figure 1.15**: cross-linking immobilization. In this method the enzymes can be connected to each other or to the polymer matrix (also called carrier), while entrapped. When they are cross-linked at each other, they act as their own carrier.[123] When the polymer matrix is cross-linked, it is the same as an entrapment but in a harder matrix. In the case of covalent cross-linking of chitosan, usual cross-linking agents are glyoxal, sodium tripolyphosphate (TPP), glutaraldehyde and genipin. El Ichi et al., have used genipin as cross-linker of chitosan to encapsulate laccase and CNTs bioelectrodes that were implanted in a rat.[136] Besides the advantages of genipin having anti-inflammatory properties and being a natural cross-linker thousands of times less toxic than glutaraldehyde, enhanced stability was obtained with such bioelectrodes.[136]

1.3.7. Direct and mediated electron transfer

Electron transfer between enzyme active sites and the electrode conducting surface can be classified in two different categories: mediated electron transfer (MET) and direct electron transfer (DET):

- in **MET**, a redox molecule (called mediator, which can be in solution or immobilized) will serve as bridge between the enzyme and the electrode surface. The enzyme catalyzes the oxidation or reduction of the mediator, and the regeneration of the mediator occurs at the electrode surface. Essential characteristics of the mediator are that it has to be a substrate for the enzymatic reaction, and its transformation has to be reversible.[137]
- in **DET**, the electron is transferred directly from the electrode to/from the substrate molecule via the active site of the enzyme. The enzyme act as a molecular transducer (term proposed by Ghindilis et al. in 1997), meaning the enzyme

converts a chemical signal into an electric signal via charge transfer, directly tunneling electrons to/from the electrode surface.[137]

Figure 1.17 shows a representation of both DET and MET processes for the oxygen reduction reaction (ORR) catalyzed by laccase enzyme, either directly, or with ABTS redox mediator, which is a common mediator for this reaction (will be further analyzed).

To date, over 1400 oxidoreductase enzymes are known, any of which could possibly be utilized as biocatalysts in an enzymatic BFCs. However, less than about a hundred of the known oxidoreductases are known to be able to communicate with an electrode surface via a DET mechanism.[63] Unfortunately, in most redox enzymes the redox center of the protein is insulated (i.e. the catalytic sites are deeply buried within the protein matrix), which prevents DET with conductive supports.[64] Therefore, the use of a variety of electron transfer mediators (electron relays) to electrically connect the biocatalyst to the electrode becomes necessary.

Despite the difficulties in achieving DET, it possesses some important advantages over MET that were highlighted by Falk et al.[63] Mediators are often health hazards and their usage can lead to voltage losses from the potential difference between the active site of the enzyme and the mediator. Employing a DET-based design allows for significant simplifications in the construction of BFCs, since membraneless systems become possible and making miniaturization easier. One of the main downsides of using the DET approach to

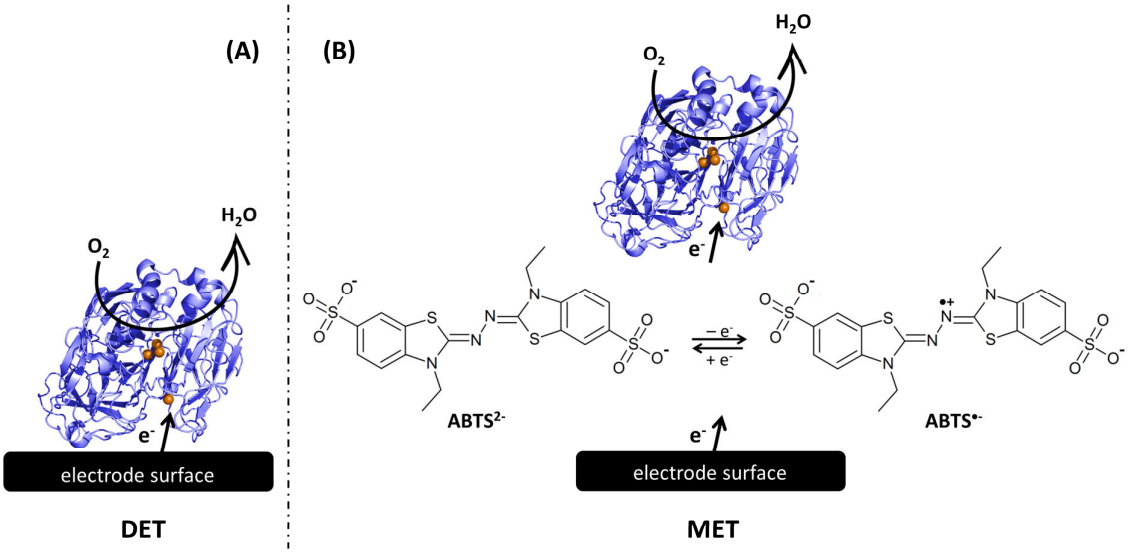

Figure 1.17. *Schematic representation of* ***(A)*** *DET and* ***(B)*** *MET processes with laccase enzyme toward ORR. Representation of MET with ABTS redox mediator.*

construct BFCs is the difficulty to electrically connect sufficient amounts of the enzymes. Limited by the active surface area, the efficiency and the power output of DET biodevices might be attenuated.[63]

An electron transfer mediator should not be confused with a cofactor. A cofactor is a catalytically essential non-protein molecule or ion that is covalently bound to the enzyme. Cofactors can be organic or inorganic, which are detailed as follows:

- **Organic cofactors** are organic molecules with small molecular weight that are bound to the enzymes and act as mediators at the redox centers. Regarding oxidoreductase enzymes, the most common organic cofactors are NAD (nicotinamide adenine dinucleotide) and FAD (flavin adenine dinucleotide), which are found in many alcohol dehydrogenases (NAD-dependent), glucose oxidases and dehydrogenases (FAD dependent).
- **Inorganic cofactors** are basically metal ions, like Cu clusters that compose the active center of laccase, or Fe ions of hydrogenase enzymes.

Mediators are typically organic molecules or ions that are used by the enzyme to help catalyze reactions, but are not a structural part of the enzyme. ABTS, *2,2'-Azino-bis(3-ethylbenzothiazoline-6-sulfonic acid) diammonium salt*, is a widely employed mediator which molecular structure is represented in **Figure 1.17**. It efficiently mediates O_2 reduction to water, and was employed in works of Palmore, Minteer, Atanasov, Cosnier and other renowned researchers in the BFCs field. One of the drawbacks of ABTS is the difficulty to immobilize it onto electrode surfaces. It easily leaks out to the solution, which reduces BFCs performances since the enzyme/electrode connection is harmed. Therefore, attempts to chemically attach ABTS to bioelectrodes have been made,[138] as well as the functionalization of the molecule.[139] Ferrocene, quinone derivatives, osmium and ruthenium-based mediators are also mediator options that have been largely employed, but will not be further detailed here.

DET have been achieved with a series of enzymes for BFCs applications like laccases,[114] glucose oxidases,[78,114] alcool dehydrogenases[81] or PQQ-dependent dehydrogenases,[82] for instance. In many cases, CNTs were employed as promoters for DET. They are very suitable in this matter thanks to the nanometric size, similar to the size of the enzymes, creating ideal conducting nanowires for efficient DET.[114] Another strategy to achieving DET is by the introduction of metallic nanoparticles along with the enzyme onto electrode surfaces,

according to the examples of Holland et al.[140] and Wang et al.,[141] who employed gold nanoparticles for that purpose in glucose/O_2 BFCs.

1.3.8. Advances in enzymatic BFCs devices

Even though BFCs can be considered to be still at a level of proof-of-concept and the majority of reported works is simply engineered, some **designs** have been created in addition to the typical two-chamber one:

- membraneless (one chamber),[114,142]
- concentric cylindrical BFCs,[130]
- with layered architecture,[143]
- systems with air biocathode,[144]
- microfluidic BFCs[145] or
- with microfibers electrodes.[71]

Few prototypes have been created, but so far have not reached commercialization, due to the drawbacks that were mentioned. Examples are the 8-cell ethanol/oxygen biofuel cell stack prototype developed by Akermin, Inc. (United States) in 2006 that operates a music player,[146] as shown in **Figure 1.18**. Furthermore, Sony Corporation (Japan) developed a glucose/O_2 BFC, with the enzymes GDH and BOD at the anode and cathode, respectively, with the electron transfer mediators VK3+NADH at the anode and potassium ferricyanide at the cathode, Poly-L-lysine was the encapsulating polymer, and porous carbon was the electrodes material (Toray). The BFC presented a V_{OC} of 0.8 V and maximum power of ~1.5 mW cm^{-2} according to the publication.[147] At Sony's website, a power of 50 mW is reported for the BFC in series, as presented in **Figure 1.19**.[148,149]

One of the most interesting target applications of BFCs is implanted *in vivo* in animals and fed by the glucose present in blood. This challenging idea was suggested in 1970,[150]

Figure 1.18. *Ethanol/air BFC stack, developed in 2006 by Akermin, Inc., that powers a music player. (reproduced from Atanassov et al.[146])*

Figure 1.19. *Photo of the prototype BFC developed by Sony in 2007.*[148]

however to the present date only a few tests have already been realized in rats, in a rabbit ear and in mollusks. Implantable abiotically catalyzed glucose fuel cells have been tested in dogs, rats, rabbits and sheeps, as highlited by Kerzenmacher in a review in 2008.[151] The aim of these implanted BFCs in the long term is to be able to power medical implanted devices like pacemakers, hearing devices, kidneys, bladder sphincters or other organs, as primary or secondary energy source, powered only by body fluids. Another feasible application would be to power (bio)sensors continuously monitoring external chemical and physical conditions. Especially in military applications or in places where there is no electricity supply to recharge batteries, BFCs would be very practical.

The group of professor Katz in the United States works with the concept of "living devices" trough the implantation of BFCs in small invertebrates like lobsters,[66] clams,[65] and snails.[152] The photo of a BFC implanted in a clam is presented in **Figure 1.20A**, along with a scheme of the functioning. Physiologically produced glucose is employed as fuel that is oxidized by PQQ-dependent glucose dehydrogenase (an enzyme that do not need any mediator and is not affected by the presence of O_2), while O_2 is used as oxidant in the cathode that is reduced by laccase, both onto commercial buckypaper deposited on ITO as electrode material. Three clams were connected together in series (V_{OC} = 800 mV and P_{max} = 5.2 μW) or in parallel (V_{OC} = 360 mV and P_{max} = 37 μW), and were able to charge a capacitor (1 F) up to 240 mV during 1 h, which was then capable of powering an electrical rotating motor (6.5 Ω) that rotated a quarter of a full turn. In a real application, however, integration with micro-power electronic devices (like sensors or wireless information transmitters) would be preferred.

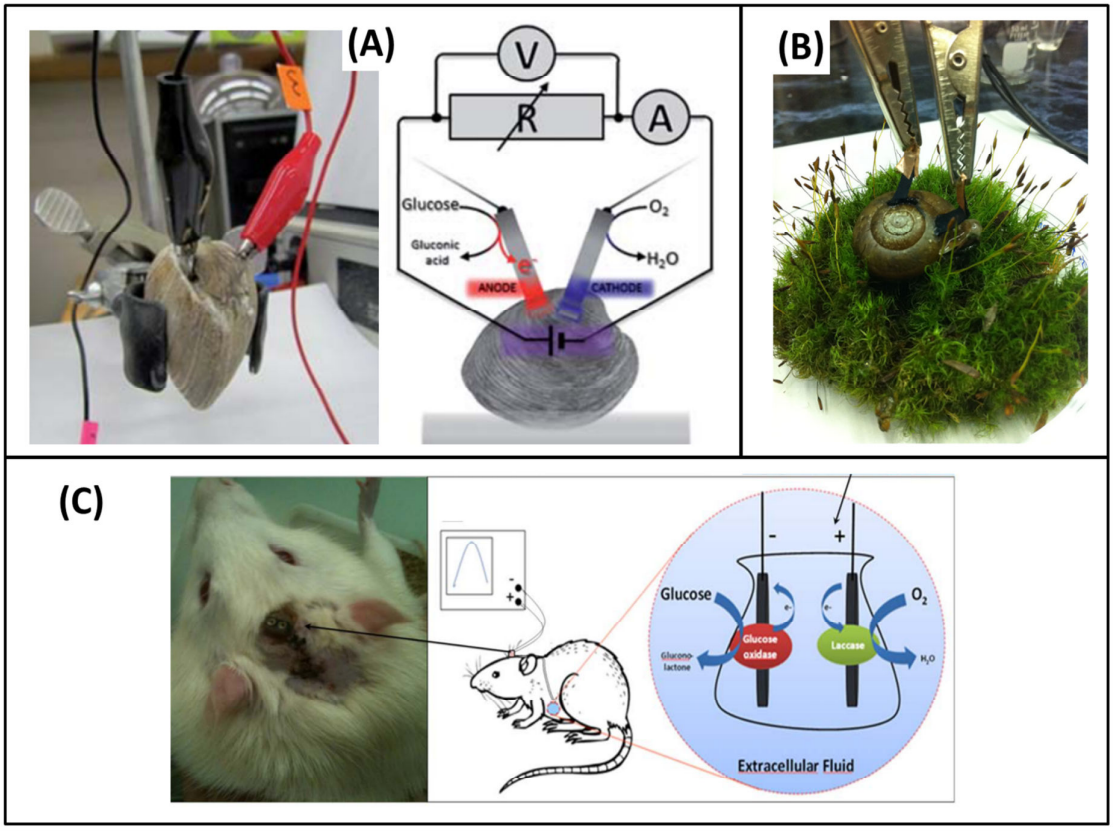

Figure 1.20. *Examples of implanted BFCs developed by researchers in the United States and in France.* ***(A)*** *BFC implanted in vivo in a clam and scheme of its functioning.*[65] ***(B)*** *BFC implanted in a living snail.*[152,153] ***(C)*** *BFC implanted in a rat and scheme of the BFC.*[68]

In **Figure 1.20B**, a photo from a snail with implanted BFC also developed by Katz et al.[152,153] is presented. Similar anode and cathode structures were used in this BFC (compared to the clam one), which produced VOC of 530 mV and power of 7.45 µW. They calculated that only 6 % of the enzymes were electrically wired onto the electrodes, which shows further improvement is still necessary. This could also be related to the fact that small species like snails do not have large amounts of glucose biofuel nor efficient blood circulation, which impair the mass transport, differently than the system of mammals.

Therefore, the group of Professor Katz also tested the same anode and cathode implanted in a lobster, which is a bigger animal compared to snails and clams. They figured the implantation of two BFCs in the same lobster would be able to double the V_{OC} of a single implanted BFC (which was V_{OC} = 540 mV, with P_{max} = 0.16 mW), and thus power a watch

(that requires 700 mV to operate). However the voltage produced from this double implanted BFC was increased only by 50 – 100 mV, which they attributed to the electrical resistance of the lobster's body tissue.[66] The important conclusion is that BFCs cannot be in series inside the same animal. In a different experiment mimicking human blood circulatory system (not implanted), they were able to power a real pacemaker (normal performance registered by an oscilloscope) for the first time, employing a series of 5 individual biofuel flow cells.[66] This is an advancement compared to other works were only simple electronic devices were powered for exemplification.

In Grenoble, France, the group of Cosnier works with BFCs implanted in rats. Their system is represented in **Figure 1.20C**. The BFC was surgically implanted in the abdominal cavity of the rat, and the wires were tunneled up to the head. They employed GOx and catalase at the anode and laccase at the cathode as enzymes, and compressed CNTs as electrode material. Catalase was used at the anode to catalyze de decomposition of H_2O_2 formed due to the presence of O_2 at the anode that was permeable to O_2 (this is a drawback of GOx). Average V_{OC} of 570 mV was achieved, with 38.7 μW of power delivered by one rat, which was able to power separately a light-emitting diode (LED) or a digital thermometer. The BFC ran for 9 days, and was stopped due to mechanical breakage of the free wires by the rat that was freely moving during the experiment.

It is known that the major drawbacks in BFCs science are the small power delivered, (compared to competing batteries) and the stability of power output, which is due to enzymes lack of stability, poor electron transfer and the small amount of effective connections between enzyme/electrode. The major problems of the already created BFCs prototypes is the low voltage produced, which is thermodynamically limited by the redox potentials of the biological fuel and oxidant.[66] Achieved V_{OC}s (usually lower than 1.0 V, as seen from the examples) are still not enough for most electronic devices, which usually require several volts for their operation. Improving efficiency of biofuel cells includes mostly increasing their current production and results in a very little effect on the voltage which is thermodynamically limited. So far two approaches have been applied to resolve the low voltage problem, as highlighted by MacVittie et al.[66]: *i)* assembling biofuel cells in series electrically, thus increasing the total output voltage and *ii)* collecting produced electrical energy in capacitors/charge pumps for the burst release in short pulses. Presently, most

works do not discuss the interface between BFCs and electronics, focusing on internal issues of BFCs. This is, therefore an important topic for the progress of the field.

1.4. Conclusion and plan

In this chapter, an overview of the basic concepts that will be explored in this work was realized. The historic development of carbon fibers was treated, from the first observation of a carbon fiber in 1879 by Thomas Edison in the light bulb, the first commercialized carbon fibers around the year 1960, until nowadays increasing demand for use in advanced materials. Electrospinning was reviewed as a useful tool for the production of polymeric nanofibers that can be further transformed to CNFs. Finally, the technology of fuel cells was introduced, followed by the emerging field of BFCs and hybrid BFCs, which key aspects were highlighted (fuels, catalysts, enzyme immobilization techniques, etc). Recent advances in the field of BFCs show that the tendency of this technology is the creation of implantable devices able to deliver power, for example, in places where electricity is not available for batteries recharging. Actual prototypes of BFCs have been already implanted in mollusks and rats, but tests in humans are still not conceivable.

One important part in any BFC is the electrode material. Its role in the performance of BFCs is major: the connection with enzymes must be optimal, otherwise the electrons produced in the anode will not reach the cathode. Some characteristics that the electrode material must present are high electrical conductivity, high specific surface, biocompatibility, chemical stability and appropriate mechanical strength.

In this work, the novelty is the use of electrospun CNFs as BFCs electrode materials, a strategy that has not been investigated so far. CNFs will be proven in this work as remarkable electrode materials since they possess appropriate specific surface and electrical conductivity, not to mention fiber properties could be tuned according to electrospinning parameters.

Given the multidisciplinary nature of this work, the present work will deal with the material preparation and characterization. Different strategies have been used to increase the performance of the material, i.e. the electrical conductivity and surface area, by varying the spatial organization of fibers or by introducing conductive nanomaterials. Thereafter, will be concerned the application of the synthesized materials as electrode materials through the modification of CNFs with enzymes or abiotic catalysts for the creation of enzymatic or

hybrid BFCs. First, the development of different O_2 biocathodes will be shown, since cathodes are usually the limiting part in both FCs and BFCs. The optimization of enzyme immobilization technique by entrapment in polymer matrixes (Nafion®, polypyrrole or chitosan) will be described. Then, the development and test of complete BFCs with the biocathodes that were optimized will be shown. The anodes employed will be either enzymatic or abiotic, powered by ethanol or glucose, and both MET and DET (mediated and direct electron transfer) strategies will be addressed.

PART 2:

ELECTRODES SYNTHESIS AND OPTIMIZATION

Introduction of Part 2

This part is dedicated to the elaboration of electrode materials and their physico-chemical characterization. Preliminary results leading to the realization of this thesis dealt with the creation of randomly organized electrospun carbon fibers that proved to be suitable as electrode material for O_2 bioelectroreduction. Therefore, several questions were raised with the objective of improving the performance of this new electrode material, for instance:

- if the spatial organization of fibers plays a role on the electron transfer,
- if enhancing the specific surface of fibers can increase electrode performance,
- if the performance can be compared to state of the art electrode materials like graphite or glassy carbon,
- if the same base material composed of CNFs is also suited for abiotic catalysis.

Different materials were synthesized in order to answer to these questions. **Chapter II** will deal with the creation of basic randomly organized CNFs that were further modified with carbon nanotubes on the surface of fibers. **Chapter III** will deal with the synthesis and characterization of aligned fibers. Finally, **Chapter IV** will deal with the synthesis of CNFs modified *in situ* with gold particles, aiming future test as glucose anodes.

In this part of the work, these materials will be characterized intrinsically, and later in Part 3, they will be modified with enzymes or other abiotic catalysts, and tested as anodes or cathodes for biofuel cells applications.

Chapter II. Randomly organized electrospun CNFs and modification with carbon nanotubes

2.1. Introduction

In this chapter, the synthesis and characterization of randomly distributed electrospun carbon fibers is detailed. The notion of "fiber direction" should be introduced here. Randomly organized fibers are, therefore, fibers that were synthesized by electrospinning on a support that was a stationary disc, so that the fibers deposit randomly onto it, in no specific direction. In the next chapter, difference should be made with aligned fibers, which are synthesized by electrospinning onto a rotating drum, so that the majority of fibers roll the drum depositing in the same direction.

Randomly organized fibers have been successfully employed as a biocathode electrode material suitable for BFCs in a previous work performed by our group.[120] Therefore, the goal of enhancing the performance of these CNFs compared to this previous work was set.

The strategy that was chosen was the modification of the CNFs through the adsorption of carbon nanotubes on its surface. CNTs possess very interesting mechanical, electrical and thermal properties, biocompatibility and chemical stability, combined with very high specific surface given by its nanometric size that could improve the properties of the electrode. CNTs have been added to polymeric nanofibers[154–157] and, for the best of our knowledge, few works have so far been published on the modification of CNFs with CNTs. In these existing reports the modification was realized by a different method than the adsorption method employed in this work, like for example the *in situ* growing of CNTs onto the fibers,[158] or the addition of CNTs on the polymeric solution prior to electrospinning.[159]

A comparison between the modification of CNFs with either multi-walled CNTs or double-walled CNTs was addressed here. Also, the developed felts modified or not by CNTs were characterized by scanning electron microscopy (SEM), Raman spectroscopy, electrical conductivity measurements and by the electrochemical technique cyclic voltammetry.

2.2. Materials and methods

2.2.1. Preparation of the randomly organized carbon nanofibers

A PAN solution in DMF (10 wt%) was stirred at 60 °C for 4 h. A web of PAN fibers was obtained by an electrospinning process under high voltage (25 kV). The feed rate and the tip–collector distance were 2.0 mL h^{-1} and 15 cm, respectively. The fiber collector consisted in a stationary disc covered in aluminum foil, so that randomly organized fibers were obtained. A picture of the electrospinning equipment employed in our laboratory can be observed in **Figure 2.1**. Two types of fiber collector can be installed: the stationary disc employed here, or a rotating drum (for the production of aligned fibers). The electrospun

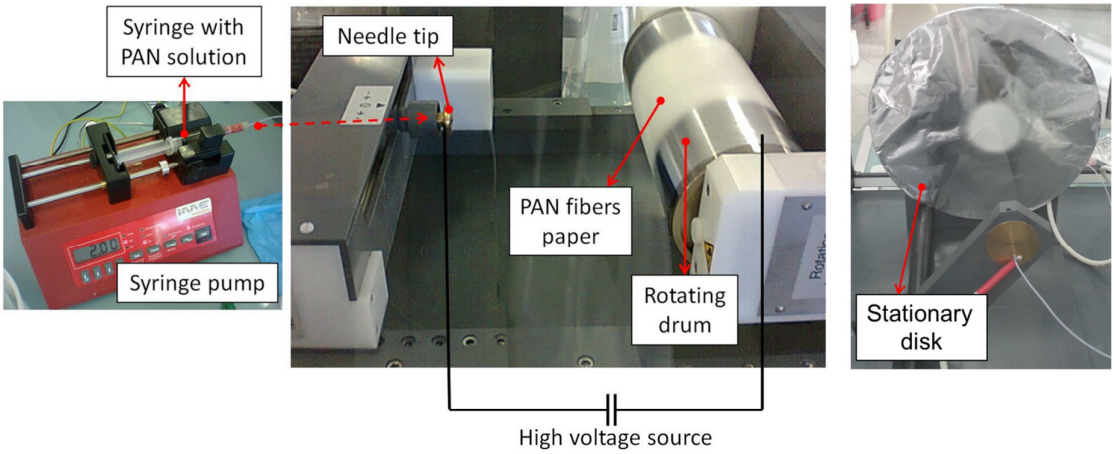

Figure 2.1. *Electrospinning equipment employed in this work, with two different fiber collectors: rotating drum (for the production of aligned fibers) or stationary disc (for random fibers).*

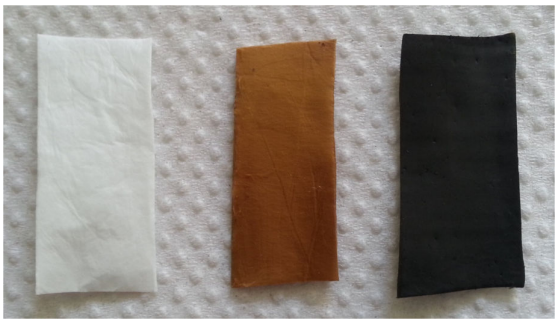

Figure 2.2. *Images of the PAN fibers mat (white), stabilized fibers (brown) and CNFs mat (black).*

nanofibers were stabilized in an air environment at 250 °C for 2 h (heating rate was 2 °C min^{-1}). Then the stabilized nanofibers were carbonized at 1000, 1200 or 1400 °C (1 h dwell) in high-purity nitrogen atmosphere (heating rate 2 °C min^{-1}). The resulted randomly organized carbon nanofibers were cut into strips of size 30 mm × 5 mm, approximately. Color changes went along with these heating treatments: white PAN fibers turned to brown (stabilized fibers) then finally black (CNFs), as depicted in **Figure 2.2**. The thickness of the felts was ~600 µm, kept constant from the electrospinning processing time, and was measured with an optical microscope.

2.2.2. Double and multi-walled carbon nanotubes characterization

Commercial double and multi-walled CNTs (Nanocyl, Belgium) were adsorbed on the surface of the developed CNFs. Previous characterization of the CNTs was realized by our collaborators from the laboratory CIRIMAT (Professor Christophe LAURENT, Toulouse, France). Some characteristics of the CNTs used in this work are listed in **Table 2.1**. The average number of walls (*N*) and average external diameter (d_{ext}) of the CNTs were determined from the measurement of about 100 CNTs on high-resolution transmission electron microscopy images. The theoretical density of the CNTs (ρ) was calculated using the CNT density chart.[160] It was attempted to evaluate the CNT length (*L*) on transmission electron microscopy images, although the measurement was very difficult to perform for the DWNTs because they tend to form bundles. Nevertheless, they were significantly longer than the MWNTs. The high-frequency range of the Raman spectra (laser excitation at 632.82 nm) showed the D band (approximately 1320 cm^{-1}) and the G band (approximately 1580 cm^{-1}). The ratio between the intensity of the D band and the G band (I_D/I_G) was equal to 0.17 and 1.90 for the DWNTs and MWNTs, respectively. An increasing I_D/I_G value

Table 2.1. *Average number of walls (N), average external diameter (d_{ext}) and approximate length (L) of the CNTs, theoretical density (ρ), specific surface area (S_{CNT}) and carbon content (C_n) in the CNT samples; the balance was mostly water and residual metal catalyst.*

Specimen	*N*	d_{ext} *(nm)*	*L (µm)*	*P (g* cm^{-3}*)*	I_D/I_G	C_n *(wt%)*	S_{CNT} *(*m^2 g^{-1}*)*
DWNTs	2	2.0	>5	1.8	0.17	88.4	923
MWNTs	8	10.2	<1.5	1.8	1.90	91.8	242

corresponds to a higher proportion of sp^3-like carbon, which is generally related to the presence of structural defects in the CNTs (more details on Raman spectroscopy will be given later on this chapter). The carbon content in the samples (C_n) was determined by flash combustion. The specific surface area of the samples (S_{CNT}) was measured by BET method using N_2 adsorption at liquid-N_2 temperature. The obtained values are in good agreement with calculations derived from geometric data.[161]

2.2.3. Adsorption of CNTs on the surface of CNFs

The adsorption of CNTs was realized by dipping the electrospun CNF felts in a dispersion of CNTs, either double or multi-walled. The CNTs were dispersed in distilled water (0.5 mg ml^{-1}) in ultrasonic bath. The dips were realized during 30 s and the felts were then rinsed with water and dried in ambient conditions. The electrodes were denominated according to their carbonization temperature (1000, 1200 or 1400 °C) and the kind of CNTs adsorbed (DWNTs or MWNTs). For example, the sample "*1200+MWNTs*" refers to the CNFs treated at 1200 °C and immersed in MWNTs dispersion. Three samples did not receive any surface modification with CNTs, and were simply denominated as "*1000*", "*1200*" and "*1400*". No surfactant was added in the CNTs dispersions, only the ultrasonic bath was employed for the dispersion. The presence of a surfactant was not desired among the nanofibers to prevent further chemical interferences in the samples. Kim et al. employed a comparable technique for the adsorption of carbon nanotubes on nylon 6 nanofibers, although they used Triton X-100 and sodium dodecyl sulfate as surfactants in water.[154] Gao et al. realized the dips simultaneously with ultrasonication, and tested the effect of adding or not a surfactant in the CNT dispersion.[156] They observed that although the surfactant guarantees the CNT uniform dispersion, it actually prevented the CNTs from adsorbing onto the nanofibers, indicating that some interaction between CNTs and surfactants may take place, which adds to the benefit of not employing a surfactant. The quantification of the amount of MWNTs adsorbed was performed by weighting the electrodes before and after adsorption. We have measured a mean value of the amount of carbon nanotubes adsorbed per unit of geometric surface of the electrode, which is **81 $\mu g_{CNT}/cm^2_{electrode}$**. Since the electrodes were not dense but composed of electrospun fibers, it was also interesting to quantify the amount of MWNTs per gram of electrospun fibers. We have thus measured a mean value of **35 $\mu g_{CNT}/mg_{fiber}$**.

The next sections will focus on the characterization of the synthesized materials, either unmodified fibers, or CNTs-modified ones, by SEM, EDX, Raman spectroscopy, electrical conductivity measurements and, finally, by cyclic voltammetry.

2.3. Morphological characterization

The morphology of the electrospun felts was observed by SEM (**Figure 2.3**). The fibers present regular and smooth fibrous morphology. During the chemical conversion of PAN to carbon, structural changes were induced and the average diameters of the fibers decreased from 450 nm (PAN fiber not thermal treated, **Figure 2.3A**) to **420 nm** (T = 1000 °C, **Figure 2.3B**), **330 nm** (T = 1200 °C, **Figure 2.3C**) and **300 nm** (T = 1400 °C, **Figure 2.3D**), due to the weight loss that takes place during thermal treatment.[162] The mean diameters were measured on about 50 fibers for each sample from SEM images.

Fibers composition on three stages of thermal treatment (PAN fibers, stabilized and carbonized ones) was assessed through energy dispersive X-ray spectroscopy (EDX). This technique allows elemental analysis by exciting the sample with an electron beam, and measuring the resulting characteristic X-ray emitted by the atoms. Each element emits X-

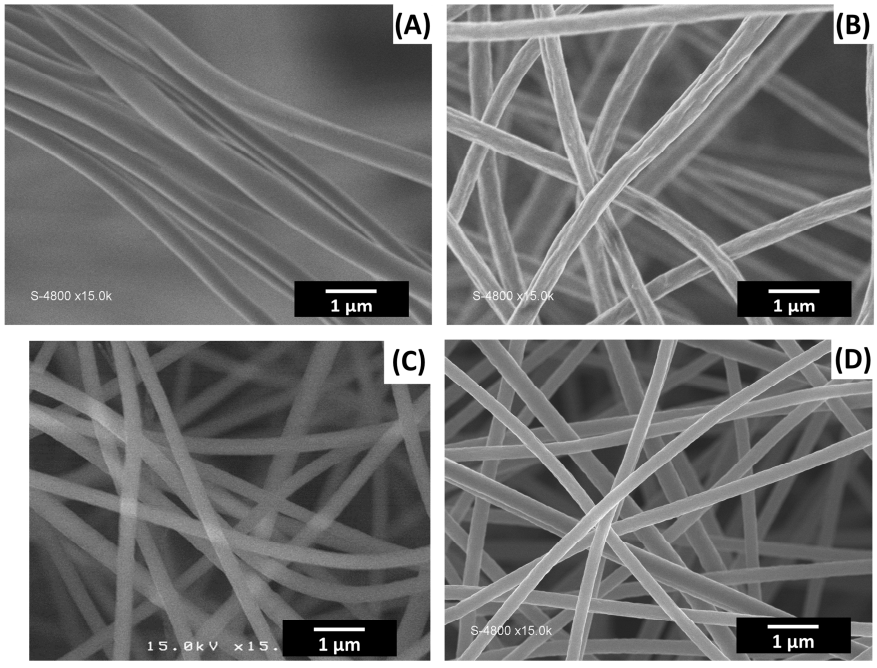

Figure 2.3. *SEM images of electrospun fibers at different carbonization temperatures.* ***(A)*** *Polymer fibers without any heat treatment.* ***(B)–(D)*** *Fibers carbonized at 1000, 1200 and 1400 °C respectively. Scale bar is 1 µm.*

rays with certain energy, allowing its identification. **Figure 2.4** presents the EDX plots of PAN fibers, stabilized fibers and carbon fibers (carbonized at 1200 °C), along with respective elemental compositions. The loss of nitrogen and oxygen during carbonization can be observed, so that a final structure composed of pure carbon is achieved.

The modification of carbon fibers with carbon nanotubes by dipping the felts in a CNTs suspension was described in 'Materials and methods' section. After the adsorption of

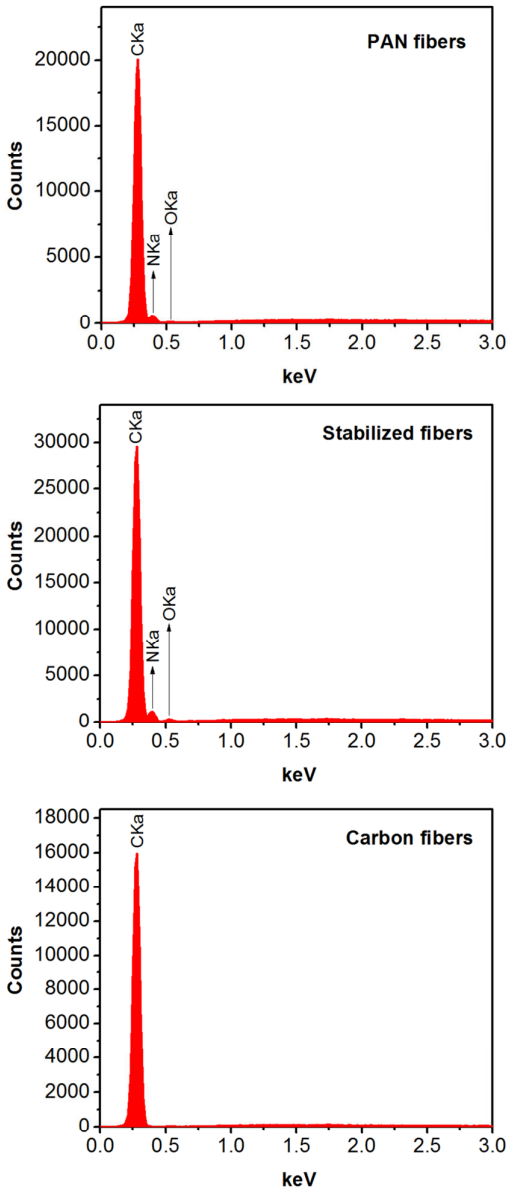

PAN fibers	keV	Mass%	Atom%
C	0.277	49.97	53.92
N	0.392	48.19	44.59
O	0.525	1.84	1.49
Total		100.00	100.00

Stabilized fibers	keV	Mass%	Atom%
C	0.277	46.55	50.56
N	0.392	50.44	46.98
O	0.525	3.01	2.46
Total		100.00	100.00

Carbon fibers	keV	Mass%	Atom%
C	0.277	100.00	100.00
Total		100.00	100.00

Figure 2.4. *EDX plots of electrospun fibers at the different stages of thermal treatment (crude, stabilized at 250 °C and carbonized at 1200 °C) with peak indications and elemental composition in weight and atomic percentages.*

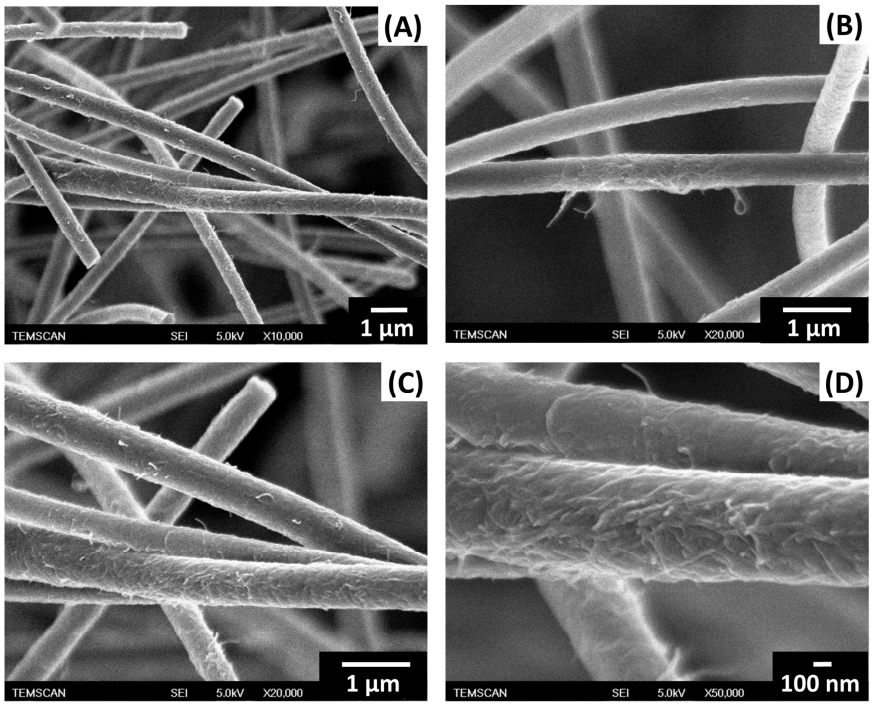

Figure 2.5. *FESEM images of the sample 1000+MWNTs showing the presence of multi-walled CNTs on the surface of electrospun carbon fibers.* ***(A)–(D)*** *shows different regions and magnifications.*

DWNTs and MWNTs onto the fibers, the different samples were observed by field-emission-gun scanning electron microscopy (FESEM). No significant structural difference was observed with the different starting fiber mats (1000, 1200 and 1400 °C). Regarding the MWNTs, typical images of *1000+MWNTs* are shown in **Figure 2.5**. Numerous MWNTs are observed on the surface of the electrospun fibers (**Figures 2.5A** and **B**). Higher magnification images (**Figures 2.5C** and **D**) show that the CNTs, isolated and in small bundles, are fairly adsorbed on the surface of the fibers. MWNTs bridging two different fibers are very rarely observed, which may reflect their short length (approximately 1.5 µm) with respect to the free space between fibers.

The suspension of DWNTs in water, without any surfactant, was unstable yielding a lack of reproducibility and homogeneity in these series of experiments. As an illustration, **Figure 2.6** shows a typical SEM image of sample *1400+DWNTs*. This image illustrates the presence of DWNTs agglomerates, which reflects the instability of the suspension. One can also notice in **Figure 2.6** the presence of bridging DWNTs, which illustrates their higher

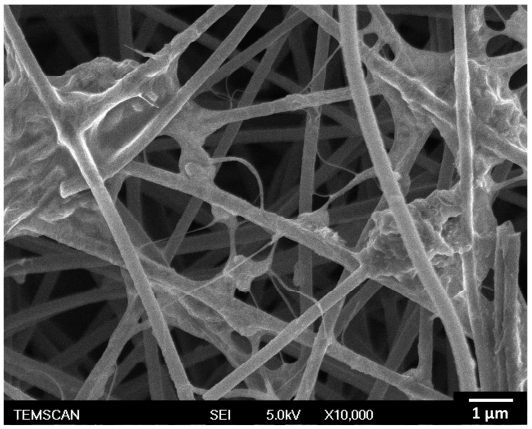

Figure 2.6. *FESEM image of sample 1400+DWNTs, illustrating the presence of CNTs bridges between the carbon fibers.*

length compared to MWNTs. However, since the formation of agglomerates was not desirable, the study was continued only with MWNTs, because they could create a uniform coating of CNTs over the fibers.

2.4. Raman spectroscopy characterization

The variations in the structural changes of the electrospun CNFs as a function of the carbonization temperature and of the presence of adsorbed CNTs were studied by Raman spectroscopy. This technique allows fast identification of any material, organic or inorganic. The principle of Raman spectroscopy is the following: a laser beam is focused on the surface of a sample, interacts with the polarizable electron density and molecular bonds of the sample, and is then scattered either with the same energy (frequency or wavelength) from the source, or with different energy. If the scattering happens with the same energy (the majority of it), it is named elastic scattering, or Rayleigh scattering. However if the scattered energy is different from the source (inelastic scattering, a small fraction of the incident light) then it is called Raman effect, and the difference in energy allows getting important information on the chemical composition of the sample. Raman spectroscopy is known to be a very useful tool for the characterization of carbon materials, which present two signature peaks: D and G, centered at respectively ca. 1355 cm^{-1} and 1580 cm^{-1}.[163]

Figure 2.7A presents the spectra of the sample *1200* with and without MWNTs. Raman spectra reveal D peak centered around 1329 cm^{-1}, and G peak centered around 1577 cm^{-1}, characteristic of disordered carbon and graphite, respectively, both of the bands are attributed to sp^2 bonded species.[164]

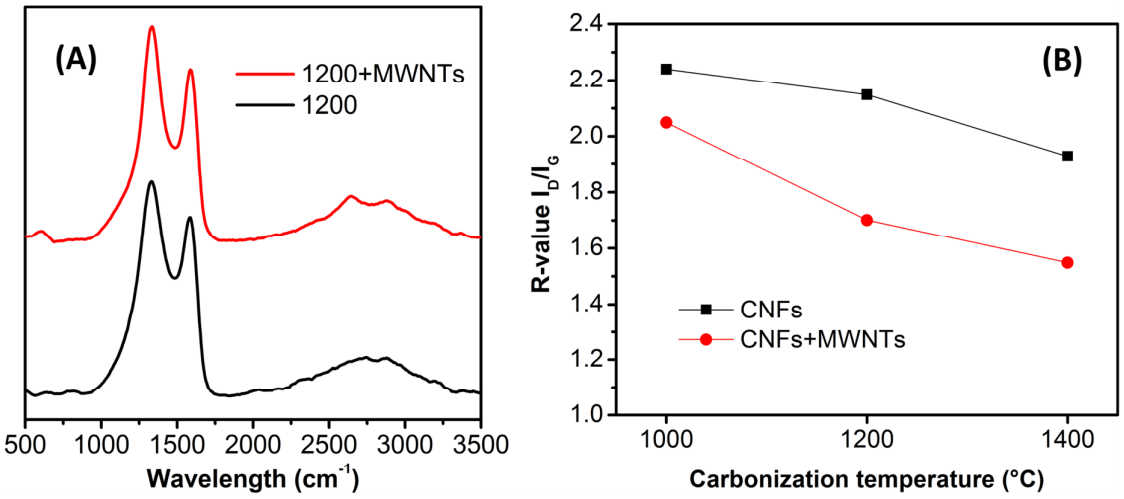

Figure 2.7. (A) *Raman spectra of the electrode 1200 with and without adsorbed MWNTs.* ***(B)*** *Ratio between D and G peaks (R) values obtained from Raman spectra according to the carbonization temperature of carbon fibers with no modification (■), carbon fibers adsorbed with MWNTs (●).*

It is well known that the R-value, the relative intensity ratio of the D band to the G band (I_D/I_G), depends on both the degree of graphitization and the alignment of graphitic planes. The lower the R-value, the higher the amount of sp^2 (graphite) groups is in the sample. The R-values of the electrodes are presented in **Figure 2.7B**. A decrease in R is observed along with increasing carbonization temperature (from 1000 to 1400 °C), representing the transformation into a more graphitized carbon. Such behavior has been observed by several authors who studied carbon materials such as CNFs.[119,165–167]

For samples with adsorbed MWNTs, R-values are smaller than the corresponding samples without MWNTs (but treated at the same temperature), and also decrease for higher temperatures. This behavior attests that the presence of MWNTs increases the relative rate of sp^2 carbon into the sample which is expected to lead to an enhanced electrical conductivity.

Finally, all the samples presented G' peak centered on 2740 cm^{-1}, additional to D and G ones. G' is approximately 2 times the frequency of D peak (i.e. the overtone of D peak), although the features of D and G' are the opposite.[165] It appears only for carbons treated higher that 1000 °C, and gets narrower and grows in amplitude as the heat treatment temperature and graphitization level increases.[165]

2.5. Electrical conductivity

The electrical conductivity of the felts was measured by the four-point probe method established by Van der Pauw.[168] This widely used technique consists of a variation of the regular four point probe technique (also known as Kelvin sensing, in which the sample must be of rectangular shape or bar shape, and the probes are positioned in an aligned manner, suitable for long samples), for samples with arbitrary shape. Between two of the four contacts on the sample a positive DC current is applied, and between the other two contacts the voltage difference is measured (this process is made twice, horizontally and vertically). The thickness (t) of the sample must be known. From the known current and voltage values, the sheet resistance (R_S) can be calculated using the Ohm's law (for more details on the calculation of R_S from the values of $R_{S\text{-horizontal}}$ and $R_{S\text{-vertical}}$, see Van der Pauw[168]). Then, the resistivity (ρ, in Ω·m) of the material is obtained from **Equation 2.1**:

$$\rho = R_S \cdot t \tag{2.1}$$

The electrical conductivity (σ, in $S \cdot m^{-1}$) is obtained as the reciprocal of the resistivity (**Equation 2.2**):

$$\sigma = \frac{1}{\rho} \tag{2.2}$$

There are four conditions that must be satisfied to use this technique:

1. The contacts are at the edges of the sample.

2. The contacts are sufficiently small.

3. The sample is homogeneous in thickness.

4. The surface of the sample is singly connected, i.e., the sample does not have isolated holes.[168]

One point to consider is the fact that carbon fibers are not the ideal candidates to be employed for the Van der Pauw technique, since it is a porous material and does not fulfill the 4th condition. It is however widely employed even for porous materials,[119,167,169,170] and therefore for the sake of comparison, will be employed here.

The conductivity values obtained are presented in **Figure 2.8** and they lay between approximately 1 and 13 S cm^{-1}. Similar values were observed by several authors who studied carbon fibers.[119,159,167,171] Kim et al. developed PAN-based carbon nanofibers with conductivity of approximately 2 S cm^{-1} when treated at 1000 °C, and approximately 15 S cm^{-1} when treated at 1500 °C.[119,167] Guo et al. obtained a conductivity of approximately

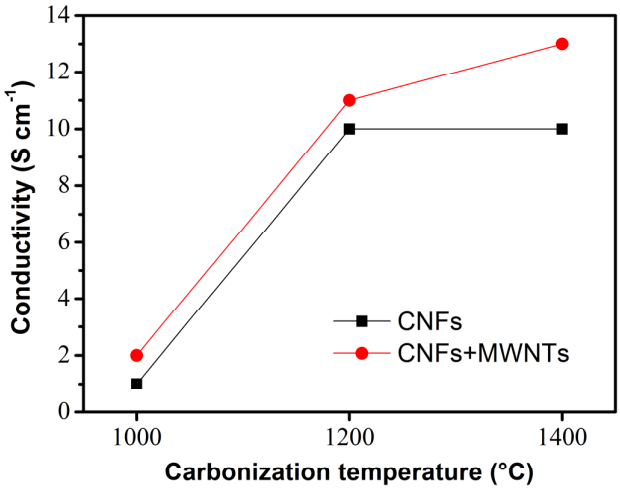

Figure 2.8. *Electrical conductivity values measured by Van der Pauw four-point probe method of carbon fibers with no modification (■) and carbon fibers adsorbed with MWNTs (●).*

5 S cm^{-1} for a hybrid material composed of CNFs containing MWNTs, prepared by the electrospinning of CNTs suspended in PAN solution followed by thermal treatments.[159] However, according to our studies, the four-point probe technique was not able to prove with certainty the beneficial effects of the presence of MWNTs on the electrical conductivity of the materials. This is probably because the characteristics of the material are not appropriated to be measured by points, due to its non-massive nature. When the four points touch the fibers in order to make the conductivity measurements, the electric current tends to flow in certain carbon fibers or carbon nanotubes that are in contact in that moment, so that it is not representative of the real behavior of the whole material. In order to show the relation between the different felts, the electron transfer was also evaluated through the electrochemical technique cyclic voltammetry.

2.6. Electrochemical behavior by cyclic voltammetry

Cyclic voltammetry (CV) is one of the most universal electrochemical techniques, in which current is recorded while the working electrode potential is swept linearly with time between two chosen values. More details about this technique can be found in **Annex 2**.

CNFs and CNTs@CNFs mats were characterized by cyclic voltammetry in phosphate buffer solution (pH 7) containing 10 mM $K_3Fe(CN)_6$ from -0.1 to 0.5 V *vs.* Ag/AgCl. For the representation of CV results, the current was reported in relation to the geometric area of

the electrodes. When used as an electrode, the resulting electrospun felts did not need the addition of any polymer binder and the structure afforded an easy handling. The influence of the carbonization temperature was studied upon the separation of the peak potentials (ΔEp) and peak current height (Ip_a) for $K_3Fe(CN)_6$ (**Figure 2.9A**).

The voltammograms are characterized by a pair of well-defined redox peaks for $Fe(CN)_6^{3-}/Fe(CN)_6^{4-}$ at $E_{1/2}$ = 0.18 mV *vs.* Ag/AgCl. When the carbonization temperature increases from 1000 to 1400 °C, ΔEp and Ip_a decreased. The trend of ΔE values ($\Delta E_{1400} < \Delta E_{1200} < \Delta E_{1000}$) indicates that the *1400* electrode presents the best reversibility in terms of ΔE due to its more organized and graphitized structure compared to *1000* and *1200* electrodes, as already observed by Raman. This result indicates faster kinetics of electron transfer that agrees with the morphology of the corresponding carbon fibers. In the case of the Ip_a trend, the peak current decreases with the heating treatment, which is attributed to the weight loss of the material during the carbonization step. The higher the heating temperature was, the lower the electroactive surface is (the higher the weight loss of the material during carbonization). Thus, since a commitment between smaller ΔE and larger Ip_a is necessary, the ***1200*** electrode was selected as the one that meets the better this condition.

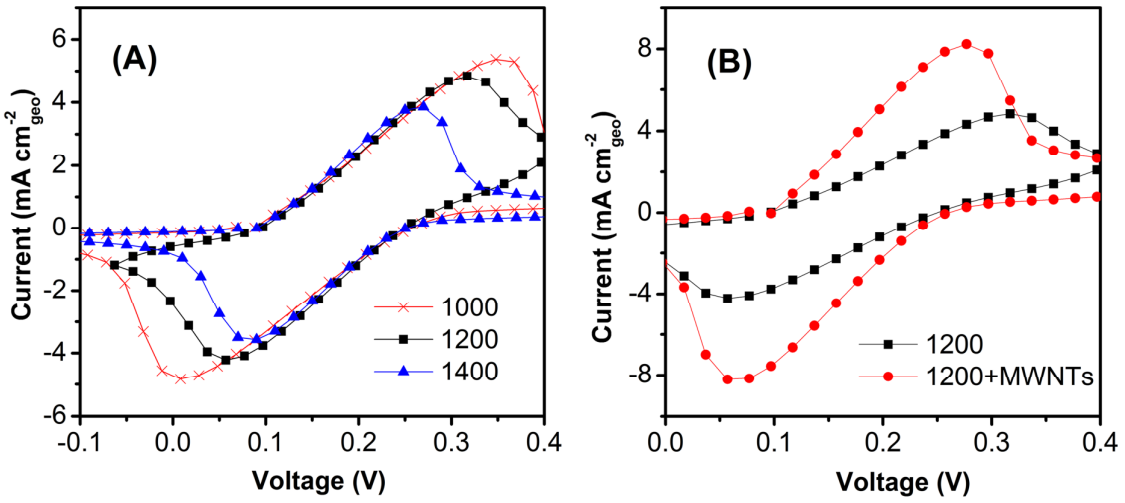

Figure 2.9. (A) *Cyclic voltammetry of 10 mM $K_3Fe(CN)_6$ at CNFs electrodes without MWNTs adsorbed, carbonized at 1000 (×), 1200 (■) and 1400 °C (▲).* ***(B)*** *Cyclic voltammetry of 10 mM $K_3Fe(CN)_6$ at CNF electrodes carbonized at 1200 °C with adsorbed MWNTs (●) and without MWNTs (■). Electrolyte: phosphate buffer pH 7, scan rate 10 mV s^{-1}.*

The benefit of adsorbing MWNTs on carbon fibers was illustrated by the evolution of both ΔEp and Ip_a. For all the samples, the reversibility of $\mathrm{Fe(CN)_6^{3-}/Fe(CN)_6^{4-}}$ was notably improved and effective electroactive surface area of the electrodes was increased in the presence of MWNTs. As shown in the case of the *1200* electrode (**Figure 2.9B**), ΔE decreases from 250 to 200 mV after immobilization of the MWNTs in the nanofibers mat and the anodic peak current is magnified 2-fold, suggesting that the presence of CNTs significantly improves the electrical conductivity and increases the effective electroactive area of the mats, which is due to the 3D structure of this CNTs@CNFs nanocomposite material. This effect was, however, not observed for the electrodes modified with DWNTs, likely as a result of the agglomerates formed on the fibers.

2.7. Conclusion

In this chapter, the preparation and material characterization of randomly organized carbon nanofibers produced by electrospinning were described. This material did not need the addition of any binder, and its structure allows easy handling. Not only it is a material with great properties that has been useful for many applications, it has also been shown as a promising material for enzymatic biocathodes in a previous work of our group.[172] Therefore, the intention of improving its performance was tested through the modification of the CNFs with the aid of CNTs: double-walled and multi-walled.

Difficulties in dispersion of the CNTs, specially the double-walled ones were encountered since the preparation of the suspensions, and confirmed by SEM images of DWNTs@CNFs. MWNTs, on the other hand, appeared well distributed onto the surface of the CNFs, according to SEM results. Raman spectroscopy analysis of the bare CNFs and modified with MWNTs showed that the R value (the ratio of the intensities of the characteristics D and G bands, I_D/I_G) was inferior for CNFs modified with MWNTs, which showed that the presence of CNTs increases the relative rate of sp^2 carbon into the sample. This was expected to lead to an enhanced electrical conductivity of the material.

However, actual electrical conductivity measurements did not show a great difference between nude CNFs and modified with MWNTs ones (that presented slightly higher conductivity), which might be related to problems during the measure of conductivity of porous materials, since the technique is not suitable for such, even if widely used. The electrical conductivity was around 10 S cm^{-1}, which is in agreement with the literature.

Finally, cyclic voltammetry analysis allowed the visualization of the effect of different carbonization temperatures on the performances of the CNFs, as well as the benefit of the presence of MWNTs on its surface. CNFs carbonized at 1200 °C were chosen as the best compromise between smaller ΔEp and higher Ip_a, and the presence of MWNTs was beneficial regarding both parameters.

Therefore, considering all the results, the intrinsic properties of the bare CNFs were indeed enhanced by the presence of MWNTs. In Part 3 of this work, these materials will be modified with enzymes and tested toward the bioelectrochemical reduction of O_2.

Chapter III. Aligned carbon fibers

3.1. Introduction

We saw in the previous chapter that randomly organized CNFs are a promising material with interesting properties regarding its structure, electrical conductivity and the possibility to use as an electrode material in electrochemical tests like cyclic voltammetry. In this chapter, the concept of aligned carbon nanofibers will be discussed in detail, whether the fact of organizing the fibers may affect its performance or not. In addition, the characteristics of these fibrous materials, aligned or random, will be compared to those of massive materials like commercial graphite or glassy carbon, and the advantages of a porous structure will be highlighted.

An important part of this chapter is the study on the electrical conductivity of fibrous materials. The evaluation of electrical conductivity of fibrous materials is a challenge and a standard measurement method for electrospun fibers felt has not yet been pointed out. Traditional techniques like the four-point probe (e.g. Van der Pauw's technique) for instance, require several conditions to be applicable. Some of these conditions are that the sample must be dense, homogeneous and isotropic,[168] as mentioned in the previous chapter. When applied to the measurement of the electrical conductivity of a felt of fibers, the four-point technique yields to various degrees in uncertainty, depending notably on the porosity of the felt.[119,167,173] Using this technique, Ra et al. have measured the conductivity of ex-PAN CNFs (i.e. stabilized PAN fibers) containing multiwall carbon nanotubes, and they have obtained values up to 35 S cm^{-1}.[174] In 2002, Wang et al. have studied the conductivity of an isolated CNF prepared by electrospinning on a substrate containing gold contacts.[47] This two-point technique gave a value of 4.9 S cm^{-1} for a single fiber prepared at 800 °C. A two-point probe configuration was also used by Zhou et al. to measure the conductivity of an anisotropic felt of CNFs.[175] However, to calculate the conductivity, the cross section of the felt is required and has been indirectly calculated by weighting. Values from 180 S cm^{-1} up to 840 S cm^{-1} have been reported for pyrolysis temperature of 1000 °C and 2200 °C, respectively. More

recently, Jia et al. have prepared carbon nanofiber yarns by solution blowing.[176] The fibers forming the yarn were very close in morphology to electrospun CNFs, even if the volumetric density of fibers in the yarn appears to be much higher than in CNFs felt. These authors have deduced the electrical conductivity from electrochemical impedance spectroscopy and a value up to 608.7 S cm^{-1} has been achieved (carbonization temperature of 1000 °C). Sui et al. have fabricated an anisotropic electrospun CNF felt by hot stretching, with fibers carbonization at 1200 °C.[177] They have studied the electrical conductivity by AC impedance analysis. The conductivity reaches 15.5 S cm^{-1} in the fibers direction. Silver paste was sputtered on the sample to improve the electrical contact. A similar strategy, gold sputtering, was used by Guo et al. for electrospun CNFs containing carbon nanotubes.[159]

The scattering of the measured values of electrical conductivity reported in the literature points out that there is no convenient and normalized measurement method allowing to take into account the features of the felt and the features of the nanofibers constituting the felt. Moreover, the contribution of the contact resistance in the overall measurements has not yet been clearly studied. The aim of this work was to make a first step in that normalization direction. For that purpose, two measurement techniques were compared (direct measurement with a micro-ohmmeter, and I-V curve plotting). The effect of contact resistances on these measurements was also evaluated.

In addition, the alignment of the CNFs in a felt was quantified by 2D Fourier Transform of SEM images, taking benefits from the pioneer works of Ayres et al.[178] The evolution of the degree of fiber alignment along with each step of the carbonization process was evaluated as well. Aligned CNFs felt, randomly distributed CNFs felt, dense graphite material were evaluated in terms of electrical conductivity, XRD and cyclic voltammetry.

3.2. Materials and methods

PAN fibers were obtained by electrospinning process. A PAN solution in DMF (10 wt.%) was stirred at 70 °C for 6 hours and electrospun under high voltage. The parameters for fabrication of both alignhed and random fibers by electrospinning are the following:

- The synthesis of randomly distributed fibers was performed between a needle (inner diameter of 800 µm) and a stationary disc covered with aluminum foil where a paper of random fibers was collected after 2 h of operation. Electrospinning voltage was 25 kV, solution feed rate 2 mL h^{-1} and tip-collector distance was fixed at 14 cm.

- The synthesis of aligned fibers was obtained on a rotating cylinder (10 cm diameter) covered by an aluminum foil. A rotation speed of 2000 RPM under a voltage of 20 kV was used. The feed rate and the tip-collector distance were 2.4 mL h^{-1} and 14 cm, respectively, and the process was carried out for 3 h.

Electrospinning conditions were such that aligned and non-aligned fibers presented approximately the same mean fiber diameter (measured with ImageJ software, NIH, *http://rsb.info.nih.gov/ij*) and thickness (~600 µm, measured with an optical microscope). The same heating treatment procedure realized in the previous chapter was employed here. Electrospun PAN nanofibers were stabilized in air environment at 250 °C for 2 h (heating rate was 2 °C min^{-1}) using a muffle furnace. The stabilized nanofibers were then carbonized at 1200 °C (1 h dwell) in high-purity nitrogen atmosphere (heating rate 2 °C min^{-1}) using a tubular furnace equipped with alumina tubes, yielding electrospun carbon nanofibers. The polymer-to-carbon conversion was performed at a temperature of 1200 °C which represents the best compromise between electrical conductivity and handling ability, as discussed in the previous chapter. The resulted aligned or randomly distributed CNFs felts were cut into strips of 3 cm × 0.7 cm in size. Clearly, the chemical structure of both aligned and random fibers is the same as presented by EDX in the previous chapter.

3.3. Materials characterization

Figure 3.1 shows SEM images of aligned and random felts at the same magnification. As illustrated by these images, the mean diameter of the fibers (330 ± 50 nm, calculated from the analysis of at least 50 fibers) is not affected by their spatial organization in the felt.

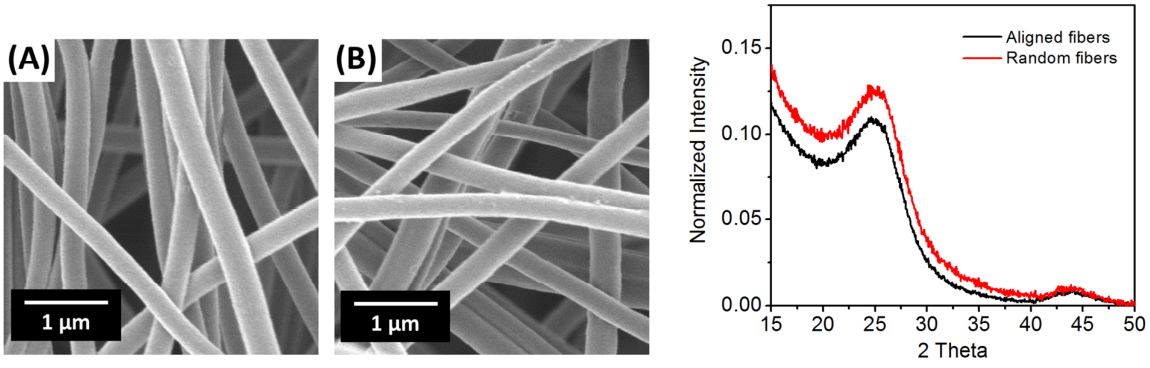

Figure 3.1. *SEM images of typical aligned felt* ***(A)*** *and random felt* ***(B)*** *of CNFs with magnification of 10,000. On the right, XRD diffractograms of the CNFs.*

This is due to the fact that no constant mechanical tension is applied to the aligned felt during air stabilization (which can significantly enhance the degree of alignment but decreasing fiber diameter).[176] This identical mean diameter of the fibers is a key-result allowing to compare the influence of the spatial organization of the fibers in a felt on their electrical properties and bioelectrode performance. Crude aligned fibers were cut into pieces before pyrolysis. Indeed, as a counterpart, the lack of mechanical tension during the thermal stabilization induces a partial loss in spatial organization of the fibers when going from crude fibers to carbon fibers. This result is illustrated by **Figure 3.2** which shows the SEM images of the aligned fibers as-collected after electrospinning synthesis (**Figure 3.2A**), after stabilization under air at 250 °C (**Figure 3.2B**) and after complete conversion into carbon at 1200 °C (**Figure 3.2C**). The spatial organization of the fibers in the carbonized sample will be deeply discussed below.

XRD analysis of aligned and random CNFs was performed, and is shown in **Figure 3.1**. Both samples present a broad peak in the region of 2θ near 25°, corresponding to the (002) planes, and a smaller one near 42°, corresponding to the (100) planes. In good agreement with the literature, this result indicates the presence of graphitic domains, even if the broad nature of the peaks implies that the fibers are turbostratic rather than crystalline.[177] Full Widths at Half Maximum (FWHM, β) and the scattering angles of (002) planes for aligned and random samples are of β = 0.0977 rad (= 5.6°) and 0.0942 rad (= 5.4°) respectively, and 2θ = 24.62° and 24.32°, respectively. The crystallite size parameters "*Lc*" can be therefore calculated in both samples using the Scherrer equation (**Equation 3.1**):

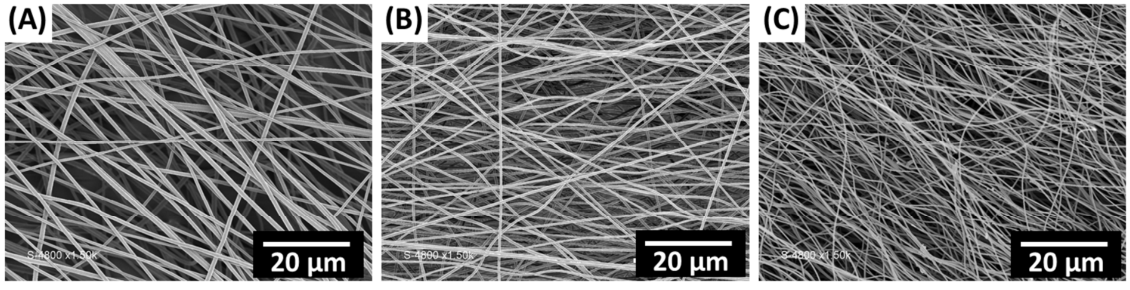

Figure 3.2. *Representative SEM images of typical aligned felt:* ***(A)*** *crude sample,* ***(B)*** *after air stabilization at 250 °C, and* ***(C)*** *after carbonization at 1200 °C. Samples were metallized by gold sputtering before observation. Magnification factor of 1,500.*

$$L_c = \frac{0.9 \cdot \lambda}{\beta \cdot \cos \theta} \quad (3.1)$$

where

- λ is the X-ray wavelength,
- β is the full width at half maximum of the peak,
- θ is the Bragg angle.

In the aligned felt, the crystallite size parameter Lc is 1.45 nm, when this value reaches 1.51 nm in the random one. This result clearly indicates that the spatial organization of the fibers does not significantly impact its crystallite sizes in our experimental conditions (no mechanical tension during air stabilization).

Finally, the specific surface area of the felts was evaluated to be $12 \pm 2\ m^2\ g^{-1}$ from Brunauer–Emmett–Teller (BET) measurements.

3.4. Evaluation of fiber alignment by Fast Fourier Transform of SEM images

The spatial organization of fibers in the felt being a key parameter for its physical properties, finding a method to evaluate this parameter was a concern during the realization of this work. In the absence of a standard characterization procedure to evaluate the alignment of fibers in the felt, the pioneer works of Ayres et al.[178] served as reference. They have demonstrated that Fast Fourier Transform (FFT) of electron microscopy images associated with a plot of the radial pixel intensity sum can allow qualifying the spatial arrangements of the fibers in the sample. They have also shown that this analysis was not dependent on SEM magnification.

3.4.1. Fast Fourier Transform method

The evaluation of fiber alignment was realized by Fast Fourier Transform (FFT).[178] This technique allows the conversion of optical information (SEM images, i.e. data from real domain) into mathematically defined frequency domain. The output transformed image consists of grayscale pixels that are distributed in a pattern that varies according to the degree of fiber alignment observed in the original SEM image. For the purpose of this work, SEM images of aligned and non-aligned fibers (8-bit grayscale TIF files) with the same

magnification factor of 1500 were cropped to 512 × 512 pixels and then processed with FFT function of ImageJ software (NIH, *http://rsb.info.nih.gov/ij*). In order to interpret the output FFT images, the pixel intensities were summed across the radius from 0 to 180° with increments of 1°. This operation was realized with ImageJ software supported with the Oval Profile plot plug-in (by Bill O'Connell, *http://imagej.nih.gov/ij/plugins/oval-profile.html*). FFT pixel intensity data was normalized to a baseline value of zero, in order to compare different samples. Then is generated the graph from the summation of the normalized pixel intensities for each degree radially along the sample, where the presence of a peak indicated the presence of a preferential alignment. The quality of this alignment is dependent on the height and shape of the peak in the plot. Full width at half maximum (FWHM) were obtained after the curves were smoothed.

3.4.2. Analysis of FFT results

In **Figure 3.3**, it is possible to observe that a random fibers sample SEM image (**Figure 3.3B**) generates an output FFT image (**Figure 3.3F**) that consists of pixels distributed in a symmetrical circular shape. This means that the frequency at which a certain pixel intensity appears on the image is identical in any direction of the sample, hence the absence of any major peak in the graph representing the pixel intensity summation of the sample between 0° and 180° (**Figure 3.3I**, red curve). On the other hand, an aligned fibers sample (**Figure 3.3A**) generates an output FFT image (**Figure 3.3E**) where the pixels are distributed in an elliptical pattern that reflects the anisotropic organization of the fibers in the sample. The pixel intensity plot at **Figure 3.3I** (black curve) highlights the presence of the peak for aligned fibers. The relative height of this peak (0.17) and its shape are featuring the fibers alignment. The full width at half maximum (FWHM) of this peak is 67.9° and further analysis were performed to determine which parameter, FWHM or peak intensity, can be representative of the alignment of the fibers.

We have first studied the effect of image colors on the results. For that purpose, cropped SEM images were converted to binary black and white images with ImageJ software (black background option). In **Figure 3.3C** and **3.3D** the resulting binary images of aligned and random felts (carbonized samples) are presented, and in **Figure 3.3G** and **3.3H**, their respective FFT images. From the curves in **Figure 3.3J** it is possible to see that the peak obtained from binary image of the aligned felt is less intense (0.125) but the peak presents a

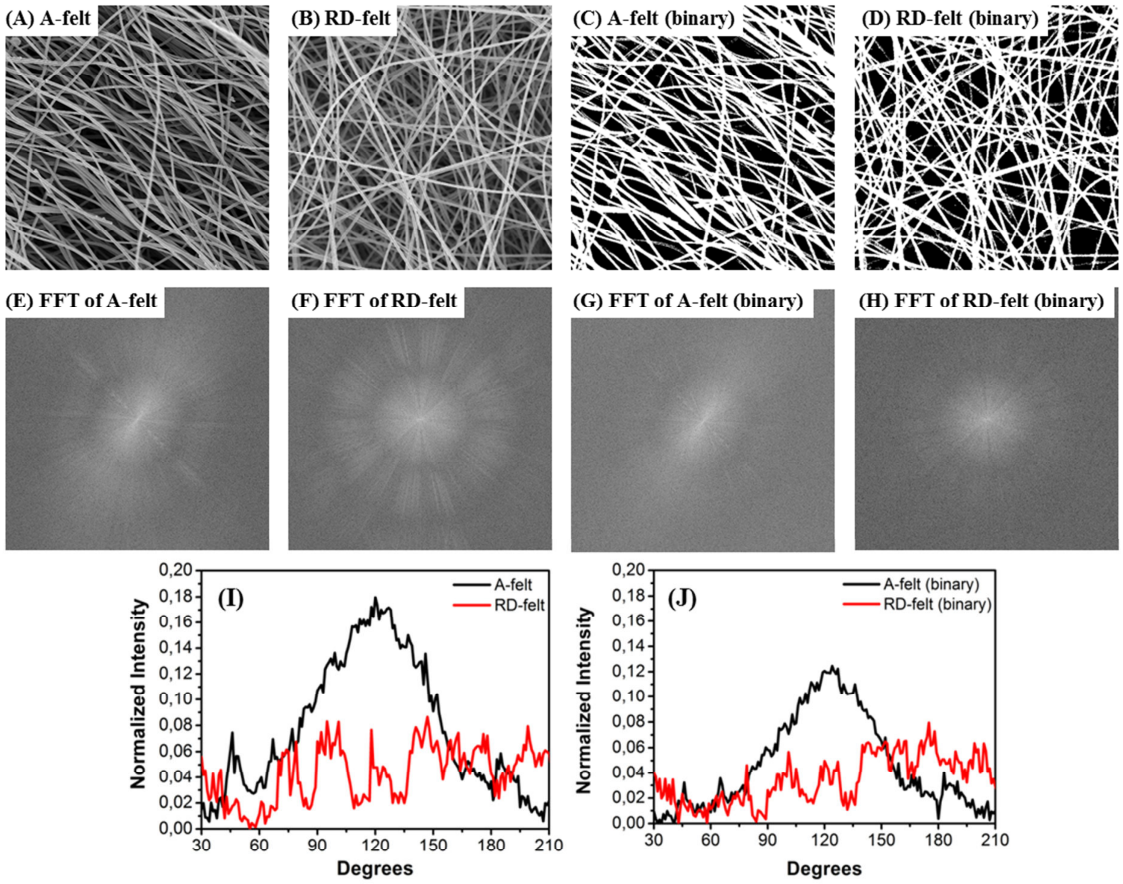

Figure 3.3. *FFT analysis of SEM images of aligned (A-felt) and randomly distributed fibers (RD-felt).* ***(A-B)*** *SEM cropped images.* ***(C-D)*** *SEM cropped images converted to binary black and white images.* ***(E-H)*** *FFT output images of the correspondent SEM image on top.* ***(I)*** *Pixel intensity plots of FFT images E and F (from grayscale MEB images) along 180°.* ***(J)*** *Pixel intensity plots of FFT images G and H (from binary black and white MEB images) along 180°.*

better resolution. This is due to the suppression of the contribution of the fibers below the SEM observation plane which appears in grey nuances in the 8-bit images. For that reason, the following analyses herein presented were performed only with binary images. The FWHM of this peak (aligned felt, binary) is of 60.8°, which at first could indicate that when the FFT analysis is made on binary images, both the intensity and the FWHM may decrease in value. This fact will be further examined.

In order to study the evolution of the alignment during the polymer-to-carbon conversion, **Figure 3.4A** presents the intensity plots resulting from FFT analysis of aligned felts on its three stages: PAN crude fibers, stabilized ex-PAN fibers (250 °C) and carbonized

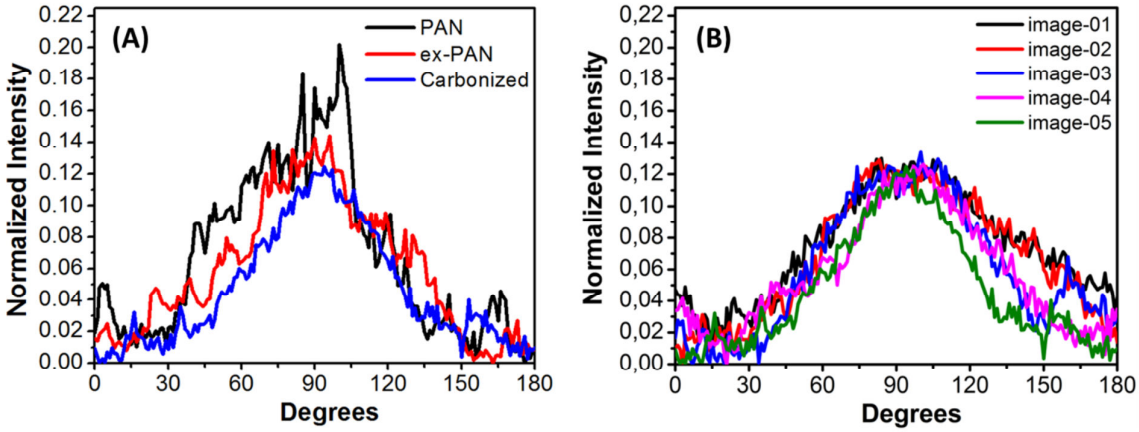

Figure 3.4. ***(A)*** *Pixel intensity plots resulted from FFT analysis of binary SEM images of aligned felts during the three stages of thermal treatment: PAN fibers, stabilized ex-PAN fibers and carbonized fibers.* ***(B)*** *Pixel intensity plots resulted from FFT analysis of several binary SEM images of the same carbonized aligned felt sample (images named from 01 to 05), in different regions.*

fibers (1200 °C). It is possible to observe that PAN crude fibers present a peak with intensity around 0.19. However, the peak of ex-PAN stabilized and carbonized fibers have lower intensity (down to 0.125), indicating that a slight loss of alignment occurs during the heat treatment. As mentioned earlier, this is due to the fact that no mechanical tension was applied to the fibers during the stabilization process, which could lead to fibers with different morphology and enhanced alignment. In addition, the act of cutting the felts in small pieces prior to carbonization is also responsible for a partial loss of alignment, which is observed in SEM image by the fact that some fibers are broken. FWHM values are 62.8, 75.7 and 60.8° respectively for PAN, ex-PAN and carbonized samples. One could think that FWHM should be lower form PAN to carbonized samples, since alignment is progressively worst, but it is not the case. So far, according to our results, FWHM does not follow a logical order.

Finally, a reproducibility test for the validation of the FFT technique was performed. Five images of the same sample (carbonized aligned felt) were analyzed, and the intensity plots obtained are presented in **Figure 3.4B**. All the curves present similar pixel intensities slightly varying around 0.125, thus confirming that the reproducibility is good. However, regarding the FWHM trend, values vary from 60.8 to 100.9°, not constant to be taken as a reproducible parameter. The conclusion obtained from the results is that the normalized

intensity of the peaks is indeed the best parameter for characterizing the fibers alignment, which is in agreement with the analysis of Ayres at al.[178]

3.5. The challenge of electrical conductivity measurements

As a way of comparing the electrical conductivity of different CNFs configurations and other materials (like graphite), the sheet resistance was chosen as a parameter. Two methods were employed for the measurements and the electrical contacts were established by two clips spaced 1 cm from each other. In the first approach, the resistance in ohms of a fiber felt was measured with the aid of a Fluke (8846A) Precision Multimeter, whereas in the second approach, the fibers were scanned from -2 V to +2 V with a step of 100 mV s^{-1} (with the aid of an Ametek potentiostat) whilst intensity currents were recorded (linear I-V curve plotting).

As a way of evaluating the contribution of the electrical contact resistances between electrical clips and CNFs, different tests were realized using or not a silver conductive paste (Silver Conductive Adhesive 478SS from Electron Microscopy Sciences). Two bands of this paste were deposited on both sides of the mat, leaving 1 cm of nude fiber mat in between (**Figure 3.5**). The coating was applied on top and bottom of each sample, over a glass slide. After applied, the coating was dried in an oven at 70 °C for 2 h before measurements.

In order to evaluate the effect of the spatial organization of the fibers on the electrical properties, resistance measurements were realized in aligned fibers while the fibers direction was parallel or perpendicular to the current flow during the measurements (schematized in **Figure 3.5**). Randomly distributed fibers resistance was also measured, as

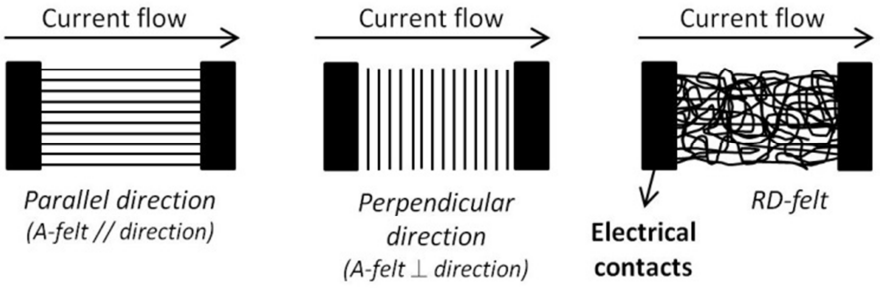

Figure 3.5. *Schemes of different measurement conditions depending on the spatial organization of CNFs in the felts (aligned = A-felt, random = RD felt). Black strips correspond to contact points with clips and where silver paste coatings were potentially disposed. The distance between clips was 1 cm.*

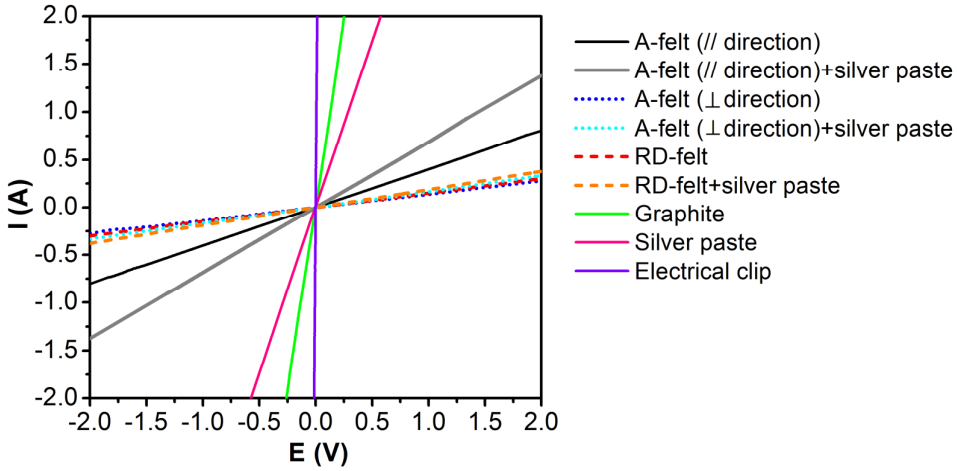

Figure 3.6. *I-V plots of different CNFs samples (aligned = A-felt, random = RD-felt), dense graphite and silver paste, with or without the assistance of a silver paste coating as interphase between the fibers and the clip.*

Table 3.1. *Electrical resistance values measured with two different techniques: directly with a Fluke Precision Multimeter or by I-V plots. Values are in Ohm for 1 cm length and 500 µm in thickness of fiber felts. The resistance of electrical clips alone was subtracted from the values obtained. Aligned = A-felt, random = RD-felt.*

		A-felt // direction	A-felt ⊥ direction	RD-felt	Graphite	Ag paste (pure)	Electrical clips
Direct contact	**R (multimeter)**	2.6	6.8	6.6	0.04	0.15	0.04
	R (I-V plot)	2.4	7.2	6.6	0.13	0.29	0.01
With Ag paste	**R (multimeter)**	1.4	5.9	5.2			
	R (I-V plot)	1.4	6.0	5.3			

well as a dense graphite sample and the pure conductive silver paste, for comparison.

Figure 3.6 presents I-V plots obtained with the different materials. The repeatability of these measurements was excellent. One can notice the linearity of the response of the materials showing ohmic behavior. Resistances (in Ohm) of the different materials were simply deduced from linear regression of the plots, and a mean value of R^2 of 0.9999 was found for all the regressions.

Resistance values obtained for both techniques (I-V plot and direct measurements) are presented in **Table 3.1**. The measurements were also performed on the electrical clips alone, and the resistance value obtained was subtracted from the values obtained for the other

materials. For each sample, the results obtained via the two techniques are quite similar, if not equal, which confirms its reproducibility, which Van der Pauw's four points technique did not provide in our previous work.[12] We observe herein that resistance values follow the order:

$$Graphite < Silver\ paste < A\text{-}felt\ //\ direction < RD\text{-}felt < A\text{-}felt \perp direction.$$

Dense crystallized Graphite sample presents evidently the smallest resistance (0.0016 ohm according to the manufacturer). Silver paste presents a resistance of 0.15 ohm which is lower than that of carbon felts, showing that it can be used as contact enhancer.

The interest of this approach is that carbon fibers are a material with voids between fibers, and then if the electrical contact is not optimal, only a certain amount of fibers may participate on the electrical conduction on the felt. The results of this investigation showed that indeed a lower resistance is observed when the conductive silver coating is applied, as presented in **Table 3.1**. The mean decrease in resistivity was of about 26 % (varied from 46 to 14 %) when the silver paste was employed as contact enhancer.

As far as carbon felts and its spatial organizations are concerned, from **Table 3.1** we observe at first that the organization providing the lowest electrical resistance is aligned fibers on the same direction as the current ("A-felt // direction"), with a resistance of 1.4 ohm (with silver paste contact). Then, "RD-felt" appears to have a slightly lower resistance than "A-felt ⊥ direction", 5.2 ohm. These results show the importance of fibers spatial organization on the conductivity of the material. The reason why "A-felt // direction" is more conductive than the other dispositions is the fact that the electron flow has fewer obstacles to surpass in their way through. In non-aligned fibers samples (RD-felts), the electrons need to jump from fiber to fiber, which is an additional resistance to the current flow. When the fibers are in perpendicular direction, a less ideal situation is created, since electrons have slightly more fiber-fiber jumps to realize than in non-aligned fiber mats, accordingly to the results.

We believe that the evaluation of the sheet resistance is a more correct way of estimating the electrical conductivity of porous felts than by using common literature methods like the Van der Pauw technique, as explained in the introduction of this chapter. When techniques like that are employed for porous materials, we are considering it as a

massive material, because the porosity is counted as if it was made of conductive material during the calculation. This procedure overestimates the conductivity value obtained. For comparison with the literature, if the conductivity here was calculated by this way (considering as a massive material), a value of 14.3 S cm^{-1} for "A-felt // direction" and of 3.39 S cm^{-1} for "A-felt ⊥ direction" would be obtained, i.e. a conductivity almost 5 times lower in this direction. Zhou et al.[22] who also studied different fiber anisotropies found a conductivity 16 times better for "A-felt // direction", although employing mechanical tension on felts during the stabilization step, with carbonization temperature of 1400 °C and in addition the cross section area of the felt was calculated indirectly by weighting, which overestimates the result. Otherwise, the calculated and overestimated value of 14.3 S cm^{-1} is in good agreement with other studies performed by Ra et al. and Sui et al.[20, 24]

3.6. Cyclic voltammetry characterization

In order to evaluate the ability of the carbon-based materials to be used as electrodes, they were characterized by cyclic voltammetry in 10 mM $K_3Fe(CN)_6$ medium in PBS (0.1 M) at pH 7.0 versus Ag/AgCl reference (**Figure 3.7**). The voltammograms present well-defined redox peaks for $Fe(CN)_6^{3-}/Fe(CN)_6^{4-}$. It is possible to evaluate the properties of the electrode material with two parameters from cyclic voltammograms: the separation of the

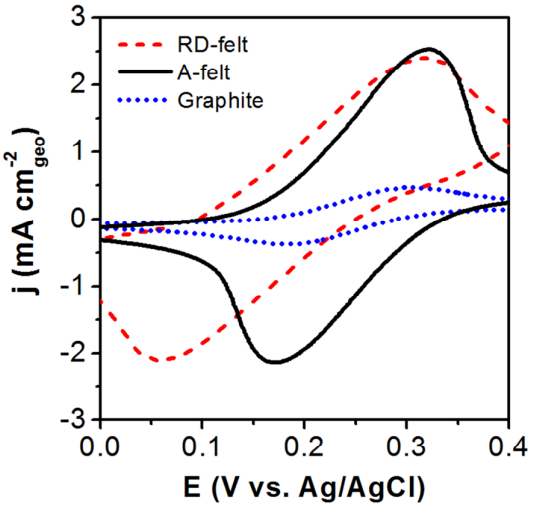

Figure 3.7. *Cyclic voltammograms of 10 mM $K_3Fe(CN)_6$ at aligned (A-felt) and randomly distributed (RD-felt) carbon felts, as well as commercial graphite, in phosphate buffer pH 7, scan rate 10 mV s^{-1}.*

peak potentials (ΔEp) and the peak current height (Ip), the first being related to the electrical conduction (electron transfer kinetics) of the material, and the second being related to the accessible redox surface for the reaction to take place onto the electrode material, as presented in **Annex 2**. As far as Ip is concerned, it is possible to observe from the voltammograms in **Figure 3.7** that Ip from CNFs is 5 times higher than from graphite (the currents were referred toward the electrodes geometric surface). This is due to the high accessible redox surface of carbon fibers, resulting from the 3D network of CNFs, aligned or not. From ΔEp trend, we observe that aligned felts notably improve the kinetics of the redox reaction comparing to random felts, as ΔE decreases from 0.25 to 0.14 V (110 mV reduction), suggesting that the spatial orientation of the fibers affects the electric transfer of the material. These results are all in agreement with the resistivity measurements presented. In addition, although commercial graphite presents a much smaller intrinsic resistivity than aligned felt, their electronic transfer properties are quite similar. This result shows that the electrochemical reactions at electrode surface depend not only on the intrinsic resistivity of the materials but as well on electron transfer rate influenced by the resistance between the interface solution/material that can be decreased in the case of the CNFs porous structure, by affording a close contact between the redox species and the material.

3.7. Conclusion

The synthesis of aligned and randomly distributed fibers obtained by electrospinning was described in this chapter. It was shown that even though aligned fibers lose some degree of alignment during the carbonization step, it is still a material with higher performance than randomly organized felts, as proved by characterizations like electrical conductivity measurements or cyclic voltammetry. The loss of alignment undergone by the felts during carbonization is mostly due to the absence of mechanical tension during heat treatment. XRD diffractograms showed that the crystallinity of CNFs was not affected by the fact the fibers were aligned or random (in the conditions employed), since aligned felts and random felts present very similar crystallite sizes. Also, the specific surface of 12 $m^2 g^{-1}$ is a satisfactory value that could be enhanced if fiber diameters were smaller than the present ones (~300 nm), but at the expense of structural properties of the felts, which could become more fragile.

Linear electrical resistivity of the fibers was measured by two different techniques: direct measurement with a precision multimeter and by I–V plots, which gave similar results. The resistivity followed the order:

Graphite < *Silver paste* < *A-felt // direction* < *RD-felt* < *A-felt* ⊥ *direction.*

The effect of the contact resistance between the clips and fibers was evaluated, and it was found that the resistivity decreased by approximately 26 % when a silver paste was employed as a contact enhancer. We proposed that the measurement of linear conductivity was more accurate than that of van der Pauw's technique, which considers the felt as a massive material. For the "*A-felt // direction"* sample, a linear conductivity of 0.71 S cm^{-1} was obtained. If it was calculated by considering the felt as a massive material, a value of 14.3 S cm^{-1} would be obtained, which is 5 times higher than the conductivity of the *"A-felt ⊥ direction"* sample.

The advantage of the porous structure of CNFs in comparison to the dense graphite was shown through cyclic voltammetry characterization. Peak intensities of CNFs electrodes were 5 times higher than graphite, showing the higher accessible surface of CNFs. This characteristic will be exploited in Part 3 of this work through the modification of CNFs with enzymes and test in BFCs half-cells or complete ones.

The results show CNFs present some interesting properties, like good specific surface and electrical conductivity, but one of the most interesting is the fact it is a freestanding felt. This is thanks to the electrospinning technique that allows the creation of very long and thin fibers that organize themselves in a non-woven manner. Therefore, these felts are able to be employed like electrodes in a wide range of applications without the need of support or binder materials.

Chapter IV. Carbon fibers decorated with Au particles

4.1. Introduction

In this chapter, the fabrication of a new nanocomposite material capable of acting as abiotic anode material for glucose electrooxidation is detailed. This material is composed of electrospun carbon fibers containing gold nanoparticles, with the advantage that the nanoparticles are formed in-situ from a polyacrylonitrile (PAN) solution of $HAuCl_4$. This approach allows the pre-reduction of gold salt by PAN in mild conditions without the need of extra energy, and leads to a very stable carbon-gold bonding with well dispersed AuNPs which, to our knowledge, has not yet been reported.

It is known that, besides enzymes and microbes, metallic electrodes and nanoparticles are able to catalyse the reaction of glucose oxidation due to their large surface area and number of surface atoms leading to a high amount of active sites.[179] However, the catalytic properties of the NPs depend on their shape, size, size distribution and environment. Great efforts have been made to develop electrode materials composed of Pt,[99] Au,[98] Au-Pt,[180,181] Pt-Pb alloy,[182] Pd,[179] and even trimetalic structures composed of Au-Pt-Pd[105] that have been proved to exhibit electrocatalytic activity in response to glucose oxidation.

Especially, gold nanoparticles (AuNPs) exhibit good activity toward glucose oxidation (with typical current values ranging from some hundreds of μA to a few mA) due to their chemical stability, good biocompatibility, high catalytic activity and resistance to surface poisoning during electrochemical processes.[183–186] Several techniques can be employed for supporting AuNPs on electrodes surface, which may vary according to the nature of the surface, such as impregnation, electrodeposition, CVD (chemical vapor deposition) or PVD (physical vapor deposition).[183–186] However, the weakness of the bonding between the NPs and the electrode material, and the heterogeneity of the coating are some limitations of such techniques. Therefore, the objective here is to overcome some of these setbacks.

By adding a gold salt in the electrospinning precursor solution, our objective is to obtain fibers that contain AuNPs after the reduction of the gold salt and particle growth. Some examples of Ni-modified carbon fibers prepared by a similar procedure as the one employed in this work can be found in the literature.[101,187] Similar approach has been employed for the synthesis of PEO fibers containing AgNPs,[188] where the PEO itself plays the role of reducing agent. Regarding AuNPs, the works of Liz-Marzan's group showed that gold salt can be reduced to AuNPs in PVP (poly(vinylpyrrolidone)) solutions, using DMF (dimethylformamide) as solvent, under reflux conditions or microwave heating.[189,190] Other reports exist on the creation of gold salt modified PAN fibers that were simultaneously[191] or subsequently[192] treated by UV irradiation for the NPs growth.

The final material developed in this chapter was characterized by SEM, EDX, XRD and electrical conductivity measurements. Cyclic voltammetry and electrochemical impedance spectroscopy (EIS) allowed the comprehension of mass and electron transfer mechanism through the felts.

4.2. Materials and methods

PAN fibers with gold salt were prepared by electrospinning, as demonstrated in the scheme in **Figure 4.1**. $HAuCl_4$ (0 or 0.5 g) was firstly mixed to preheated DMF (10 mL at 70 °C), and then PAN (1.0 g) was added slowly. The mixture was stirred at 70 °C for 3 hours. The amount of gold salt in the solution was limited to 0.5 g in 10 mL because at that point the solution was already well charged and fiber formation during electrospinning became difficult (jet instability). The solution with no added gold was electrospun on a drum (10 cm diameter) covered by aluminum foil, rotating at 2,000 RPM, under a voltage of 20 kV, with feed rate of 2.4 mL h^{-1} and tip to collector distance of 14 cm. The solution loaded with 0.5 g of $HAuCl_4$ (solution named $AuCl_4^-$*+PAN+DMF*), was electrospun under a voltage of 22 kV, drum speed of 1000 RPM, with feed rate of 2 mL h^{-1} and tip to collector distance of 8 cm (electrospinning parameters are different for the solution containing gold because solution properties are different). The inner diameter of the needle was 800 µm and the process was carried out for 2 hours. Photos of the resulting felts obtained with 0.5 g $HAuCl_4$ show a yellowish color, while felts with no added gold are white, as depicted in **Figure 4.1**.

The electrospun felts obtained were stabilized in air environment at 250 °C for 2 hours (heating rate of 2 °C min^{-1}) in a muffle furnace (Vecstar Ltd.). The stabilized fibers were then

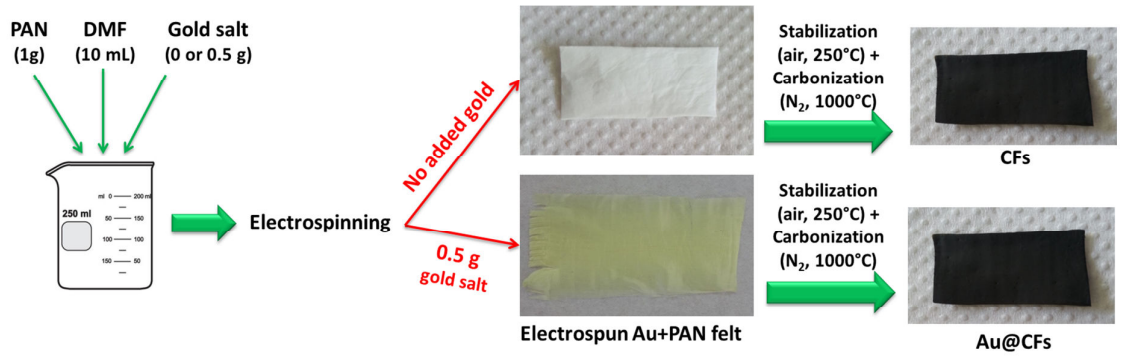

Figure 4.1. *Scheme of the synthesis process, with photos of the as-electrospun felts obtained from precursor solutions with 0 or 0.5 g of $HAuCl_4$ (white and yellowish felts), and the carbonized felt, which is black in both cases (with or without added gold).*

carbonized at 1,000 °C (1 h dwell) in high-purity nitrogen atmosphere (heating rate 2 °C min^{-1}) using a tubular furnace (Vecstar Ltd, VTF-4 furnace model) equipped with alumina tubes, yielding either pure electrospun carbon fibers (*CFs*) or AuNPs-modified carbon fibers (*Au@CFs*). The resulted felts were cut into squares of 0.8 × 0.8 cm in size and used as electrodes for glucose electrooxidation.

4.3. Study on the Au particles formation and materials characterization

Au particles embedded in carbon fibers were prepared by a one-pot route using electrospinning technique, as described. In **Figure 4.2**, SEM images of the precursor Au@PAN fibers are presented. It is observed that the crude PAN fibers (directly collected after electrospinning) possess metallic particles when observed with back-scattered electron detector. With this type of analysis, a material with higher atomic number appears brighter than a lighter material. Thus, the shiny particles in **Figure 4.2B** represent the Au particles (which cannot be observed with the regular secondary electrons detector in **Figure 4.2A**, presumably due to the non-conductive property of the PAN fibers). This leads to the conclusion that the Au particles formation started before the heat treatment step. The studies of the Liz-Marzán group show that DMF solvent is an appropriate reaction medium for the synthesis of metal NPs,[190] which is combined to poly(vinylpyrrolidone) (PVP) as capping agent[189] and with the help of extra energy (reflux conditions or microwave heating).

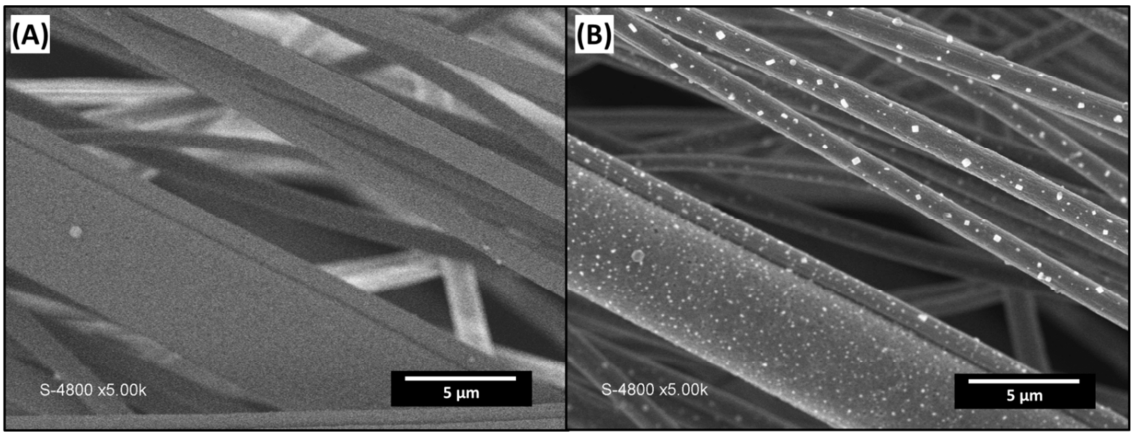

Figure 4.2. *SEM images of Au@PAN fibers (yellowish tissue collected directly after electrospinning process) observed* ***(A)*** *with regular secondary electrons detector and* ***(B)*** *with back-scattered electrons detector.*

The PAN+DMF couple can also be employed as medium for AuNPs growth, according to the works of Anka *et al.* and Sawada *et al*,[191,192] but a subsequent UV-irradiation treatment is employed for the NPs growth according to their works. Therefore, in both cases, extra energy is required to produce the gold nanoparticles.

In order to understand the particle growth, the precursor solution ($AuCl_4^-$*+PAN+DMF*) was deposited in the form of a film by spin-coating on a glass substrate. According to the works of Liz-Marzán's group,[189,190] we suspect the DMF to act as a reductive agent for gold, the same precursor solution was also prepared in DMSO medium for comparison. It is important to note that DMSO is not known for acting as NPs reducing agent. Also, DMSO was chosen because it is able to dissolve PAN. Fibers and films were then characterized by XRD, as shown in **Figure 4.3** (**Figure 4.3A** shows crude fibers and films, whereas **Figure 4.3B** shows carbonized fibers).

First, the crude PAN fibers and films obtained with gold salt were analyzed by XRD (**Figure 4.3A**). Besides the broad peak at ~17° that corresponds to PAN orthorhombic chain packing,[193] peaks of crystalline gold are observed for all samples, meaning Au particles are already present in the crude fibers, in agreement with SEM analysis. The strong relative intensity of the (111) peaks compared to the diffractograms of carbonized samples on **Figure 4.3B** can be noticed. This result can be explained either by an anisotropy of the sample during analysis in the Bragg Brentano configuration[194] or more probably by an anisotropy during the initial steps of NPs growth, i.e. formation of anisotropic gold seeds.[195]

Figure 4.3A also shows the presence of a peak at 31.6° which is not present anymore in the carbonized fibers (**Figure 4.3B**) nor in the crude film that does not contain gold (PAN+DMF) (XRD presented in **Figure 4.4**). We assume that this peak is related to gold salt crystallites that remain in the sample. In the literature, this peak was precisely attributed to the presence of AuCl [196] despite their diffraction peaks values are not in agreement with calculated data.[197] This means that the Au particles start to be formed during the solution preparation and/or shaping step, which is remarkable since the experimental conditions are mild (stirring at 70 °C). It is, to our knowledge, the first time that no extra energy is required to form Au particles in DMF solutions.

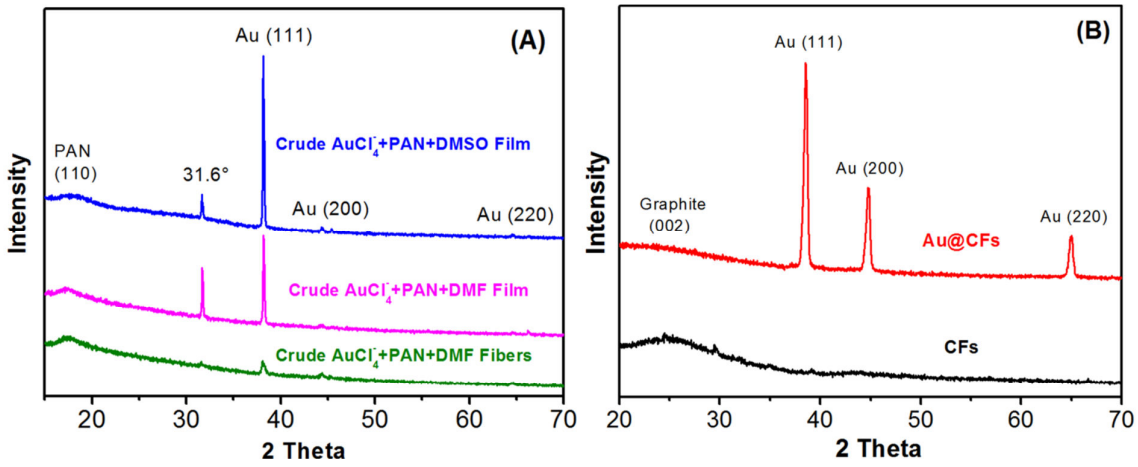

Figure 4.3. (A) *Diffractograms of crude fibers obtained from the solution containing* $AuCl_4^-$*+PAN+DMF (green curve), crude film from the same solution (pink curve), and crude film from the solution prepared in DMSO (*$AuCl_4^-$*+PAN+DMSO) (blue curve).* ***(B)*** *XRD diffractograms of carbonized fibers with no Au (black curve) and Au@CFs (red curve).*

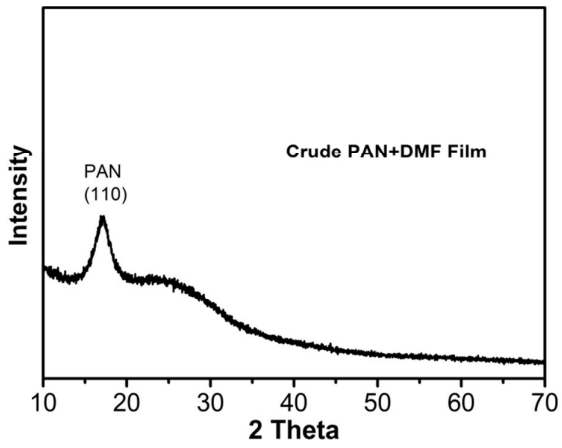

Figure 4.4. *XRD diffractogram of PAN+DMF film.*

The role of DMF in Au particles formation was studied by using DMSO solutions, since DMSO is also a solvent to PAN and it is not known to act as reducing agent, as mentioned earlier. **Figure 4.3A** (blue curve) shows that there is no dependence of the solvent composition on the gold nanoparticles formation. We assume therefore that PAN polymer is acting as a reductive agent and is able to reduce gold salt in mild conditions (70 °C) without the need of extra energy (microwave or UV radiation).

Regarding **Figure 4.3B**, both carbonized fiber samples present on their diffractograms a broad peak in the region of 2θ around 25° that corresponds to the (002) planes, which indicates the presence of graphitic domains according to the literature.[177] For Au@CFs, the other peaks located at 2θ around 38.5°, 44.8° and 64.9° correspond respectively to the (111), (200) and (220) planes of pure face-centred crystalline structure of gold (according to the PDF Card number 00-004-0784 and the literature[198–200]). With the aid of the Scherrer equation (**Equation 3.1** in Chapter III) it is possible to calculate the crystallite size *Lc* of the sample. The value obtained from the XRD peak corresponding to the (111) plane (i.e. peak at 38.5°) is *Lc* = 19.31 nm for gold crystallites on *Au@CFs*.

It is important to note, however, that during the carbonization step at 1000 °C, the NPs growth process continues, given the disappearance of the peak at 31.6° and the increase of peaks (200) and (220).

SEM images of the carbonized fibers prepared from PAN solutions charged with $HAuCl_4$, are presented in **Figure 4.5**, and in **Figure 4.6**, a SEM image of pure *CFs* is presented. Mean fiber diameters are 242 ± 27 nm for pure *CFs* and 691 ± 140 nm for *Au@CFs*. The difference in fiber diameters between pure *CFs* and *Au@CFs* is due to changes in electrospinning dynamics when gold is added to the solution.

The chemical composition of the particles was determined as gold by EDX analysis, as shown in **Figure 4.7**. The element compositions of the *Au@CFs* obtained by EDX are summarized in **Table 4.1**, where we observe that 0.96 atom% or 13.09 mass% of Au is present in the samples. The great majority of the samples are composed of carbon, as

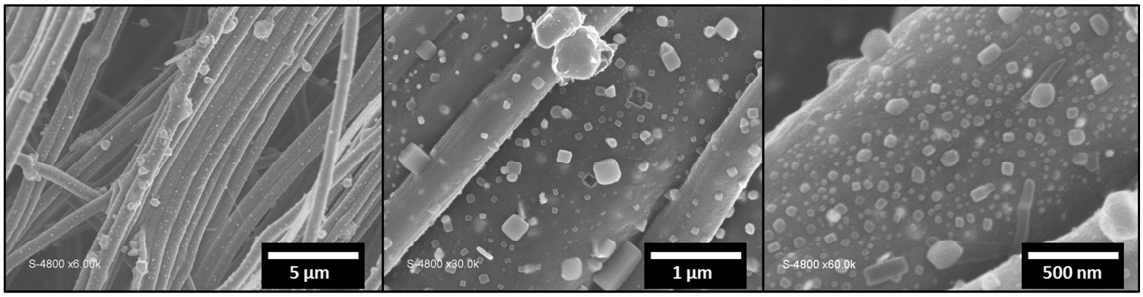

Figure 4.5. *SEM images of Au@CFs at different magnifications.*

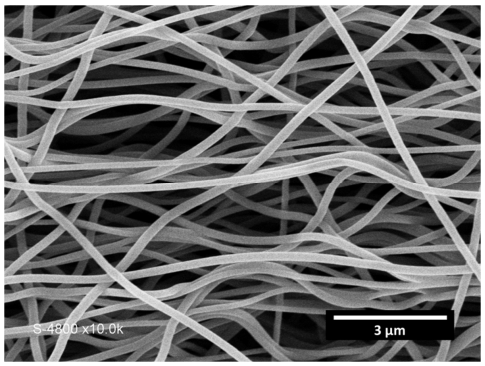

Figure 4.6. *SEM image of pure CFs, carbonized at 1000 °C under N_2.*

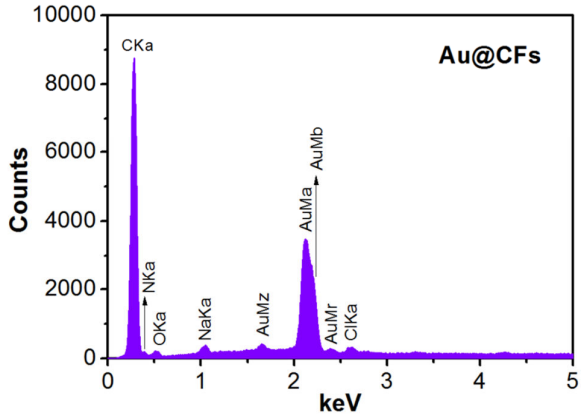

		Au@CFs	
	keV	Mass%	Atom%
C	0.277	58.85	70.86
N	0.392	23.75	24.52
O	0.525	3.65	3.30
Na	1.041	0.42	0.27
Cl	2.621	0.23	0.09
Au	2.121	13.09	0.96
Total		100.00	100.00

Figure 4.7. *EDX plots of Au@CFs with peak indications. The table shows the Elemental composition in weight and atomic percentages determined from the EDX plot. (The Na peak is originated from the conductive tape used on the sample holder of the equipment).*

expected, since the heating temperature of 1000 °C leads to almost all the PAN present on the precursor fibers to carbonize.[10] Since the EDX beam is larger than the particles, it was not possible to analyze one single particle alone (the composition obtained is always a mixture of gold and carbon).

As illustrated by **Figure 4.5**, two ranges of particle sizes are observed: ***i.*** large gold particles with mean size of 214 ± 91 nm; and ***ii.*** small nanoparticles with mean size of 50 ± 13 nm. In order to understand this size distribution, the localization of the nanoparticles in the sample was studied through SEM images recorded at different voltages (1, 5, 15 and 30 kV) (**Figure 4.8**). At lower voltages, only the large surface nanoparticles are detected. As the voltage is increased, the depth of penetration of the SEM electron beam in the sample increases, and smaller NPs embedded in the carbon fibers are then revealed. We can conclude therewith that small NPs are located inside the fibers, while the large ones are on the surface of fibers. This means that the large particles are the ones effectively capable of reacting, for example in the case of glucose oxidation, and the small NPs can play a role in the physical properties of the carbon felts.

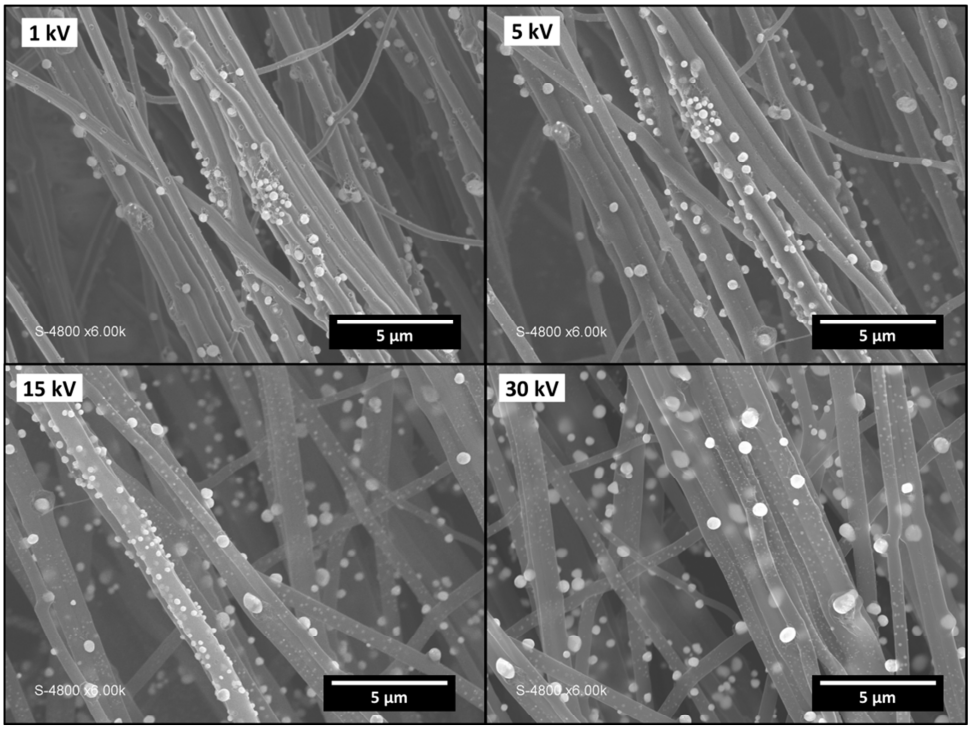

Figure 4.8. *SEM images of Au@CFs carbonized at 1000 °C. Images obtained at different SEM voltages (1, 5, 15 and 30 kV).*

TGA (showed in **Figure 4.9**) was employed for the determination of the amount of gold present on the carbonized samples (*Au@CFs*). TGA of CFs without gold (blue line) shows the combustion of carbon at temperature around 500 °C, and the totality of the sample is decomposed at 600 °C. When gold is present (red line), the combustion of carbon starts at lower temperature (around 450 °C), as expected. The amount of Au on *Au@CFs* was found to be 25.5 wt.% Au (all the rest is due to carbon). Aiming to evaluate the amount of particles distributed internally and on the surface of the fibers, *Au@CFs* were treated in aqua regia (3 parts HCl : 1 part HNO3) for 12 h, so that the Au on the surface of fibers is dissolved in the acid, and only the internal NPs remain within the fibers. Then, TGA was performed (**Figure 4.9**, red line). It was calculated that 8.3 % of the sample is composed of Au present inside the fibers, and therefore 17.2 % of the sample is composed of Au on the surface.

Aiming to study the stability of the Au particles, we performed a simple test by extending the time of the carbonization step from 1 h to 10 h dwell at 1000 °C for the *Au@CFs* sample. SEM images of this sample annealed for 10 h are presented in **Figure 4.10**. The main observation is that two ranges of particles sizes are still present on the sample (with approximately the same diameter that when annealed for only 1 h). The fact that the particles can resist for a long time at high temperature is a good indication that this material is suitable for high temperature applications and especially high temperature catalysis.

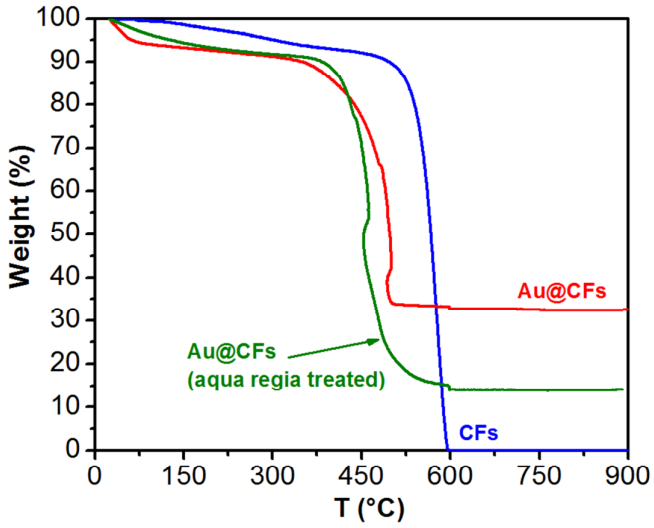

Figure 4.9. *TGA curves of the bare CFs and Au@CFs performed at 10 °C min^{-1} in air (1 h dwell at 600 °C).*

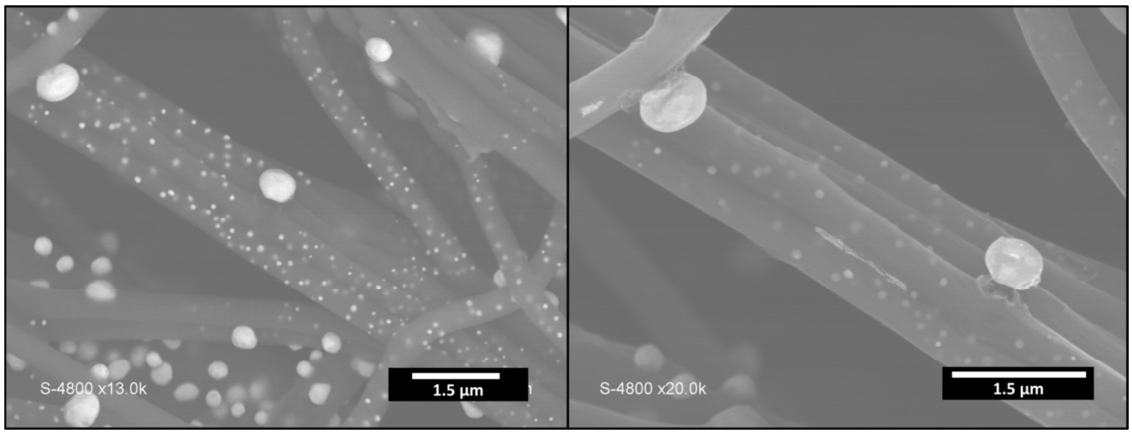

Figure 4.10. *SEM images of Au@CFs at different magnifications after carbonization at 1000 °C for 10 h instead of 1 h. The presence of small and large particles is still observed.*

4.4. Electrical conductivity of the felts

In order to evaluate if the presence of Au could have an effect on the electrical conductivity of the material, electrical conductivity measurements were performed in a Swagelok cell, where the felts were pressed between two stainless steel plates. This method was chosen for simplicity and to check how different methods of measurement affect the results of electrical conductivity of fibers. The conductivity of the bare *CFs* was calculated to be around 3 S m^{-1}. Regarding the gold modified fibers, *Au@CFs,* the conductivity was around 10 S m^{-1}. This increase may be thanks to the presence of gold, since during the measure in the Swagelok cell the felts are pressed, which allows gold NPs to create a preferential path for electrons flow. However, it may also be simply due to the variation on electrospinning conditions with gold salt in the solution, which resulted in different fiber diameters.

The conductivity of the bare randomly organized CNFs studied in Chapter II (also carbonized at 1000 °C) was measured by the Van der Pauw four-point probe method and a value of 1,000 S m^{-1} (10 S cm^{-1}) was obtained.[172] The difference between the two methods is due to the fact that, with the four point probe, the conductivity results from the flow of the electrical current along the longitudinal direction of the felt and not along the transverse direction. Although, to our knowledge no work reports on conductivity measurements in Swagelok cell for electrospun carbon felts, electrical conductivity in the same order of

magnitude were obtained with the Swagelok cell for other carbon materials, like single and double layer papers composed of lithium iron phosphate, Super P carbon particles and nano-fibrillated cellulose (0.02 and 0.14 S m^{-1}).[169]

4.5. Cyclic voltammetry and electrochemical impedance spectroscopy characterization

In order to evaluate the electrochemical and diffusion behavior of the electrodes *CFs* and *Au@CFs*, CV and EIS were performed in the presence of the redox probe $Fe(CN)_6^{3-/4-}$ in 0.1 M KOH medium. **Figure 4.11A** shows the typical CVs that depict the oxidation and reduction peaks of ferricyanide/ferrocyanide at the scan rate 10 mV s^{-1}, for both felts with and without gold. The values of the peak-to-peak separation *ΔEp* are 300 mV and 250 mV for electrodes with and without gold, respectively, due to small differences in fiber morphology (electrospinning conditions). For each electrode, CVs were performed at several scan rates varying from 2 to 1,000 mV s^{-1}. For each voltammogram, peak shape is observed, which represents linear diffusion. From the plot of the peak-to-peak separation *ΔEp versus* ln $v^{1/2}$ (where *v* is the scan rate) presented in **Figure 4.11B**, according to the Nicholson's method (explained in Chapter 1.4), it is possible to calculate the apparent rate constants (k°_{app}) of heterogeneous electron transfer at high scan rates, where the mass transport is not limiting.

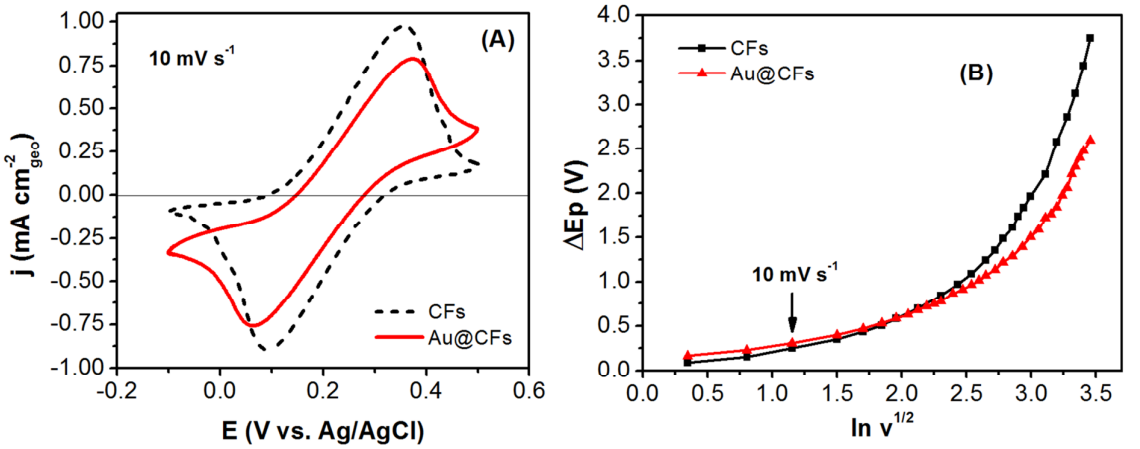

Figure 4.11. (A) *Cyclic voltammetry realized in 10 mM* $Fe(CN)_6^{3-}/Fe(CN)_6^{4-}$*, in 0.1 M KOH medium at the electrodes CFs and Au@CFs at 10 mV* s^{-1}*.* ***(B)*** *plot of ΔEp versus ln* $v^{1/2}$ *(v is the scan rate, varied from 2 to 1,000 mV* s^{-1}*) for the same electrodes, according to the Nicholson's method.*

The shape of the curves presents two zones: the first where the electrodes are characterized by similar *ΔEp*, and the second where *ΔEp* differences are accentuated (for $v > 160$ mV s^{-1}, or ln $v^{1/2} > 2.5$). At the second region the comparison of carbon felt electrodes with and without the presence of gold can be realized.

The k°_{app} obtained for the electrodes are presented in **Table 4.2**, and represent the influence of the nature of the electrodes surface on the reaction kinetics. The redox probe $Fe(CN)_6^{3-/4-}$ is known to be very sensitive to surface modification.[201,202] The k°_{app} value calculated for *Au@CFs* is twice as high as the one obtained for bare *CFs* electrode, which clearly indicates that the presence of gold on the electrode improves the electron transfer kinetics.

The k°_{app} values can be employed for the calculation of the theoretical charge transfer resistances (R_{ct}) on the electrodes, according to the **Equation 4.2**:

$$R_{ct} = \frac{RT}{F^2 K^{\circ}_{app} AC} \qquad (4.2)$$

where

- *R (J K^{-1} mol^{-1})* is the gas constant,
- *T (K)* the temperature,
- *F (C mol^{-1})* the Faraday constant,
- *A* (cm) the electrode surface area,
- *C (mol cm^{-3})* the concentration of ferricyanide/ferrocyanide in the medium.

Table 4.2. *Values for the apparent rate constant k°_{app} (cm s^{-1}) determined from CVs, charge transfer resistance R_{ct} (ohm) obtained by calculation and experimentally from Nyquist plots, and Warburg coefficients σ (ohm $s^{-1/2}$) obtained by calculation and experimentally from EIS analysis.*

		Charge Transfer Resistance (ohm)		**Warburg coefficient σ (ohm $s^{-1/2}$)**	
	k°_{app} (cm s^{-1})	R_{ct} theoretical *(from Eq. 1)*	R_{ct} experimental *(from semicircle diameters of EIS plots)*	σ_{exp} *(slope of -Z'' vs. $\omega^{-1/2}$)*	σ_{theo} *(from Eq. 2)*
CFs	$(1.0 \pm 0.2) .10^{-2}$	36	16	189	271
Au@CFs	$(2.0 \pm 0.2) .10^{-2}$	9	13	242	254

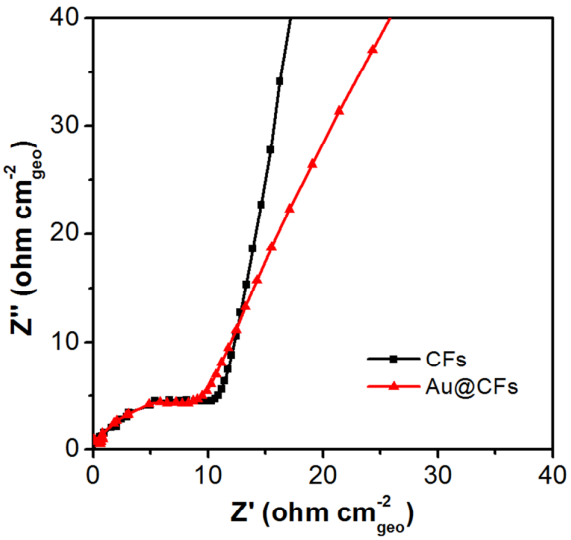

Figure 4.12. *Nyquist plots of bare CFs and Au@CFs in 0.1 M KOH containing 10 mM* $Fe(CN)_6^{3-}/Fe(CN)_6^{4-}$. *Frequency range from 10 kHz to 0.1 Hz, with 10 points per decade, at the half wave potential (*$E_{1/2}$ *= 0.208 V vs. Ag/AgCl).*

The theoretical R_{ct} values are presented in **Table 4.2** and we can observe that the presence of gold on the electrodes results in a reduction in the electrochemical resistance, as expected.

This result can be verified by EIS measurements. In **Figure 4.12**, Nyquist plots present a semicircle at high frequencies, followed by a linear region at low frequencies. When this line is at 45°, it means the behavior is typical of Warburg impedance (i.e. linear semi-infinite diffusion of species), which is not the case. It is common to interpret Warburg governed EIS spectra by the Randles equivalent circuit. However, Randles circuit was not able to fit the EIS data of **Figure 4.12**. This means the equivalent circuit that corresponds to the behavior of bare *CFs* and the *Au@CFs* electrodes is more complicated than the Randles circuit, which takes into account the electrolyte resistance, the charge transfer resistance, the Warburg coefficient and the double layer capacitance of the system. In the case of the nanostructured electrodes developed here, additional phenomena are relevant and the charge transfer resistance should be consisted of several terms regarding the electron transfer between

i) the solution and the carbon fibers,

ii) the solution and the Au particles, and also

iii) between the Au particles and the carbon fibers.

Besides, the mass transport of the redox species is composed of the diffusion that occurs in the bulk and inside the fiber mat (including the diffusion layer at individual fibers and at multiple single fibers, depending on the interfiber distance). Each of these

phenomena would add in the complexity of the equivalent circuit. Since it is not the objective here, we did not go further on the fitting of the EIS data to a more complex circuit. It is known, however, that the diameter of the semicircle in Nyquist plots is equivalent to R_{ct}.[201] R_{ct} values obtained from the plots (measuring of semicircle diameters) are depicted in **Table 4.2**, and are in the same order of magnitude of the ones obtained by calculation, which validates the analysis.

Finally, the Warburg coefficients were obtained by two ways. First, experimentally, considering that when the mass transport is governed by diffusion, the plot of the imaginary part of the impedance *-Z'' versus* $\omega^{-1/2}$ (ω is the angular frequency) gives a line whose slope is the Warburg coefficient (σ_{exp}).[201] The second way was theoretical, by considering the **Equation 4.3**:

$$\sigma_{theo} = \frac{RT}{F^2 A\sqrt{2}} \left(\frac{1}{D_{ox}^{1/2} C_{ox}^{*}} + \frac{1}{D_{red}^{1/2} C_{red}^{*}} \right) \quad (4.3)$$

where

- D ($D_{ox} = D_{red} = 7.0 \times 10^{-6}$ cm² s^{-1}) is the diffusion coefficient of the oxidized and reduced species, and
- C is the bulk concentrations of oxidized and reduced species ($C_{ox} = C_{red} = 0.5$ mM).

The results obtained experimentally or theoretically (presented in **Table 4.2**) are similar for both techniques of calculation. Since σ values are close for both electrodes, the mass transport is not affected by the presence of gold.

4.6. Conclusion

The one pot route synthesis of a new nanocomposite material composed of gold particles embedded in carbon fibers was reported in this chapter. The material was characterized by SEM where two ranges of particles sizes were measured. By performing SEM analysis at different voltages, it was determined that the smaller range of NPs was located inside the carbon fibers, whereas the larger particles are located on their surface. This might mean that only the particles located on the surface can act as catalysts, whereas the interior particles might participate on physical properties of the fibers. We have determined for the first time that PAN polymer is acting as a reductive agent and was able to generate gold nanoparticles at moderate temperature. The nanocomposite exhibits

remarkable high temperature stability since the gold nanoparticles were able to support a thermal treatment of 10 h at 1,000 °C without losing their nanostructuration. Electrical conductivity was measured with a Swagelok cell, and the values of 3 S m^{-1} (bare CFs) and 10 S m^{-1} (*Au@CFs*) were obtained. Gold modified fibers present higher electrical conductivity because during the measure in the Swagelok cell, the felts are pressed, which allows gold NPs to create a preferential path for electrons flow.

Electrochemical analysis (CVs and EIS) were crucial for the better understanding of electron transfer and diffusion through the electrolyte/carbon/gold system. Apparent rate constants for the ferricyanide/ferrocyanide redox reaction were calculated, enabling the calculation of the charge transfer resistance of each electrode. *Au@CFs* provides faster kinetics than *CFs*. The Warburg coefficient was also calculated, and similar values were obtained for both electrodes studied, meaning that the presence of gold does not affect the diffusion of the species in the felt. The electrodes were also tested towards the electrochemical oxidation of glucose in alkaline medium, which proved its efficiency thanks to current densities of about 2 mA cm^2. The perspectives for the new material developed in this work are, at first, the use as anodes in a complete hybrid glucose fuel cell, as will be shown in Chapter 7.3. Secondly, high temperature catalysis applications can be envisaged due to the exceptional thermal stability of the nanocomposite, as well as other monosaccharide oxidation reactions catalyzed by gold.

Conclusion of Part 2

The synthesis and characterization of electrospun CNFs was described in Part 2. Different CNF-based materials were presented: randomly organized fibers modified or not with carbon nanotubes onto fibers surface, aligned fibers and CFs modified *in situ* with gold particles. Electrical conductivity measurements as well as cyclic voltammetry results showed that improvements were achieved compared with the basic unmodified CNFs: when CNFs were modified with adsorbed CNTs, the available surface increased compared to bare CNFs, and aligned fibers presented better electron transfer than random ones. Also, CNFs modified *in situ* with gold particles were successfully achieved by a simple method, and it was found that Au-modified fibers allow faster kinetics than the bare CNFs. These results mean the goals that were set were so far accomplished.

The random CNFs, CNTs@CNFs and aligned CNFs materials will be employed as electrode materials for the biocathode compartment of a BFC in Part 3 of this work. They will be modified with enzymes and electron transfer mediators and tested in a half-cell biocathode for the O_2 reduction reaction (ORR). Au-modified CFs will, on the other hand, be tested as electrodes for glucose electrooxidation, since gold can catalyse this reaction.

PART 3:

BIOFUEL CELL ASSEMBLY

Introduction of Part 3

In this part of the work, the materials presented in Part 2 will be employed as electrode materials for bioelectrochemical reactions. Firstly, in **Chapter V**, the enzyme immobilization technique will be optimized onto the developed fibers by testing different strategies. Focusing on the O_2 reduction reaction (ORR), which is typical in the cathode compartment of BFCs, appropriate enzymes will be entrapped onto the CNFs with different polymers (Nafion, polypyrrole or chitosan).

The following chapters will be dedicated to the test of complete BFCs, employing biocathodes that were optimized in Chapter V. In **Chapter VI**, the creation and test of an enzymatic BFC powered by ethanol will be presented, where the bioanode was developed with similar optimized technique to the biocathode. Finally in **Chapter VII**, two different hybrid BFCs powered by glucose will be shown. In the first one the anode compartment is composed of aligned CNFs modified with metallic nanoparticles: Au-based nanoparticles modified with Pt and/or Pd. This anodic structure was developed by a partner from IC2MP laboratory. The second hybrid BFC will employ as anode the gold-modified CNFs that were presented in Chapter IV, which will be shown to be able to catalyze glucose oxidation.

Chapter V. Optimization of the enzyme immobilization technique onto CNFs for O_2 reduction reaction

5.1. Introduction

Enzymatic reduction of O_2 is an important topic in biofuel cells development.[89] For this reason, development of cathodes modified with redox enzymes is a challenge since it allows to perform oxygen reduction at low overpotential.[86] As seen in Chapter I, considering the application in biofuel cells, many are the possible enzyme immobilization strategies, and each one has its pros and cons. In this chapter, the immobilization techniques we explored will be presented. They consist of encapsulation and reticulation techniques, where a polymer matrix entraps all the species, the polymer being reticulated or not. Three different polymers were employed for entrapment of species: Nafion®, Polypyrrole and the biopolymer Chitosan. In this chapter, both MET and DET (i.e. mediated and direct electron transfer) will be addressed. First, MET will be achieved through the immobilization of species in Nafion® or Polypyrrole matrixes. Then, DET between the enzyme and electrode material will be performed with chitosan in the presence of CNTs.

Two enzymes are employed in this work as catalysts for the O_2 reduction reaction: laccase and BOD (bilirubin oxidase). Both are multicopper oxidoreductases that catalyze the 4-electron reduction of O_2 completely to H_2O, which can be achieved in the presence of the electron transfer mediator ABTS.[86] By oxidizing the mediator $ABTS_{red}$, laccase acquires the necessary electrons to reduce dioxygen into water, and $ABTS_{ox}$ is reduced on the electrode surface. Direct heterogeneous electron transfer (DET) between redox centers of the enzyme and electrode (i.e. without ABTS) has been achieved by proper immobilization using carbon nanotubes as promoters for suitable orientation.[203]

The laccase enzyme employed here has its maximum activity when working in a solution at pH 5. For this reason, it would not be suitable for applications in implantable devices, since they operate under physiological conditions (pH around 7 – 7.4 and temperature around 30 – 37 °C). BOD enzyme (from Amano), on the other hand, has its optimal pH range at neutral pH. It was thus employed aiming future applications in implantable devices.

For the Nafion® encapsulation, known quantities of enzyme and mediator were mixed together in the presence of the polymer matrix. Polypyrrole entrapment strategy was a little different, since after a coating of enzyme, polypyrrole was electropolymerized onto the electrode along with ABTS, so that the actual amount of ABTS that was entrapped was not known. Chitosan immobilization was accomplished in the absence of ABTS (DET). A film of chitosan was placed on top of the enzymes onto the electrode, creating a protective film layer.

The porous structure and the large surface area of CNFs felts makes them ideal for enzyme immobilization leading to high content of electrically contacted enzyme molecules per unit of geometric surface area of the electrode and thus higher catalytic current density.[204] In this chapter, both randomly organized CNFs felts and aligned felts will be employed as bioelectrode materials, and the performance will be characterized. Only half-cell performances will be evaluated (i.e. cathodic side toward O_2 reduction), and in the following chapters, complete biofuel cells will be presented. To our knowledge, this was the first time that the anisotropic properties of carbon fibers were employed for the benefit of bioelectrochemical applications, such as the one explored here, and that can be extended to the more general application that are biofuel cells electrodes.

5.2. Laccase entrapped in Nafion® matrix

We showed in Chapter II the synthesis of random fibers carbonized at different temperatures (1000, 1200 and 1400 °C) that were characterized through cyclic voltammetry. This analysis allowed the selection of the CNFs treated at 1200 °C as the best compromise between small ΔEp (good electron transfer kinetics) and higher Ip_a (more accessible electroactive surface). In this section, random and aligned CNFs carbonized at 1200 °C that were presented in Part 2 are employed and compared as electrode material for O_2 electroreduction, covered on the surface by a mixture of laccase, ABTS and carbon Vulcan

particles entrapped in Nafion® polymer. The presence of carbon Vulcan is a common option to increase enzyme loading.[205] The performance of the bare random CNFs is also compared with CNTs-modified random CNFs, as a continuation of characterizations realized in Chapter II. CNTs have been extensively used for the construction of bioelectrodes, due to their ability to promote electron transfer reactions between immobilized enzymes and electrodes.[206] The advantages of electrospun CNFs and CNTs were combined to develop suitable conductive support for enzyme immobilization.The CNTs@CNFs electrodes were also tested with and without ABTS in order to test the potential of such electrodes for achieving DET.

5.2.1. Materials and methods

The bioelectrodes to be employed in the electroreduction of oxygen were prepared by adsorption of enzymes and mediators on the surface of the electrodes by drop casting technique. This procedure, schematized in **Figure 5.1**, consisted in depositing on the electrodes surface (geometric surface: 2 faces of 0.25 cm^2, thus 0.5 cm^2 in total) a droplet of 20 µL of a mixture containing laccase from *Trametes versicolor* (7.5 mg mL^{-1}, from Sigma Aldrich, ≥10 U mg^{-1}), ABTS (2.4 mg mL^{-1}, from Sigma Aldrich), carbon vulcan (7.5 mg mL^{-1},

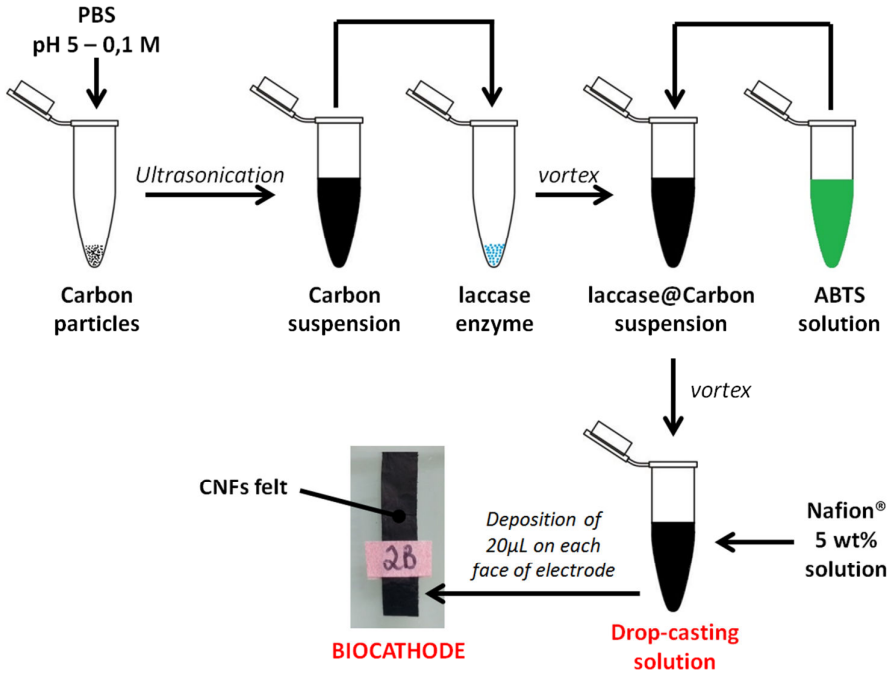

Figure 5.1. *Scheme of cathodes preparation: laccase entrapped in Nafion® polymer matrix.*

from Cabot Corporation) and Nafion® perfluorinated resin solution (5.0 vol% in lower aliphatic alcohols and water, from Sigma Aldrich) in PBS (pH 5, 0.1 M, prepared from $NaH_2PO_4 \cdot 2H_2O$ and Na_2HPO_4 from Sigma Aldrich using ultrapure water, 18.2 MΩ·cm, 25 °C). The samples were then dried at 5 °C overnight. The enzyme loading was estimated to 300 µg cm^{-2} (taking into account the geometric surface area of the electrode). Linear scan voltammetry measurements at scan rate of 3.3 mV s^{-1} were determined in dioxygen-saturated PBS at pH 5 after stabilization of the cathode open circuit potential. The current density was determined from the geometric surface area of the electrodes.

5.2.2. Test of biocathodes toward ORR with random CNFs electrodes

Figure 5.2 presents linear scan voltammetry measurements to evaluate the electrochemical performance of the biocathodes towards O_2 reduction, in buffer solution (pH 5.0) saturated in oxygen, with a typical three electrode system composed of working electrode (CNFs), reference electrode (Ag/AgCl saturated KCl) and counter electrode

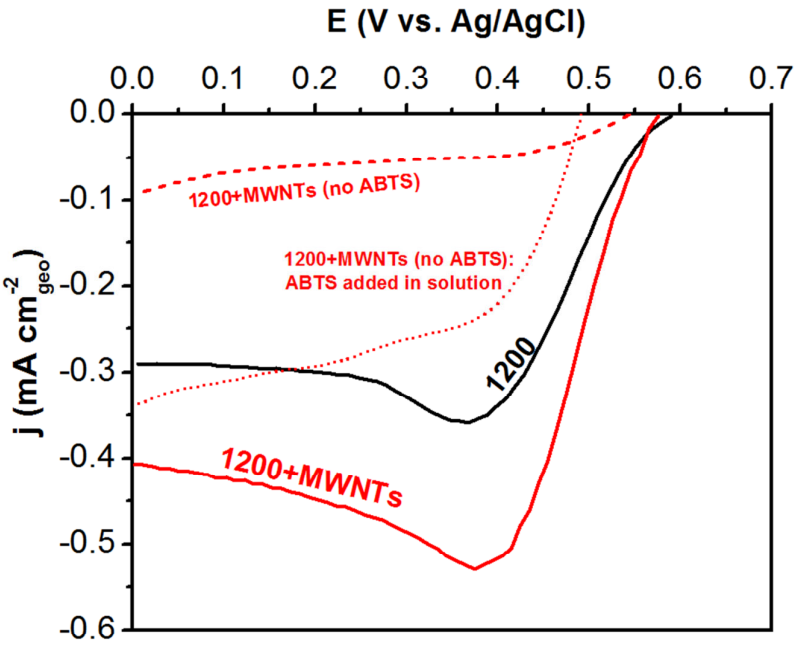

Figure 5.2. *Polarization curves of a laccase/ABTS/Nafion modified electrode in O_2 saturated PBS (pH 5.0, 0.1 M). Comparison between electrodes carbonized at 1200 °C with MWNTs adsorbed (red line) and without MWNTs (black line) on CNFs. Dashed line: 1200+MWNTs electrode prepared with no ABTS. Dotted line: 3 mM ABTS is added in the solution of the electrode with no immobilized ABTS. Scan rate 3.3 mV s^{-1}.*

(stainless steel plate) connected to a potentiostat (Ametek VersaStat). This assembly was the same throughout this work, and more details are presented in **Annex 2**. Polarization curves (obtained from scanning the electrode potential from the open circuit voltage, V_{OC}, to 0 V vs. Ag/AgCl) show high current density values, in the range 300 – 400 μA cm^{-2}, associated to the enzymatic O_2 reduction. The oxygen reduction current begins at 0.6 V *vs.* Ag/AgCl, without overpotential, and current densities feature a semi-plateau that indicates the control of the catalytic reaction by diffusion of the oxygen to the electrode surface.

Current densities are improved by 33% for random electrospun CNFs modified with MWNTs (0.4 mA cm^{-2}), with no variation of V_{OC}, which make such new electrodes attractive as cathodes for biofuel cells. This result demonstrates that enhancing effective electroactive surface area of the electrode with the presence of CNTs is a key feature regarding enzyme immobilized reactions. Although comparison with the reported literature is not obvious, our system presents competitive efficiency with other reported values focusing on the immobilization of the couple laccase/ABTS by encapsulation in silica matrix on porous carbon paper supports[207] (450 μA cm^{-2} at pH 6 with estimated laccase loading of 190 μg cm^{-2}), by entrapment within layered double hydroxides[208] (70 μA cm^{-2} at pH 6 with estimated laccase loading of 600 μg cm^{-2}) or by entrapment in polypyrrole on porous carbon tubes[209] (300 μA cm^{-2} at pH 4.8, with estimated laccase loading of 190 μg cm^{-2}).

The CNTs@CNFs electrodes were also tested in the absence of ABTS, as shown by the dashed curve in **Figure 5.2**. V_{OC} in this case (0.54 V) is slightly lower than electrodes containing ABTS ($V_{OC} \cong 0.57 – 0.6$ V, which is close to the theoretical redox potential of laccase of 0.59 V vs. Ag/AgCl or 0.79 V vs. SHE [112]), and the current density attains only 0.1 mA cm^{-2}, which is 4 times lower than when ABTS is present as electron transfer mediator. This shows DET is achieved at some extent (not only thanks to the current delivered, but also because V_{OC} without ABTS is almost unchanged, meaning the enzymes are still "wired"), but it appears the amount of CNTs present on the surface of CNFs might not be sufficient for enabling DET of all the enzymes present, since current density is much lower. The role of CNTs is mainly related to electroactive surface properties. The proof that not all the enzymes are "wired" by the CNTs is clear when an excess of ABTS (3 mM) is added in the solution. The current density increases until more than 0.3 mA cm^{-2}, which is almost the original current of the 1200+MWNTs electrode. In this study, no effort was done to

modify the CNTs in order to orientate the site T_1 of the enzyme for more efficient direct electron transfer, which is a possible strategy.

An observation concerning the article in journal Nanotehnology where these results have been published is necessary. There,[172] the electrodes geometric surface that was considered for the normalization of the results in mA cm^2 was only one face of the felts. However, we understand that the reaction takes place on both sides of the electrodes, since their structure is porous, and the enzyme solution is able to cross the whole felt, being available from both sides of the electrode. Therefore, the results from the publication were divided by 2, considering the surface as 2 faces. Figure 5.1 depicts the new results where the correct surface area is considered (in the following of this work, 2 faces were always considered).

We acknowledge that by referring the current density toward the geometric surface, we do not take into account the three dimensional structure of our electrodes, since the current density is normalized by the projected surface area of the electrodes. As mentioned by the works of Mano at al.[210], the projected area bears no relation between the volume, the geometry and weight of the electrode material, and should not be the appropriate normalization criteria.

5.2.3. Test of biocathodes toward ORR with aligned CNFs electrodes

Aligned CNFs were employed as well as electrode materials and modified with laccase, carbon particles and ABTS in a Nafion matrix. Polarization curves obtained in O_2-saturated PBS are presented in **Figure 5.3** (blue curve), in comparison with the curve obtained with random CNFs (dashed gray line, the same as black line in **Figure 5.2**). The V_{OC} obtained with aligned CNFs is slightly higher than the V_{OC} of random CNFs, around 0.63 V. The current density obtained with aligned CNFs as electrodes is of 0.4 mA cm^{-2}, while random CNFs deliver around 0.3 mA cm^{-2}. This result highlights the advantages of the spatial organization of CNFs, which have already been analyzed in Chapter III, however here it is possible to observe that the enhanced electronic transfer through aligned CNFs is also useful toward ORR.

Furthermore, the current density obtained with aligned CNFs is very similar to that obtained with random CNFs modified with MWNTs. Therefore, it is very likely that the current density of aligned CNFs could still be enhanced via modification with MWNTs.

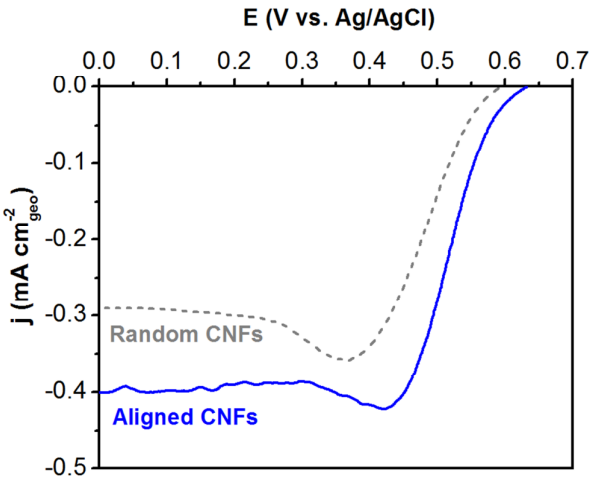

Figure 5.3. *Polarization curves of laccase/ABTS/Nafion modified electrodes in O_2 saturated PBS at pH 5.0, 0.1 M. Comparison between the random CNFs electrode presented in Figure 5.2 (here in gray dashed line), and an electrode composed of aligned CNFs (blue line), both carbonized at 1200 °C. Scan rate 3.3 mV s^{-1}.*

However, this strategy is not explored here, mostly because the amount of MWNTs that is adsorbed in the surface of CNFs by dipping is not sufficient for achieving DET (at least in the conditions employed here, with no surfactants or other agents), as shown previously, which is a key point for the creation of a viable BFC. In a forward section, MWNTs will be employed along with aligned fibers, not via the dipping method, but in a strategy that shall allow DET.

5.3. BOD enzyme entrapped in Nafion® matrix

Aligned felts were seen in Chapter III to present enhanced performance concerning electrical conductivity measurements compared to randomly organized CNFs. In addition, in the previous section their performance toward ORR was shown to be higher than random CNFs when the simple immobilization technique with Nafion polymer was employed. In this section, the enzyme BOD will be employed with the same immobilization technique, with the advantage that BOD can operate at neutral pH, instead of laccase (pH 5). Thus, applications in the field of implantable devices can be envisaged. A complete optimization of the biocathode composition is presented regarding the ratio of BOD and ABTS quantities in the film, the quantity of enzyme given a fixed ratio of ABTS, the concentration of Nafion® and finally the stability over time of the biocathodes. A comparison was made between the

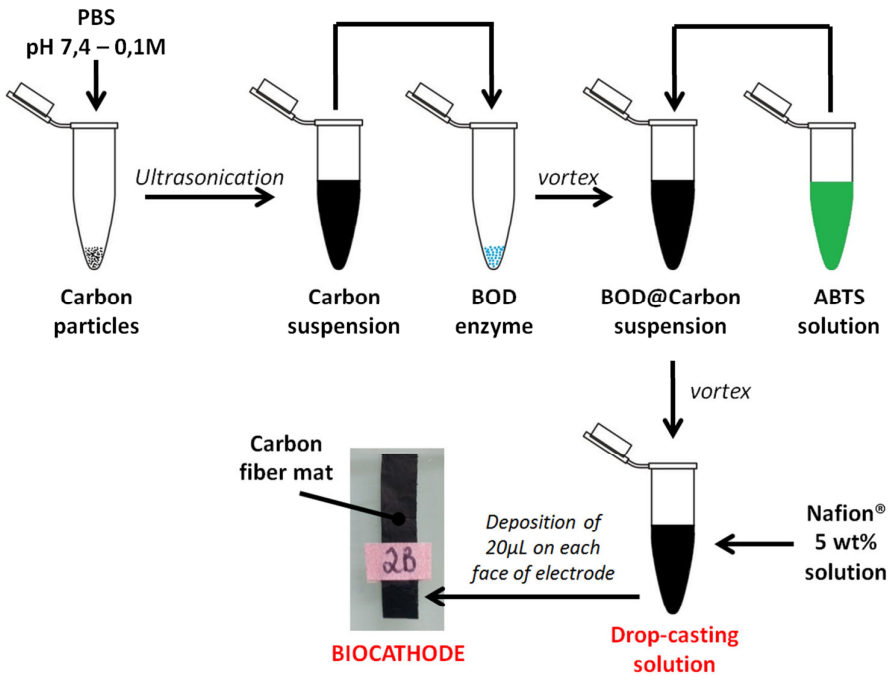

Figure 5.4. *Scheme of cathodes preparation: BOD entrapped in Nafion® polymer matrix.*

aligned CNFs felts and a dense glassy carbon electrode, and the advantages of the porous structure were highlighted.

The results from this section were published in a paper in collaboration with our colleagues from Poitiers, France (IC2MP laboratory) in The Journal of Physical Chemistry C.[106]

5.3.1. Materials and methods

The preparation protocol, which is depicted in **Figure 5.4**, consisted on, first, ultrasonicating carbon particles (0.04 µm grain size, specific surface area 62 $m^2 g^{-1}$, Super P from Timcal) with an optimized concentration of 7.5 mg mL^{-1} in PBS (pH 7.4, 0.1 M, prepared from $NaH_2PO_4 \cdot 2H_2O$ and Na_2HPO_4 from Sigma Aldrich using ultrapure water) for 30 minutes in a sonication bath. Then, BOD enzyme (33.6 mg mL^{-1}, from Amano, 3.04 U mg^{-1}) and ABTS (3.4 mg mL^{-1}, from Sigma Aldrich) were added to this solution and mixed in a vortex for 20 minutes. Nafion® perfluorinated resin solution (5.0 vol% in lower aliphatic alcohols and water, from Sigma Aldrich) was added thereafter in a concentration of 5.0 vol.%, and rapidly mixed together, thus finalizing the enzyme solution preparation. 40 µL of the final solution were dropped on the electrode (geometric surface of 0.7 × 0.7 cm^2 each face, i.e. 0.98 cm^2)

and left to dry overnight at 5 °C. Nafion® acts as an insoluble polymer electrolyte to hold the species on the electrode surface. The enzyme loading was varied on the electrode: 2.8, 5.6, 8.4, 11.2, 16.8 and 22.4 nmol cm^{-2} were deposited relative to the electrode geometric surface (considering both faces).

5.3.2. Test of biocathodes toward ORR

The catalytic activity of BOD was studied in the presence of the mediator ABTS as an electron relay. The composition of the coating solution was optimized in terms of the ratio between the ABTS and BOD concentrations. For optimal ABTS/BOD ratio, the amount of BOD enzyme was varied on the electrode surface, as well as the amount of Nafion® polymer in the coating solution. A study of the stability of the bioelectrodes over time and the advantages of the porous structure in comparison with a dense structure was also performed.

5.3.3. Optimization of the biocathode composition

Influence of the ratio between ABTS and BOD concentrations. The coating solution composition was optimized in terms of the molar ratio between ABTS and BOD. During the catalysis process, 4 electrons are transferred from ABTS to the active sites of BOD composed of four copper sites to reduce subsequently dioxygen into 2 equivalents of water (as shown previously in Chapter I). However, since ABTS is a small and soluble molecule that is difficult to keep immobilized onto the electrode, it becomes necessary to add a higher amount of ABTS regarding the enzyme. In this work, the molar ratio of ABTS/BOD was varied between 100 (highest ABTS concentration) to 10 (lowest ABTS concentration) and compared with the electroactivity of two reference cathodes modified only with BOD or ABTS.

The polarization curves obtained for the CNFs electrodes modified according to these ratios are showed in **Figure 5.5A**. In the absence of BOD, the cathode consisting of ABTS/Super P/Nafion® ink shows extremely low electrochemical activity for the ORR beginning at a potential 0.52 V *vs.* Ag/AgCl. However, the cathode BOD/Super P/Nafion® ink, in the absence of ABTS, shows an onset potential 50 mV more positive with higher delivered current densities, pointing out direct electron transfer between a portion of the immobilized enzymes and the electrode. When BOD and ABTS are co-immobilized on the CNFs cathodes, higher current densities are delivered and the significantly decreased slope of the

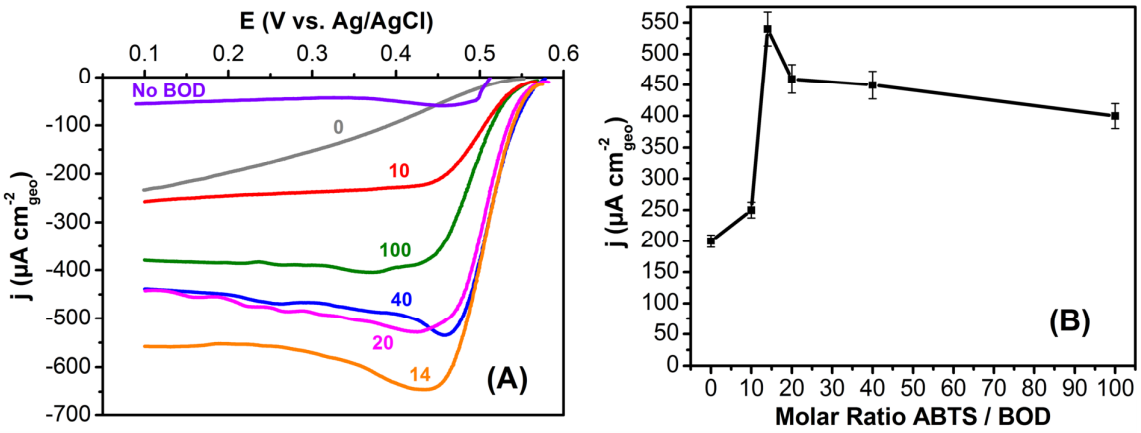

Figure 5.5. (A) *O_2 reduction polarization curves of CNFs biocathodes with different molar ratios between ABTS/BOD (indicated next to the curves) immobilized on the electrode surface (other components concentrations kept constant), and* ***(B)*** *comparison of the maximum cathodic current density obtained according to the molar ratio ABTS/ BOD of the coating solution (j_{max} read at 0.2 V vs. Ag/AgCl). Scan rate of 3.33 mV s^{-1}, PBS 0.1 M, pH 7.4 at 34 °C saturated with O_2.*

polarization curves corresponds to almost no activation losses, attributed to enhanced electronic communication between the enzymes and the electrode promoted by the presence of ABTS. **Figure 5.5B** presents the trend of j delivered at 0.2 V *vs.* Ag/AgCl, where we can observe that the ideal ratio between ABTS and BOD, necessary for the achievement of optimal j, is around 14. For higher ratio, the excess of ABTS does not contribute favorably to the increase of j, even leading to lower electrochemical activity for the ORR. According to previous works, an excess of ABTS can lead to instability and fast deactivation of the enzymes.[203] Considering these results, the ratio ABTS/BOD of 14 was selected for the following tests.

Variation of BOD enzyme amount. From the optimal ratio ABTS/BOD, the amount of BOD on the electrode surface was optimized, as presented in **Figure 5.6A** with the evolution of the maximal current density j_{max} (at 0.2 V vs. Ag/AgCl) in function of enzyme amount (nmol cm^{-2}). As observed, j_{max} increases sharply with increasing amounts of biocatalysts from 2.8 to 5.6 nmol cm^{-2}. For higher BOD loadings, the increase is less pronounced indicating that not all of the immobilized enzymes participate in the ORR. The BOD amount was thus fixed to 11.2 nmol cm^{-2}, as the best compromise.

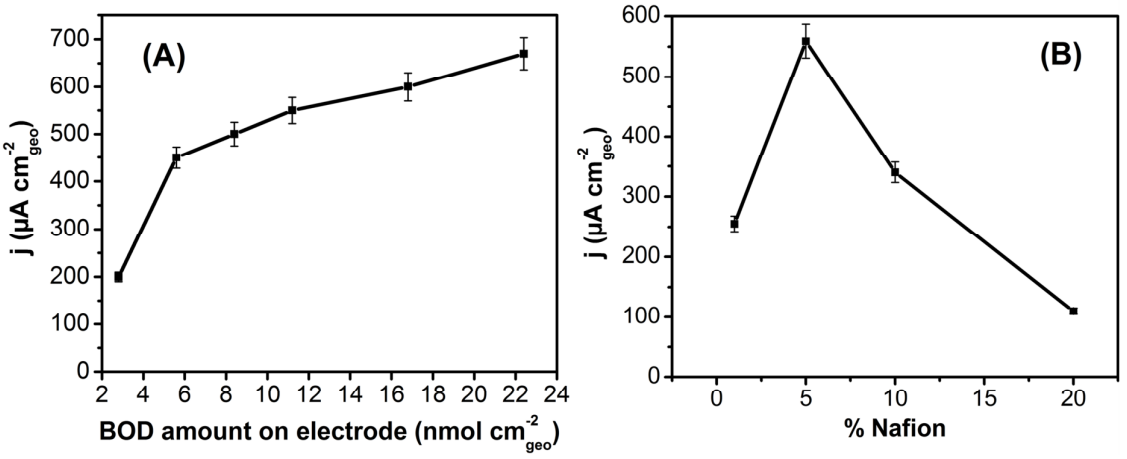

Figure 5.6. *Evolution of the maximum cathodic current density j_{max} (at 0.2 V vs. Ag/AgCl) according to* ***(A)*** *the enzyme amount on the electrode and* ***(B)*** *the Nafion® concentration, with the ratio ABTS/BOD constant to 14 and the optimized BOD concentration.*

Influence of Nafion® concentration in the coating solution. In order to optimize the immobilization of enzyme and mediator on the surface of the carbon fibers via entrapment in Nafion®, the influence of this polymer concentration was studied. Nafion® should prevent the release of the entrapped components to the solution, and allows for H^+ and O_2 diffusion to the electrode surface. Nafion® concentration was varied from 1 to 20 % in the coating solution containing optimized amount of BOD enzyme, ABTS mediator and Super P carbon particles. As observed in **Figure 5.6B**, j_{max} increases sharply (at 0.2 V vs. Ag/AgCl) when Nafion® amount varies between 1 and 5 %. However, higher amounts are harmful to the efficiency of the biocathode, probably due to the thickness of the polymer layer that prevents the diffusion of O_2 within the enzyme layer. An amount of Nafion® of 5 % has thus been chosen to construct the biocathodes.

Although comparison with literature is not straightforward (due to differences in enzyme nature and activity, concentrations, cell designs, electrode materials, etc.), these CNFs-based biocathodes present competitive efficiency with other reported works[48,49] focusing on nanostructured electrodes for bioelectrocatalysis of dioxygen reduction.

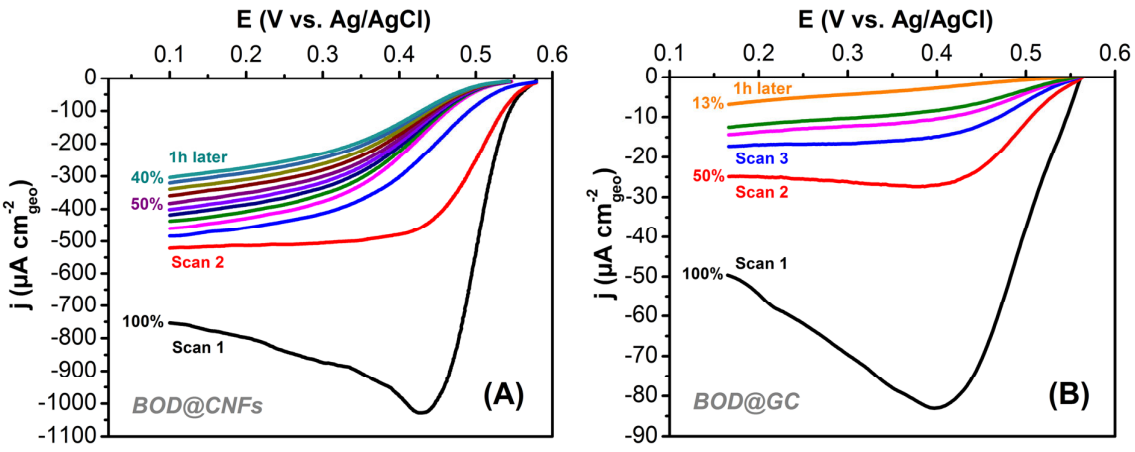

Figure 5.7. *Polarization curves of the biocathode towards ORR with BOD/ABTS immobilized on* ***(A)*** *CNFs electrode (porous structure) and* ***(B)*** *Glassy Carbon electrode (dense structure). Both electrodes contain the same enzyme loading relative to its geometric surface. Scan rate of 3.33 mV* s^{-1}*, PBS 0.1 M, pH 7.4 at 34 °C saturated with* O_2*.*

5.3.4. Advantage of the porous structure and stability over time

The benefit of the highly porous three-dimensional structure of the CNFs was highlighted by comparing the bioelectroactivity efficiency with a modified glassy carbon (GC) electrode. In **Figures 5.7A** and **5.7B**, we observe successive polarization curves for ORR on the optimized biocathode either with CNFs or GC as electrode, respectively. A proportional amount of the coating solution was dropped on the surface of both electrodes so that both contain the same loading of all components according to its geometric surface. Firstly, the results show that the porous structure of the CNFs dramatically increases the electrode surface area, improves the accessibility to the reactive species and provides 15 times higher current densities than that obtained with GC at 0.2 V vs. Ag/AgCl. Secondly, successive scans show the loss of the initial maximum current density for both electrodes, due mostly of leaking of entrapped ABTS from electrodes surface.[110] The loss is more pronounced for the GC electrode attributed to the release of the species out of the film, which points out the advantage of the 3D nanostructure of the electrospun carbon fibers to entrap species and to offer extended stability.

The optimized BOD/ABTS/Super P/Nafion® cathode was polarized under a constant voltage of 0.3 V *vs*. Ag/AgCl and the delivered current density was measured (**Figure 5.8**) for one hour in oxygen saturated solution. The cathode delivers a catalytic current of

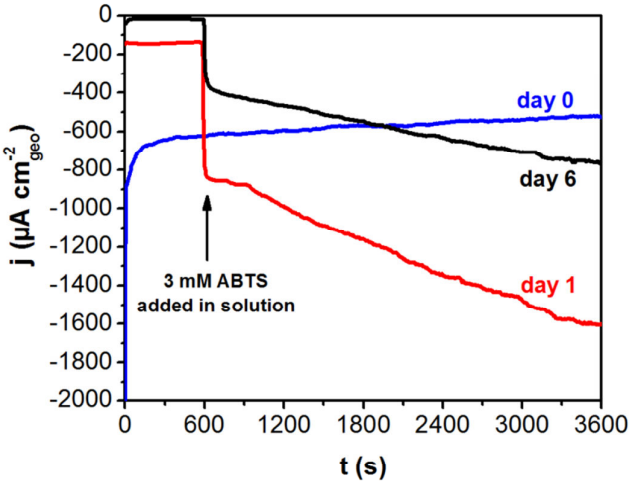

Figure 5.8. *Chronoamperometry measurements of the optimized BOD/ABTS/SuperP/Nafion® cathode based on electrospun carbon fibers obtained at the constant voltage of 0.3 V vs. Ag/AgCl. Stability tests realized on day 1 and day 6, 3 mM of ABTS were added in solution after 600 s. PBS 0.1 M, pH 7.4 at 34 °C saturated with O_2.*

600 µA cm^{-2} that decreases by 15 % after 1 h, illustrating the operational stability of the electrode. However, the experiment repeated after 24 h shows a lower catalytic current decreased by 3.5 times (or ~70%) due mostly to ABTS leaking from the electrode surface or conformational changes of the enzymes. Indeed, the addition of ABTS in the solution (3 mM) induces increasing current densities to 900 µA cm^{-2} that continuously increase over 1 h, indicating that the enzymes retain their catalytic activity towards ORR and the presence of ABTS in solution promotes the electronic communication of a larger amount of immobilized BOD within the film. After one week, the delivered current density further decreases, but still reaches the initial current density when 3 mM ABTS is added in solution.

The results point out the usefulness of the CNFs to construct BFCs, where total current and stability are among the most important issues.

5.4. Laccase entrapped in polypyrrole matrix

Aligned electrospun carbon fibers felts were compared to randomly distributed CNFs felt, here with a different enzyme immobilization technique. In this section, their performance as bioelectrodes for the bioelectroreduction of oxygen using laccase enzyme will be explored.

Enzyme immobilization was realized via the deposition of species followed by entrapment in a polypyrrole matrix (with and without ABTS). This is achieved through the electropolymerization of pyrrole monomer onto the CNFs along with ABTS. Polypyrrole has the advantage of being a polymer capable of conducting electricity, which might be helpful in the electrons transfer that happens during enzymatic reactions onto the electrodes. However, in this method, the actual amount of entrapped ABTS is not known.

5.4.1. Materials and methods

The bioelectrodes to be employed in electroreduction of oxygen were prepared by adsorption of laccase enzyme on the surface of the electrodes followed by entrapment along with ABTS mediator in a polypyrrole film. This procedure (**Figure 5.9**) consisted in depositing on each face of the electrodes (geometric area of 0.7 × 0.7 cm^2 each face) a droplet of 20 µL of a mixture containing laccase from *Trametes versicolor* (7.5 mg mL^{-1}, from Sigma Aldrich, ≥10 U mg^{-1}) and carbon particles (7.5 mg mL^{-1}, 0.04 µm grain size, specific surface area 62 m^2 g^{-1}, Super P from Timcal) in PBS (pH 5.0). The samples were then dried under air flow. The laccase enzyme loading was estimated to 300 µg cm^{-2} (relative to electrode geometric

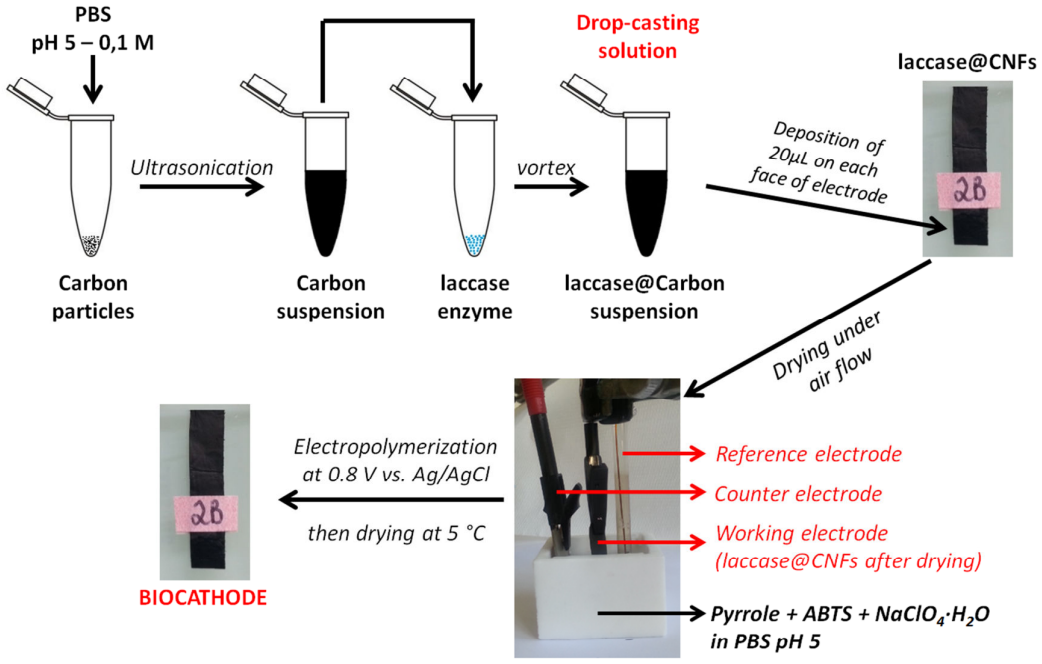

Figure 5.9. *Scheme of cathodes preparation: laccase entrapped in polypyrrole polymer matrix.*

surface). This laccase loading was optimized from previous works in our group. After drying, polypyrrole electropolymerization was carried out onto CNFs felts electrodes dipped in a solution containing pyrrole (200 mM, from Sigma Aldrich), ABTS (20 mM, from Sigma Aldrich) and $NaClO_4 \bullet H_2O$ (0.1 M, from Sigma Aldrich) in PBS (pH 5.0, prepared from $NaH_2PO_4 \cdot 2H_2O$ and Na_2HPO_4 from Sigma Aldrich using ultrapure water), at +0.8 V vs. Ag/AgCl until a charge of 1.0 Coulomb has passed. This charge value was optimized from tests with charges varying from 0.1 to 3.0 C. The complete polymerization of any pyrrole excess that may have remained between the carbon fibers was achieved by cycling the biocathodes in clean PBS (pH 5.0) from 0 to 0.8 V (5 cycles at scan rate of 50 mV s^{-1}). Note that even though polypyrrole is a conductive polymer, it does not affect the overall conductivity of the CNFs, since it is only present in the extremity part of the CNFs electrode, where enzyme coating is.

5.4.2. Characterization of the bioelectrodes towards O_2 electroreduction

CNFs were modified with enzyme laccase followed by entrapment in a polypyrrole film containing ABTS as electron transfer mediator. The assembly employed for the characterization of the biocathodes was presented in Chapter 1.4. **Figure 5.10** presents polarization curves realized in O_2 saturated PBS at pH 5.0. From the polarization curves, the

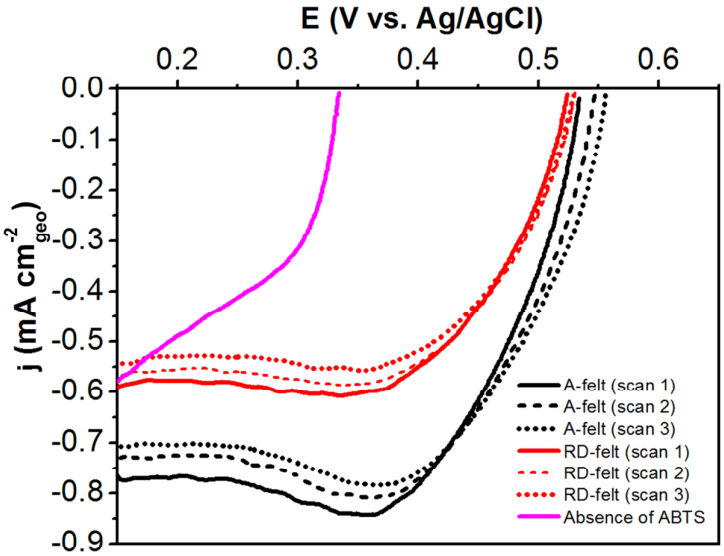

Figure 5.10. *Polarization curves for electroreduction of O_2 onto aligned and random felts (A-felt and RD-felt) and graphite electrodes modified with laccase entrapped in polypyrrole film with ABTS in O_2-saturated phosphate solution (pH 5.0, 0.1 M), as well as an aligned felt electrode without ABTS in the same medium. Scan rate 3.3 mV s^{-1}.*

oxygen reduction current begins at around 0.53 V vs Ag/AgCl, without overpotential, and the current densities feature a semi-plateau that indicates the control of the electrocatalytic reaction by diffusion of the oxygen to the electrode surface. Stability tests were performed periodically until the 7th day after keeping the electrodes at 5 °C in a humid environment. **Figure 5.10** shows that an aligned felt delivers a current density of about 740 µA cm^{-2}, which is about 30 % higher than that of a random felt. Successive scans lead to gradual loss of the initial electrochemical activity, and after 7 days, the activity of both aligned and non-aligned electrodes has decreased of about 60 % of its original activity (not shown). This is due mostly to the loss of entrapped ABTS from electrodes surface to the solution.[110] In the absence of immobilized ABTS mediator on aligned fibers, the current density is only about 30 % lower, which indicates that the adsorbed enzymes are well oriented for direct electron transfer (DET) between the electrode, the copper centers of laccase and the oxygen molecules. DET with laccase enzyme has already been reported by several authors.[211–213] However, in this case the V_{OC} is 0.34 V *vs.* Ag/AgCl, fixed by the polypyrrole electroconductivity which also participates in the electron transfer. When only polypyrrole is deposited onto CNFs (without enzyme nor ABTS), the V_{OC} is 0.2 V vs. Ag/AgCl (not shown). This shows that ABTS is being crucial for enzyme connection in the film, since in the absence of ABTS the V_{OC} drops towards the potential of pure polypyrrole. When laccase and ABTS are co-immobilized onto aligned felt electrodes, the bioelectroreduction of oxygen is enhanced, given not only higher cathodic currents, but also a modulation of the V_{OC} values at which oxygen reduction begins: about 0.34 V *vs.* Ag/AgCl in the absence of ABTS, and about 0.53 V *vs.* Ag/AgCl for the laccase + ABTS couple. Although comparison with literature is not straightforward (due to differences in enzyme activities, concentrations, cell designs, electrode materials, etc.), aligned CNFs felt present competitive efficiency with other reported works focusing on nanostructured electrodes for bioelectrocatalysis of dioxygen reduction.[207,214,215]

Comparison of both techniques presented so far, Nafion® and polypyrrole entrapment, shows that in general current densities are similar at the first day of test of the biocathodes. The major difference is regarding the stability, where polypyrrole entrapment appears to be more advantageous. For polypyrrole, -60 % of the original activity is lost after 1 week, whereas for Nafion the activity is negligible after 1 week, unless more ABTS is added in solution (as seen in **Figure 5.8**). These results show that unless mediator molecules are strongly attached to the immobilized structure, DET strategy must be addressed, since it is

not viable, for example, to have mediator leaking from biocathodes in an implanted application.

Despite this inconvenient, the promising results can be attributed to the porous structure of the CNFs that affords a close contact between the electrode material and the enzymes, and relieves the mass-transfer limitation of the species through the fiber mat. Also, it is thanks to the anisotropic properties of aligned fibers. Moreover, it points out the high benefit and the future applications of aligned electrospun carbon fibers to increase the performance of enzymatic electrodes.

5.5. Chitosan: DET with BOD enzyme

We saw in previous sections the advantages aligned CNFs can offer compared to random ones, especially concerning the enhanced electron transfer. Therefore, in this section aligned CNFs will be employed as electrode materials for the development and optimization of an enzyme immobilization technique based on the use of the biopolymer chitosan as entrapment matrix. Chitosan is the second most abundant biopolymer after cellulose, possessing great film properties that make it a good candidate for enzyme immobilization. Chitosan is not yet widely employed for such application, few examples being found in the literature. It can be employed alone as a film, if the pH of the solution it will be immersed is superior to 6.5 (otherwise it might disintegrate), or it can be reticulated to form a gel. Both strategies will be employed in this section, the second one with the cross-linking agent glutaraldehyde, widely employed for this purpose.

No electron transfer mediator will be employed here, in an attempt to achieve DET between enzymes and the CNFs electrode. Systems with DET are simpler and more adapted for possible future applications in implanted devices, since many MET systems require the electron transfer mediator to be in solution, which is not possible when implanted. We saw previously that when the immobilization was realized with Nafion (**Figures 5.2** and **5.5**) or polypyrrole (**Figure 5.10**), DET can be achieved, but with low efficiency. Here, MWNTs will be employed along with the enzymes, since they are known to promote DET.

The bioelectrodes will be tested toward O_2 electroreduction, either by polarization curves (where the potential of the electrode is scanned while making current readings), or by chronoamperometry (where the current is read at a fixed chosen potential, for a certain

amount of time). Both techniques allow the evaluation of the bioelectrodes performance, and will be employed here in conjunction for comparison.

5.5.1. Materials and methods

The immobilization of enzymes was achieved via entrapment in a chitosan matrix. This method was optimized, so that several immobilization procedures were tested. Chitosan needs to be dissolved in acidic conditions, therefore an acetic acid solution was employed. PBS solutions (pH 5.0 or 7.0 at 0.1 M) were prepared from $NaH_2PO_4 \cdot 2H_2O$ and Na_2HPO_4 from Sigma Aldrich using ultrapure water (18.2 MΩ·cm at 25 °C). MWNTs were obtained from Nanocyl, and were either 95 % or 95 % COOH-modified, as will be mentioned in the results section. BOD was purchased from Amano, 2.51 U mg^{-1} (note that the activity of BOD here is different from the one employed in section 5.3 because different enzyme batches were used. However, the mass was calculated so that the same amount of activity units are employed). Laccase from *Trametes versicolor*, ≥10 U mg^{-1}, was purchased from Sigma Aldrich. Total surface of electrodes was ≅ 2 cm^2. Enzyme loading was calculated to be 1.56 mg cm^{-2} of electrode geometric surface for BOD, and 0.3 mg cm^{-2} of electrode geometric surface for laccase. Several immobilization procedures tested (A to E) are described as follows:

Preparation of chitosan solution: Acetic acid (≥ 99 % from Sigma Aldrich) was dissolved in water at a 1 vol.% concentration. Then appropriate amount of chitosan (low molecular weight, from crab shells, Sigma Aldrich) was dissolved in 1000 µL of the acetic acid solution (1 vol.%) in a vortex stirrer until complete dissolution. Two chitosan concentrations were tested: 1 or 4 mg mL^{-1}, as will be mentioned. When mentioned, 50 µL glutaraldehyde (25 % solution in H_2O, from Sigma Aldrich) was added to 1000 µL of the chitosan solution, and stirred for 1 h in a vortex stirrer for reticulation of the chitosan molecules.

Procedure A*:* this procedure (represented in **Figure 5.11A**) was based on the Nafion method previously shown, where all the species are mixed togheter along with the polymer and then drop-casted onto the CNFs electrode. Here, MWNTs were suspended in the chitosan solution (chitosan concentration of 1 mg mL^{-1}, containing or not glutaraldehyde) at a concentration of 7.5 mg mL^{-1} with the aid of an ultrasonication tip that was immersed in the solution for 1 minute. Then BOD in a concentration of 39 mg mL^{-1} was mixed with the MWNTs+chitosan solution in a vortex for 15 min. This solution was drop-casted onto CNFs at

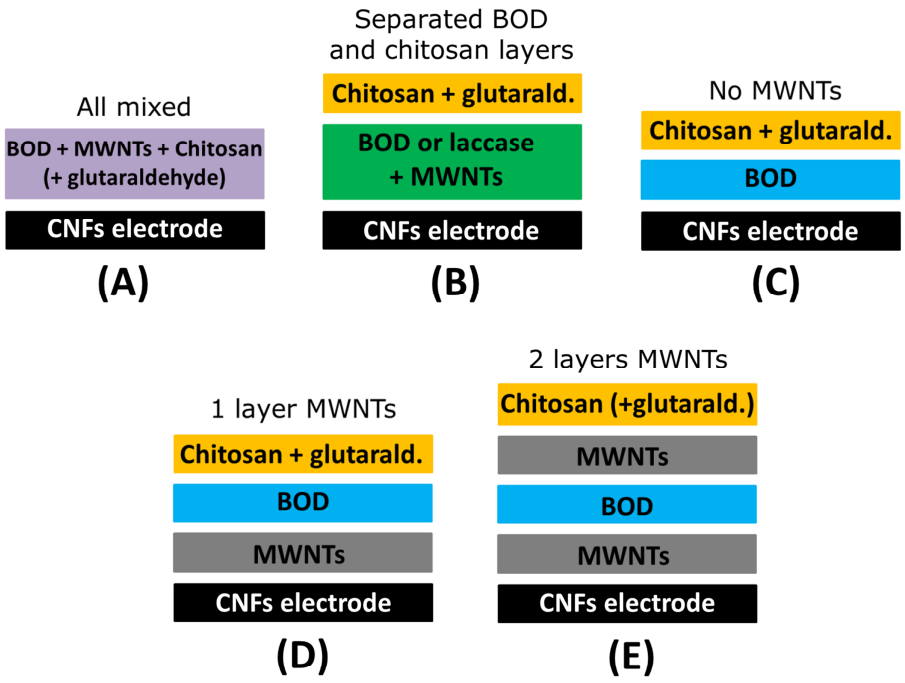

Figure 5.11. *Representation of the layers structures employed in the different immobilization procedures (named from A to E).*

a loading of 40 µL cm^{-2} of electrode geometric surface. The electrodes were left to dry at 5 °C for 48 h.

Procedure B: In this procedure, two layers were drop casted onto the CNFs. For the first layer, 7.5 mg mL^{-1} of MWNTs were dissolved in PBS at pH 7.0 (for BOD coating) or pH 5.0 (for laccase coating), and suspended with the aid of an ultrasonication tip that was immersed in the solution for 1 minute. **BOD solution:** BOD (concentration of 39 mg mL^{-1}) and the MWNTs solution at pH 7.0 were mixed in a vortex stirrer for 15 min. **Laccase solution:** laccase was mixed with the MWNTs solution at pH 5.0, in a concentration of 7.5 mg mL^{-1}, in a vortex stirrer for 15 min. Either laccase+MWNTs or BOD+MWNTs solutions were drop casted onto CNFs at a loading of 40 µL cm^{-2} of electrode geometric surface and let to dry under air flow. After drying, the second layer was drop-casted, which consisted in the chitosan solution (with chitosan concentration of 1 mg mL^{-1}) containing glutaraldehyde at a loading of 40 µL cm^{-2} of electrode geometric surface. The electrodes were left to dry at 5 °C for 48 h. This procedure is represented in **Figure 5.11B**.

Procedure C: No MWNTs were added in this coating. The first layer consisted in BOD solution in PBS pH 7.0 at a concentration of 39 mg mL^{-1}, which was stirred for 15 min in a vortex stirrer. The solution was drop-casted at a loading of 40 µL cm^{-2} of electrode geometric surface and let to dry under air flow. After drying, the second layer was coated (same volumetric loading of 40 µL cm^{-2}), which consisted in the chitosan solution (chitosan concentration of 1 mg mL^{-1}) containing glutaraldehyde. The electrodes were left to dry at 5 °C for 48 h. This procedure is represented in **Figure 5.11C**.

Procedure D: The first layer (drop casted at the same loading) consisted in a suspension of MWNTs in PBS at pH 7.0 in a concentration of 7.5 mg mL^{-1}, which was mixed with the aid of an ultrasonication tip that was immersed in the solution for 1 minute. After drying under air flow, the second layer was drop-casted, which consisted in the same BOD layer employed in procedure C. Then after drying of the second layer, the same chitosan layer (1 mg mL^{-1}, containing glutaraldehyde) employed in procedure C was drop casted and let to dry at 5 °C for 48 h. This procedure is represented in **Figure 5.11D**.

Procedure E: This procedure is similar to the procedure C, except that after the BOD layer, an additional layer of MWNTs was drop-casted and let to dry under air flow (so that there are two MWNTs layers, one before and one after the BOD layer, as can be visualized in **Figure 5.11E**). Then, the same chitosan layer (1 mg mL^{-1} or 4 mg mL^{-1}, when mentioned, containing or not glutaraldehyde) was also drop casted and let to dry at 5 °C for 48 h.

5.5.2. Characterization of the bioelectrodes towards O_2 electroreduction

Aligned CNFs that were modified as described by procedures A to E (schematized in **Figure 5.11**), with enzymes and carbon nanotubes in a chitosan film, were next tested toward ORR as previously done in this work. The objective in this section was not to employ an electron transfer mediator as in previous sections, so that DET can be achieved, and to increase the stability of the biocathodes via the immobilization in a chitosan matrix. Procedures A to E describe the optimization of this immobilization technique, which results will be presented as follows.

BOD was firstly immobilized following a similar procedure that the one employed with Nafion® previously, which means all the components were mixed together in a solution that was then casted onto the CNFs. MWNTs-95 % were employed for this test, chitosan concentration of 1 mg mL^{-1} and the effect of the presence of glutaraldehyde as cross-linking

agent was tested. The polarisation curve is shown in **Figure 5.12A** (full red line). When no glutaraldehyde is present, the V_{OC} is of 0.5 V, and the bioelectrode delivers a current density around 0.3 mA cm^{-2}. This value can be compared with previous tests for the biocathode with BOD enzyme entrapped in Nafion in the absence of ABTS that delivered 0.2 mA cm^{-2}, in **Figure 5.5A**. The increase in the current density value between the two immobilization methods can be due to the fact that MWNTs were employed here, whereas carbon particles were employed in the tests of **Figure 5.5A**, besides the different nature of the entrapping polymer. Still, 0.3 mA cm^{-2} is not a great performance, which needs to be optimized. When glutaraldehyde is employed in the mixed layer of procedure A (result shown in dotted red line of **Figure 5.12A**), the current delivered is even lower (0.15 mA cm^{-2}). The purpose of employing glutaraldehyde is to reticulate the film in order to create a denser and more stable structure, able to keep the enzymes active. What we observe here is that, since all components are mixed together, glutaraldehyde is being capable to reticulate not only the chitosan but the enzymes as well. Apparently, since the enzymes are reticulated in the matrix, their movements have been diminished, which lead to lower current density.

With that in mind, a different strategy was adopted, which is procedure B, showed in **Figure 5.12B**. In this procedure, the enzyme and MWNTs were separated in a different layer from chitosan and glutaraldehyde. In the case of BOD (red line), we can see the current delivered increases to 0.6 mA cm^{-2}, thanks to the fact here the enzymes are not being

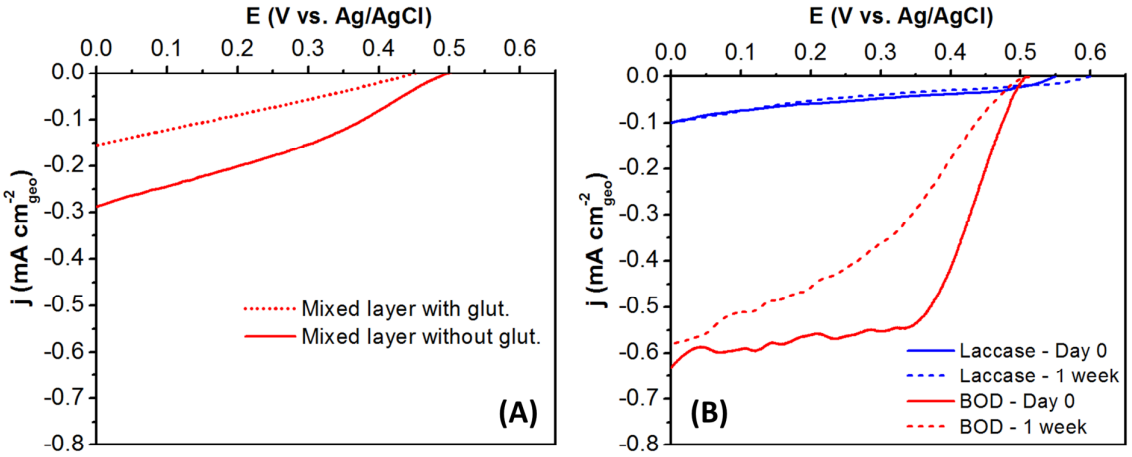

Figure 5.12. *ORR polarization curves obtained for* ***(A)*** *BOD (test in PBS pH 7) immobilized according to procedure A, and* ***(B)*** *laccase (test in PBS pH 5.0) or BOD (test in PBS pH 7.0) immobilized according to procedure B. Scan rate of 3 mV* s^{-1} *in* O_2 *saturated PBS.*

reticulated by glutaraldehyde. This result is surprisingly good, since it shows the achievement of similar current densities through DET that have been obtained with ABTS. This procedure was chosen to compare BOD with laccase enzyme (which works at pH 5.0) (blue line in **Figure 5.12B**), but a much lower current density is observed (0.1 mA cm^{-2}). We think this is due to the fact the chitosan film dissolves at some extent in acidic solution, which might release enzymes to the solution, inactivating them. However, some amount of enzymes remain onto the CNFs electrode, since when the test is realized again after 1 week (blue dashed curve), almost the same performance is retrieved. For BOD, similar behavior is found after 1 week as well (dashed red line), which highlights the benefits of chitosan immobilization.

The effect of the layered structure and of the amount of MWNTs was further studied through procedures C, D and E. In procedure C, no MWNTs were added, only one layer of BOD and one chitosan layer were present. In procedure D, the first layer was composed of MWNTs, then a BOD layer, and finally a chitosan layer (chitosan concentration of 1 mg mL^{-1} and with glutaraldehyde). In procedure D, two layers of MWNTs were present before and after the BOD layer, plus a chitosan layer on top. Glutaraldehyde was employed along with chitosan, and the MWNTs employed here were 95 % purity modified with COOH functions (readily bought from Nanocyl). The effect of MWNTs type will be discussed next. Polarization curves with the results of bioelectrodes prepared according to procedures C, D and E tested for ORR can be found in **Figure 5.13A**. When no MWNTs are present (blue dotted line), DET is not achieved, and the current delivered is negligible. This proves the role of MWNTs on electron transfer, crucial for DET when no mediator is present. When one layer of MWNTs is present (red line), current density is of 0.9 mA cm^{-2}. We can see that this value is higher than the one obtained when MWNTs and BOD were mixed in the same layer (red line in **Figure 5.12A**), which highlights the beneficial effect of layered disposition for better electron transfer. MWNTs might be more available for electrical connections between enzymes and the CNFs surface when added first, in a separate layer, as suggested by the results. Finally, when 2 layers of MWNTs (one on top and one on the bottom of BOD enzyme) are present, the current density is yet increased to 1.2 mA cm^{-2}, which is a remarkable result when comparing to the state of the art O_2 biocathodes so far.[114,135,136,214] With two MWNTs layers, remaining BOD molecules that were nor "wired" on the one-layer configuration are then able to participate on the electron transfer. These bioelectrodes were also tested by

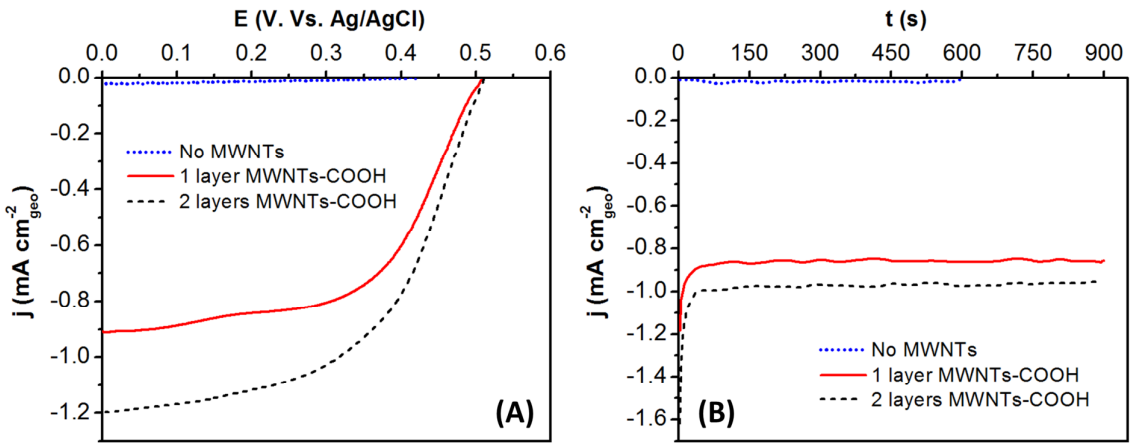

Figure 5.13. *ORR polarization curves* ***(A)*** *and chronoamperometry curves (obtained at 0.1 V vs. Ag/AgCl)* ***(B)*** *obtained with BOD bioelectrodes prepared according to the procedures C, D and E described earlier, with either no MWNTs, one layer or two layers of MWNTs, along with a BOD layer and a chitosan+glutaraldehyde layer. Scan rate of 3 mV* s^{-1} *in* O_2 *saturated PBS (pH 7.0).*

chronoamperometry at 0.1 V vs. Ag/AgCl for 15 min, as presented in **Figure 5.13B**. The current delivered is in the form of a plateau during the period of the experiment, which shows good stability and integrity of the biocathodes in the solution with time. In addition, the values of current obtained by this method are slightly lower than the ones obtained by polarization, which comes from the fact that this technique represents a more real way to test the electrodes, closer to the conditions found in an actual biofuel cell.

Regarding the type of MWNTs employed, two samples of MWNTs with purity of 95 % from Nanocyl were tested, one that was untreated, and one that possessed COOH functions on its surface. Both MWNTs were tested in the two-layers configuration (procedure E), with chitosan concentration of 1 mg mL^{-1} and with glutaraldehyde. Results are presented in **Figure 5.14**. The difference between both types is clear, COOH-modified MWNTs delivering 1.2 mA cm^{-2} versus 0.8 mA cm^{-2} for the untreated MWNTs, by polarization curves. Results obtained by chronoamperometry (**Figure 5.14B**), are also a bit lower, but still represent the same behavior. One reason for this difference might come from the fact that, since no surfactants were employed, the untreated MWNTs were much more hydrophobic than the COOH ones. Therefore, the quality of the suspension formed with the COOH-modified MWNTs is better, capable to create a more uniform covering onto the CNFs, and thus be

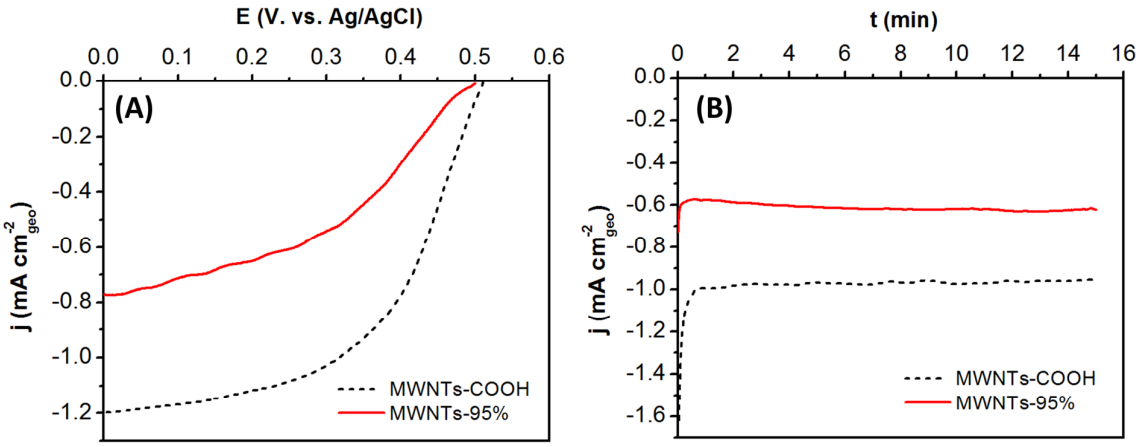

Figure 5.14. *ORR polarization curves* ***(A)*** *and chronoamperometry curves (obtained at 0.1 V vs. Ag/AgCl)* ***(B)*** *obtained with BOD bioelectrodes prepared according to procedure E described earlier, with either untreated MWNTs (95 % purity) or COOH-modified MWNTs (same purity). Scan rate of 3 mV* s^{-1} *in* O_2 *saturated PBS (pH 7.0).*

more accessible for electron transferring. The second and most probable reason for achieving better performance with COOH-modified MWNTs is the fact that carboxyl groups are important for binding BOD enzyme in an orientation allowing fast electron transfer, as proposed by the work of Armstrong et al.[216] and highlighted by Atanassov et al.[217]

The effect of chitosan concentration was also evaluated, for electrodes prepared by procedure E, with COOH-modified MWNTs and with glutaraldehyde in the chitosan layer. We expect chitosan concentration to play a role especially in the stability of electrodes, since the layers underneath the chitosan layer would be more "protected" by a film of increased concentration. However, at the same time, this extra protection might prevent the diffusion of oxygen and electrons through the film, reducing the overall performance. The stability of the bioelectrodes was measured weekly by polarization curves, and the electrodes were stored at 5 °C in PBS solution at pH 7.0 in between tests.

Typically, a concentration of 1 mg mL^{-1} of chitosan was employed (dashed curve in **Figure 5.15**). This bioelectrode presented an average decrease in activity of 30 % of the original current density after 1 week, and of 60 % after 1 month. The concentration of 4 mg mL^{-1} was also tested for comparison. This bioelectrode delivers mean current density of 0.8 mA cm^{-2}, which is 33 % lower than the current obtained with 1 mg mL^{-1} of chitosan. Here the current density obtained by chronoamperometry is also slightly lower than the one

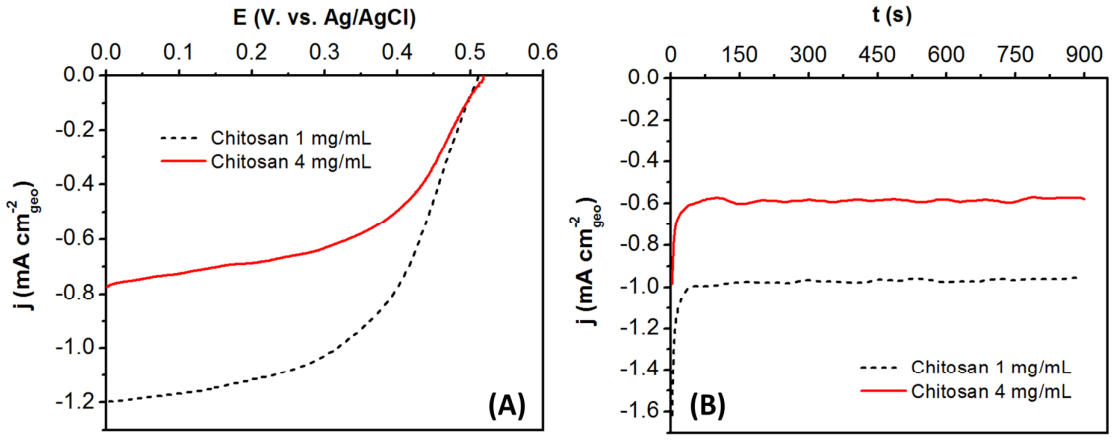

Figure 5.15. *ORR polarization curves* ***(A)*** *and chronoamperometry curves (obtained at 0.1 V vs. Ag/AgCl)* ***(B)*** *obtained with BOD bioelectrodes prepared according to procedure E described earlier (with COOH-modified MWNTs, with glutaraldehyde), with different chitosan concentrations of 1 and 4 mg* mL^{-1}*. Scan rate of 3 mV* s^{-1} *in* O_2 *saturated PBS (pH 7.0).*

obtained by polarization. This result testifies that increased polymer concentration prevents the diffusion of species through the film. Regarding the stability of the biocathode with chitosan concentration of 4 mg mL^{-1}, the current density decreased only 20 % after 1 week, and 32 % after 1 month, which proves that increased concentration actually improves stability. Given the higher current delivered by the bioelectrode with chitosan concentration of 1 mg mL^{-1}, this composition was chosen for future tests, even though the stability is inferior.

Finally, the presence of glutaraldehyde was also studied as a parameter able to play a role in the long term stability of biocathodes. Stability should be enhanced when the film of chitosan is cross-linked by glutaraldehyde because the structure becomes more rigid, preventing the loss of immobilized species. At the first day of test, no difference was observed in the intensity of current delivered by biocathodes prepared in the presence and absence of glutaraldehyde in the chitosan layer, as can be observed in **Figure 5.16**, which were as well tested by polarization curves and chronoamperometry. However, with regard to stability, the presence of glutaraldehyde was actually able to give a positive effect. The electrodes with glutaraldehyde presented an average decrease in activity of 30 % of the original current density after 1 week, and of 60 % after 1 month. At the same time,

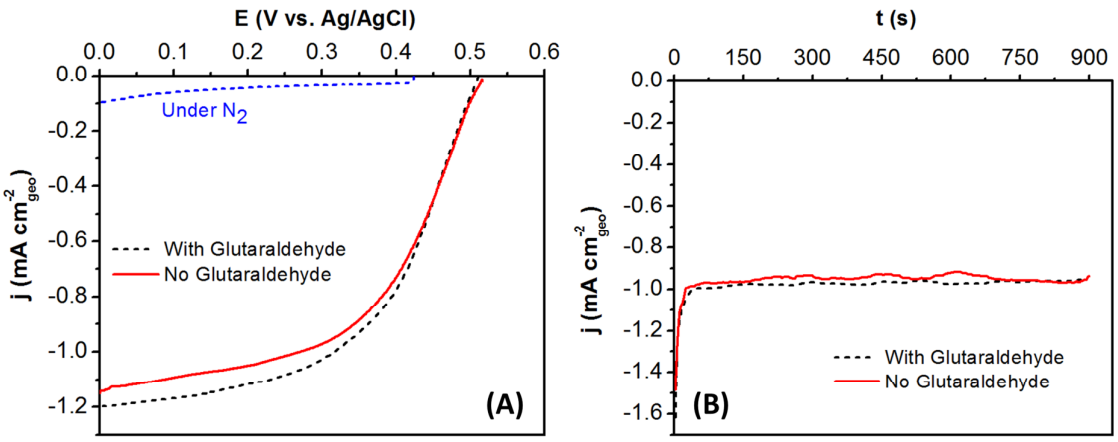

Figure 5.16. *ORR polarization curves* ***(A)*** *and chronoamperometry curves (obtained at 0.1 V vs. Ag/AgCl)* ***(B)*** *obtained with BOD bioelectrodes prepared according to procedure E described earlier (with COOH-modified MWNTs, with chitosan concentration of 1 mg mL^{-1}), with and without glutaraldehyde in the chitosan layer. Scan rate of 3 mV s^{-1} in O_2 saturated PBS (pH 7.0). In* ***(A)****, electrode with glutaraldehyde tested under N_2 (instead of O_2) as well.*

electrodes without glutaraldehyde presented an average decrease of 45 % after 1 week, and of 70 % after 1 month.

Thanks to the optimization results presented, the biocathodes prepared by the procedure E, with two layers of COOH-modified MWNTs, one layer of BOD enzyme, all covered by a layer of chitosan (1 mg mL^{-1}) cross-linked with glutaraldehyde was chosen as the best composition. This bioelectrode was tested under N_2 as well, as can be seen in **Figure 5.16** (blue dashed line). The solution was bubbled with N_2 over nigh, and then the bioelectrode was inserted in the cell and the solution was further bubbled for 1.5 more hours. Only a small residual catalytic current of 0.1 mA cm^{-2} can be observed, which can be attributed to the presence of traces of O_2 between the fibers of the electrode.

The stability of this optimized biocathode was tested by polarization curve after 3 months (storage in PBS at pH 7.0, at 5 °C), as showed in **Figure 5.17**. The cathodic current delivered after this period of time was of 0.28 mA cm^{-2}, while at day 0 it was 1.2 mA cm^{-2}. This means after 3 months the current decreased 76 % from the original value, which is a remarkable stability. This result also shows the loss of stability is not linear: an important loss of activity happened on the first month (discussed earlier), and then the loss became slower. Regarding the V_{OC}, it decreased from 0.52 V to 0.47 V after 3 months. This optimized

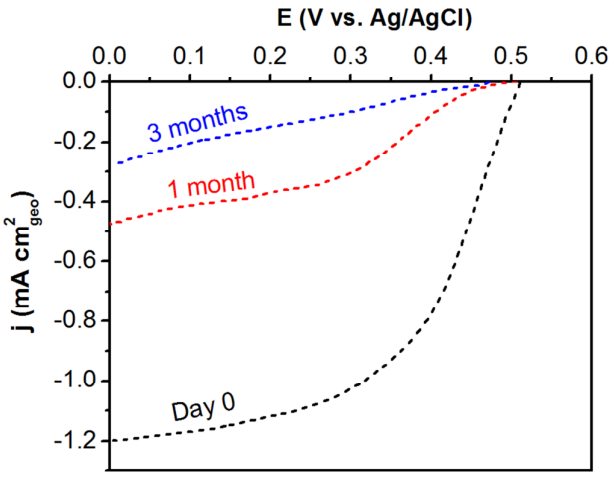

Figure 5.17. *Stability of the optimized biocathode along 3 months. Polarization curves realized at scan rate of 3 mV s^{-1} in O_2 saturated PBS (pH 7.0). Electrodes stored in PBS at 5 °C between measurements.*

biocathode was employed for the creation of a hybrid biofuel cell where the anode was composed of the CNFs modified with Au particles (Chapter IV). This BFC will be presented in Chapter VII.

5.6. Conclusion

In this chapter, randomly organized and aligned CNFs felts were modified with the enzymes laccase or BOD entrapped in Nafion®, polypyrrole or chitosan films, either through MET with ABTS, or through DET in the presence of MWNTs and without ABTS, and were further tested for the electroreduction of oxygen.

When laccase was immobilized onto randomly organized felts in a Nafion® matrix, better results are obtained when MWNTs are adsorbed on the fibers surface. However, the amount of MWNTs present was not sufficient for achieving DET. The same technique was employed with aligned CNFs as electrode material, and the performance was similar to the one of MWNTs-modified random CNFs. This result showed that it was more practical to work with aligned CNFs, which could enhance the electron transfer with fewer steps.

Nafion® technique was also employed for the entrapment of BOD onto aligned felts, and the composition of these films was fully optimized. It was found that the stability of the biocathodes is impaired by the loss of ABTS from the film, since when excess of ABTS is added in solution, initial performances can be retrieved even after one week.

The better performance of aligned felts in comparison with random ones was confirmed when laccase was entrapped in polypyrrole films onto both types of electrodes. Aligned felts delivered a cathodic current that was 30 % higher than that of random felts, confirming that the organization of fibers is a factor capable of enhancing not only the intrinsic electrical conductivity, but also the response to bio-electrochemical reactions, such as enzymatic oxygen reduction. DET was achieved, but the presence of ABTS mediator was crucial for "wiring" the enzymes with better V_{OC} values. After one week, the electrodes have lost 60 % of the initial performance, also due to the loss of ABTS that was entrapped. However, stability with polypyrrole entrapment appears to be higher than with Nafion®, even though performances are similar in the first day of tests.

Through immobilization in a chitosan matrix, DET was achieved between BOD enzyme and aligned CNFs surface, with the presence of MWNTs. When MWNTs were COOH-modified, better performance was achieved, since carboxyl groups are known to bind BOD enzyme in an orientation allowing fast electron transfer. Increased stability was also achieved with chitosan, biocathodes lost -60 % of the original current density after 1 month, and -76 % after 3 months, which highlights the benefits of chitosan immobilization.

Comparison of the three strategies (Nafion, polypyrrole or chitosan) is not evident, given that both MET and DET were tested. The two main parameters for comparison are the current delivered or the stability. Considering the current delivered, polypyrrole and chitosan were the most promising. Nafion and polypyrrole present similar current densities, but polypyrrole was more stable. As for the stability, chitosan is clearly the most stable, but further optimization on the polypyrrole immobilization technique could probably lead to better stability as well. However, clearly the calculation of current densities of porous electrodes in relation to the geometric surface of the electrodes is not the most appropriate way. Using the specific surface or the volume of electrodes might be better options. The only reason for not doing so is the need to compare performances with the literature, which is at the same time difficult and unavoidable.

In the next chapters, bioelectrodes modified by Nafion and chitosan will be employed for the construction of complete biofuel cells. Polypyrrole biocathodes were not employed for the construction of complete BFCs in this work, which is a perspective for future researches.

Chapter VI. Development of an enzymatic biofuel cell powered by ethanol

6.1. Introduction

After the optimization of the cathode enzyme immobilization technique, some of the developed cathodes will be connected to anodes to create a complete BFC. In this chapter, an enzymatic anode powered by ethanol that have been previously developed in our group has been selected to complete the enzymatic BFC.

Ethanol BFCs emerged from the challenge in creating traditional fuel cells with ethanol as a fuel, since platinum-based catalysts are unable to efficiently catalyze the oxidation of ethanol reaction, being quickly passivated.[142] At the same time, living organisms (like Pseudomonas aeruginosa, acetobacter, gluconobacter) contain oxidoreductase enzymes that are able to oxidize ethanol. Thus, ethanol biological fuel cells became an attractive alternative to eliminate the dependence on precious metal catalysts.

In this section, an ethanol BFC with electrodes composed of CNFs as electrode material will be presented. The importance of the structure of the electrode material is highlighted by developing the same BFC either with electrodes composed of aligned carbon fibers or by graphite. Graphite was chosen since it is the reference material commonly used in the literature.

Regarding the anode, it is the site of ethanol oxidation to acetaldehyde by the enzyme alcool desydrogenase (ADH) and its cofactor NAD. The regeneration of the cofactor is achieved by using the additional redox protein diaphorase (DP) which operates efficiently in the presence of the redox mediator K3 vitamin (VK3).[218] This anodic system, which have been employed previously in our group[84] was discussed in Chapter 1. **Figure 6.1** depicts a representation of the chain of electrochemical reactions that happen in the anode, being ethanol in solution, and other components immobilized on the surface of the electrode material. The reaction that takes place at the anode is presented in **Equation 6.1**: ethanol oxidizes to acetaldehyde liberating 2 protons and 2 electrons per molecule.

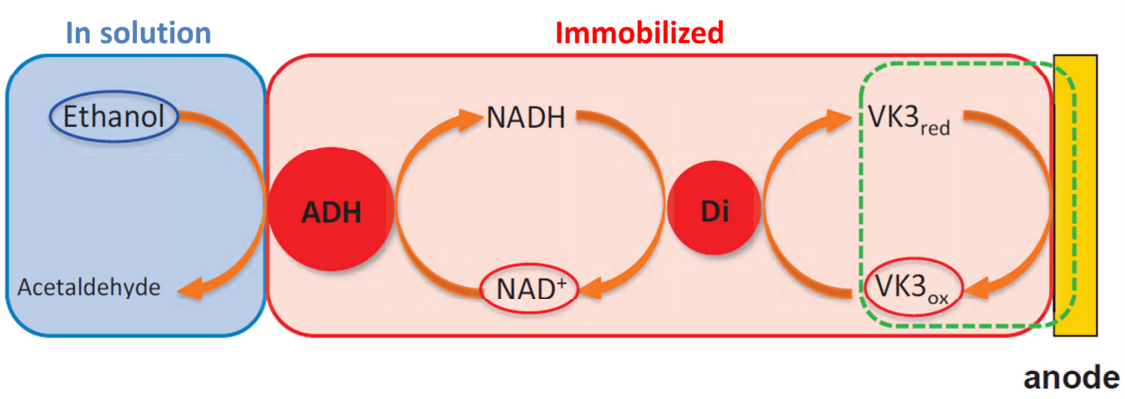

Figure 6.1. *Representation of the cascade of electrochemical reactions taking place at the anode where ethanol is oxidized. (Scheme from Techer, 2013 [84]).*

The cathode employed in this BFC, composed of laccase and ABTS immobilized in a Nafion® matrix has been thoroughly discussed. The reaction taking place at the cathode is presented in **Equation 6.2**, which was also mentioned: oxygen is reduced directly to water with 4 electrons and 4 protons, thanks to laccase enzyme. For each oxygen molecule, 2 ethanol molecules are needed to complete the cycle. The global reaction of the complete BFC is, therefore, presented in **Equation 6.3**.

$$2\ CH_3CH_2OH \xrightarrow{ADH/NAD/DP/VK3} 2\ CH_3CHO + 4H^+ + 4e^- \quad (6.1)$$

$$O_2 + 4H^+ + 4e^- \xrightarrow{laccase/ABTS} 2H_2O \quad (6.2)$$

$$2\ CH_3CH_2OH + O_2 \longrightarrow 2\ CH_3CHO + 2H_2O \quad (6.3)$$

In this chapter, both anode and cathode will first be tested separately, and then in a two-chamber cell, separated with a Nafion membrane. The BFC will be tested by the CRD (constant resistance discharge) technique, which means a set of electrical resistances are connected to the cell, as well as a voltmeter and an amperemeter. When the resistance value is at its highest and no current passes through the external circuit, the V_{OC} of the cell can be read. Then, the resistance is lowered step by step, and at each step voltage and current readings are made. At the end, the power of the cell can be calculated simply from

P = E × I, and plotted against the current density. Cell voltage is also plotted against the current density, which is the polarization curve of the cell. More details about BFC tests can be found in **Annex 2**. Some results presented in this chapter were published in an invited contribution to the journal *L'Actualité Chimique* in 2014.[219]

6.2. Materials and methods: preparation of the biocathode

The immobilization of laccase and ABTS onto aligned CNFs was accomplished thanks to a Nafion polymeric matrix, according to the protocol discussed in Chapter 5, sections 5.2 and 5.3: carbon particles solution at a concentration of 7.5 mg mL^{-1} (0.04 µm grain size, specific surface area 62 $m^2 g^{-1}$, Super P from Timcal) was prepared in PBS (0.1 M at pH 5, prepared from $NaH_2PO_4 \cdot 2H_2O$ and Na_2HPO_4 from Sigma Aldrich using ultrapure water, 18 MΩ·cm at 25 °C). Then laccase from *Trametes versicolor* (7.5 mg mL^{-1}, from Sigma Aldrich, ≥10 U mg^{-1}), ABTS (2.4 mg mL^{-1}, from Sigma Aldrich) and 5 vol.% Nafion perfluorinated resin solution (5 vol.% in lower aliphatic alcohols and water, from Sigma Aldrich) were added to this solution and carefully stirred in a vortex mixer. Enzyme solution loading was 66 µL cm^{-2} of geometric electrode surface (CNFs – considering both sides – or graphite). Aligned CNFs were chosen as electrode material, since its performance was shown to be superior than the randomly organized ones.

6.3. Materials and methods: preparation of the bioanode

Regarding the anodic chamber, ethanol was catalyzed by a multienzymatic cascade system with the enzymes alcool desydrogenase (ADH) and diaphorase (DP), with nicotinamide dinucleotide (NAD) as cofactor and K3 vitamine (VK3) as mediator, immobilized in a Nafion® matrix. The reactions that take place through this scheme were demonstrated in the beginning of this section.

The protocol for the preparation of such bioanodes (depicted in **Figure 6.2**) is the following:

- The buffer solution at pH 9 was prepared from a phosphate buffer solution at pH 7 (0.1 M) by adding sufficient amount of KOH until it reached pH 9.

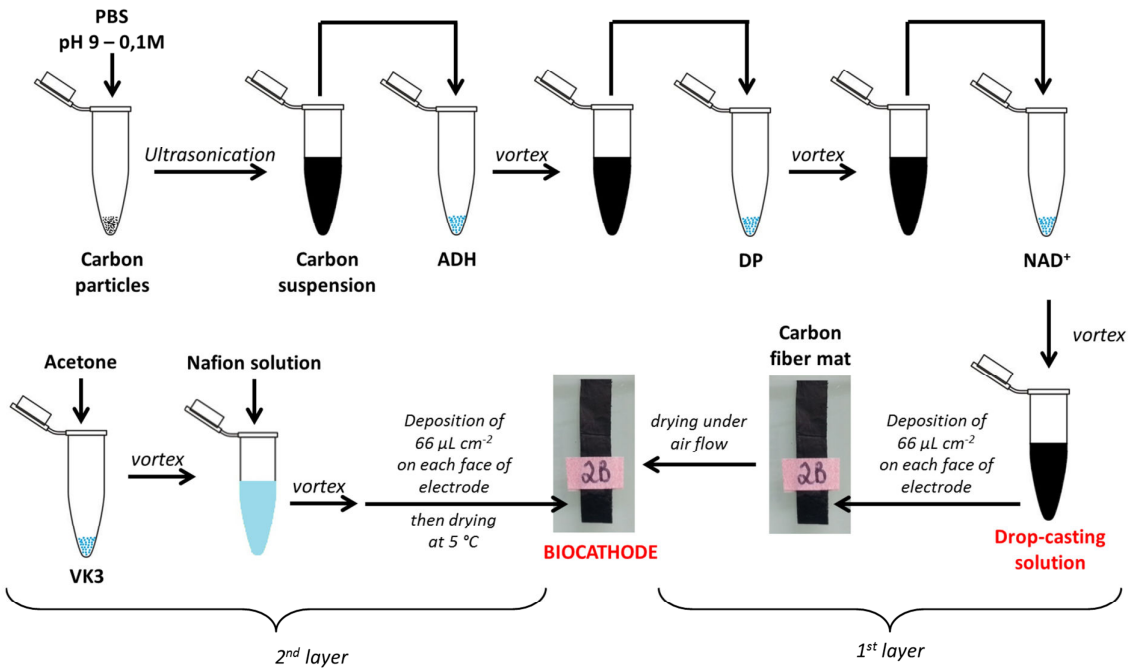

Figure 6.2. *Scheme of bioanode preparation.*

- **First layer:** Super P carbon particles suspension is prepared with the buffer solution at pH 9, at a concentration of 15 mg mL^{-1} (ultrasonication bath is used for easier dispersion). Then, ADH [28 mg mL^{-1}], DP [16.4 mg mL^{-1}] and NAD [20 mg mL^{-1}] are added to the Super P solution, and after the addition of each component, the solution is homogenized in a vortex stirrer. The final solution was deposited with a loading of 66 µL cm^{-2} of electrode surface and let to dry under air flow. In the case of CNFs felt, both faces of the felt were coated with the solution.
- **Second layer:** VK3 is diluted in acetone in a concentration of 63 mg mL^{-1} and thoroughly stirred in a vortex stirrer, then Nafion® solution is added (5 vol.%) and the whole is properly stirred as well. The second layer solution was coated on top of the first dried layer, also with a loading of 66 µL cm^{-2} of electrode surface, and let to dry at 5 °C overnight.

6.4. Half-cell test of anode and cathode performance

CNFs or graphite were modified with enzymes and mediators (anodic or cathodic), with the same amount of species regarding the geometric surface of the electrodes.

The test of the cathode towards O_2 reduction reaction followed the same protocol of the previous chapter dedicated to it. Since laccase is the enzyme of choice, the test was realized in PBS solution at pH 5, saturated with O_2. The anode was tested in the same buffer solution at pH 9 used for the preparation of the electrodes, with 3.0 mM of NAD^+ in solution and 4.0 $\mu L_{ETHANOL}$ per mL of buffer solution. In the case of the anode, open circuit voltage is negative, and the potential is scanned towards positive values. Both anode and cathode electrodes were stored at 5 °C in a humid environment after the tests.

Figure 6.3 presents the polarization curves of both the anode (upper graph with positive j) and the cathode (lower graph with negative j), for both types of electrodes (CNFs and graphite). All current density readings were made at 0.1 V *vs.* Ag/AgCl, and the values of j were reported to the geometric surface of the electrodes.

The anode with CNFs electrode delivers 830 µA cm^{-2}, while the graphite one delivers 22 % less. The CNFs electrode presents a high oxidation peak that is lower for graphite. This peak is attributed to the oxidation of the large amount of VK3. Thanks to the porous structure, more VK3 species are in intimate contact on the surface of the material, enabling efficient electrical contact. However, after 1 day, neither of the anodes are active towards ethanol oxidation. This might be due to the inactivation of the enzymes caused by

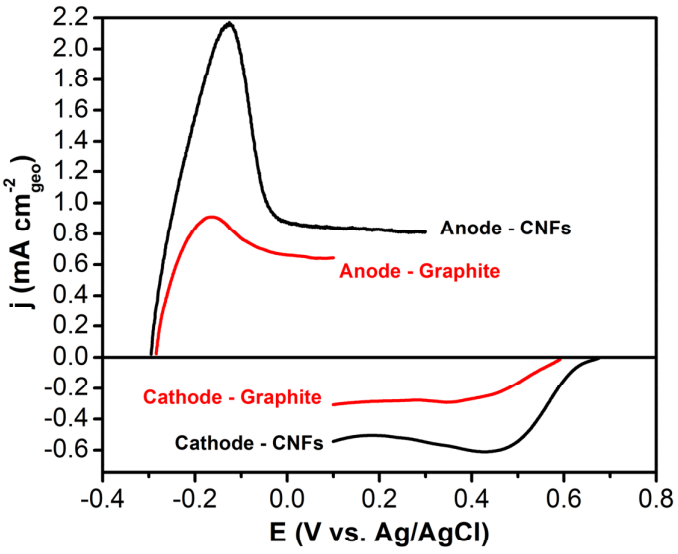

Figure 6.3. *Polarization curves of the anode (positive j) for the oxidation of ethanol, and cathode (negative j) for the reduction of O_2. Anode: 3.0 mM of NAD in solution and 4.0 $\mu L_{ETHANOL}$ per mL of buffer solution at pH 9.0. Cathode: pH 5 saturated with O_2. Scan rate = 3.33 mV s^{-1}.*

insufficient proton diffusion in the enzymatic film, which creates a microenvironment with decreased pH, unfavorable for the enzymes, as proposed by Sakai et al.[147] They show that when increasing the concentration of the buffer solution, the problem of pH reduction can be avoided. However, they mention higher buffer solution concentration is yet another cause of enzyme deactivation.[147] Several alcohol BFCs in the literature also report difficulty to efficiently immobilize NAD^+ at the electrode surface, influencing anode stability, which explains why many operate with the cofactor NAD^+ in solution.[142,220] Moreover, diffusion of NAD to the active sites must be weak in the anode presented here, which is yet another cause for the low stability.

Regarding the cathode, CNFs electrode delivers a cathodic current of around 550 µA cm^{-2}, while the graphite electrode delivers 45 % less, with only 300 µA cm^{-2}. After 1 day, CNFs electrode have lost 55 % of their initial current densities, which was certainly due to the loss of ABTS into the solution, because when more ABTS was added in solution (3 mM), the CNFs electrode regain almost all of its initial current.

6.5. Test of complete BFC

The BFC was assembled in a two chamber cell, with a proton exchange membrane

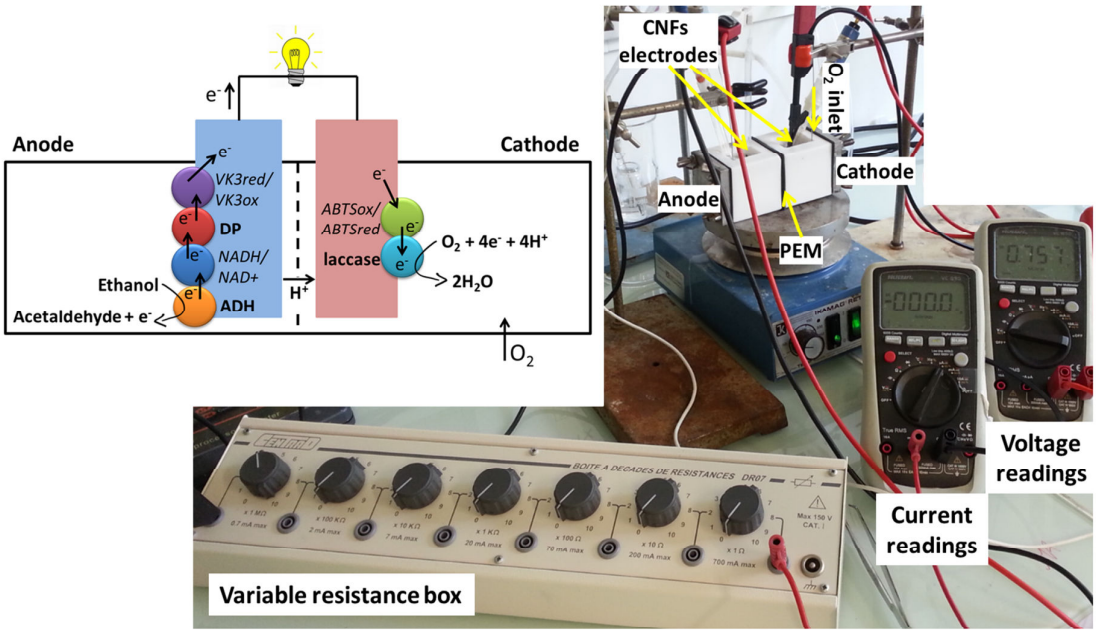

Figure 6.4. *Scheme of the enzymatic biofuel cell powered by ethanol, and picture of the laboratory assembly employed for BFC tests.*

(Nafion 117®) separating both chambers. A scheme and a picture of the BFC is shown in **Figure 6.4**. The cell was tested according to the method called "constant resistance discharge", as discussed in Chapter 1.4. This method consist of varying the resistance connected to the anode and cathode, step by step starting from the highest resistance of 10 MΩ, and making E and I readings at each step.

Figure 6.5 presents the performance curves of the developed BFC. Cell voltage (dashed lines) and power densities (full lines) are plotted against the current density of the cell; red lines corresponding to the BFC developed with CNFs electrodes in both anode and cathode, and black lines to graphite electrodes. According to the polarization curve j *vs.* E, the region of ohmic polarization of the BFC with CNFs as electrodes present less pronounced slope then the one with graphite electrodes. This means that the ohmic resistance of the BFC (resistance of electrons flow through electrode and connections, of the proton exchange membrane and electrolyte) is higher for the graphite BFC (Logan et al.[221] well explained this behavior). However since in both BFCs (CNFs and graphite) the proton exchange membrane and electrolytes are the same, the electrons flow through electrode itself is to blame. The ohmic region is followed by a sharp drop of E, which represents the limitation of mass

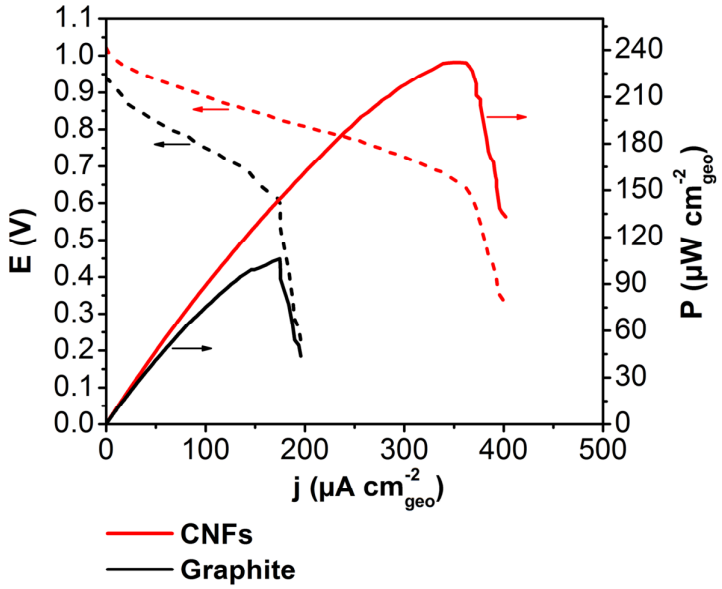

Figure 6.5. *Characterization of the two enzymatic BFCs realized with electrodes (anode and cathode) composed of CNFs (red lines) or graphite (black curves). Anode: ADH+NAD+DP+VK3, 3.0 mM of NAD in solution and 4.0 $\mu L_{ETHANOL}$ per mL of buffer solution at pH 9.0. Cathode: laccase, pH 5.0 saturated with O_2.*

transfer of O_2 and ethanol through the respective enzymatic films, either due to the exhaustion of the reactants at higher currents, or due to the accumulation of the products formed. Regarding the open circuit voltage, when graphite electrodes are employed, V_{OC} is 950 mV, whereas CNFs electrodes allow attaining a remarkable V_{OC} of 1020 mV, which is certainly amongst the highest V_{OC} in the literature of ethanol BFCs. For example, Deng et al. developed a BFC with V_{OC} of 860 mV when powered by ethanol, and of 780 mV when powered by commercial alcoholic beverage (maximum power density of 1.78 mW cm^{-2}).[222] Ramanavicius et al. created a single chamber BFC where the anode and cathode were powered by ethanol, with V_{OC} of 240 mV (power density of 1.5 μW cm^{-2}).[223] Topcagic et al. developed a BFC with V_{OC} of 680 mV when operating with two chambers separated by a membrane, and 510 mV when operating membraneless (power density of 300 μW cm^{-2}).[142] Clearly, it is difficult to make a relevant comparison of the delivered powers with the literature, since it is not an intrinsic value of the cell, but the result of preparation experimental conditions and that can be optimized by a convenient electrode design.

However, it is in terms of power that the advantage of employing porous electrodes is clearer, given that the CNFs BFC reaches 230 μW cm^{-2}, which is twice the power achieved by the graphite BFC. This is due to the higher amount of enzymes that is effectively immobilized on the surface of the electrode, and to the more efficient mass transport. Even if the same amount of species was deposited onto each electrode per cm^2 geometrically, those that are not able to be close to the surface leak into the solution or are inactive to the reaction. Moreover, on the CNFs electrode, all the species are closer to the electrode surface (i.e. the surface of the individual fibers), which ease the electrical and mass transfer. The opposite happens with graphite, where a thicker layer of enzymes and mediators is on the surface and may lead to transfer resistance.

One downside of the BFC developed is certainly its stability, which was very low. This is due to the anode stability, which is affected by a series of factors like the deactivation of the enzyme from insufficient proton diffusion in the film, or from the weak diffusion of NAD present in solution to the active sites of the reaction, as mentioned.

6.6. Conclusion

An ethanol BFC with CNFs as electrode material was presented in this chapter. The anode composition was successfully adapted from previous works in our group (with gold electrodes), and the performance with CNFs was higher than graphite as electrode material (current density with graphite as electrode material was 22 % lower). However we acknowledge that the comparison between the two electrodes was made from the projected surface area of each electrode, which is probably not the most accurate method.

Anode and cathode were connected in a two-chamber device, separated with Nafion membrane, and the performance of the complete BFC was tested by the CRD technique, with variable resistances connected to the BFC. The BFC with CNFs as electrodes material presented V_{OC} of 1020 mV, which is remarkable compared to the literature of ethanol BFCs, whereas the BFC with graphite as electrodes material presented V_{OC} of 950 mV. The power density was of 230 $\mu W\ cm^{-2}$ when CNFs were employed as electrodes, which is twice the power obtained with graphite as electrode.

These results highlight the benefits of the porous structure on the performance of the BFC, which is the objective of this work. The porous 3D structure allows for higher enzyme loading and effective mass transport. However, the stability of this device is very low due to the loss of anode performance.

Chapter VII. Development of hybrid biofuel cells powered by glucose

7.1. Introduction

For the fabrication of a glucose BFC (GBFC), glucose oxidation at the anode, catalyzed by glucose oxidase (GOx) or glucose dehydrogenase (GDH) is limited by the regeneration of the enzyme at the anode. Moreover, in the case of GOx, a parasite reaction between glucose and O_2 generates H_2O_2, leading to inevitable degradation of GBFC performance.[114] For glucose oxidation in sensors or glucose BFCs, abiotic nanomaterials have been advocated because of their high available specific electrochemical surface area (SECSA)[151] and their high catalytic activity. The long-term stability of this kind of electrode material is well known in conventional FCs systems. Abiotic glucose catalysts are not selective, compared to enzymes, and might also be poisoned by the reaction with O_2, but its stability and catalytic activity overcome these drawbacks.

In this chapter, two hybrid biofuel cells with abiotic anode and enzymatic cathode will be presented. These systems work from the electrocatalytic glucose oxidation combined to the O_2 reduction.

In section 7.2, abiotic anodes composed of palladium or platinum-modified gold nanocatalysts (Au_xPd_y and Au_xPt_y) for the oxidation of glucose were tested along with a BOD/ABTS@CNFs biocathode prepared with a Nafion matrix. The abiotic anodes were synthesized by our partner from Poitiers, France (IC2MP, *Institut de Chimie des Milieux et Matériaux de Poitiers*), and the preparation and characterization of the nanomaterials is briefly presented, along with BFCs characterizations. These results have been published in the journal ChemElectroChem in 2015.[105]

In section 7.3, the abiotic anode composed of CNF modified *in situ* by Au particles able to perform the oxidation of glucose in alkaline medium (deeply explored in Chapter IV), will

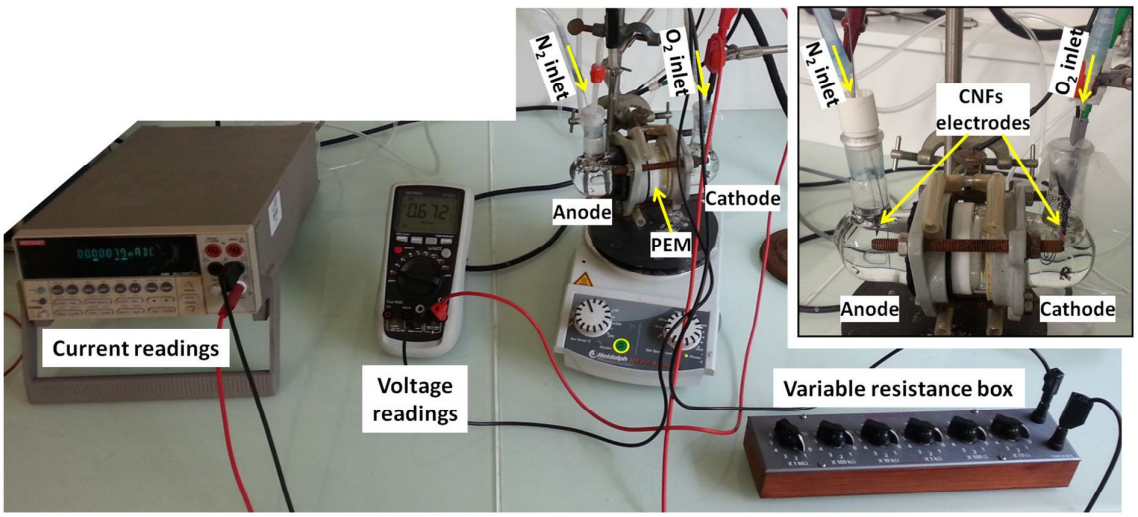

Figure 7.1. *Photos of the laboratory assembly used for h-BFCs tests.*

be employed. This anode was tested in a two-chamber biofuel cell along with the BOD/MWNTs@CNFs biocathode prepared in a chitosan film (presented in Chapter V).

The BFCs were tested through the CRD method (see Annex 2 for details). A picture of the assembly employed for h-BFCs tests is presented in **Figure 7.1**.

7.2. h-BFC powered by glucose with trimetalic NPs-decorated CNFs as abiotic anode and enzymatic biocathode

In this section, the design of a hybrid glucose biofuel cell (h-GBFC) is reported, with aligned electrospun CNFs as electrode materials in the anode and cathode compartments operating at pH 7.4 and 37 °C. The operating conditions are physiological, meaning that this h-BFC is a first step towards the creation of an implantable BFC. Unlike traditional batteries, where environmental concerns and recharging delays are a strong issue, implantable BFCs can count on constant replenishing of fresh fuel from the body, being theoretically able to operate indefinitely.[151] Being glucose one of the most available biofuels, many systems have been implanted in some animals and plants, like the works of Prof. Katz who developed the first pacemaker powered by a BFC implanted in lobsters,[66] and other systems implanted in snails[152] and clams.[65] In addition, French researchers created an enzymatic BFC implanted in rats that was able to power a light emitting diode (LED) or a digital thermometer.[68] The advantage of enzymes over traditional metallic catalysts has been addressed in this work,

but despite all the advantages, enzymatic BFC have not yet been commercialized due to their limited lifetime and stability.

For glucose oxidation at the anode, the synthesis of very small and well- dispersed metal nanostructures composed of Au, Pt and Pd was carried out with the so-called bromide anion exchange (BAE) method,[224] followed by adsorption onto carbon particles that were further immobilized on the surface of CNFs. Regarding O_2 reduction at the cathode compartment, BOD enzyme immobilization was accomplished in this work by entrapment in a Nafion polymer matrix, and ABTS was employed as electron-transfer mediator. Cathode composition was kept constant during all the tests. The h-GBFC was compartmentalized with a Nafion proton exchange membrane separating the chambers, using the as-synthesized abiotic catalysts at the anode and the commercial BOD at the cathode, both immobilized on the surface of aligned electrospun CNFs.

7.2.1. Materials and methods

Abiotic anode. Gold-based electrocatalysts for the anode compartment were synthesized through the BAE method by our partners from IC2MP laboratory. A description of the synthesis procedure follows: "*Typically, a suitable amount of metal(s) salt(s) was dissolved in a thermostatted glass reactor (100 mL ultrapure water) with magnetic stirrer, initially maintained at 25 °C. Potassium bromide was then added, according to a molar ratio ϕ = n(KBr)/n(metal(s)) of 1.5, under vigorous stirring. The value of ϕ was set after different tests. After a few minutes homogenization, a suitable amount of Vulcan XC 72R carbon black was added under constant ultrasonic homogenization to obtain a metal loading of 20 wt.%. The materials Pt/C, Au/C, and* $Au_{80}Pt_{20}$*/C were synthesized by using* $NaBH_4$ *(0.1 mol* L^{-1}*, 15 mL), and* $Au_{70}Pt_{15}Pd_{15}$*/C and* $Au_{60}Pt_{20}Pd_{20}$*/C using AA [L-ascorbic acid] (0.1 mol* L^{-1}*, 13 mL) as reducing agent, respectively. After dropwise addition of the reducing agent, the reactor temperature was elevated at 40 °C. After 2 h, the Vulcan-supported nanomaterials were filtered, rinsed several times with ultrapure water, and dried at 40 °C in an oven for 12 h."*[105]
The preparation of the catalytic ink and of the final CNFs anodes is depicted in **Figure 7.2**.

The electrochemical set-up for anode characterization consisted in a conventional three-electrode cell with temperature control. The reference electrode was a homemade reversible hydrogen electrode (RHE). To avoid any potential loss due to reactions occurring

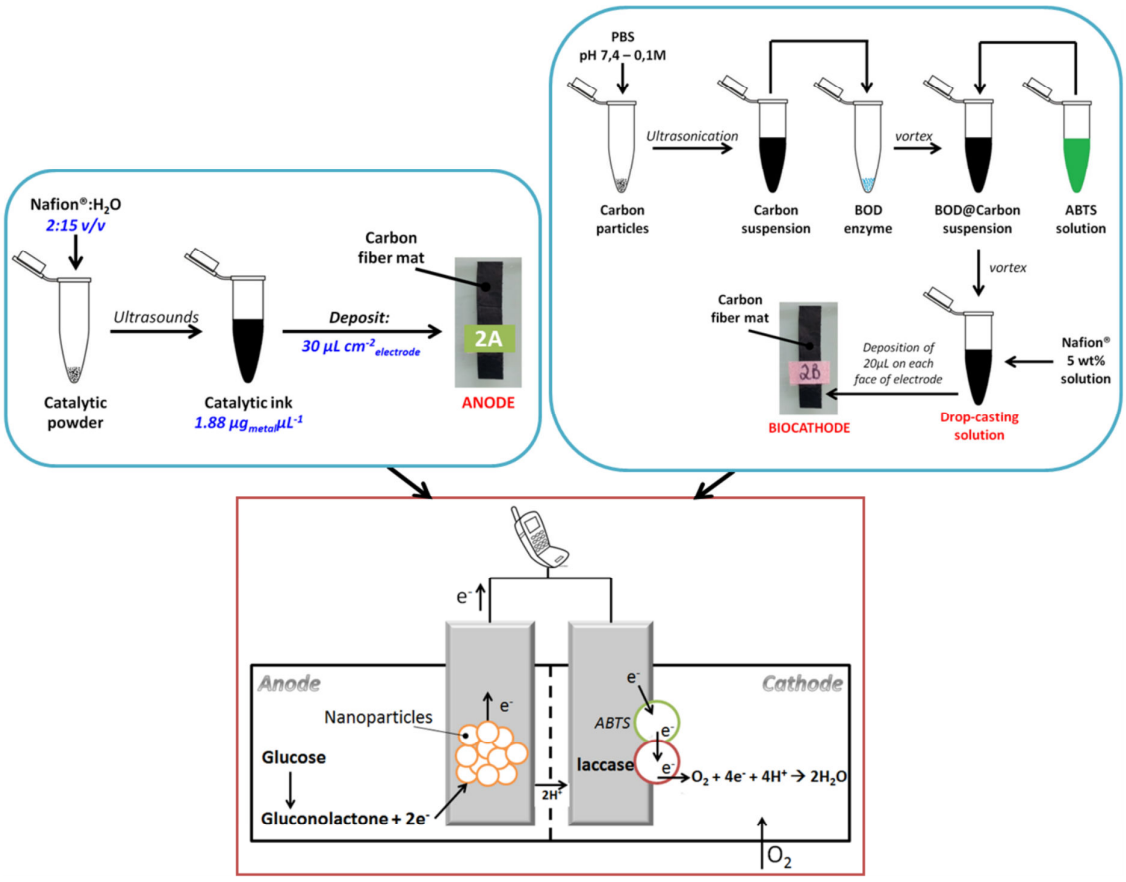

Figure 7.2. *Schematic anode and biocathode preparation for the h-GBFC configuration.*

at the working electrode (WE), the RHE was secluded from the WE compartment; this was achieved by strategically separating the RHE from the solution (WE compartment) by using a Luggin capillary tip. A glassy carbon counter electrode was used. The WE consisted of 1 × 1 cm CNFs, on which a catalytic ink (20 µL cm^{-2}) was deposited for each test. Details regarding the catalytic ink preparation can be found in previous reports.[225,226] Cyclic voltammetry (CV) experiments were conducted in PBS (0.2 M, pH 7.4, prepared from $NaH_2PO_4 \cdot 2H_2O$ and Na_2HPO_4 salts from Sigma Aldrich). Solutions were bubbled with N_2 for 30 min prior to experiments to remove O_2 interferences. The anodic catalytic activity was investigated with D-(+)-glucose (10 mM in PBS, from Sigma Aldrich), and the mass current density was normalized with the weight value assessed by TGA analysis.

Biocathode. The composition of the biocathode employed in the h-GBFCs is similar to the one presented in Chapter 5.5. Briefly, enzyme, mediator, and carbon particles were immobilized on the surface of the CNFs in a Nafion® matrix by using the drop-casting technique. The principle involved depositing a droplet (20 mL) of a mixture containing BOD (16 mg mL^{-1}, 3.04 U mg^{-1} from Amano), ABTS (1.71 mg mL^{-1}, from Sigma Aldrich), Super P carbon particles (7.5 mg mL^{-1} from Timcal), and Nafion® perfluorinated resin solution (5.0 vol.% in lower aliphatic alcohols and water, from Sigma Aldrich) in PBS (0.1 M, pH 7.4) on each face of the electrodes (geometric area of 0.7×0.7 cm^2, i.e. a total of 0.98 cm^2). First, Super P particles in PBS were ultrasonicated for 30 min in a sonication bath. After the addition of the other components, the solution was mixed in a vortex for 20 min, then Nafion® was added, rapidly mixed in vortex, and the drop-casting was carried out. **Figure 7.2** depicts the process. The samples were then dried overnight at 5 °C. The enzyme loading was estimated at 680 µg cm^{-2} relative to electrode geometric surface. Linear scan voltammetry measurements were determined at scan rate of 3.3 mV s^{-1} in O_2-saturated PBS at pH 7.4 after stabilization of the cathode open circuit potential. The current density was determined from the geometric surface area of the electrodes. Biocathode tests are also described in **Annex 2**.

7.2.2. Electrochemical study of glucose oxidation reaction on nanoparticles

This section depicts the characterization of the abiotic anodes separately, as performed by our colleagues from IC2MP, and is reproduced for better understanding of the whole h-GBFC system.

Before performing glucose electrooxidation, the electrochemical behavior of the anode materials in 0.2 M phosphate buffer solution (PBS; pH 7.4 and 37 °C) was checked. Typical steady state cyclic voltammograms (CVs) are displayed in **Figure 7.3A**. The shape of Pt/C CV at pH 7.4 is slightly different to those in alkaline or acidic media, but all the regions can be seen distinctly. During the forward scan, hydrogen desorption from Pt surface occurs at a potential lower than 0.40 V versus RHE (-0.23 V *vs.* Ag/AgCl). Then, Pt oxidation begins at approximately 0.82 V versus RHE (0.18 V *vs.* Ag/AgCl). In the reverse scan, Pt oxides are reduced at around 0.75 V versus RHE (0.12 V *vs.* Ag/AgCl), whereas hydrogen adsorption on the different crystallographic facets starts at approximately 0.40 V versus RHE (-0.23 V *vs.*

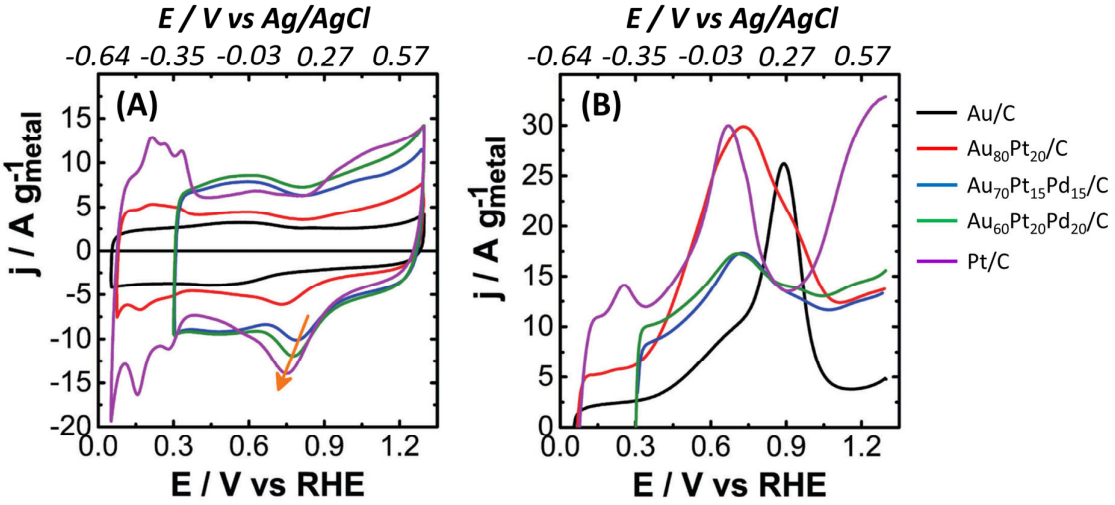

Figure 7.3. *Electrochemical tests recorded at 20 mV s^{-1} in PBS (0.2 M, pH 7.4) at 37 °C on abiotic catalysts Au/C, $Au_{80}Pt_{20}$/C, $Au_{70}Pt_{15}Pd_{15}$/C, $Au_{60}Pt_{20}Pd_{20}$/C and Pt/C:* ***(A)*** *CVs without glucose, and* ***(B)*** *CVs in the presence of glucose (10 mM).*

Ag/AgCl). Taking into account that one monolayer of hydrogen is desorbed from the Pt surface in the forward scan, the specific electrochemical surface area (SECSA) of the Pt electrode is determined by using a charge of 210 mC cm^{-2} as reference.[227] For a CV recorded at 50 mV s^{-1}, a value of 27 m^2 g^{-1} was evaluated which is higher than values reported,[228] meaning the Pt synthesized in this work is expected to be more active. In the case of Au/C, no sign of Au can be seen in the CV. On the other hand, XRD, TEM, and EDX (not shown) and TGA investigations have shown the presence of gold in the sample. Moreover, a CV plotted in alkaline medium showed the presence of gold.[224]

Finally, the catalytic performance of the electrocatalysts was evaluated in the presence of 10 mM glucose. The normalized polarization curves (at 20 mV s^{-1}) are depicted in **Figure 7.3B**. For the mono and bimetallic catalysts, the dehydrogenation properties of the catalysts toward glucose at lower potentials decrease when the Pt content is diminished. Glucose dehydrogenation starts at approximately 0.1 V versus RHE (-0.53 V *vs.* Ag/AgCl). For the trimetallic catalysts, the oxidation starts earlier but, in this case, the curves started at 0.3 V versus RHE for reasons that are explained in detail elsewhere.[225,226] Taking into account the different experimental conditions, the performances obtained herein (in terms of onset potential and peak currents) are superior to those reported for abiotic catalysts (AuPt,[103,130] Pt[184]) or enzymes.[147,229]

7.2.3. Oxygen reduction by BOD

Figure 7.4 presents the polarization curves of the BOD-modified CNFstoward the O_2 enzymatic reduction. Tests were performed in O_2-saturated PBS (0.1 M, pH 7.4) at 30 °C. The oxygen reduction current begins at around 0.55 V *vs.* Ag/AgCl. The electrocatalytic reaction is controlled by diffusion of the oxygen molecules to the electrode surface, giving rise to a semi-plateau in the plot. A cathodic current of approximately 400 µA cm^2 is obtained, relative to the geometric area of the electrode (i.e. two sides of 0.7 × 0.7 cm = 0.98 cm^2). This cathodic current is comparable to those reported in other studies.[88,130] For example, Habrioux et al. obtained a cathodic current of approximately 600 µA cm^2 with BOD-ABTS-Nafion modified porous carbon tube electrodes, with almost three times more active BOD than that used in this work.

Successive scans were realized on the electrodes. The electrode was prepared at day 0. The polarization curves start from an open-circuit voltage (V_{OC}) of around 0.55 V *vs.* Ag/AgCl to 0.1 V *vs*. Ag/AgCl in O_2-saturated PBS, and then following scans were realized after the

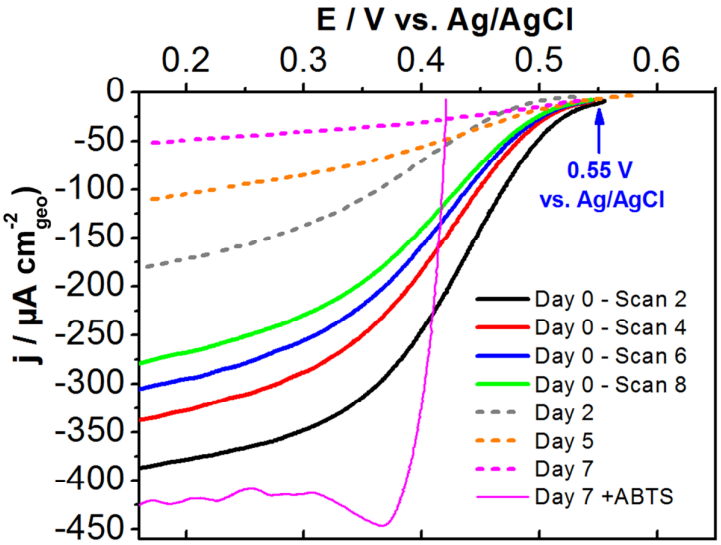

Figure 7.4. *Polarization curves for ORR on aligned CNFs electrodes modified with enzyme BOD entrapped in Nafion matrix along with ABTS, realized in O_2-saturated PBS (0.1 M, pH 7.4) at 30 °C. Sequence of stability tests performed during repeated scans over one week. After 7 days, polarization realized with the addition of ABTS (3 mM) to the solution. Scan rate 3.3 mV s^{-1}.*

recovery of V_{OC}. Successive scans lead to the gradual loss of the initial electrochemical activity. Stability tests were performed periodically until the 7th day, keeping the electrode at 5 °C in a humid environment between each test. After 7 days, the electrode had lost 85 % of its original activity. This loss of activity was mainly due to the loss of ABTS to the solution during tests,[230] as shown by observing the polarization curve realized on the 7th day after addition of 3 mM of ABTS to the solution. A cathodic current even higher than that obtained on day 0 was delivered and was stable on successive scans. This means that most enzymes have kept their activity, but they cannot perform DET, the electrode performance being limited by the ABTS loss. After 2 weeks, the biocathode had lost 50 % of its cathodic current density even in the presence of ABTS in the solution, owing to enzyme denaturation or leakage.

7.2.4. Hybrid glucose BFCs tests

Complete BFC tests were realized in a two-chamber cell, separated with a Nafion membrane. The anode compartment (10 mM glucose solution in PBS pH 7.4) was fed with N_2 gas during the test (for removal of O_2), and the cathode compartment was saturated with O_2. PBS at pH 7.4 was the electrolyte solution in both compartments. More details about BFC tests can be found in Annex 2 of this manuscript.

Monitoring the anode and cathode electrode potentials. An h-GBFC test was performed by introducing a reference electrode (RE) in each compartment to follow the evolution of each electrode potential, then, the constant resistance discharge (CRD) technique was employed. This technique consisted in varying the resistance applied to the cell step by step, while making current and voltage readings, as described in **Annex 2**. This type of investigation allows the identification of the limiting electrode.[231] In FCs science, it is known that the cathode reaction typically limits cell performance. For the purpose of this test, the abiotic anode material was Au/C. **Figure 7.5** displays the anodic and cathodic polarization curves (black and red lines). The anode potential goes from 0.30 to 0.50 V versus RHE (-0.33 to -0.13 V *vs.* Ag/AgCl), meaning ΔE_{anode} = 200 mV. The variation of the cathode potential is more important. It starts at approximately 1.21 V versus RHE (0.57 V *vs.* Ag/AgCl) and falls to 0.70 V versus RHE (0.07 V *vs.* Ag/AgCl) with 113 µA cm^{-2}, meaning

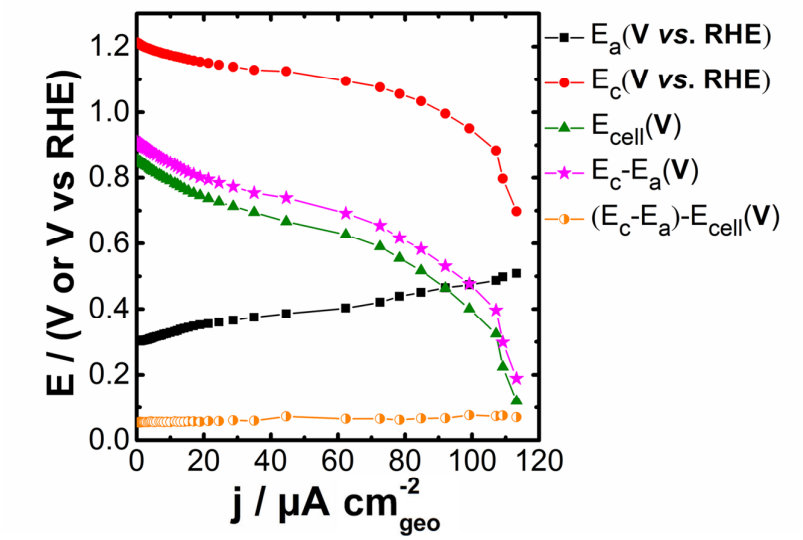

Figure 7.5. *h-GBFC tests with Au/C as anode catalyst and BOD/ABTS as cathode biocatalyst, recorded in PBS (0.1 M; pH 7.4) at 37 °C containing glucose (10 mM) at the anode, and O_2 saturated PBS at the cathode. A reference electrode was immersed in each compartment.*

$\Delta E_{cathode}$ = 510 mV. This rapid variation of the cathode potential limits the activity of the anode, which full potential is not exploited.

In **Figure 7.5**, the green curve represents the cell voltage (E_{cell}), showing V_{OC} of 854 mV. The pink curve shows the theoretical cell voltage (obtained from the difference of $E_{cathode} - E_{anode}$). Around the ohmic drop region, the corresponding internal resistance (R_{int}) has been evaluated from the difference between theoretical and real cell voltages $(E_{cathode} - E_{anode}) - E_{cell}$ (represented by the orange curve) as 2 kΩ (obtained from Ohm's law), which is a high value compared with conventional FCs R_{int} values. R_{int} includes the ohmic resistance (R_Ω) of the system which results from the transfer of protons in electrolyte and electrons close to electrode surface, including resistance of electrode and other contact resistances.[231] This value can be reduced, for example, by the removal of the Nafion membrane between the two compartments to facilitate proton transfer. Also, Han et al. proposed to reduce the activation resistance by modifying the electrode surface, such as immobilizing carbon nanotubes to improve the surface property of electrodes, which will increase the number of catalytic species attaching to the electrodes and thus enhance the efficiency of electron transfer.[231]

Effect of abiotic catalysts. **Figure 7.6** shows the comparative performance of the h-GBFC produced by the CRD method. The left y axis displays the voltage polarization curves $E_{cell} = f(j)$ whereas the right y axis shows the output power density $P = f(j)$. The values of P were calculated by simple multiplication of the cell voltage by the current density at each point. In FCs science, one of the most important parameters is the value of V_{OC}, which provides substantial information on the activation region. Therefore, V_{OC}, and the

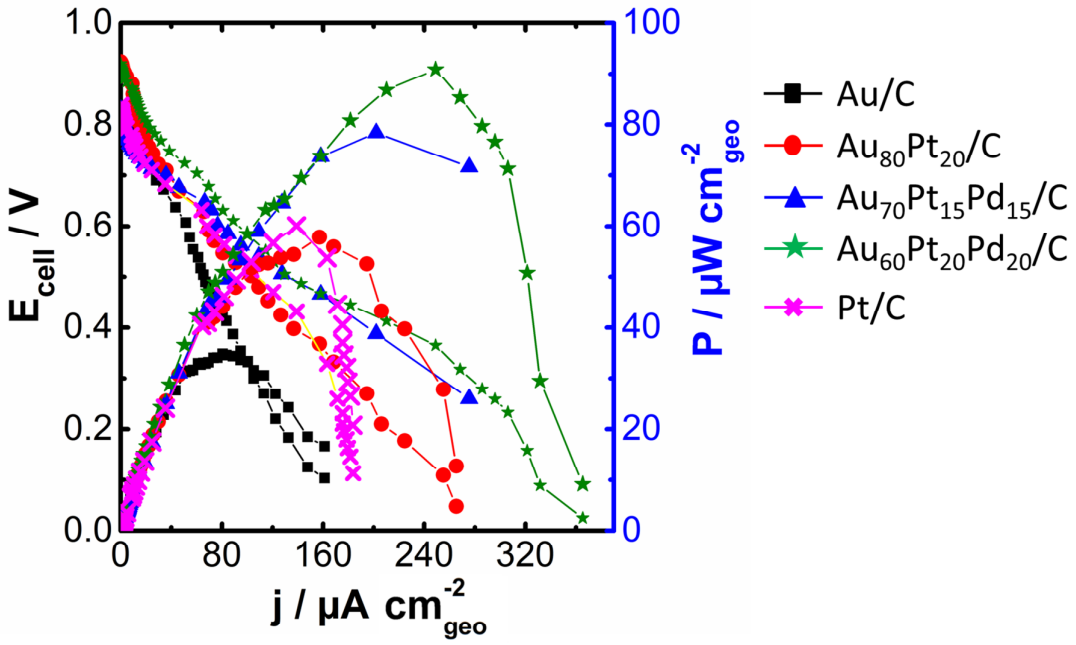

Figure 7.6. *Comparative performances of h-GBFCs: with Au/C, $Au_{80}Pt_{20}$/C, $Au_{70}Pt_{15}Pd_{15}$/C, $Au_{60}Pt_{20}Pd_{20}$/C and Pt/C as anode catalysts, and BOD/ABTS as cathode biocatalyst, recorded in PBS (0.1 M, pH 7.4) at 37 °C containing glucose (10 mM) at the anode and O_2 saturated PBS at the cathode.*

Table 7.1. *Comparative performance of the h-GBFC.*

		Point of maximum power density		
Anode	**Initial V_{OC} (mV)**	**E_{cell} (mV)**	**j (µA cm^{-2})**	**P (µW cm^{-2})**
Au/C	833	432	81	35
$Au_{80}Pt_{20}$/C	924	368	157	58
$Au_{70}Pt_{15}Pd_{15}$/C	830	388	202	78
$Au_{60}Pt_{20}Pd_{20}$/C	820	365	249	91
Pt/C	839	432	139	60

characteristics of the power peak are presented in **Table 7.1**, according to the anode catalyst employed (with the same cathode).

These are the highest values obtained for biofuel cells using abiotic nanomaterials at the anode and BOD at the cathode. Habrioux et al.[130] reported an V_{OC} of 750 mV with $Au_{50}Pt_{50}$/C synthesized from the microemulsion method. This large improvement is attributed to the use of the BAE method for the synthesis of abiotic catalysts. For comparison, for enzymatic GBFCs (not hybrid), different values of V_{OC} have been reported, like 950 mV,[114] 730 mV and 830 mV,[232] and 780 mV.[233] Regarding living systems (*in vivo*), different BFCs have been tested with 200 mV,[67] 300 mV,[65] 810 mV,[69] and 600 mV[66] in pacemaker applications. The anode materials presented here are undoubtedly able to provide good performance upon optimization of each compartment.

From Table 1, the maximum output power density for each anode increases in the order:

$$Au/C < Au_{80}Pt_{20}/C \approx Pt/C < Au_{70}Pt_{15}Pd_{15}/C < Au_{60}Pt_{20}Pd_{20}/C$$

For the monometallic anode materials, P = 35 mW cm^2 for Au/C (at 432 mV) and 60 mW cm^2 for Pt/C (at 432 mV). Reported values are approximately 50 and 30 mW cm^2 for Au/C and Pt/C.[130] Therefore, the Pt/C developed here is two times more powerful. Furthermore, the multimetallic catalysts exhibit better performance in terms of output power density than monometallic catalysts. The trimetallic $Au_{60}Pt_{20}Pd_{20}$/C catalyst shows the best performance, with a value of 91 mW cm^2 at 365 mV, it is almost the same value reported by Habrioux et al. for their best abiotic catalyst ($Au_{70}Pt_{30}$).[130] The synergistic effect between gold and palladium explained this highly improved performance as already observed in alkaline medium.[234] In addition, the improvement on the catalytic performance has been attributed to the fact that Pt/C is more poisoned by the strongly adsorbed species. Otherwise, the competitive adsorption between phosphate ions and glucose on the catalytic sites may explain these observations.

The performance of $Au_{80}Pt_{20}$/C compared with the trimetallic catalyst composition was unexpected. In fact, all the electrochemical tests (cyclic voltammetry, long-term chronoamperometry) suggested that this material was amongst the most active. Moreover,

this catalyst has lower activation energy compared with $Au_{70}Pt_{15}Pd_{15}$/C which shows better performance in h-GBFC. The activation energy in the operating anode potential window (E < 0.7 V *vs.* RHE) is lower than 20 kJ mol^{-1} for $Au_{80}Pt_{20}$/C and lower than 25 kJ mol^{-1} for $Au_{70}Pt_{15}Pd_{15}$/C, as we published (more details found in the publication).[105] Regarding the BOD biocathode reaction, Mano et al. evaluated an activation energy of 34.3 kJ mol^{-1}, whereas for an enzymatic anode composed of GOx the activation energy they report is 28.3 kJ mol^{-1},[71] meaning the cathode activation energy tends to be higher than that of the anode.

Therefore, taking into account: *i)* the electrode potentials evolution in h-GBFC (**Figure 7.5**), *ii)* the polarization curves in a single half-cell, and *iii)* the activation energies, it can be concluded that the performance of the present h-GBFC is still limited by the enzymatic oxygen reduction reaction. The best alternative envisaged to address this issue would be a direct electron-transfer system between the enzyme BOD and the electrode material, which is the topic of the next section. Despite this feature, the h-GBFCs developed in this section represent significant progress in the field, offering exciting prospects for future studies

7.3. h-BFC powered by glucose with Au@CFs prepared *in situ* as abiotic anode and enzymatic biocathode

Another glucose h-BFC will be reported in this section, however with several differences from the one presented in the previous section. Here, the anode is composed of carbon fibers modified *in situ* with Au particles (Au@CFs), a material which synthesis was presented in Chapter IV. The main difference from the CNFs modified with metallic particles from the previous section (which are adsorbed onto the surface of final CNFs) is that here the Au particles are formed *in situ* in the fibers, from the addition of a gold salt in the precursor solution for electrospinning. We showed in Chapter IV that the salt is reduced to metallic Au by reductive properties of PAN polymer in mild conditions, even though the carbonization treatment also provides a reducing environment for the formation of Au particles and NPs, which might complete the process of metallic Au formation.

Glucose oxidation is a reaction that can be catalyzed by gold, which is normally achieved in alkaline conditions. In the previous section this reaction was being catalyzed at neutral pH, which was, amongst others, one of the advantages of that anodic structure.

Since here alkaline conditions will be employed at the anode, this h-BFC cannot be considered for implantable applications. It can, however, be considered for other devices like alkaline BFCs of other types of glucose sensors.

The biocathode employed here is composed of BOD and MWNTs immobilized onto aligned CNFs, entrapped in a chitosan matrix. Differently from other BFCs presented in this work, electron transfer at the cathode is achieved through a DET process, with no electron transfer mediators. The optimization of this biocathode was presented in Chapter V.

Complete BFC test was realized in a two-chamber cell (given the pH difference between anode and cathode), separated with a Nafion membrane, at 37 °C. Stability tests were realized to assess the long-term performance of the h-BFC.

7.3.1. Materials and methods

Abiotic anode. CNFs modified with Au particles (Au@CFs) that were presented in Chapter IV are employed here with no further modification as electrode material, Au particles being responsible for glucose oxidation at the anode chamber. Before complete BFC tests, half-cell tests were performed by cyclic voltammetry (CV) in KOH solution (0.1 M in water, from Merck), containing or not (blanc tests) D-(+)-glucose (10 mM from Sigma Aldrish) under N_2 bubbling, in typical three-electrode system (more details in **Annex 2**). Glucose solution was prepared by stirring for 24 hours.

Biocathode. Biocathode composition employed here is the optimized one that was presented in Chapter V, with BOD and MWNTs in a chitosan and glutaraldehyde matrix. It corresponds to Procedure E, with a first layer of COOH-modified MWNTs, second layer of BOD enzyme in PBS pH 7.0, third layer also of COOH-modified MWNTs and fourth layer of chitosan with glutaraldehyde as cross-linking agent. Each layer was dried prior to the addition of the next layer. The exact synthesis procedure is described in Chapter V, section 5.5, procedure E. Half-cell tests of the biocathode will not be presented in this chapter.

7.3.2. Au@CNFs as abiotic anodes for glucose oxidation

The electrocatalytic activity of the *Au@CFs* electrodes toward glucose oxidation was evaluated by CV in 0.1M KOH containing 10 mM glucose, and the bare CFs electrode was also tested for comparison (**Figure 7.7**).These materials are flexible and free-standing, so no additive or support material was necessary for the final application.

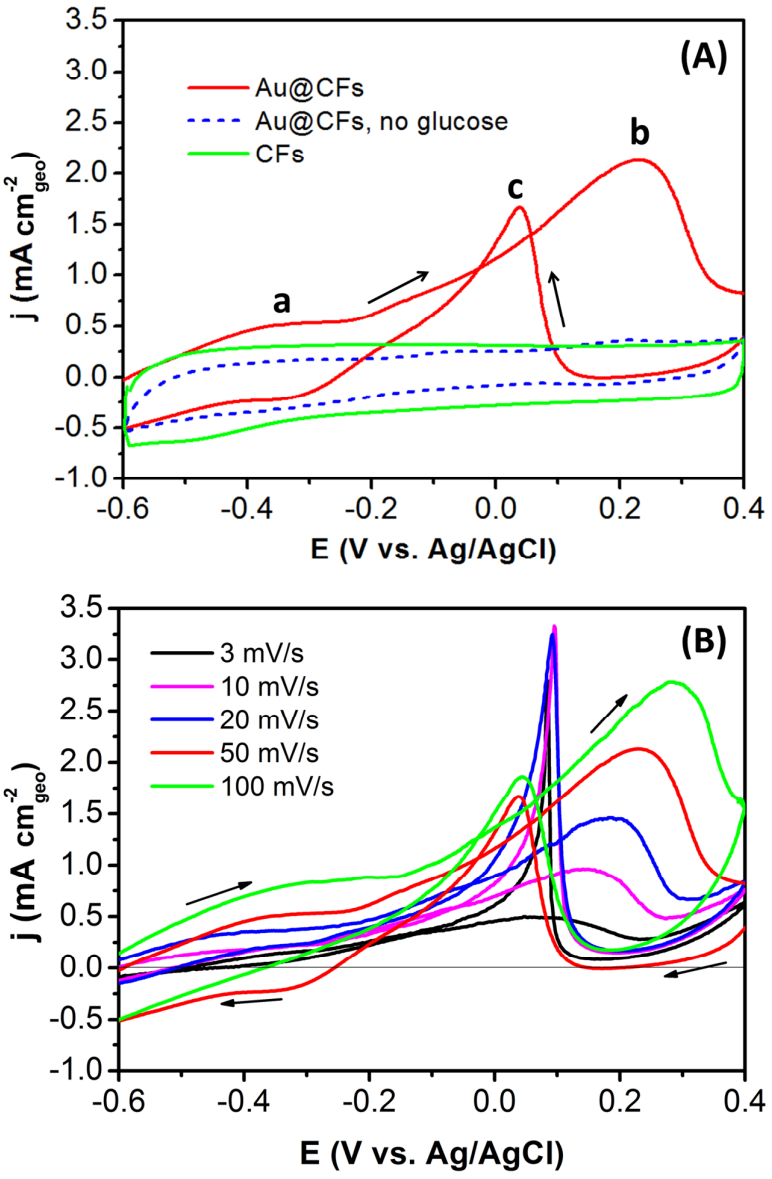

Figure 7.7. (A) *CV of Au@CFs and bare CFs in 10 mM glucose in 0.1 M KOH at 50 mV s*$^{-1}$*, compared with the CV of Au@CFs in the absence of glucose (dashed line).* ***(B)*** *Cyclic voltammograms of Au@CFs at various scan rates in 10 mM glucose in 0.1 M KOH.*

In the absence of glucose (**Figure 7.7A**, dashed line), the CV of the *Au@CFs* electrode exhibits the two small electrochemical processes at 0.2 and 0.1 V *vs.* Ag/AgCl relative to gold surface oxides formation and reduction, respectively, in alkaline media.[98] In the presence of glucose, one can first observe that pure *CFs* exhibit high capacitive currents and are not active for glucose electrooxidation in the potential range investigated (**Figure 7.7A**, green curve). However, *Au@CFs* electrode shows tipical voltammetric behavior in the presence of glucose (**Figure 7.7A**, red curve). Two main oxidation peaks (a, b) appear during the positive potential scan. The peak "a", located at -0.35 V, is due to the dehydrogenation of the anomeric carbon of glucose molecules on Au particles that produce a layer of adsorbed glucose intermediates on the electrode surface.[98,184,235,236] These intermediates are then oxidized to gluconolactone species (peak "b") at around 0.2 to 0.4 V *vs.* Ag/AgCl (according to the scan rate, as demonstrated in **Figure 4.13B**) which is in agreement with the literature.[235,237,238] The peak "c" located in the negative return scan, an intense oxidative peak at around 0.18 V, corresponds to the re-adsorption and oxidation of glucose. This peak intensity is highly dependent on the pH of the reaction medium and reaction conditions (like the nature of the buffer solution or the glucose concentration, for instance).[239] It is important to note that the peaks are dislocated (**Figure 7.7B**) when varying the scan rate, which is also a point to consider when comparing different works.

Regarding peak intensities, *Au@CFs* provides defined and intense peaks. Overall, an intensity of around 2 mA cm^{-2} is obtained for peak "b" at *Au@CFs*, which is a competitive value compared to the present literature on glucose oxidation by materials decorated with gold nanoparticles.[183,186,235,238,240] For example, El-Ads *et al.*[240] created AuNPs modified graphite electrodes that displayed current response of 0.5 mA toward glucose oxidation. This current was further increased to 3 mA when the electrodes were modified with $SrPdO_3$. The work of Hebié et al.[185] highlighted the fact that when different Au forms are employed, different results can be obtained. Comparison of Au nanocuboids, Au spherical NPs, Au nanorods and Au polyhedrons was performed, and maximum current densities of around 5 mA cm^{-2} were obtained for Au spherical NPs. Similar analysis was performed by Tung *et al.*[186] When carbon papers were modified with Au nanocorals, Au nanoparticles or sputered Au, current densities of around 4.0, 3.0 and 2.0 mA cm^{-2} were respectively obtained toward glucose oxidation in alkaline media. Besides, Pasta *et al.*[235] when performing glucose

oxidation with electrodeposited AuNPs on CNTs-textile electrodes obtained around 7 mA cm^{-2}. Clearly, the comparison with literature is not evident since **i)** it is not obvious to calculate and compare the amount of active AuNPs on the electrodes which depends on the methods of preparation, and **ii)** even the Au form is an important factor that play a role in the obtained current densities, as mentioned above.

The greatest advantage of the *Au@CFs* electrodes developed in this work is the one-pot route to prepare the electrodes that leads to strongly attached Au particles to the carbon fibers since they are growing *in situ*. Thereby, we expect no gold nanoparticles leaching to the solution during tests, as opposed to other deposition techniques where the particles are just adsorbed onto a substrate. This fact can be relevant for other gold catalyzed reactions that could benefit of the electrodes herein developed (for example: oxidation of other monosaccharides besides glucose,[241] gas phase oxidation of alcohols,[242] liquid phase oxidation of alcohols,[243] amongst others).

7.3.3. Hybrid glucose BFC tests

A cell with two compartments was employed for the tests, as mentioned, with a Nafion proton exchange membrane separating both compartments. The anode solution was composed of 10 mM glucose prepared in 0.1 M KOH with N_2 bubbling, while PBS at pH 7 was in the cathode, saturated with O_2. The h-BFC was tested by the CRD technique with variable resistances, which consisted in varying the resistance applied to the cell step by step, while making current and voltage readings. More details about BFC tests can be found in **Annex 2** of this manuscript.

Monitoring the anode and cathode electrode potentials. During h-BFC test by CRD technique, a reference electrode was inserted in each compartment in order to observe the evolution of the anode and cathode individually. In the previous section, this approach allowed to identify the cathode as the limiting electrode, since its potential varied too rapidly. In **Figure 7.8** the cell voltage is represented (green line with triangles). The V_{OC} of the cell is around 0.75 V, which is not ideally high but still a good value in comparison with other reported cells. The potential of the cell decreases smoothly, do not presenting sharp variations, and a maximum current density of 200 µA cm^{-2} is delivered. The anode polarization curve (black line with squares) and cathode polarization curve (red line with

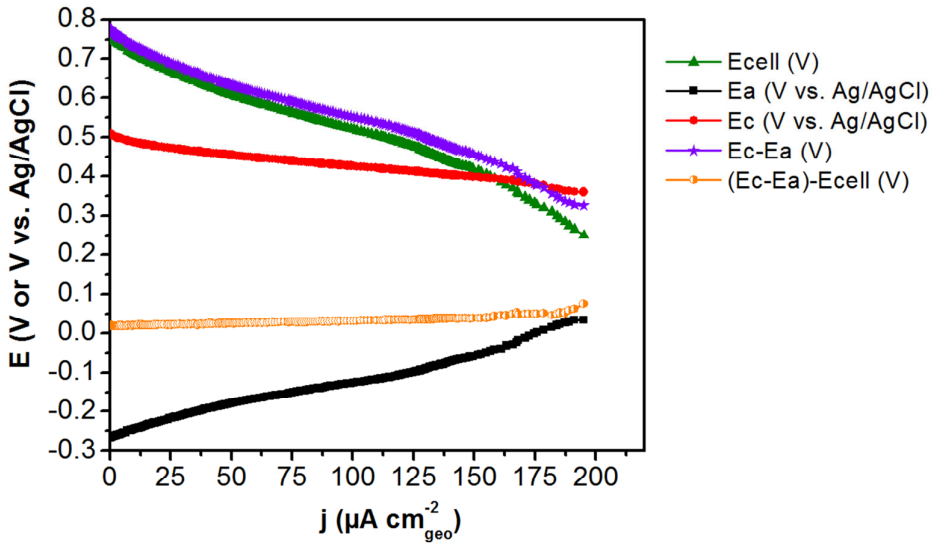

Figure 7.8. *h-GBFC test with Au@CFs anode and BOD/MWNTs@CNFs biocathode, recorded in PBS (0.1M, pH 7.0) at ~37°C containing 10 mM glucose at the anode and O_2-saturated PBS at the cathode compartment. Ag/AgCl reference electrodes immersed in each compartment.*

circles) are also represented (in V vs. Ag/AgCl). The anode potential goes from -0.27 until 0.05 V vs. Ag/AgCl, undergoing a variation of ΔE_{anode} = 0.32 V. At the same time, the cathode potential varies from 0.52 V vs. Ag/AgCl (V_{OC} in agreement with polarization curves from Chapter 5.5) until 0.37 V vs. Ag/AgCl, meaning $\Delta E_{cathode}$ = 0.15 V. Roughly, the anode varied twice as the cathode. From these results, unlike what happened in the previous section, cathode is not the limiting electrode. We can say that chitosan immobilization with DET contributed for the greater stability of the cathode, and chitosan film is ensuring a good microenvironment for the enzyme.

Also in **Figure 7.8**, the purple curve represents the theoretical cell voltage, which was calculated from the difference $E_{cathode} - E_{anode}$. From the difference between these two curves (real and theoretical cell voltages, represented by the orange curve), the internal resistance (R_{int}) of the cell can be calculated by the Ohm's law in the ohmic drop region of the curve, and this value was of ~400 Ω. The physical meaning of this resistance was mentioned in the previous section, where R_{int} was 2 kΩ. We think R_{int} is lower here thanks to the enhanced electron transfer achieved in the cathode by DET with the presence of

MWNTs, as mentioned by Han et al.[231] They proposed that by improving the surface property of electrodes and increasing electron transfer, this resistance could be reduced.

h-BFC performance and stability. In **Figure 7.9** are represented the typical power curves of the h-GBFC from the first test (day 0) until 3 weeks. The left y axis displays the cell polarization curves $E_{cell} = f(j)$ and the right y axis shows the output power density $P = f(j)$. Power curves were calculated by the multiplication of the cell voltage and the current density at each point. After each test, the enzymatic electrode was stored in the fridge in PBS solution at pH 7.0, and the BFC was reassembled after 1 week for the next test.

The results show that maximum power density of ~70 µW cm^{-2} is achieved with the h-GBFC, with V_{OC} of around 0.75 – 0.8 V and maximum current density of around 200 µA cm^{-2}. More interestingly, the performance of the cell remains intact after 3 weeks, and after 3 months, the power density decreases to 30 µW cm^{-2}, which means a decrease in 56 % of the original power. After 3 months, the V_{OC} of the cell is reduced to 0.65 V. This is thanks to the abiotic anode, which stability is naturally high, and to the enhanced stability of the optimized biocathode developed with DET and a chitosan matrix.

However, these results do not reflect the real stability of the BFC in a real application,

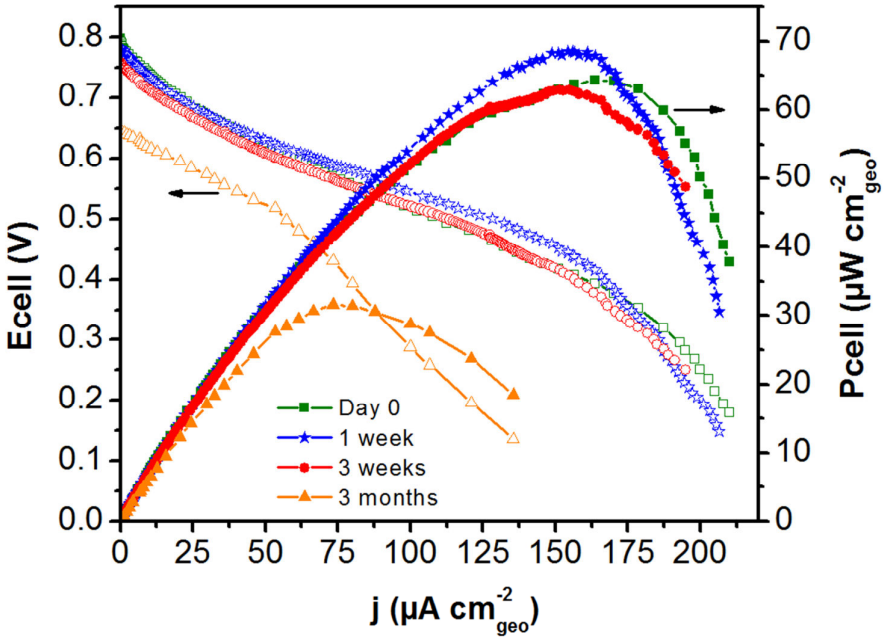

Figure 7.9. *Power curve of the h-GBFC tested by the CRD method, recorded in PBS (0.1 M, pH 7.0) at ~37 °C containing 10 mM glucose at the anode and O_2-saturated PBS at the cathode compartment.*

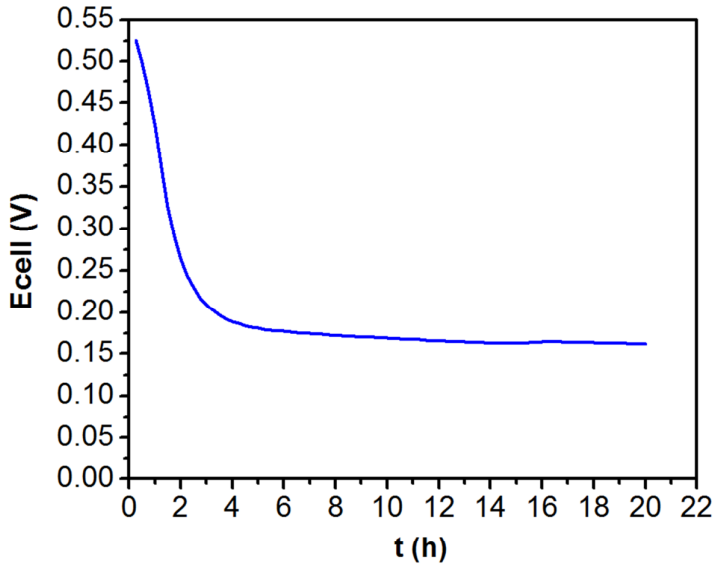

Figure 7.10. *Stability of the h-GBFC tested with fixed resistance of 3.5 kΩ, which corresponds to 75 %P_{max}. Cell voltage values were measured every 10 min for 20 h.*

because after the realization of each test, the biocathode (which stability is obviously more susceptible to losses) was stored at 5 °C in the PBS until the next test was performed. At least from these results we can say the enzymes remain active after 3 months, but it is not possible to say if this behavior would remain in the case of constant discharge of the BFC during the same amount of time, which is more similar to a real operation.

Therefore, in order to test the stability of the cell from a more real perspective, a fixed resistance (3.5 kΩ) was applied to the cell and the voltage was measured every 10 minutes for 20 hours. The resistance chosen corresponded to 75 % of P_{max} in the power curve, which is a value in agreement to the operation of a real device (devices do not operate at maximum power, but slightly lower). The curve obtained from this constant operation of the h-GBFC is presented in **Figure 7.10**. It is observed that for 5 hours the voltage of the cell decreases, and then it stabilizes at around 0.17 V. Even though this value is less important, it is not overestimated and reflects the real capabilities of the h-BFC.

7.4. Conclusion

Through the example of the hybrid BFCs presented in this Chapter, it was possible to show that electrospun CNFs are indeed an excellent electrode material for BFCs. It is a promising support for catalyst immobilization either the catalyst is abiotic or enzymatic.

In the first h-GBFC showed here, Au-based nanoscale materials containing Pt and Pd synthesized by the BAE method were supported onto CNFs and employed as anode material, showing stable catalytic activity in half-cell tests. The cathode was composed of BOD and ABTS immobilized onto CNFs in a Nafion matrix. According to h-GBFC tests, a higher open circuit potential of 0.924 V was reached with the abiotic $Au_{80}Pt_{20}$/C nanocatalyst, which is the best reported value for an h-GBFC operating in a buffer solution at pH 7.4. From the considered anode materials, the highest power density that can be delivered by the h-GBFC was 91 μW cm^{-2} at 0.36 V cell voltage, with $Au_{60}Pt_{20}Pd_{20}$/C as the anode material. The performance of the h-GBFC are limited by the stability of the cathode, which is mostly due to the failure of the immobilization procedure to efficiently entrap ABTS molecules; this is an issue commonly observed that could be overcome by the adoption of a DET strategy.

In the second h-GBFC presented, a different procedure was employed for the synthesis of the abiotic anode. Au particles were produced *in situ* in the CNFs, from the addition of a gold salt in the electrospinning precursor solution. This new material, that was presented and characterized in Chapter IV, was also tested in half-cell toward glucose oxidation in alkaline medium, showing competitive performances with maximum current density of ~2 mA cm^{-2}. The biocathode employed here was composed of BOD and MWNTs immobilized in CNFs through a chitosan matrix. This biocathode that operates with DET was presented and optimized in Chapter V. Complete h-GBFC tests in a two-chamber cell showed that the biocathode is not the limiting electrode anymore, thanks to the DET strategy. Maximum power of ~70 μW cm^{-2} was achieved at ~0.45 V, with V_{OC} of ~0.8 V, and after 3 months the power decreased of 56 % (not in continuous operation).

The advantage of the first h-GBFC presented here was the ability to operate at physiological conditions, whereas the second h-GBFC needed alkaline conditions in the anode. This means the second h-GBFC is not suitable for application in implanted devices. It can, however, be considered for application in alkaline BFCs or other glucose sensors.

Conclusion and perspectives

The field of biofuel cells is still at early stages of development, but advances are making increasingly possible the creation of prototypes that might soon be the subject of industrial development.

In this thesis, carbon nanofibers were employed for the first time as electrode material in enzymatic and hybrid BFCs applications. Focus was given to the synthesis and characterization of different types of CNFs that could present enhanced properties, like electrical conductivity and specific surface, which are crucial in BFCs technology. Therefore, randomly organized CNFs modified or not with CNTs, aligned CNFs or gold-modified CNFs were presented. We showed that when CNTs are adsorbed onto fibers, surface properties are enhanced. The comparison of random and aligned fibers showed that, indeed, fiber alignment plays a role in the electrical conductivity of the material, which is interesting considering the simplicity of the fiber fabricating method. Finally, gold-modified CNFs also provided a simple route to fabricate a material that is able to catalyze glucose electrooxidation.

These electrodes were tested with different enzymes (laccase and BOD) and enzyme immobilization techniques (entrapment in Nafion® polypyrrole or chitosan matrices) in the basic O_2 biocathode. The main goal was to prove CNFs are very promising for such application, and that simple modifications like the spatial organization of fibers can increase not only intrinsic material properties, but electron transfer, for instance.

Nonetheless, the results obtained here for biocathodes are amongst the highest in the literature, and complete BFCs also presented promising results. The hybrid BFC developed with Pt and Pd-modified Au catalysts onto CNFs as anode material was shown to have its stability limited by the cathode performance, which was composed of BOD immobilized with ABTS in a Nafion matrix. After the optimization of the biocathode by achieving DET of BOD enzyme with MWNTs in a chitosan matrix, the test of the second hybrid BFC, where the anode was composed of CNFs modified *in situ* with Au particles, no longer was limited by the

cathode performance. This h-BFC not only presented increased stability, but operated in the absence of electron transfer mediator.

The results obtained in this work were able to demonstrate the promising perspectives of 3D materials with high specific surface to enhance the performance of biofuel cells, if compared to dense materials. Considering the multidisciplinarity of this work and the many optimization possibilities, many perspectives exist for the continuation of this work.

For example, many more advanced strategies could have been undertaken as far as enzyme immobilization engineering is concerned, like the use of linkers that allow enzyme orientation, or the chemical modification or functionalization of CNTs, ABTS, Nafion® or pyrrole prior to immobilization, as a way of creating more stable films. However, considering that this work was a first attempt to employ CNFs as electrode material, some aspects could not be further investigated.

Other perspective would be the use of the biocathode entrapped with polypyrrole, which presented promising results, in a complete BFC. The development of an anodic structure entrapped with polypyrrole is also envisaged. Preliminary tests have been realized for the creation of a fully enzymatic glucose BFC. GOx enzyme is employed at the anode, operating with DET, similarly to the biocathode structure immobilized with chitosan that was developed here. Also, first results were obtained for a microbial-enzymatic BFC with CNFs electrodes on both compartments, which could benefit from the enhanced stability of the biocathode developed here. In addition, a biocathode employing the gold-modified CNFs for enzyme attachment onto Au particles with the help of a specific linker is under development. The porous structure of CNFs would also be suitable for the creation of an “air breathing” biocathode, which has the advantage of enhancing oxygen access to the active sites.

Concerning fibers structure, one interesting strategy would be the addition of porosity on the carbon fibers in order to increase the specific surface of the material. Preliminary tests have been realized on this matter. Moreover, the synthesis of CNFs with different metallic structures embedded in/on the fibers is envisaged. In order to produce harmless PAN precursor fibers, electrospinning tests have been carried employing DMSO as solvent instead of DMF, which can be interesting for larger scale applications. It is noteworthy that

different carbon structures like graphene would be options to CNTs with potential to, allied to CNFs, increase electrode performance.

With all these research possibilities, it is expected that this work will be the first of other scientific advancements contributing to the vast fields of BFCs and electrospun CNFs.

Scientific contributions

Publications

A Both Engel, A Cherifi, S Tingry, D Cornu, A Peigney and Ch Laurent. "*Enhanced performance of electrospun carbon fibers modified with carbon nanotubes: promising electrodes for enzymatic biofuel cells*". **Nanotechnology**, 2013, 24 245402. DOI: 10.1088/0957-4484/24/24/245402.

URL: http://iopscience.iop.org/0957-4484/24/24/245402/media

Adriana Both Engel , Aziz Cherifi , David Cornu , Sophie Tingry. "*Amélioration des performances des biopiles enzymatiques par le design de nouveaux matériaux d'électrode*". **L'Actualité Chimique**, November 2014, n° 390.

URL: http://www.lactualitechimique.org/spip.php?numero_article3072

Yaovi Holade, Adriana Both Engel, Sophie Tingry, Aziz Cherifi, David Cornu, Karine Servat, Têko W. Napporn and Kouakou B. Kokoh. "*Insights on Hybrid Glucose Biofuel Cells Based on Bilirubin Oxidase Cathode and Gold-Based Anode Nanomaterials*". **ChemElectroChem**, 2014, Volume 1, Issue 11, pages 1976-87. DOI: 10.1002/celc.201402142

URL: http://onlinelibrary.wiley.com/doi/10.1002/celc.201402142/abstract

Adriana Both Engel, Aziz Cherifi, Mikhael Bechelany, Sophie Tingry and David Cornu. "*Control of Spatial Organization of Electrospun Fibers in a Carbon Felt for Enhanced Bioelectrode Performance"*, front cover. **ChemPlusChem**, 2015, Volume 80, Issue 3. DOI: 10.1002/cplu.201402324.

URL: http://onlinelibrary.wiley.com/doi/10.1002/cplu.201402324/abstract

Adriana Both Engel, Yaovi Holade, Sophie Tingry, Aziz Cherifi, David Cornu, Karine Servat, Teko W. Napporn and Kouakou B. Kokoh. *"Electrospun Carbon Fibers: Promising Electrode Material for Abiotic and Enzymatic Catalysis"*. **JPhysChem C**, 2015, 119(29), ppt 16724-16733. DOI: 10.1021/acs.jpcc.5b04352.

URL: http://pubs.acs.org/doi/abs/10.1021/acs.jpcc.5b04352

Adriana Both Engel, Mikhael Bechelany, Olivier Fontaine, Aziz Cherifi, David Cornu and Sophie Tingry. *"One-pot route to gold nanoparticles embedded in electrospun carbon fibers as an efficient catalyst material for hybrid alkaline glucose biofuel cells"*. **ChemElectroChem**, 2016. DOI: 10.1002/celc.201500537.

URL: http://onlinelibrary.wiley.com/doi/10.1002/celc.201500537/abstract

Participation in national conferences (France)

July, 2013. **Journées d'Electrochimie**, Paris.

✓ Oral presentation : "*Des fibres de carbone obtenues par electrospinning modifiées avec des CNTs : des matériaux d'électrodes prometteurs pour les biopiles*".
Adriana Both Engel, Aziz Cherifi, Christophe Laurent, Allan Peigney, David Cornu, Sophie Tingry.

October 2013. **Journées Méditerranéennes des Jeunes Chercheurs**, Montpellier.

✓ Poster presentation (best poster prize): "*New enzymatic biofuel cells electrodes composed of carbon fibers created by electrospinning*".
Adriana Both Engel, Aziz Cherifi, Sophie Tingry, David Cornu.

December, 2013. **4^{éme} Colloque de la Féderation Gay Lussac – La Chimie et la Ville de Demain**, Paris.

✓ Oral presentation: *"Nouvelles électrodes pour biopiles enzymatiques obtenues à partir de fibres de carbone electrospun".*
Adriana Both Engel, Morgane Ramade, Aziz Cherifi, Christophe Laurent, Allan Peigney, David Cornu, Sophie Tingry.

March, 2014. **Ecole d'Energies et Recherches**, Roscoff.

✓ Flash presentation and Poster: *"Développement de nouvelles biopiles enzymatiques à base d'électrodes à grande surface spécifique obtenues par electrospinning"*.
Adriana Both Engel, Aziz Cherifi, Sophie Tingry, David Cornu.

September 2014. **XIV^{éme} Colloque du Groupe Français de Bioelectrochimie**, Sète.

✓ Poster presentation: *"Biopiles enzymatiques et la technologie des matériaux d'électrode"*.
Adriana Both Engel, Aziz Cherifi, Sophie Tingry, David Cornu.

Participation in international conferences

September 2013. **HeteroNanoCarb 2013,** Barcelone, Spain.

✓ Oral presentation: *"CNT-reinforced electrospun carbon fibers: promising electrodes for energy production by enzymatic biofuel cells".*
Sophie Tingry, Adriana Both Engel, Aziz Cherifi, David Cornu, Christophe Laurent.

December 2013. **Thermec'2013 (International Conference on Processing & Manufacturing of Advanced Materials)**, Las Vegas, USA.

✓ Oral presentation: *"Electrospun carbon fibers as promising electrodes for enzymatic biofuel cells".*
David Cornu, Adriana Both Engel, Aziz Cherifi, Sophie Tingry.

August 2014. **Electrospin 2014 – 3rd International Conference on Electrospinning**, San Francisco, USA.

✓ Oral presentation: *"Electrospun carbon fibers as promising electrodes for enzymatic biofuel cells"*
Adriana Both Engel, Aziz Cherifi, Mikhael Bechelany, Sophie Tingry, David Cornu.
✓ Oral presentation: *"One-pot route to Carbon Electrospun Fibers decorated with Metal-based Nanomaterials"*
Adriana Both Engel, Aziz Cherifi, Mikhael Bechelany, Sophie Tingry, David Cornu.

September 2014. **International Society of Electrochemistry (ISE) 65th Annual Meeting**, Lausanne, Switzerland.

✓ Oral presentation: *"Electrospun carbon fibers: a promising electrode material for abiotic and enzymatic catalysis in hybrid biofuel cells"*
Sophie Tingry, Adriana Both Engel, Aziz Cherifi, David Cornu, Yaovi Holade, Karine Servat, Boniface Kokoh, Teko Napporn.

March 2015. **International Workshop: Nanomaterials for Energy and Environment,** Paris, France.

✓ Poster presentation: *"Advanced micro-power fuel cell for bionanotechnology application"*
Yaovi Holade, Kevin MacVittie, Adriana Both Engel, Karine Servat, Sophie Tingry, Teko W. Napporn, Evgeny Katz, Jean-Marc Berjeaud, K. Boniface Kokoh.

June 2015. **11th International Symposium on Ceramic Materials and Components for Energy and Environmental Applications**, Vancouver, Canada.

- ✓ Oral presentation: *"Design of electrospun carbon fiber electrodes for enzymatic biofuel cells"*

  Adriana Both Engel, Aziz Cherifi, Mikhael Bechelany, Sophie Tingry, David Cornu.
- ✓ Oral presentation: *"One-pot route to electrospun carbon fibers decorated with gold (nano)particles for the electrochemical oxidation of glucose"*

  David Cornu, Adriana Both Engel, Aziz Cherifi, Mikhael Bechelany, Sophie Tingry.

October 2015. **International Symposium on Nanotechnologies : Research , Innovation and Economic Challenges**, Casablanca, Morocco.

- ✓ Oral presentation: *"Electrospun carbon felts – bare and modified with gold nanoparticles – as electrode materials for biofuel cells"*

  Adriana Both Engel, Mikhael Bechelany, Sophie Tingry, David Cornu.

References

(1) Messina, G.; Santangelo, S. *Carbon - The Future Material for Advanced Technology Applications*; Messina, G.; Santangelo, S., Eds.; Springer-Verlag Berlin Heidelberg, 2006.

(2) Rufford, T. E.; Zhu, J.; Hulicova-Jurcakova, D. *Green Carbon Materials: Advances and Applications*; Rufford, T. E.; Zhu, J.; Hulicova-Jurcakova, D., Eds.; CRC Press, 2014.

(3) Falcao, E. H. L.; Wudl, F. Carbon Allotropes: Beyond Graphite and Diamond. *J. Chem. Technol. Biotechnol.* **2007**, *82*, 524–531.

(4) Mantell, C. L. *Carbon and Graphite Handbook*; Interscience Publishers: New York, 1968.

(5) Huang, X. Fabrication and Properties of Carbon Fibers. *Materials (Basel).* **2009**, *2*, 2369–2403.

(6) Prescott, R.; Orr, I. W. Process for the Manufacture of Continuous High Modulus Carbon Yarns and Monofilaments. 3533743, 1970.

(7) Edison, T. A. Electric Lamp. 223898, 1880.

(8) Bacon, R. Filamentary Graphite and Method for Producing the Same. 2957756, 1960.

(9) High Performance Carbon Fibers - American Chemical Society National Historic Chemical Landmark http://www.acs.org/content/acs/en/education/whatischemistry/landmarks/carbonfibers.html (accessed Aug 5, 2015).

(10) Rahaman, M. S. A.; Ismail, A. F.; Mustafa, A. A Review of Heat Treatment on Polyacrylonitrile Fiber. *Polym. Degrad. Stab.* **2007**, *92*, 1421–1432.

(11) Edie, D. D. The Effect of Processing on the Structure and Properties of Carbon Fibers. *Carbon N. Y.* **1998**, *36*, 345–362.

(12) Brisson, M. The global market for PAN-based carbon fiber http://www.jeccomposites.com/news/composites-news/global-market-pan-based-carbon-fibre (accessed Aug 5, 2015).

(13) Carbon Fiber Reinforced Polymers Composites Market Forecast 2015 https://www.visiongain.com/blog/index.php/carbon-fibre-reinforced-polymers-composites-market-forecast-2015/ (accessed Aug 5, 2015).

(14) 12% growth in carbon fiber predicted http://www.materialstoday.com/carbon-fiber/news/12-growth-in-carbon-fiber-predicted/ (accessed Aug 5, 2015).

(15) Nataraj, S. K.; Yang, K. S.; Aminabhavi, T. M. Polyacrylonitrile-Based nanofibers—A State-of-the-Art Review. *Prog. Polym. Sci.* **2012**, *37*, 487–513.

(16) Morita, K.; Murata, Y.; Ishitani, A.; Murayama, K.; Ono, T.; Nakajima, A. Characterization of Commercially Available PAN (polyacrylonitrile)-Based Carbon Fibers. *Pure Appl. Chem.* **1986**, *58*, 455–468.

(17) Houtz, R. C. "Orlon" Acrylic Fiber: Chemistry and Properties. *Text. Res. J.* **1950**, *20*, 786–801.

(18) David, L. I. B.; Ismail, A. F. Influence of the Thermostabilization Process and Soak Time

during Pyrolysis Process on the Polyacrylonitrile Carbon Membranes for O2/N2 Separation. *J. Memb. Sci.* **2003**, *213*, 285–291.

(19) Wu, M.; Wang, Q.; Li, K.; Wu, Y.; Liu, H. Optimization of Stabilization Conditions for Electrospun Polyacrylonitrile Nanofibers. *Polym. Degrad. Stab.* **2012**, *97*, 1511–1519.

(20) Gupta, A.; Harrison, I. R. New Aspects in the Oxidative Stabilization of PAN-Based Carbon Fibers: II. *Carbon N. Y.* **1997**, *35*, 809–818.

(21) Liu, C.-K.; Lai, K.; Liu, W.; Yao, M.; Sun, R.-J. Preparation of Carbon Nanofibres through Electrospinning and Thermal Treatment. *Polym. Int.* **2009**, *58*, 1341–1349.

(22) Zhu, D.; Chu, C.; Nakura, N.; Matsuo, M. Study of Carbon Films from PAN/VGCF Composites by Gelation/crystallization from Solution. *Carbon N. Y.* **2002**, *40*, 363–373.

(23) Fitzer, E.; Frohs, W. The Influence of Carbonization and Post Treatment Conditions on the Properties of PAN- Based Carbon Fibers. In *Carbon '88 Proceedings of the International Carbon Conference*; Carbon: Newcastle upon Tyne, U.K., 1988; pp. 298–300.

(24) Iijima, S. Helical Microtubules of Graphitic Carbon. *Nature* **1991**, *354*, 56–58.

(25) Kim, Y. A.; Hayashi, T.; Endo, M.; Dresselhaus, M. S. Carbon Nanofibers. In *Springer Handobook of Nanomaterials*; Vajtai, R., Ed.; Springer, 2013; pp. 233–262.

(26) Liu, J.; Yue, Z.; Fong, H. Continuous Nanoscale Carbon Fibers with Superior Mechanical Strength. *Small* **2009**, *5*, 536–542.

(27) Arshad, S. N.; Naraghi, M.; Chasiotis, I. Strong Carbon Nanofibers from Electrospun Polyacrylonitrile. *Carbon N. Y.* **2011**, *49*, 1710–1719.

(28) Yao, J.; Bastiaansen, C.; Peijs, T. High Strength and High Modulus Electrospun Nanofibers. *Fibers* **2014**, *2*, 158–186.

(29) Zhang, L.; Aboagye, A.; Kelkar, A.; Lai, C.; Fong, H. A Review: Carbon Nanofibers from Electrospun Polyacrylonitrile and Their Applications. *J. Mater. Sci.* **2013**, *49*, 463–480.

(30) Reneker, D. H.; Chun, I. Nanometre Diameter Fibres of Polymer, Produced by Electrospinning. *Nanotechnology* **1996**, *7*, 216.

(31) Subianto, S.; Cornu, D.; Cavaliere, S. Fundamentals of Electrospinning. In *Electrospinning for Advanced Energy and Environmental Applications*; Cavaliere, S., Ed.; CRC Press, 2015; p. 288 Pages.

(32) Bognitzki, M.; Czado, W.; Frese, T.; Schaper, a.; Hellwig, M.; Steinhart, M.; Greiner, a.; Wendorff, J. H. Nanostructured Fibers via Electrospinning. *Adv. Mater.* **2001**, *13*, 70–72.

(33) Bhardwaj, N.; Kundu, S. C. Electrospinning: A Fascinating Fiber Fabrication Technique. *Biotechnol. Adv.* **2010**, *28*, 325–347.

(34) Tucker, N.; JJ, S.; MP, S.; H, R.; K, H. The History of the Science and Technology of Electrospinning from 1600 to 1995. *J. Eng. Fibers Fabr. - JEFF* **2012**.

(35) Morton, W. J. Method of Dispersing Fluids. US 705691 A, 1902.

(36) Formhals, A. Process and Apparatus for Preparing Artificial Threads. US1975504, 1934.

(37) Lukáš, D.; Sarkar, A.; Martinová, L.; Vodsed'álková, K.; Lubasová, D.; Chaloupek, J.; Pokorný, P.; Mikeš, P.; Chvojka, J.; Komárek, M. Physical Principles of Electrospinning

(Electrospinning as a Nano-Scale Technology of the Twenty-First Century). *Text. Prog.* **2009**, *41*, 59–140.

(38) Persano, L.; Camposeo, A.; Tekmen, C.; Pisignano, D. Industrial Upscaling of Electrospinning and Applications of Polymer Nanofibers: A Review. *Macromol. Mater. Eng.* **2013**, *298*, 504–520.

(39) Taylor, G. Disintegration of Water Drops in an Electric Field. *Proc. R. Soc. - A. Math. Phys. Sci.* **1964**, *280*.

(40) Taylor, G. The Force Exerted by an Electric Field on a Long Cylindrical Conductor. *Proc. R. Soc. London - A. Math. Phys. Sci.* **1966**, *291*.

(41) Taylor, G. Electrically Driven Jets. *Proc. R. Soc. London - A. Math. Phys. Sci.* **1969**, *313*.

(42) Doshi, J.; Reneker, D. H. Electrospinning Process and Applications of Electrospun Fibers. In *Conference Record of the 1993 IEEE Industry Applications Conference Twenty-Eighth IAS Annual Meeting*; IEEE: Toronto, 1993; pp. 1698–1703.

(43) Srinivasan, G.; Reneker, D. H. Structure and Morphology of Small Diameter Electrospun Aramid Fibers. *Polym. Int.* **1995**, *36*, 195–201.

(44) Ramakrishna, S.; Fujihara, K.; Teo, W.-E.; Lim, T.-C.; Ma, Z. *An Introduction to Electrospining and Nanofibers*; World Scientific Publishing Co. Pte. Ltd.: Singapore, 2005.

(45) Zussman, E.; Chen, X.; Ding, W.; Calabri, L.; Dikin, D. a.; Quintana, J. P.; Ruoff, R. S. Mechanical and Structural Characterization of Electrospun PAN-Derived Carbon Nanofibers. *Carbon N. Y.* **2005**, *43*, 2175–2185.

(46) Gomes, D. S.; Silva, A. N. R.; Morimoto, N. I.; Furlan, R.; Ramos, I. Characterization of an Electrospinning Process Using Different PAN / DMF Concentrations. **2007**, *17*, 206–211.

(47) Wang, Y. U.; Serrano, S.; Santiago-Aviles, J. J. Conductivity Measurement of Electrospun PAN-Based Carbon Nanofiber. *J. Mater. Sci. Lett.* **2002**, *21*, 1055–1057.

(48) Luo, C.; Stoyanov, S.; Stride, E.; Pelan, E.; Edirisinghe, M. Electrospinning versus Fibre Production Methods: From Specifics to Technological Convergence. *Chem. Soc. Rev.* **2012**, *41*, 4708–4735.

(49) Capone, G. J. Wet-Spinning Technology. In *Acrylic Fiber Technology and Applications*; Masson, J., Ed.; 1995; pp. 69–99.

(50) Rodriguez, N. M. A Review of Catalytically Grown Carbon Nanofibers. *J. Mater. Res.* **1993**, *8*, 3233–3250.

(51) Endo, M.; Kim, Y. a.; Hayashi, T.; Nishimura, K.; Matusita, T.; Miyashita, K.; Dresselhaus, M. S. Vapor-Grown Carbon Fibers (VGCFs) - Basic Properties and Their Battery Applications. *Carbon N. Y.* **2001**, *39*, 1287–1297.

(52) Li, D.; Xia, Y. Electrospinning of Nanofibers: Reinventing the Wheel? *Adv. Mater.* **2004**, *16*, 1151–1170.

(53) Nain, A. S.; Sitti, M.; Jacobson, A.; Kowalewski, T.; Amon, C. Dry Spinning Based Spinneret Based Tunable Engineered Parameters (STEP) Technique for Controlled and Aligned Deposition of Polymeric Nanofibers. *Macromol. Rapid Commun.* **2009**, *30*, 1406–1412.

(54) Jiang, X. CVD Growth of Carbon Nanofibers. *Phys. Status Solidi* **2014**, *211*, 2679–2687.

(55) Tibbetts, G.; Lake, M.; Strong, K.; Rice, B. A Review of the Fabrication and Properties of Vapor-Grown Carbon Nanofiber/polymer Composites. *Compos. Sci. Technol.* **2007**, *67*, 1709–1718.

(56) Kirubakaran, A.; Jain, S.; Nema, R. K. A Review on Fuel Cell Technologies and Power Electronic Interface. *Renew. Sustain. Energy Rev.* **2009**, *13*, 2430–2440.

(57) Gross, D. Fuel Cells: 170 years of technology development – and Space Age experience! http://www.cleantechinvestor.com/portal/fuel-cells/6455-fuel-cell-history.html (accessed Aug 26, 2015).

(58) Larminie, J.; Dicks, A. *Fuel Cell Systems Explained*; 2nd ed.; Wiley, 2003; Vol. 93.

(59) Potter, M. C. Electrical Effects Accompanying the Decomposition of Organic Compounds. *Proc. R. Soc. B Biol. Sci.* **1911**, *84*, 260–276.

(60) Cohen, B. The Bacterial Culture as an Electrical Half-Cell. *J. Bacteriol.* **1931**, *21*, 18–19.

(61) Yahiro, A. T.; Lee, S. M.; Kimble, D. O. Bioelectrochemistry: I. Enzyme Utilizing Bio-Fuel Cell Studies. *Biochim. Biophys. Acta - Spec. Sect. Biophys. Subj.* **1964**, *88*, 375–383.

(62) Barton, S. C.; Gallaway, J.; Atanassov, P. Enzymatic Biofuel Cells for Implantable and Microscale Devices. *Chem. Rev.* **2004**, *104*, 4867–4886.

(63) Falk, M.; Blum, Z.; Shleev, S. Direct Electron Transfer Based Enzymatic Fuel Cells. *Electrochim. Acta* **2012**, *82*, 191–202.

(64) Katz, E.; Shipway, A. N.; Willner, I. Chapter 21 - Biochemical Fuel Cells. In *Handbook of Fuel Cells – Fundamentals, Technology and Applications*; Vielstich, W.; Gasteiger, H. A.; Lamm, A., Eds.; John Wiley & Sons, Ltd, 2003; Vol. 1.

(65) Szczupak, A.; Halámek, J.; Halámková, L.; Bocharova, V.; Alfonta, L.; Katz, E. Living Battery – Biofuel Cells Operating in Vivo in Clams. *Energy Environ. Sci.* **2012**, *5*, 8891.

(66) MacVittie, K.; Halámek, J.; Halámková, L.; Southcott, M.; Jemison, W. D.; Lobel, R.; Katz, E. From "cyborg" Lobsters to a Pacemaker Powered by Implantable Biofuel Cells. *Energy Environ. Sci.* **2013**, *6*, 81–86.

(67) Cinquin, P.; Gondran, C.; Giroud, F.; Mazabrard, S.; Pellissier, A.; Boucher, F.; Alcaraz, J.-P.; Gorgy, K.; Lenouvel, F.; Mathé, S.; et al. A Glucose Biofuel Cell Implanted in Rats. *PLoS One* **2010**, *5*, 1–7.

(68) Zebda, A.; Cosnier, S.; Alcaraz, J.-P.; Holzinger, M.; Le Goff, A.; Gondran, C.; Boucher, F.; Giroud, F.; Gorgy, K.; Lamraoui, H.; et al. Single Glucose Biofuel Cells Implanted in Rats Power Electronic Devices. *Sci. Rep.* **2013**, *3*, 1–5.

(69) Miyake, T.; Haneda, K.; Nagai, N.; Yatagawa, Y.; Onami, H.; Yoshino, S.; Abec, T.; Nishizawa, M. Enzymatic Biofuel Cells Designed for Direct Power Generation from Biofluids in Living Organisms. *Energy Environ. Sci.* **2011**, *4*, 5008–5012.

(70) Holade, Y.; MacVittie, K.; Conlon, T.; Guz, N.; Servat, K.; Napporn, T. W.; Kokoh, K. B.; Katz, E. Wireless Information Transmission System Powered by an Abiotic Biofuel Cell Implanted in an Orange. *Electroanalysis* **2015**, *27*, 276–280.

(71) Mano, N.; Mao, F.; Heller, A. Characteristics of a Miniature Compartment-Less Glucose-O2 Biofuel Cell and Its Operation in a Living Plant. *J. Am. Chem. Soc.* **2003**, *125*, 6588–6594.

(72) Poulpiquet, A. de; Ciaccafava, A.; Gadiou, R.; Gounel, S.; Giudici-Orticoni, M. T.; Mano, N.; Lojou, E. Design of a H2/O2 Biofuel Cell Based on Thermostable Enzymes. *Electrochem. commun.* **2014**, *42*, 72–74.

(73) Xu, L.; Armstrong, F. A. Pushing the Limits for Enzyme-Based Membrane-Less Hydrogen Fuel Cells – Achieving Useful Power and Stability. *RSC Adv.* **2015**, *5*, 3649–3656.

(74) Hao Yu, E.; Scott, K. Enzymatic Biofuel Cells—Fabrication of Enzyme Electrodes. *Energies* **2010**, *3*, 23–42.

(75) Wu, X.; Zhao, F.; Varcoe, J. R.; Thumser, A. E.; Avignone-Rossa, C.; Slade, R. C. T. A One-Compartment Fructose/air Biological Fuel Cell Based on Direct Electron Transfer. *Biosens. Bioelectron.* **2009**, *25*, 326–331.

(76) Stoica, L.; Dimcheva, N.; Ackermann, Y.; Karnicka, K.; Guschin, D. A.; Kulesza, P. J.; Rogalski, J.; Haltrich, D.; Ludwig, R.; Gorton, L.; et al. Membrane-Less Biofuel Cell Based on Cellobiose Dehydrogenase (Anode)/Laccase (Cathode) Wired via Specific Os-Redox Polymers. *Fuel Cells* **2009**, *9*, 53–62.

(77) Ivanov, I.; Vidaković-Koch, T.; Sundmacher, K. Recent Advances in Enzymatic Fuel Cells: Experiments and Modeling. *Energies* **2010**, *3*, 803–846.

(78) Zhang, X.; Liu, D.; Li, L.; You, T. Direct Electrochemistry of Glucose Oxidase on Novel Free- Standing Nitrogen-Doped Carbon Nanospheres@Carbon Nanofibers Composite Film. *Sci. Rep.* **2015**, *5*, 1–11.

(79) Tasca, F.; Gorton, L.; Harreither, W.; Haltrich, D.; Ludwig, R.; Nöll, G. Highly Efficient and Versatile Anodes for Biofuel Cells Based on Cellobiose Dehydrogenase from Myriococcum Thermophilum. *J. Phys. Chem. C* **2008**, *112*, 13668–13673.

(80) Coman, V.; Ludwig, R.; Harreither, W.; Haltrich, D.; Gorton, L.; Ruzgas, T.; Shleev, S. A Direct Electron Transfer-Based Glucose/Oxygen Biofuel Cell Operating in Human Serum. *Fuel Cells* **2010**, *10*, 9–16.

(81) Lima, F.; Maia, G. Direct Electron Transfer from Alcohol Dehydrogenase. *RSC Adv.* **2014**, *4*, 22575.

(82) Aquino Neto, S.; Suda, E. L.; Xu, S.; Meredith, M. T.; De Andrade, A. R.; Minteer, S. D. Direct Electron Transfer-Based Bioanodes for Ethanol Biofuel Cells Using PQQ-Dependent Alcohol and Aldehyde Dehydrogenases. *Electrochim. Acta* **2013**, *87*, 323–329.

(83) Palmore, G. T. R.; Bertschy, H.; Bergens, S. H.; Whitesides, G. M. A Methanol / Dioxygen Biofuel Cell That Uses NAD(+)-Dependent Dehydrogenases as Catalysts: Application of an Electro-Enzymatic Method to Regenerate Nicotinamide Adenine Dinucleotide at Low Overpotentials. *J. Electroanal. Chem.* **1998**, *443*, 155–161.

(84) Techer, V. Electrodes Catalytiques à Base D'enzymes Pour Le Développement de Biopiles Alcool/oxygène Microfluidiques (Catalytic Electrodes Based on Enzymes for the Development of Microfluidic Alcohol/oxygen Biofuel Cells), Université Montpellier, 2013.

(85) Brocato, S.; Lau, C.; Atanassov, P. Mechanistic Study of Direct Electron Transfer in Bilirubin Oxidase. *Electrochim. Acta* **2012**, *61*, 44–49.

(86) Bilewicz, R.; Opallo, M. Biocathodes for Dioxygen Reduction in Biofuel Cells. In *Fuel*

Cell Science: Theory, Fundamentals, and Biocatalysis; Wieckowski, A.; Nørskov, J. K., Eds.; John Wiley & Sons, Inc.: Hoboken, NJ, USA, 2010.

(87) Madhavi, V.; Lele, S. S. Laccase: Properties and Applications. **2009**, *4*, 1694–1717.

(88) Mano, N.; Edembe, L. Bilirubin Oxidases in Bioelectrochemistry: Features and Recent Findings. *Biosens. Bioelectron.* **2013**, *50*, 478–485.

(89) Palmore, G. T. R.; Kim, H.-H. Electro-Enzymatic Reduction of Dioxygen to Water in the Cathode Compartment of a Biofuel Cell. *J. Electroanal. Chem.* **1999**, *464*, 110–117.

(90) Reuillard, B.; Goff, A. Le; Agnès, C.; Zebda, A.; Holzinger, M.; Cosnier, S. Direct Electron Transfer between Tyrosinase and Multi-Walled Carbon Nanotubes for Bioelectrocatalytic Oxygen Reduction. *Electrochem. commun.* **2012**, *20*, 19–22.

(91) Rodgers, C. J.; Blanford, C. F.; Giddens, S. R.; Skamnioti, P.; Armstrong, F. A.; Gurr, S. J. Designer Laccases: A Vogue for High-Potential Fungal Enzymes? *Trends Biotechnol.* **2010**, *28*, 63–72.

(92) Opallo, M.; Bilewicz, R. Recent Developments of Nanostructured Electrodes for Bioelectrocatalysis of Dioxygen Reduction. *Adv. Phys. Chem.* **2011**, *2011*, 1–21.

(93) Song, C.; Zhang, J. Electrocatalytic Oxygen Reduction Reaction. In *PEM Feul Cell Electrocatalyst and Catalyst Layers. Fundamentals and Applications*; Zhang, J., Ed.; Springer, 2008; pp. 89–134.

(94) Yeager, E. Dioxygen Electrocatalysis: Mechanisms in Relation to Catalyst Structure. *J. Mol. Catal.* **1986**, *38*, 5–25.

(95) Song, C.; Zhang, J. Electrocatalytic Oxygen Reduction Reaction. In *PEM Fuel Cell Electrocatalysts and Catalyst Layers*; Zhang, J., Ed.; Springer London, 2008; pp. 89–134.

(96) Ren, X.; Chen, D.; Meng, X.; Tang, F.; Hou, X.; Han, D.; Zhang, L. Zinc Oxide Nanoparticles/glucose Oxidase Photoelectrochemical System for the Fabrication of Biosensor. *J. Colloid Interface Sci.* **2009**, *334*, 183–187.

(97) Neto, S. A.; Andrade, A. R. De. New Energy Sources: The Enzymatic Biofuel Cell. *J. Braz. Chem. Soc.* **2013**, *24*, 1891–1912.

(98) Pasta, M.; Ruffo, R.; Falletta, E.; Mari, C. M.; Pina, C. Della. Alkaline Glucose Oxidation on Nanostructured Gold Electrodes. *Gold Bull.* **2010**, *43*, 57–64.

(99) Blaesi, A. H.; Buie, C. R. Characterization of the Electrochemical Oxidation of Glucose on Pt Nanoparticle Catalysts in pH Neutral Phosphate Buffer Solution. *ECS Trans.* **2011**, *33*, 41–48.

(100) Quan, H.; Park, S.-U.; Park, J. Electrochemical Oxidation of Glucose on Silver Nanoparticle-Modified Composite Electrodes. *Electrochim. Acta* **2010**, *55*, 2232–2237.

(101) Li, L.; Zhou, T.; Sun, G.; Li, Z.; Yang, W.; Jia, J.; Yang, G. Ultrasensitive Electrospun Nickel-Doped Carbon Nanofibers Electrode for Sensing Paracetamol and Glucose. *Electrochim. Acta* **2015**, *152*, 31–37.

(102) Yi, Q.; Niu, F.; Yu, W. Pd-Modified TiO2 Electrode for Electrochemical Oxidation of Hydrazine, Formaldehyde and Glucose. *Thin Solid Films* **2011**, *519*, 3155–3161.

(103) Habrioux, A.; Sibert, E.; Servat, K.; Vogel, W.; Kokoh, K. B.; Alonso-Vante, N. Activity of Platinum-Gold Alloys for Glucose Electrooxidation in Biofuel Cells. *J. Phys. Chem. B*

2007, *111*, 10329–10333.

(104) Tonda-Mikiela, P.; Napporn, T. W.; Morais, C.; Servat, K.; Chen, A.; Kokoh, K. B. Synthesis of Gold-Platinum Nanomaterials Using Bromide Anion Exchange-Synergistic Electroactivity toward CO and Glucose Oxidation. *J. Electrochem. Soc.* **2012**, *159*, H828–H833.

(105) Holade, Y.; Both Engel, A.; Tingry, S.; Cherifi, A.; Cornu, D.; Servat, K.; Napporn, T. W.; Kokoh, K. B. Insights on Hybrid Glucose Biofuel Cells Based on Bilirubin Oxidase Cathode and Gold-Based Anode Nanomaterials. *ChemElectroChem* **2014**, *1*, 1976–1987.

(106) Both Engel, A.; Holade, Y.; Tingry, S.; Cherifi, A.; Cornu, D.; Servat, K.; Napporn, T. W.; Kokoh, K. B. Electrospun Carbon Fibers: Promising Electrode Material for Abiotic and Enzymatic Catalysis. *J. Phys. Chem. C* **2015**, *119*, 16724–16733.

(107) Yang, X.-Y.; Tian, G.; Jiang, N.; Su, B.-L. Immobilization Technology: A Sustainable Solution for Biofuel Cell Design. *Energy Environ. Sci.* **2012**, *5*, 5540–5563.

(108) Zloczewska, A.; Jönsson-Niedziolka, M.; Rogalski, J.; Opallo, M. Vertically Aligned Carbon Nanotube Film Electrodes for Bioelectrocatalytic Dioxygen Reduction. *Electrochim. Acta* **2011**, *56*, 3947–3953.

(109) Tam, T. K.; Pita, M.; Ornatska, M.; Katz, E. Biofuel Cell Controlled by Enzyme Logic Network--Approaching Physiologically Regulated Devices. *Bioelectrochemistry* **2009**, *76*, 4–9.

(110) Kim, J.; Yoo, K.-H. Glucose Oxidase Nanotube-Based Enzymatic Biofuel Cells with Improved Laccase Biocathodes. *Phys. Chem. Chem. Phys.* **2013**, *15*, 3510–3517.

(111) Xiao, Y.; Patolski, F.; Katz, E.; Hainfeld, J. F.; Willner, I. "Plugging into Enzymes": Nanowiring of Redox Enzymes by a Gold Nanoparticle. *Science (80-.).* **2003**, *299*, 1877–1881.

(112) Shleev, S.; Jarosz-Wilkolazka, A.; Khalunina, A.; Morozova, O.; Yaropolov, A.; Ruzgas, T.; Gorton, L. Direct Electron Transfer Reactions of Laccases from Different Origins on Carbon Electrodes. *Bioelectrochemistry* **2005**, *67*, 115–124.

(113) Kim, J.; Parkey, J.; Rhodes, C.; Gonzalez-Martin, A. Development of a Biofuel Cell Using Glucose-Oxidase- and Bilirubin-Oxidase-Based Electrodes. *J. Solid State Electrochem.* **2008**, *13*, 1043–1050.

(114) Zebda, A.; Gondran, C.; Le Goff, A.; Holzinger, M.; Cinquin, P.; Cosnier, S. Mediatorless High-Power Glucose Biofuel Cells Based on Compressed Carbon Nanotube-Enzyme Electrodes. *Nat. Commun.* **2011**, *2*, 370–375.

(115) Li, X.; Zhang, L.; Su, L.; Ohsaka, T.; Mao, L. A Miniature Glucose/O2 Biofuel Cell With a High Tolerance Against Ascorbic Acid. *Fuel Cells* **2009**, *9*, 85–91.

(116) Bessel, C. A.; Laubernds, K.; Rodriguez, N. M.; Baker, R. T. K. Graphite Nanofibers as an Electrode for Fuel Cell Applications. *J. Phys. Chem. B* **2001**, *105*, 1115–1118.

(117) Serp, P.; Corrias, M.; Kalck, P. Carbon Nanotubes and Nanofibers in Catalysis. *Appl. Catal. A Gen.* **2003**, *253*, 337–358.

(118) Kim, C.; Yang, K. S. Electrochemical Properties of Carbon Nanofiber Web as an Electrode for Supercapacitor Prepared by Electrospinning. *Appl. Phys. Lett.* **2003**, *83*,

1216.

(119) Kim, C.; Yang, K. S.; Kojima, M.; Yoshida, K.; Kim, Y. J.; Kim, Y. a.; Endo, M. Fabrication of Electrospinning-Derived Carbon Nanofiber Webs for the Anode Material of Lithium-Ion Secondary Batteries. *Adv. Funct. Mater.* **2006**, *16*, 2393–2397.

(120) Che, A.-F.; Germain, V.; Cretin, M.; Cornu, D.; Innocent, C.; Tingry, S. Fabrication of Free-Standing Electrospun Carbon Nanofibers as Efficient Electrode Materials for Bioelectrocatalysis. *New J. Chem.* **2011**, *35*, 2848.

(121) Chen, S.; He, G.; Carmona-Martinez, A. A.; Agarwal, S.; Greiner, A.; Hou, H.; Schröder, U. Electrospun Carbon Fiber Mat with Layered Architecture for Anode in Microbial Fuel Cells. *Electrochem. commun.* **2011**, *13*, 1026–1029.

(122) Spahn, C.; Minteer, S. D. Enzyme Immobilization in Biotechnology. *Recent Patents Eng.* **2008**, *2*, 195–200.

(123) Hanefeld, U.; Gardossi, L.; Magner, E. Understanding Enzyme Immobilisation. *Chem. Soc. Rev.* **2009**, *38*, 453–468.

(124) Pizzariello, A.; Stred'ansky, M.; Miertus, S. A Glucose/hydrogen Peroxide Biofuel Cell That Uses Oxidase and Peroxidase as Catalysts by Composite Bulk-Modified Bioelectrodes Based on a Solid Binding Matrix. *Bioelectrochemistry* **2002**, *56*, 99–105.

(125) Tingry, S.; Cretin, M.; Innocent, C. Les Biopiles Enzymatiques Pour Produire de L ' électricité (Enzymatic Biofuel Cells for the Production of Electricity). *Actual. Chim.* **2013**, *373*, 18–25.

(126) Gutiérrez-Sánchez, C.; Pita, M.; Vaz-Domínguez, C.; Shleev, S.; De Lacey, A. L. Gold Nanoparticles as Electronic Bridges for Laccase-Based Biocathodes. *J. Am. Chem. Soc.* **2012**, *134*, 17212–17220.

(127) Mauritz, K. a; Moore, R. B. State of Understanding of Nafion. *Chem. Rev.* **2004**, *104*, 4535–4585.

(128) Moehlenbrock, M. J.; Minteer, S. D. Extended Lifetime Biofuel Cells. *Chem. Soc. Rev.* **2008**, *37*, 1188–1196.

(129) Sadowska, K.; Stolarczyk, K.; Biernat, J. F.; Roberts, K. P.; Rogalski, J.; Bilewicz, R. Derivatization of Single-Walled Carbon Nanotubes with Redox Mediator for Biocatalytic Oxygen Electrodes. *Bioelectrochemistry* **2010**, *80*, 73–80.

(130) Habrioux, A.; Servat, K.; Tingry, S.; Kokoh, K. B. Enhancement of the Performances of a Single Concentric glucose/O2 Biofuel Cell by Combination of Bilirubin oxidase/Nafion Cathode and Au-Pt Anode. *Electrochem. commun.* **2009**, *11*, 111–113.

(131) Sadki, S.; Schottland, P.; Brodie, N.; Sabouraud, G. The Mechanisms of Pyrrole Electropolymerization. *Chem. Soc. Rev.* **2000**, *29*, 283–293.

(132) Wang, L.-X.; Li, X.-G.; Yang, Y.-L. Preparation, Properties and Applications of Polypyrroles. *React. Funct. Polym.* **2001**, *47*, 125–139.

(133) Lalaoui, N.; Elouarzaki, K.; Le Goff, A.; Holzinger, M.; Cosnier, S. Efficient Direct Oxygen Reduction by Laccases Attached and Oriented on Pyrene-Functionalized Polypyrrole/carbon Nanotube Electrodes. *Chem. Commun.* **2013**, *49*, 9281–9283.

(134) Vaghari, H.; Jafarizadeh-Malmiri, H.; Berenjian, A.; Anarjan, N. Recent Advances in Application of Chitosan in Fuel Cells. *Sustain. Chem. Process.* **2013**, *1*, 1–12.

(135) Ichi, S. El; Zebda, A.; Laaroussi, A.; Reverdy-Bruas, N.; Chaussy, D.; Belgacem, M. N.; Cinquin, P.; Martin, D. K. Chitosan Improves Stability of Carbon Nanotube Biocathodes for Glucose Biofuel Cells. *Chem. Commun.* **2014**, *50*, 14535–14538.

(136) El Ichi, S.; Zebda, A.; Alcaraz, J.-P.; Laaroussi, A.; Boucher, F.; Boutonnat, J.; Reverdy-Bruas, N.; Chaussy, D.; Belgacem, M. N.; Cinquin, P.; et al. Bioelectrodes Modified with Chitosan for Long-Term Energy Supply from the Body. *Energy Environ. Sci.* **2015**, *8*, 1017–1026.

(137) Ghindilis, A. L.; Atanasov, P.; Wilkins, E. Enzyme-Catalyzed Direct Electron Transfer: Fundamentals and Analytical Applications. *Electroanalysis* **1997**, *9*, 661–674.

(138) Nazaruk, E.; Sadowska, K.; Biernat, J. F.; Rogalski, J.; Ginalska, G.; Bilewicz, R. Enzymatic Electrodes Nanostructured with Functionalized Carbon Nanotubes for Biofuel Cell Applications. *Anal. Bioanal. Chem.* **2010**, *398*, 1651–1660.

(139) Bourourou, M.; Elouarzaki, K.; Holzinger, M.; Agnès, C.; Le Goff, A.; Reverdy-Bruas, N.; Chaussy, D.; Party, M.; Maaref, A.; Cosnier, S. Freestanding Redox Buckypaper Electrodes from Multi-Wall Carbon Nanotubes for Bioelectrocatalytic Oxygen Reduction via Mediated Electron Transfer. *Chem. Sci.* **2014**, *5*, 2885–2888.

(140) Holland, J. T.; Lau, C.; Brozik, S.; Atanassov, P.; Banta, S. Engineering of Glucose Oxidase for Direct Electron Transfer via Site-Specific Gold Nanoparticle Conjugation. *J. Am. Chem. Soc.* **2011**, *133*, 19262–19265.

(141) Wang, X.; Falk, M.; Ortiz, R.; Matsumura, H.; Bobacka, J.; Ludwig, R.; Bergelin, M.; Gorton, L.; Shleev, S. Mediatorless Sugar/oxygen Enzymatic Fuel Cells Based on Gold Nanoparticle-Modified Electrodes. *Biosens. Bioelectron.* **2012**, *31*, 219–225.

(142) Topcagic, S.; Minteer, S. D. Development of a Membraneless Ethanol/oxygen Biofuel Cell. *Electrochim. Acta* **2006**, *51*, 2168–2172.

(143) Miyake, T.; Haneda, K.; Yoshino, S.; Nishizawa, M. Flexible, Layered Biofuel Cells. *Biosens. Bioelectron.* **2013**, *40*, 45–49.

(144) Higgins, S. R.; Lau, C.; Atanassov, P.; Minteer, S. D.; Cooney, M. J. Hybrid Biofuel Cell : Microbial Fuel Cell with an Enzymatic Air-Breathing Cathode. *ACS Catal.* **2011**, *1*, 994–997.

(145) Kjeang, E.; Djilali, N.; Sinton, D. Microfluidic Fuel Cells: A Review. *J. Power Sources* **2009**, *186*, 353–369.

(146) Atanassov, P.; Apblett, C.; Banta, S. Enzymatic Biofuel Cells. *Electrochem. Soc. Interface* **2007**, *16*, 28–31.

(147) Sakai, H.; Nakagawa, T.; Tokita, Y.; Hatazawa, T.; Ikeda, T.; Tsujimura, S.; Kano, K. A High-Power Glucose/oxygen Biofuel Cell Operating under Quiescent Conditions. *Energy Environ. Sci.* **2009**, *2*, 133–138.

(148) Burton, N. Sugar-powered electronics http://www.rsc.org/Publishing/ChemTech/Volume/2008/11/sugar_powered_electronics.asp (accessed Aug 26, 2015).

(149) Sony Corporation. Sony Develops “Bio Battery” Generating Electricity from Sugar http://www.sony.net/SonyInfo/News/Press/200708/07-074E/index.html.

(150) Drake, R. F.; Kusserow, B. K.; Messinger, S.; Matsuda, S. A Tissue Implantable Fuel Cell

Power Supply. *Trans. Am. Soc. Artif. Intern. Organs* **1970**, *16*, 199–205.

(151) Kerzenmacher, S.; Ducrée, J.; Zengerle, R.; von Stetten, F. Energy Harvesting by Implantable Abiotically Catalyzed Glucose Fuel Cells. *J. Power Sources* **2008**, *182*, 1–17.

(152) Halámková, L.; Halámek, J.; Bocharova, V.; Szczupak, A.; Alfonta, L.; Katz, E. Implanted Biofuel Cell Operating in a Living Snail. *J. Am. Chem. Soc.* **2012**, *134*, 5040–5043.

(153) Clarkson University Scientists Implant Biofuel Cell in Living Snail http://www.clarkson.edu/news/2012/news-release_2012-03-15-3.html.

(154) Kim, H. S.; Jin, H.-J.; Myung, S. J.; Kang, M.; Chin, I.-J. Carbon Nanotube-Adsorbed Electrospun Nanofibrous Membranes of Nylon 6. *Macromol. Rapid Commun.* **2006**, *27*, 146–151.

(155) Naebe, M.; Lin, T.; Wang, X. Carbon Nanotubes Reinforced Electrospun Polymer Nanofibres. In *Nanofibers*; Kumar, A., Ed.; InTech, 2010; pp. 309–328.

(156) Gao, J.; Hu, M.; Li, R. K. Y. Ultrasonication Induced Adsorption of Carbon Nanotubes onto Electrospun Nanofibers with Improved Thermal and Electrical Performances. *J. Mater. Chem.* **2012**, *22*, 10867.

(157) Wang, K.; Gu, M.; Wang, J.; Qin, C.; Dai, L. Functionalized Carbon Nanotube/polyacrylonitrile Composite Nanofibers: Fabrication and Properties. *Polym. Adv. Technol.* **2012**, *23*, 262–271.

(158) Hou, H.; Reneker, D. H. Carbon Nanotubes on Carbon Nanofibers: A Novel Structure Based on Electrospun Polymer Nanofibers. *Adv. Mater.* **2004**, *16*, 69–73.

(159) Guo, Q.; Zhou, X.; Li, X.; Chen, S.; Seema, A.; Greiner, A.; Hou, H. Supercapacitors Based on Hybrid Carbon Nanofibers Containing Multiwalled Carbon Nanotubes. *J. Mater. Chem.* **2009**, *19*, 2810.

(160) Laurent, C.; Flahaut, E.; Peigney, A. The Weight and Density of Carbon Nanotubes versus the Number of Walls and Diameter. *Carbon N. Y.* **2010**, *48*, 2994–2996.

(161) Peigney, A.; Laurent, C.; Flahaut, E.; Bacsa, R. R.; Rousset, A. Specific Surface Area of Carbon Nanotubes and Bundles of Carbon Nanotubes. *Carbon N. Y.* **2001**, *39*, 507–514.

(162) Kim, J. M.; Song, I. S.; Cho, D.; Hong, I. Effect of Carbonization Temperature and Chemical Pre-Treatment on the Thermal Change and Fiber Morphology of Kenaf-Based Carbon Fibers. *Carbon Lett.* **2011**, *12*, 131–137.

(163) Schwan, J.; Ulrich, S.; Batori, V.; Ehrhardt, H.; Silva, S. Raman Spectroscopy on Amorphous Carbon Films. *J. Appl. Phys.* **1996**, *80*, 440–447.

(164) Dresselhaus, M. S.; Dresselhaus, G.; Pimenta, M. A.; Eklund, P. C. Raman Scattering in Carbon Materials. In *Analytical Application of Raman Spectroscopy*; Pelletier, M. J., Ed.; Blackwell: London, UK, 1999.

(165) Vidano, R.; Fischbach, D. B. New Lines in the Raman Spectra of Carbons and Graphite. *J. Am. Ceram. Soc.* **1978**, *61*, 13–17.

(166) Wang, Y.; Serrano, S.; Santiago-Avilés, J. J. Raman Characterization of Carbon Nanofibers Prepared Using Electrospinning. *Synth. Met.* **2003**.

(167) Kim, C.; Park, S.-H.; Cho, J.-I.; Lee, D.-Y.; Park, T.-J.; Lee, W.-J.; Yang, K.-S. Raman

Spectroscopic Evaluation of Polyacrylonitrile-Based Carbon Nanofibers Prepared by Electrospinning. *J. Raman Spectrosc.* **2004**, *35*, 928–933.

(168) L. J. van der Pauw. A Method of Measuring Specific Resistivity and Hall Effect of Discs of Arbitrary Shape. *Philips Res. Rep.* **1958**, *13*, 1–9.

(169) Leijonmarck, S.; Cornell, A.; Lindbergh, G.; Wågberg, L. Flexible Nano-Paper-Based Positive Electrodes for Li-Ion batteries—Preparation Process and Properties. *Nano Energy* **2013**, *2*, 794–800.

(170) Lu, H.; Liang, F.; Gou, J.; Leng, J.; Du, S. Synergistic Effect of Ag Nanoparticle-Decorated Graphene Oxide and Carbon Fiber on Electrical Actuation of Polymeric Shape Memory Nanocomposites. *Smart Mater. Struct.* **2014**, *23*, 085034–085040.

(171) Li, M.; Han, G.; Yang, B. Fabrication of the Catalytic Electrodes for Methanol Oxidation on Electrospinning-Derived Carbon Fibrous Mats. *Electrochem. commun.* **2008**, *10*, 880–883.

(172) Both Engel, A.; Cherifi, A.; Tingry, S.; Cornu, D.; Peigney, A.; Laurent, C. Enhanced Performance of Electrospun Carbon Fibers Modified with Carbon Nanotubes: Promising Electrodes for Enzymatic Biofuel Cells. *Nanotechnology* **2013**, *24*, 245402.

(173) Zhou, W.; Tang, Y.; Song, R.; Jiang, L.; Hui, K. S.; Hui, K. N. Characterization of Electrical Conductivity of Porous Metal Fiber Sintered Sheet Using Four-Point Probe Method. *Mater. Des.* **2012**, *37*, 161–165.

(174) Ra, E. J.; An, K. H.; Kim, K. K.; Jeong, S. Y.; Lee, Y. H. Anisotropic Electrical Conductivity of MWCNT/PAN Nanofiber Paper. *Chem. Phys. Lett.* **2005**, *413*, 188–193.

(175) Zhou, Z.; Lai, C.; Zhang, L.; Qian, Y.; Hou, H.; Reneker, D. H.; Fong, H. Development of Carbon Nanofibers from Aligned Electrospun Polyacrylonitrile Nanofiber Bundles and Characterization of Their Microstructural, Electrical, and Mechanical Properties. *Polymer (Guildf).* **2009**, *50*, 2999–3006.

(176) Jia, K.; Zhuang, X.; Cheng, B.; Shi, S.; Shi, Z.; Zhang, B. Solution Blown Aligned Carbon Nanofiber Yarn as Supercapacitor Electrode. *J. Mater. Sci. Mater. Electron.* **2013**, *24*, 4769–4773.

(177) Sui, G.; Sun, F.; Yang, X.; Ji, J.; Zhong, W. Highly Aligned Polyacrylonitrile-Based Nano-Scale Carbon Fibres with Homogeneous Structure and Desirable Properties. *Compos. Sci. Technol.* **2013**, *87*, 77–85.

(178) Ayres, C.; Bowlin, G. L.; Henderson, S. C.; Taylor, L.; Shultz, J.; Alexander, J.; Telemeco, T. a; Simpson, D. G. Modulation of Anisotropy in Electrospun Tissue-Engineering Scaffolds: Analysis of Fiber Alignment by the Fast Fourier Transform. *Biomaterials* **2006**, *27*, 5524–5534.

(179) Matveeva, V.; Bykov, A.; Doluda, V.; Sulman, M.; Kumar, N.; Dzwigaj, S.; Marceau, E.; Kustov, L.; Tkachenko, O.; Sulman, E. Direct D-Glucose Oxidation over Noble Metal Nanoparticles Introduced on Polymer and Inorganic Supports. *Top. Catal.* **2009**, *52*, 387–393.

(180) Zhang, H.; Toshima, N. Synthesis of Au/Pt Bimetallic Nanoparticles with a Pt-Rich Shell and Their High Catalytic Activities for Aerobic Glucose Oxidation. *J. Colloid Interface Sci.* **2013**, *394*, 166–176.

(181) Gao, H.; Xiao, F.; Ching, C. B.; Duan, H. One-Step Electrochemical Synthesis of PtNi

Nanoparticle-Graphene Nanocomposites for Nonenzymatic Amperometric Glucose Detection. *ACS Appl. Mater. Interfaces* **2011**, *3*, 3049–3057.

(182) Cui, H. F.; Ye, J. S.; Liu, X.; Zhang, W. D.; Sheu, F. S. Pt-Pb Alloy Nanoparticle/carbon Nanotube Nanocomposite: A Strong Electrocatalyst for Glucose Oxidation. *Nanotechnology* **2006**, *17*, 2334–2339.

(183) Zhao, J.; Kong, X.; Shi, W.; Shao, M.; Han, J.; Wei, M.; Evans, D. G.; Duan, X. Self-Assembly of Layered Double Hydroxide nanosheets/Au Nanoparticles Ultrathin Films for Enzyme-Free Electrocatalysis of Glucose. *J. Mater. Chem.* **2011**, *21*, 13926.

(184) Yan, X.; Ge, X.; Cui, S. Pt-Decorated Nanoporous Gold for Glucose Electrooxidation in Neutral and Alkaline Solutions. *Nanoscale Res. Lett.* **2011**, *6*, 313–318.

(185) Hebié, S.; Kokoh, K. B.; Servat, K.; Napporn, T. W. Shape-Dependent Electrocatalytic Activity of Free Gold NPs toward Glucose Oxidation. *Gold Bull.* **2013**.

(186) Tung, S.-P.; Huang, T.-K.; Lee, C.-Y.; Chiu, H.-T. Electrochemical Growth of Gold Nanostructures on Carbon Paper for Alkaline Direct Glucose Fuel Cell. *RSC Adv.* **2012**, *2*, 1068–1073.

(187) Gao, D.; Wang, L.; Xia, X.; Qiao, H.; Cai, Y. Preparation and Characterization of Porous Carbon / Nickel Nanofibers for Supercapacitor. *J. Eng. Fiber. Fabr.* **2013**, *8*, 108–113.

(188) Saquing, C. D.; Manasco, J. L.; Khan, S. A. Electrospun Nanoparticle-Nanofiber Composites via a One-Step Synthesis. *Small* **2009**, *5*, 944–951.

(189) Pastoriza-Santos, I.; Liz-Marzán, L. M. Preparation of PVP Protected Metal Nanoparticles in DMF. *Langmuir* **2002**, *18*, 2888–2894.

(190) Pastoriza-Santos, I.; Liz-Marzán, L. M. N,N-Dimethylformamide as a Reaction Medium for Metal Nanoparticle Synthesis. *Adv Funct Mater* **2009**, *19*, 679–688.

(191) Anka, F. H.; Perera, S. D.; Ratanatawanate, C.; Balkus, K. J. Polyacrylonitrile Gold Nanoparticle Composite Electrospun Fibers Prepared by in Situ Photoreduction. *Mater. Lett.* **2012**, *75*, 12–15.

(192) Sawada, K.; Sakai, S.; Taya, M. Polyacrylonitrile-Based Electrospun Nanofibers Carrying Gold Nanoparticles in Situ Formed by Photochemical Assembly. *J. Mater. Sci.* **2014**, *49*, 4595–4600.

(193) Sawai, D.; Miyamoto, M.; Kanamoto, T.; Ito, M. Lamellar Thickening in Nascent Poly (acrylonitrile) upon Annealing. *J. Polym. Sci. Part B Polym. Phys.* **2000**, *38*, 2571–2579.

(194) Hristu, R.; Stanciu, S. G.; Tranca, D. E.; Matei, A.; Stanciu, G. A. Nonlinear Optical Imaging of Defects in Cubic Silicon Carbide Epilayers. *Sci. Rep.* **2014**, *4*, 1–6.

(195) Tohidi, M.; Mahyari, F. A.; Safavi, A. A Seed-Less Method for Synthesis of Ultra-Thin Gold Nanosheets by Using a Deep Eutectic Solvent and Gum Arabic and Their Electrocatalytic Application. *RSC Adv.* **2015**, *5*, 32744–32754.

(196) Zehani, F.; Sebais, M.; Zaioune, H. Elaboration and Characterization of AuCl Semiconductor Nanocrystals Embedded in KCL Single Crystals. *J. Mod. Phys.* **2012**, *3*, 534–537.

(197) Janssen, E. M. W.; Folmer, J. C. W.; Wiegers, G. A. The Preparation and Crystal Structure of Gold Monochloride, AuCl. *J. Less Common Met.* **1974**, *38*, 71–76.

(198) Feng, X.; Hu, J.; Chen, X.; Xie, J.; Liu, Y. Synthesis and Electron Transfer Property of

Sulfhydryl-Containing Multi-Walled Carbon Nanotube/gold Nanoparticle Heterojunctions. *J. Phys. D. Appl. Phys.* **2009**, *42*, 042001.

(199) Ban, Z.; Barnakov, Y. A.; Li, F.; Golub, V. O.; O'Connor, C. J. The Synthesis of Core–shell Iron@gold Nanoparticles and Their Characterization. *J. Mater. Chem.* **2005**, *15*, 4660–4662.

(200) Uosaki, K.; Shen, Y.; Kondo, T. Preparation of a Highly Ordered Au (111) Phase on a Polycrystalline Gold Substrate by Vacuum Deposition and Its Characterization by XRD, GISXRD, STWAFM, and Electrochemical Measurements. *J. Phys. Chem.* **1995**, *99*, 14117–14122.

(201) Bard, A. J.; Faulkner, L. R. *Electrochemical Methods: Fundamentals and Applications*; 2nd ed.; Wiley, 2001.

(202) Zoski, C. *Handbook of Electrochemistry*; Zoski, C., Ed.; Elsevier: Las Cruces, USA, 2006.

(203) Ivnitski, D.; Artyushkova, K.; Atanassov, P. Surface Characterization and Direct Electrochemistry of Redox Copper Centers of Bilirubin Oxidase from Fungi Myrothecium Verrucaria. *Bioelectrochemistry* **2008**, *74*, 101–110.

(204) Stolarczyk, K.; Nazaruk, E.; Rogalski, J.; Bilewicz, R. Nanostructured Carbon Electrodes for Laccase-Catalyzed Oxygen Reduction without Added Mediators. *Electrochim. Acta* **2008**, *53*, 3983–3990.

(205) Minteer, S. D.; Atanassov, P.; Luckarift, H. R.; Johnson, G. R. New Materials for Biological Fuel Cells. *Mater. Today* **2012**, *15*, 166–173.

(206) Davis, J. J.; Coleman, K. S.; Azamian, B. R.; Bagshaw, C. B.; Green, M. L. H. Chemical and Biochemical Sensing with Modified Single Walled Carbon Nanotubes. *Chem. - A Eur. J.* **2003**, *9*, 3732–3739.

(207) Farneth, W. E.; D'Amore, M. B. Encapsulated Laccase Electrodes for Fuel Cell Cathodes. *J. Electroanal. Chem.* **2005**, *581*, 197–205.

(208) Ding, S.-N.; Holzinger, M.; Mousty, C.; Cosnier, S. Laccase Electrodes Based on the Combination of Single-Walled Carbon Nanotubes and Redox Layered Double Hydroxides: Towards the Development of Biocathode for Biofuel Cells. *J. Power Sources* **2010**, *195*, 4714–4717.

(209) Servat, K.; Tingry, S.; Brunel, L.; Querelle, S.; Cretin, M.; Innocent, C.; Jolivalt, C.; Rolland, M. Modification of Porous Carbon Tubes with Enzymes: Application for Biofuel Cells. *J. Appl. Electrochem.* **2007**, *37*, 121–127.

(210) Flexer, V.; Brun, N.; Courjean, O.; Backov, R.; Mano, N. Porous Mediator-Free Enzyme Carbonaceous Electrodes Obtained through Integrative Chemistry for Biofuel Cells. *Energy Environ. Sci.* **2011**, *4*, 2097–2106.

(211) Hussein, L.; Rubenwolf, S.; von Stetten, F.; Urban, G.; Zengerle, R.; Krueger, M.; Kerzenmacher, S. A Highly Efficient Buckypaper-Based Electrode Material for Mediatorless Laccase-Catalyzed Dioxygen Reduction. *Biosens. Bioelectron.* **2011**, *26*, 4133–4138.

(212) Kuwahara, T.; Asano, T.; Kondo, M.; Shimomura, M. Bioelectrocatalytic O2 Reduction with a Laccase-Bearing poly(3-Methylthiophene) Film Based on Direct Electron Transfer from the Polymer to Laccase. *Bioelectrochemistry* **2013**, *91*, 28–31.

(213) Jensen, U. B.; Vagin, M.; Koroleva, O.; Sutherland, D. S.; Besenbacher, F.; Ferapontova, E. E. Activation of Laccase Bioelectrocatalysis of O2 Reduction to H2O by Carbon Nanoparticles. *J. Electroanal. Chem.* **2012**, *667*, 11–18.

(214) Kim, J.; Yoo, K.-H. Glucose Oxidase Nanotube-Based Enzymatic Biofuel Cells with Improved Laccase Biocathodes. *Phys. Chem. Chem. Phys.* **2013**, *15*, 3510–3517.

(215) Karnicka, K.; Miecznikowski, K.; Kowalewska, B.; Skunik, M.; Opallo, M.; Rogalski, J.; Schuhmann, W.; Kulesza, P. J. ABTS-Modified Multiwalled Carbon Nanotubes as an Effective Mediating System for Bioelectrocatalytic Reduction of Oxygen. *Anal. Chem.* **2008**, *80*, 7643–7648.

(216) Dos Santos, L.; Climent, V.; Blanford, C. F.; Armstrong, F. a. Mechanistic Studies of the "Blue" Cu Enzyme, Bilirubin Oxidase, as a Highly Efficient Electrocatalyst for the Oxygen Reduction Reaction. *Phys. Chem. Chem. Phys.* **2010**, *12*, 13962–13974.

(217) Ulyanova, Y.; Babanova, S.; Pinchon, E.; Matanovic, I.; Singhal, S.; Atanassov, P. Effect of Enzymatic Orientation through the Use of Syringaldazine Molecules on Multiple Multi-Copper Oxidase Enzymes. *Phys. Chem. Chem. Phys.* **2014**, *16*, 13367–13375.

(218) Togo, M.; Takamura, A.; Asai, T.; Kaji, H.; Nishizawa, M. An Enzyme-Based Microfluidic Biofuel Cell Using Vitamin K3-Mediated Glucose Oxidation. *Electrochim. Acta* **2007**, *52*, 4669–4674.

(219) Engel, A. B.; Cherifi, A.; Cornu, D.; Tingry, S. Amélioration Des Performances Des Biopiles Enzymatiques Par Le Design de Nouveaux Matériaux D'électrode (Design of Advanced Electrode Materials for Performance Enhancement of Enzymatic Biofuel Cells). *Actual. Chim.* **2014**, *November*, 36–38.

(220) Moore, C. M.; Minteer, S. D.; Martin, R. S. Microchip-Based Ethanol/oxygen Biofuel Cell. *Lab Chip* **2005**, *5*, 218–225.

(221) Logan, B. E.; Hamelers, B.; Rozendal, R.; Schröder, U.; Keller, J.; Freguia, S.; Aelterman, P.; Verstraete, W.; Rabaey, K. Microbial Fuel Cells: Methodology and Technology. *Environ. Sci. Technol.* **2006**, *40*, 5181–5192.

(222) Deng, L.; Shang, L.; Wen, D.; Zhai, J.; Dong, S. A Membraneless Biofuel Cell Powered by Ethanol and Alcoholic Beverage. *Biosens. Bioelectron.* **2010**, *26*, 70–73.

(223) Ramanavicius, A.; Kausaite, A.; Ramanaviciene, A. Enzymatic Biofuel Cell Based on Anode and Cathode Powered by Ethanol. *Biosens. Bioelectron.* **2008**, *24*, 767–772.

(224) Holade, Y. Transformation électrocatalytique de Sucres Couplée à La Réduction Enzymatique de L'oxygène Moléculaire Pour La Production D'énergie, Université de Poitiers, 2015.

(225) Holade, Y.; Morais, C.; Arrii-Clacens, S.; Servat, K.; Napporn, T. W.; Kokoh, K. B. New Preparation of PdNi/C and PdAg/C Nanocatalysts for Glycerol Electrooxidation in Alkaline Medium. *Electrocatalysis* **2013**, *4*, 167–178.

(226) Holade, Y.; Morais, C.; Servat, K.; Napporn, T. W.; Kokoh, K. B. Toward the Electrochemical Valorization of Glycerol: Fourier Transform Infrared Spectroscopic and Chromatographic Studies. *ACS Catal.* **2013**, *3*, 2403–2411.

(227) Chatterjee, S. K. *X-Ray Diffraction: Its Theory and Applications*; 2nd ed.; Prentice-Hall of India Pvt.Ltd: New Delhi, India, 2010.

(228) Coutanceau, C.; Croissant, M. J.; Napporn, T.; Lamy, C. Electrocatalytic Reduction of Dioxygen at Platinum Particles Dispersed in a Polyaniline Film. *Electrochim. Acta* **2000**, *46*, 579–588.

(229) Habrioux, A.; Merle, G.; Servat, K.; Kokoh, K. B.; Innocent, C.; Cretin, M.; Tingry, S. Concentric glucose/O2 Biofuel Cell. *J. Electroanal. Chem.* **2008**, *622*, 97–102.

(230) Nogala, W.; Rozniecka, E.; Zawisza, I.; Rogalski, J.; Opallo, M. Immobilization of ABTS – Laccase System in Silicate Based Electrode for Biolectrocatalytic Reduction of Dioxygen. *Electrochem. commun.* **2006**, *8*, 1850–1854.

(231) Han, Y.; Yu, C.; Liu, H. A Microbial Fuel Cell as Power Supply for Implantable Medical Devices. *Biosens. Bioelectron.* **2010**, *25*, 2156–2160.

(232) Gao, F.; Viry, L.; Maugey, M.; Poulin, P.; Mano, N. Engineering Hybrid Nanotube Wires for High-Power Biofuel Cells. *Nat. Commun.* **2010**, *1*, 2.

(233) Mano, N.; Mao, F.; Shin, W.; Chen, T.; Heller, A. A Miniature Biofuel Cell Operating at 0.78 V. *Chem. Commun.* **2003**, *2*, 518–519.

(234) Simoes, M.; Baranton, S.; Coutanceau, C. Electrooxidation of Sodium Borohydride at Pd, Au, and Pd xLAu1-X Carbon-Supported Nanocatalysts. *J. Phys. Chem. C* **2009**, *113*, 13369–13376.

(235) Pasta, M.; Hu, L.; La Mantia, F.; Cui, Y. Electrodeposited Gold Nanoparticles on Carbon Nanotube-Textile: Anode Material for Glucose Alkaline Fuel Cells. *Electrochem. commun.* **2012**, *19*, 81–84.

(236) Tominaga, M.; Shimazoe, T.; Nagashima, M.; Taniguchi, I. Electrocatalytic Oxidation of Glucose at Gold Nanoparticle-Modified Carbon Electrodes in Alkaline and Neutral Solutions. *Electrochem. commun.* **2005**, *7*, 189–193.

(237) Zhu, C.; Guo, S.; Dong, S. PdM (M = Pt, Au) Bimetallic Alloy Nanowires with Enhanced Electrocatalytic Activity for Electro-Oxidation of Small Molecules. *Adv. Mater.* **2012**, *24*, 2326–2331.

(238) Wojnicki, M.; Luty-B., M.; Dobosz, I.; Grzonka, J.; Pac, K. Electro-Oxidation of Glucose in Alkaline Media on Graphene Sheets Decorated with Gold Nanoparticles. *Mater. Sci. Appl.* **2013**, *4*, 162–169.

(239) Makovos, E. B.; Liu, C. C. A Cyclic-Voltammetric Study of Glucose Oxidation on a Gold Electrode. *Bioelectrochemistry Bioenerg.* **1986**, *211*, 157–165.

(240) El-Ads, E. H.; Galal, A.; Atta, N. F. Electrochemistry of Glucose at Gold Nanoparticles Modified graphite/SrPdO3 Electrode – Towards a Novel Non-Enzymatic Glucose Sensor. *J. Electroanal. Chem.* **2015**, *749*, 42–52.

(241) Parpot, P.; Nunes, N.; Bettencourt, A. P. Electrocatalytic Oxidation of Monosaccharides on Gold Electrode in Alkaline Medium: Structure–reactivity Relationship. *J. Electroanal. Chem.* **2006**, *596*, 65–73.

(242) Biella, S.; Rossi, M. Gas Phase Oxidation of Alcohols to Aldehydes or Ketones Catalysed by Supported Gold. *Chem. Commun.* **2003**, *2003*, 378–379.

(243) Prati, L.; Porta, F. Oxidation of Alcohols and Sugars Using Au/C Catalysts - Part 1. Alcohols. *Appl. Catal. A Gen.* **2005**, *291*, 199–203.

(244) Girault, H. H. Cyclic Voltammetry. In *Analytical and Physical Electrochemistry*; EPFL

Press - Marcel Dekker, 2004; pp. 375–409.

(245) Mabbott, G. A. An Introduction to Cyclic Voltammetry. *J. Chem. Educ.* **1983**, *60*, 697–702.

(246) Nicholson, R. S. Theory and Application of Cyclic Voltammetry for Measurement of Electrode Reaction Kinetics. *Anal. Chem.* **1965**, *37*, 1351–1355.

(247) Zhao, F.; Slade, R. C. T.; Varcoe, J. R. Techniques for the Study and Development of Microbial Fuel Cells: An Electrochemical Perspective. *Chem. Soc. Rev.* **2009**, *38*, 1926–1939.

(248) Kloke, A.; Biller, B.; Kräling, U.; Kerzenmacher, S.; Zengerle, R.; Von Stetten, F. A Single Layer Glucose Fuel Cell Intended as Power Supplying Coating for Medical Implants. *Fuel Cells* **2011**, *11*, 316–326.

(249) Bunte, C.; Hussein, L.; Urban, G. A. Performance of Non-Compartmentalized Enzymatic Biofuel Cell Based on Buckypaper Cathode and Ferrocene-Containing Redox Polymer Anode. *J. Power Sources* **2014**, *247*, 579–586.

Annex 1

Materials details

Electrospinning equipment: IME Technologies, The Netherlands.

Stabilization of PAN fibers realized in an ashes furnace (Thermolyne 4800).

Carbonization of stabilized fibers realized in a tubular furnace (Vecstar VTF-4, England).

Optical microscope for felts thickness measurement: Olympus BX41 coupled with an Olympus MPlan 5x/0.10 objective.

Raman spectroscope: Jobin-Yvon LabRAM HR 800 spectrometer, laser excitation at 632.82 nm.

SEM equipment: Hitachi S4800 microscope.

EDX equipment: Jeol JCM-6000PLUS Neoscope Benchtop SEM coupled with EDX.

XRD equipment: PANalytical Xpert-PRO diffractometer equipped with an X'celerator detector using Ni-filtered Cu Kα-radiation at wavelength of 1.5406 Å.

Ultrasonic homogenizer: Bandelin Sonopuls UW 3100

TGA equipment: SDT 2960 Simultaneous from TA Instruments.

Potentiostat employed for electrochemical measurements: Ametek VersaStat 3.

Annex 2

Electrochemical characterization techniques of electrode materials, half-cells and complete BFCs

In this section, a theoretical overview of the electrochemical techniques employed in this work will be presented. Notably, cyclic voltammetry was employed for the characterization of the electrodes, composed of CNFs, graphite or glassy carbon. Bare CNFs and gold-modified CNFs were also characterized by electrochemical impedance spectroscopy in Chapter IV. When electrodes were modified with enzymes (Part 3 of this work), polarization curves were employed for half-cell tests, either as anode or as cathode. Finally, complete BFC test was realized by varying the external resistance applied to the cell.

It is important to highlight here the equation that governs electrochemical systems: the Nernst Equation (**Equation A.1**) which provides a link between electrode potential E and the concentrations of participants in a given electrode process of the type "O + *ne* → R", where O is the oxidized form, and R is the reduced form of a certain species.[201]

$$E_{SHE} = E^0_{SHE} + \frac{RT}{nF} ln\left(\frac{C_{ox}}{C_{red}}\right) \quad \text{(A.1)}$$

where **E** = electrode potential, [V] (i.e. $E_{working} - E_{reference}$ *vs.* SHE for a half cell, or the electromotive force, E_{cell}, for a complete cell)

E^0 = standard potential, [V] (i.e. the standard reduction potential *vs.* SHE for a half-cell, or the standard cell potential for a complete cell)

R = gas constant, [8.314 J K^{-1} mol^{-1}]

T = temperature, [K]

n = number of mols of electrons transferred in the reaction, dimensionless

F = Faraday constant, [9.6485 x 10^4 C mol^{-1}]

C_{ox} and **C_{red}** = concentration of oxidized and reduced species, by considering the activity a = 1 (diluted solutions)

Nernst equation governs processes where the concentrations of oxidized and reduced species at the electrode surface can be assumed to be at equilibrium with the

electrode potential and current, if the kinetics of electron transfer is rapid. The net rate of electrode reaction is governed by the rate at which electroactive species are brought to the surface by mass transfer. Therefore when the main species obey thermodynamic relationships at the electrode surface, the system is called *reversible* or *nernstian*,[201] which will be considered herein.

In this work, electrochemical characterizations were realized with a typical three electrode system composed of a reference electrode (Ag/AgCl saturated KCl), a working electrode (CNFs felt developed by electrospinning, further modified or not) and a counter electrode (stainless steel) connected to a potentiostat, in a Teflon open cell under magnetic stirring on a heating plate. A picture of the cell is presented on **Figure A.1**, as well as the typical electrode composed of CNFs, which only the bottom part was dipped in the solution for measurements. The solution content varied according to the characterization realized.

Cyclic voltammetry

Cyclic voltammetry is a potential sweeping method, in which the current is recorded while the working electrode potential is changed linearly with time between two chosen values.[202] It is, according to Girault, the most universal electrochemical technique, used either to elucidate reaction mechanisms or to carry out quantitative analysis. The technique consists of varying the electrode potential in a linear fashion between two limits: the initial electrode potential E_i and the final electrode potential E_f (known as switching potential,

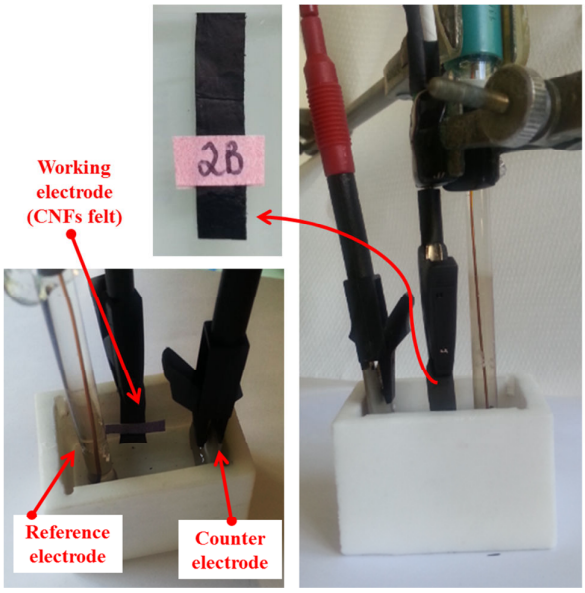

Figure A.1. *Assembly employed for electrochemical characterizations, composed of typical three electrode system, as well as a photo of a typical CNFs electrode (only the bottom part is dipped in the solution).*

where the direction of the scan is reversed), in order to probe the reactivity of the electrochemical system over a large range of potentials in a single sweep. In a typical voltammogram, like the one presented in **Figure A.2**, oxidation and reduction peaks are observed at the respective potentials E_{ox} and E_{red}. By varying the sweep rate, the kinetics of the reactions and/or the mass transfer process can also be examined. On the reverse scan, part of the species oxidized in the forward scan are reduced.[244]

Considering a reversible system (one where the reaction is fast enough to maintain the concentrations of the oxidized and reduced forms in equilibrium with each other at the electrode surface[245]), like $Fe(CN)_6^{3-}$, a typical voltammogram (current response plotted as a function of the applied potential) shows the oxidation and reduction peaks, as presented in **Figure A.2**. The more reversible is the reaction, the closer together are the peaks, so that the ΔE difference can be correlated to the kinetics of the electric transfer (the lower the ΔE, the better the electric transfer for a given species at a given electrode surface). The current obtained depends on two steps in the overall process, the movement of electroactive species to the surface and the electron transfer reaction, since it is a nernstian process.[245]

One topic that will be employed in Chapter IV should be highlighted here: the Nicholson method[246] for the determination of standard rate constants (k^0) for electron transfer in quasireversible systems. According to this method, which was well explained by Bard[201], the variation of ΔE with scan rates (v) in cyclic voltammetry must be determined. Nicholson showed that ΔE is a function of the single dimensionless kinetic parameter ψ (**Equation A.2**):

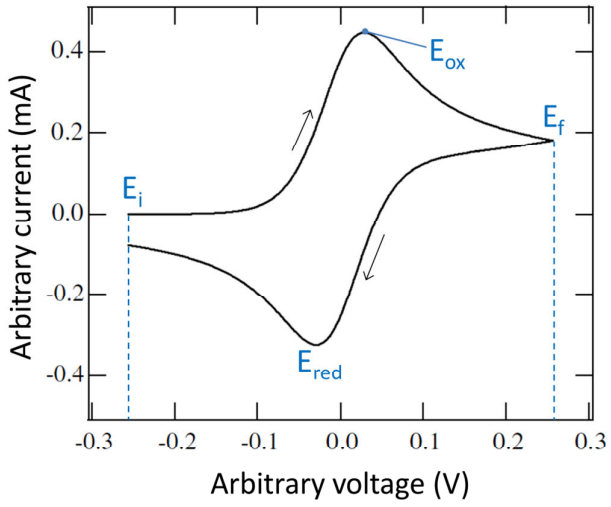

Figure A.2. *Typical cyclic voltammogram of a reversible system.*

$$\psi = k^0 \frac{\left(\frac{D_{ox}}{D_{red}}\right)^{\frac{\alpha}{2}}}{\sqrt{\pi D_{ox} v F (R T)^{-1}}} \quad \text{(A.2)}$$

where **ψ** = dimensionless rate parameter in cyclic voltammetry
k^0 = standard rate constant, [cm s^{-1}]
D_{ox} and **D_{red}** = diffusion coefficient of oxidized and reduced species, [cm^2 s^{-1}]
α = transfer coefficient, dimensionless, typical value of 0.5 was employed
v = scan rate of cyclic voltammogram, [V s^{-1}]
F = Faraday constant, [9.6485 x 10^4 C mol^{-1}]
R = gas constant, [8.314 J K^{-1} mol^{-1}]
T = temperature, [K]

After measuring ΔE for several *v*, the table that relates ψ and ΔE proposed by Nicholson (not shown here) can be used to find the corresponding value of ψ.[202] Then, K^0 can be easily calculated from **Equation A.2** for several *v*, and a mean value of K^0 can be determined.

Electrochemical impedance spectroscopy (EIS)

EIS is another technique employed in Chapter IV for the comparison of electron transfer efficiency between bare CNFs and gold-modified CNFs.

Ohm's law, E = R × I, defines resistance in terms of the ratio between voltage, E, and current, I, and E and I signals (which are alternating sinusoidal signals with a certain angular frequency ω) must be in phase with each other (ideal system), according to **Figure A.3A**.

Real circuit elements do not present ideal behavior (do not follow Ohm's law), thus impedance concept is employed instead of the concept of resistance. Impedance is also a measurement of the ability of a circuit to resist the flow of electrical current. However in non-ideal circuits, E and I signals are not in phase with each other, meaning there is a phase shift between them, as represented by **Figure A.3B**.

Potential and current can be therefore written as:

$e = E \sin(\omega t)$

$i = I \sin(\omega t + \theta)$

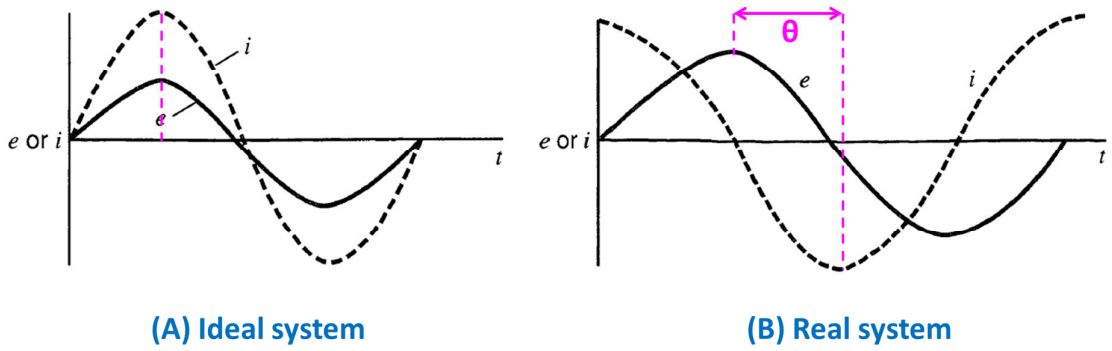

Figure A.3. *Relation between current and voltage signals in* ***(A)*** *an ideal system and* ***(B)*** *a real (non-ideal) system. [Adapted from Bard*[201]*]*

where *e* and *i* are the potential and current at any given moment, and E and I are the maximum amplitude of the signal.

Impedance is, therefore, a complex variable that must be written: $Z(\omega) = Z_{re} - j.Z_{im}$; and Ohm's law can be rewritten in terms of the impedance: $E = Z \times I$.

EIS technique is realized in an electrochemical cell containing a redox species in solution. In this work, $Fe(CN)_6^{3-}$ was employed in the typical three electrode cell (Figure 1.22). The experiment is realized at a fixed electrode potential: here the $E_{1/2}$ (i.e. the mean between E_{ox} and E_{red}) of $Fe(CN)_6^{3-/4-}$ reaction was chosen, because at this potential no redox peaks are present. Then the frequency of the system is scanned over a high range of frequency values, while making impedance (Z) readings, thus generating an impedance spectrum. The variation of impedance and frequency can be displayed in different ways. Z_{re} can be plotted against Z_{im}, which consists the *Nyquist* plot, or $\log|Z|$ and θ can be plotted against $\log(\omega)$, which consists the *Bode* plot.

In order to interpret the obtained plots, electrochemical systems are often represented in terms of an equivalent electrical circuit of resistors, capacitors, inductors, etc. A frequently used circuit, called the *Randles* equivalent circuit, is shown in **Figure A.4**. In this circuit, R_Ω represents the solution resistance, C_d the double layer capacitance, and the impedance Z_f is normally separated in two terms: R_{ct} (charge transfer resistance) and Z_w (Warburg impedance, which represents a mass transfer resistance). All these components can be calculated allowing comparison between different systems, for instance. For more

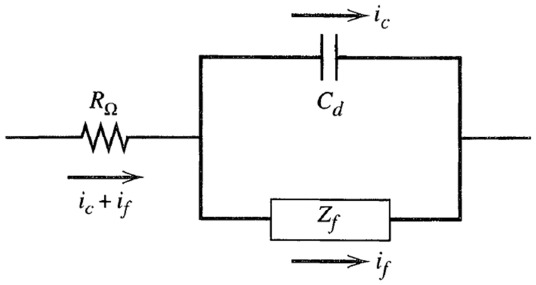

Figure A.4. *Randles equivalent circuit. [From Bard[201]]*

complicated electrochemical systems (e.g. layered electrodes, porous structures, presence of enzymes or other catalysts), more complicated circuits must be developed. More details on this matter are, however, not on the scope of this work. EIS technique has been applied to a variety of electrochemical systems, including those involved in corrosion, electrodeposition, polymer films, semiconductor electrodes, photovoltaics, biosensing, organic coatings on metals, etc.

Half-cell polarization curves

Half-cell tests were realized on the same three electrode system presented in **Figure A.1**, either with an O_2 gas entry to saturate the PBS solution, in the case of a biocathode, or with the anodic substrate (glucose, alcohol), depending on the case. The working electrode in half-cell test was composed of the CNFs modified with the specific enzyme, depending on the reaction to be accomplished (laccase for O_2 reaction, GOx for glucose oxidation, for example).

O_2 biocathodes were chosen as model reaction in this work for the comparison of enzyme immobilization techniques or different electrode materials. ORR, one of the most important reactions in life processes such as biological respiration, has been widely studied for the application in O_2 cathodes in electrochemical energy conversion systems (like FCs). ORR in aqueous solutions occurs mainly by two pathways: the direct 4-electron reduction pathway from O_2 to H_2O (as mentioned in Section 1.3.2), and the 2-electron reduction pathway from O_2 to hydrogen peroxide (H_2O_2). In non-aqueous aprotic solvents and/or in alkaline solutions, the 1-electron reduction pathway from O_2 to superoxide (O_2^-) can also occur.[95] Normally, kinetics of ORR is very slow, so that a catalyst in needed, platinum being one of the best catalysts for this reaction, even though commercially unviable.

For the 4-electron reduction pathway from O_2 to H_2O (the one that preferably happens at enzymatic BFCs), the thermodynamic electrode potential in acidic aqueous solution is 1.229 V *vs.* SHE (which corresponds to ~0.6 V *vs.* Ag/AgCl). It is desirable that the reaction occurs at a potential as close as possible to the thermodynamic electrode potential, with satisfactory reaction rate and low overpotential (i.e. the potential difference between the thermodynamic potential and the experimentally observed potential).[95]

One of the possible techniques for ORR catalysis studies is steady-state polarization, which was the technique employed in this work. In a polarization curve, the potential of the electrode surface shifts away from its equilibrium value, leading to an electrochemical reaction. This process follows the *Butler-Volmer* equation (not shown here) for electrode heterogeneous kinetics. A steady-state polarization curve describes the relationship between the electrode potential and the current density, which is recorded by either holding the electrode potential and recording the stable current response, or holding the current density and recording the stable potential response. In this work, all the polarization curves were recorded by varying the potential and recording the current density response. Typical polarization curves are presented in **Figure A.5**. It is possible to observe the important decrease in overpotential achieved with laccase-modified carbon electrode compared to Pt electrode.[92] The plateau observed with laccase electrodes means electron transfer at high current densities is limited by the diffusion of species onto the electrode, and can be overcome with different enzyme immobilization techniques, for example.

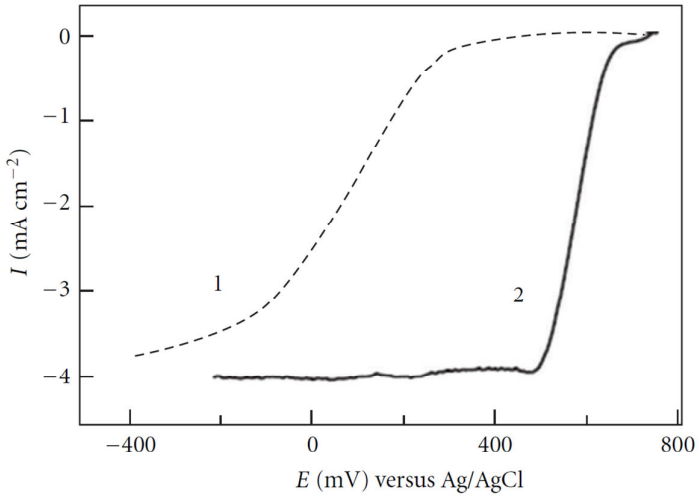

Figure A.5. *Typical linear sweep voltammograms (polarization curves) of ORR onto* ***(1)*** *Platinum electrode, and* ***(2)*** *laccase adsorbed carbon aerogel electrode, at pH 5, obtained with rotating disc electrode at 1000 RPM at a scan rate of 0.02 V* s^{-1}*. [Reproduced from Opallo*[92]*]*

In the case of a cathode, it is established that the current is negative, while for anodes it is positive. Anodic polarization curves were realized by the same technique for alcohol bioanodes developed in Chapter VI. It is important to note that half-cell reaction can also be studied by cyclic voltammetry, as will be the case for glucose anodes in this work. Specific peaks of glucose oxidation depend on the electrode material employed. For example, abiotic oxidation onto gold particles will be discussed in Chapter IV, and bio-oxidation with GOx, in Chapter VI.

Complete BFC tests

In biofuel cell (BFC) science, there are four basic techniques available to test and validate cell voltage and output current performance:[247]

- **CRD** or "*constant resistance discharge*" consists of connecting different resistors to the BFC and measuring the resulting currents and voltages, point per point, starting with the higher resistor.[66,69,105]
- **PDP** or "*potentiodynamic polarization*" involves conducting linear sweep voltammetry (LSV) to record the current at slow voltage scan rate, generally at 1 mV s^{-1}.[221]
- **GSD** or "*galvanostatic discharge*" method involves controlling the applied current when the resulting voltage is measured.[248]
- In **PSD** or "*potentiostatic discharge*" the voltage is controlled and the resulting current is measured.[249]

Zhao et al. highlighted the strengths and weaknesses of each of these methods. According to their analysis, PSD measurements may be the most suitable for investigations because it probes the fundamental science that is involved in microbial or biofuel cells, especially when the electrochemistry of enzymes is involved.[247] One of the given reasons is the sudden deactivation of the enzyme when the potentials are raised beyond a certain point in CRD, PDP, or GSD methods.

In conventional FC studies, the GSD protocol is preferred. The performance during CRD, GSD, and PSD depend strongly on the delay in the acquisition time. For example, the duration of each step in GSD or PSD has a critical role in determining the obtained measured variable (cell voltage for GSD and output current for PSD).

The determination of BFC performance (cell voltage and output power) using LSV is inappropriate, because a steady-state (equilibrium) cannot be reached during such a test. More importantly, it is known that during LSV experiments, the measured current depends strongly on the scan rate, so that the obtained power density ($P_{cell} = E_{cell} \times j$) also depends on the scan rate. Also, it is known that the current increases when the scan rate increases. Thus, it is impossible to compare the performance of two BFCs when the value of the scan rate is not reported (which usually happens in published works). Unfortunately, in many works there is not enough information about the kind of test the authors have used to characterize BFCs, so that it is not possible to properly compare different works.

In this work, the CRD technique was employed for the evaluation of BFCs performance because in this techniques the BFC is connected to an external load that reflects the real situation to activate implantable biomedical devices. During CRD test, a housing resistor ranging from 10 MΩ to 0 Ω was employed, along with multimeters for voltage and current readings, as shown in the scheme of **Figure A.6**: the variable resistance box and amperemeter are connected to the anode and cathode in series to each other, while the voltmeter is connected in parallel with the whole system.

At 10 MΩ, the open circuit voltage (V_{OC}) is noted, then the resistance is lowered step by step, and E and I readings are noted at each step. BFC tests were performed in PBS solution (0.1 M) at 37 °C in two-compartment configuration. Nafion® 117 perfluorinated membrane was used to separate the compartments. BFCs were evaluated in terms of the V_{OC}; cell voltage or tension (E_{cell}); output current density (j) and power density (P, calculated from E and I readings), using the geometric surface area of the electrodes.

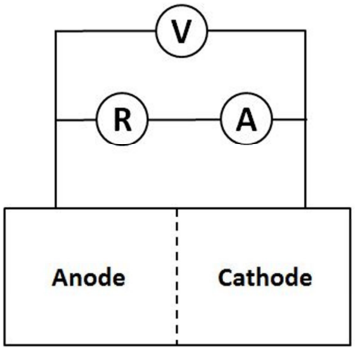

Figure A.6. *Scheme of the circuit employed for BFCs tests by the CRD method, containing a variable resistance box, an amperemeter and a voltmeter connected to the anode and cathode of the BFC.*

An ideal polarization curve $E_{cell} = f(j)$ of a BFC (obtained from the readings of the CRD method), the typical curve shown in **Figure A.7**, presents three different zones, according to Zhao et al.[247]

- First, there is the region of charge transfer overpotentials, also known as the activation region, which is located at low currents and derives from the slowness (irreversibility) of the reactions taking place on the surface of the electrodes. Some of the parameters that govern this region are the nature of the electrode materials, catalysts, reactant activities, electrolyte including any spectator species that may be present, electrochemical mediators, electrode microstructure, enzyme species and their metabolisms, and operational conditions such as the temperature.
- The second region is the ohmic overpotentials, situated at intermediary currents in the polarization curve. Their origin is due to the ionic resistances in the electrolyte, membrane, and the electrical resistances in the electrodes and current collector connectors. Generally, the cell voltage varies very slightly in this current range.
- At higher current, the so-called mass-transport overpotentials results from the change in concentration of the reactants/products at the interface electrode/bulk electrolyte.

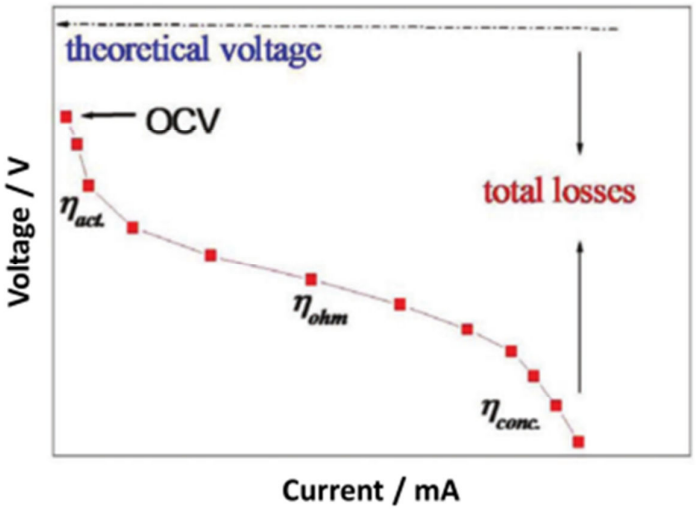

Figure A.7. *Ideal current-voltage polarization curve of a typical BFC. (from Zhao et al.[247])*

Résumé

Ce manuscrit de thèse présente la synthèse et l'optimisation d'un nouveau matériau d'électrode adapté aux biopiles enzymatiques et hybrides qui sont des systèmes capables de convertir de l'énergie chimique en énergie électrique en utilisant des catalyseurs enzymatiques. Ce matériau est constitué de nanofibres de carbone fabriquées par la technique d'*electrospinning* à partir d'une solution de polyacrylonitrile, suivi de traitements thermiques appropriés. Les propriétés structurales et électriques des nanofibres de carbone les rendent très intéressantes en tant que matériaux d'électrode tridimensionnels pour développer des systèmes de conversion d'énergie. Dans ce travail, les propriétés des électrodes à base de nanofibres de carbone ont été améliorées par adsorption de nanotubes de carbone ou croissance *in situ* de particules d'or. D'autre part, l'influence de l'organisation spatiale des fibres a été étudiée avec la synthèse de fibres alignées et non alignées. Des bioélectrodes ont été préparées à partir de ces différents types de matériaux en utilisant des enzymes oxydoréductases. Ces enzymes ont été encapsulées dans des matrices de Nafion, polypyrrole ou chitosan pour réaliser soit du transfert médiaté, soit du transfert direct. Ces bioélectrodes ont été employées par la première fois dans des biopiles enzymatiques et hybrides utilisant comme combustible soit de l'éthanol ou du glucose. Les résultats obtenus dans ce travail ont démontré toute la potentialité des matériaux à base de nanofibres de carbone pour la construction de biopiles performantes, ce qui représente une avancée significative vers un futur developpement industriel.

Abstract

This thesis manuscript presents the synthesis and optimization of a new electrode material suitable for enzymatic and hybrid biofuel cells, which are systems capable of converting chemical energy into electrical energy by using enzymatic catalysts. This material is composed of carbon nanofibers fabricated by the electrospinning of a polyacrylonitrile solution, followed by appropriate thermal treatments. Carbon nanofibers structural and electrical properties make them very suitable for application as tridimensional electrode materials for the development of energy conversion systems. In this work, the properties of electrodes composed of carbon nanofibers were enhanced through the adsorption of carbon nanotubes, or the *in situ* growing of gold particles. In a different strategy, the influence of the fibers spatial organization was studied through the synthesis of aligned and randomly organized fibers. Bioelectrodes were prepared from these different types of materials with oxidoreductase enzymes. Enzymes were entrapped in matrixes composed of Nafion, polypyrrole or chitosan in order to realize either mediated or direct electron transfer. These bioelectrodes were employed for the first time in enzymatic and hybrid biofuel cells, with ethanol or glucose as fuels. The results obtained in this work were able to demonstrate the potential of materials based of carbon nanofibers for the construction of performing biofuel cells, which represents a significant advance toward future industrial development.